

**HYDROPHOBICALLY MODIFIED LOW MOLECULAR
WEIGHT CHITOSAN FOR DRUG DELIVERY**

TIEW SHU XIAN

**FACULTY OF SCIENCE
UNIVERSITY OF MALAYA
KUALA LUMPUR**

2018

**HYDROPHOBICALLY MODIFIED LOW MOLECULAR
WEIGHT CHITOSAN FOR DRUG DELIVERY**

TIEW SHU XIAN

**THESIS SUBMITTED IN FULFILMENT OF
THE REQUIREMENTS FOR THE DEGREE
OF DOCTOR OF PHILOSOPHY**

**DEPARTMENT OF CHEMISTRY
FACULTY OF SCIENCE
UNIVERSITY OF MALAYA
KUALA LUMPUR**

2018

UNIVERSITY OF MALAYA
ORIGINAL LITERARY WORK DECLARATION

Name of Candidate: **TIEW SHU XIAN**

Matric No: **SHC140014**

Name of Degree: **DOCTOR OF PHILOSOPHY**

Title of Project Paper/Research Report/Dissertation/Thesis (“this Work”):
**HYDROPHOBICALLY MODIFIED LOW MOLECULAR WEIGHT
CHITOSAN FOR DRUG DELIVERY**

Field of Study: **PHYSICAL CHEMISTRY (BIOCOLLOID)**

I do solemnly and sincerely declare that:

- (1) I am the sole author/writer of this Work;
- (2) This Work is original;
- (3) Any use of any work in which copyright exists was done by way of fair dealing and for permitted purposes and any excerpt or extract from, or reference to or reproduction of any copyright work has been disclosed expressly and sufficiently and the title of the Work and its authorship have been acknowledged in this Work;
- (4) I do not have any actual knowledge nor do I ought reasonably to know that the making of this work constitutes an infringement of any copyright work;
- (5) I hereby assign all and every rights in the copyright to this Work to the University of Malaya (“UM”), who henceforth shall be owner of the copyright in this Work and that any reproduction or use in any form or by any means whatsoever is prohibited without the written consent of UM having been first had and obtained;
- (6) I am fully aware that if in the course of making this Work I have infringed any copyright whether intentionally or otherwise, I may be subject to legal action or any other action as may be determined by UM.

Candidate’s Signature

Date:

Subscribed and solemnly declared before,

Witness’s Signature

Date:

Name:

Designation:

HYDROPHOBICALLY MODIFIED LOW MOLECULAR WEIGHT CHITOSAN FOR DRUG DELIVERY

ABSTRACT

Hydrophobically modified chitosan which are able to self-aggregate as a hydrophobic core and a hydrophilic corona architecture in an aqueous physiological environment are drawing attention and developing tremendously in drug delivery due to their numerous advantages and biological potentials. In this study, 25 kDa low molecular weight chitosan (Ch3) was prepared via depolymerization with nitrous acid for better solubility and introduced with different chain lengths of hydrophobic alkyl groups to obtain butyryl (ChC4), hexanoyl (ChC6), octanoyl (ChC8), decanoyl (ChC10) and lauryl chitosan (ChC12) for the evaluation as drug carriers. The successful acylation of the alkyl chain was confirmed via fourier-transform infrared (FTIR), ^1H and ^{13}C nuclear magnetic resonance (NMR) analyses, as well as the change in zeta potential to a negative value after acylation. The water solubility, critical aggregation concentration and particle size were greatly influenced by the alkyl chain length and degree of substitution (DS) of acylated low molecular weight chitosan (ChA). Thermogravimetric analysis (TGA), X-ray diffraction (XRD) and viscosity showed the effect of acylation to the hydrogen bonding of the chitosan. Observations from both transmission electron microscope (TEM) and field-emission scanning electron microscope (FE-SEM) showed that ChA formed spherical particles, in which longer chain acylated chitosan have larger particle size due to possible larger occupancy volume. The encapsulation of ChA with four model analgesic drugs of different solubilities including salicylic acid (SA), lidocaine (LID), acetaminophen (ACE) and caffeine (CAF), demonstrated that the encapsulation efficiency was dependent on the drug solubility and alkyl chain length. The particle size of ChA was larger after loading with slightly soluble drugs such as SA and LID compared to those of sparingly soluble drugs such as ACE and CAF. Additionally, the size

increment was more pronounced in short alkyl chain acylated chitosan (ChC4 and ChC6) with higher rigidity. The morphology from TEM micrographs showed that ChA maintained their spherical shape after drug loading. The *in vitro* drug release from ChA in phosphate buffer saline pH 7.4 for topical delivery using inline vertical Franz diffusion cells and in simulated gastric fluid (SGF) pH 1.2 for oral delivery using dialysis tubing demonstrated that ChA were able to slow down the release of free drug solutions by following the Korsmeyer-Peppas model, where both swelling and diffusion were involved in the release mechanism. The hydrophobically modified low molecular weight chitosan were promising carriers to prolong drug release, with lauryl chitosan showing the best drug sustainability among the ChA.

Keywords: Chitosan, low molecular weight, hydrophobic modification, drug delivery.

KITOSAN BERJISIM MOLEKUL RENDAH DENGAN PENGUBAHSUAIAN KUMPULAN HIDROFOBİK BAGI PENGHANTARAN UBAT

ABSTRAK

Kitosan yang diubahsuai dengan kumpulan hidrofobik yang dapat beragregat dengan reka bentuk teras hidrofobik dan korona hidrofilik dalam persekitaran fisiologi akueus manusia berjaya mengundang perhatian penyelidikan dan berkembang pesat dalam penghantaran ubat disebabkan oleh kebaikan dan potensi biologinya. Dalam kajian ini, kitosan yang berjisim molekul rendah, 25 kDa (Ch3) disedia dengan pendepolimeran menggunakan asid nitrus bagi keterlarutan yang lebih baik dan diubahsuai dengan kumpulan hidrofobik yang berlainan kepanjangan rantaian untuk menghasilkan kitosan butiril (ChC4), heksanoyil (ChC6), oktanoyil (ChC8), dekanoyil (ChC10) dan lauril (ChC12) bagi mengkaji potensi sebagai penghantar ubat. Kejayaan pengasilan rantaian alkil pada kitosan disah dengan analisis inframerah transformasi fourier (FTIR), ^1H dan ^{13}C resonans magnet nukleus (NMR), dan juga perubahan keupayaan zeta yang bertukar ke negatif selepas pengasilan. Keterlarutan, kepekatan agregat genting dan saiz partikel banyak dipengaruhi oleh kepanjangan rantaian alkil dan darjah penukargantian kitosan berjisim molekul rendah yang berasal (ChA). Analisis termogravimetri (TGA), belauan sinar-X (XRD) dan kelikatan menunjukkan kesan pengasilan terhadap ikatan hidrogen kitosan. Pemerhatian daripada kedua-dua mikroskop electron transmisi (TEM) dan elektron pengimbas-emisi medan (FE-SEM) menunjukkan bahawa ChA membentuk partikel bulat, di mana kitosan yang berasal rantaian panjang mempunyai saiz partikel yang lebih besar, berkemungkinan disebabkan oleh pengisian isipadu yang lebih besar. Pengkapsulan ChA dengan empat jenis model ubat analgesik yang berlainan keterlarutan, termasuklah asid salisilik (SA), lidokain (LID), asetaminofen (ACE), dan kafeina (CAF), menunjukkan bahawa kecekapan pengkapsulan bergantung pada keterlarutan ubat dan kepanjangan rantaian alkil. Saiz partikel ChA adalah lebih besar selepas dimuat dengan

ubat yang terlarut sedikit seperti SA dan LID berbanding dengan ubat yang agak terlarut seperti ACE dan CAF. Tambahan pula, peningkatan saiz ChA lebih menonjol pada kitosan yang berasal rantaian alkil pendek (ChC4 dan ChC6) yang lebih tinggi ketegaran. Morfologi daripada mikrograf TEM menunjukkan bahawa ChA kekal sebagai partikel bulat selepas pemuatan ubat. Pelepasan ubat *in vitro* dari ChA dalam larutan garam penimbal fosfat pH 7.4 menggunakan sel difusi Franz tegak sebaris bagi penghantaran ubat secara topikal dan dalam cecair gastrik simulasi pH 1.2 menggunakan tiub dialysis bagi penghantaran ubat melalui mulut menunjukkan bahawa ChA dapat melambatkan pelepasan ubat mengikut model Korsmeyer-Peppas, di mana kedua-dua process pengembangan dan difusi terlibat dalam mekanisme pelepasan ubat. Kitosan berjisim molekul rendah yang diubahsuai dengan kumpulan hidrofobik berpotensi untuk memanjangkan tempoh pelepasan ubat, di mana kitosan lauril menunjukkan keupayaan menahan pelepasan ubat yang tertinggi antara ChA.

Kata kunci: Kitosan, berjisim molekul rendah, pengubahsuaian hidrofobik, penghantaran ubat.

ACKNOWLEDGEMENTS

“The essence of all beautiful art is gratitude.” –Friedrich Nietzsche

There are many people who become part of the essence in my colourful study life. I appreciate the people who always provide support, advices and help for me throughout these years of research. First of all, I would like to express the highest gratitude to my supervisor Prof. Dr. Misni Misran who not only give me guidances, advices and courage in the academic research study, but also instill and shape better character in me. Of course, a heartfelt gratitude is dedicated to my labmates and friends for their advices, experiences sharing and help. I am thankful for their motivations and humor shared in our Colloid chat group to brighten and cheer up the days. I appreciate the moments with them whether during formal research discussions or festival celebration or leisure gathering. We learned, grew and laughed together, life would have been dull without them. I would like to thank the lab assistants who offered me technical support and advices for instrumental operations. Special thanks to the staffs of Chemistry Department and the University of Malaya (UM) management for their assiduous commitment. In addition, the support, care and tolerance of my family members over the years are much appreciated as psychological nutrients during my study journey. The last but not least, I would like to render my gratitude for the financial support from the UM Institute of Research and Monitoring (IPPP) for the expenses of the research project, and also UM Fellowship Scheme (SBUM) and MyBrainSc scholarships from Malaysia Ministry of Higher Education for sponsoring my study.

TABLE OF CONTENTS

Abstract.....	iii
Abstrak.....	v
Acknowledgements.....	vii
Table of Contents.....	viii
List of Figures.....	xii
List of Tables.....	xvii
List of Symbols and Abbreviations.....	xx
CHAPTER 1: INTRODUCTION.....	1
1.1 Drug delivery.....	1
1.2 Polymeric particles in drug delivery.....	2
1.3 Polysaccharides in drug delivery.....	3
1.4 Chitosan.....	5
1.4.1 Potentials of chitosan.....	6
1.4.2 Limitations of chitosan.....	7
1.5 Objectives.....	8
CHAPTER 2: LITERATURE REVIEW.....	9
2.1 Modifications of chitosan.....	9
2.1.1 Depolymerization.....	11
2.1.1.1 Low molecular weight chitosan (LMWC).....	12
2.1.2 Hydrophobic modifications.....	15
2.1.2.1 Acylation.....	18
2.1.2.2 Physicochemical properties of HMC.....	20
2.2 Chitosan for drug delivery.....	22
2.2.1 Chitosan for topical delivery.....	22
2.2.2 Chitosan for oral delivery.....	24
2.3 Analgesic drugs.....	26
2.3.1 Examples of analgesic drugs.....	28
2.3.1.1 Salicylic acid (SA).....	28
2.3.1.2 Lidocaine (LID).....	28
2.3.1.3 Acetaminophen (ACE).....	29
2.3.1.4 Caffeine (CAF).....	29

2.3.2	Chitosan for delivery of analgesic drugs.....	30
-------	---	----

CHAPTER 3: MATERIALS AND METHODS.....32

3.1	Materials.....	32
3.2	Sample preparation.....	32
3.2.1	Preparation of depolymerized chitosan.....	32
3.2.2	Preparation of <i>N</i> -acylated chitosan.....	33
3.2.3	Preparation of analgesic drugs loaded acylated chitosan.....	34
3.2.4	Preparation of buffer solutions.....	34
3.3	Equipments and instrumentations.....	35
3.3.1	pH measurement.....	35
3.3.2	Centrifugation.....	35
3.3.3	Determination of average molecular weight.....	36
3.3.4	Structural analysis of chitosan.....	38
3.3.4.1	Fourier-transform infrared (FTIR).....	38
3.3.4.2	¹ H and ¹³ C Nuclear magnetic resonance (NMR).....	39
3.3.5	Particle size and zeta potential.....	39
3.3.6	Powder X-ray diffraction (XRD).....	41
3.3.7	Thermogravimetric analysis (TGA).....	42
3.3.8	Determination of water solubility and critical aggregation concentration (CAC) using ultraviolet-visible (UV-Vis) spectroscopy.....	43
3.3.9	Kinematic viscosity measurement.....	45
3.3.10	Determination of swelling percentage.....	46
3.3.11	Morphology observations.....	46
3.3.11.1	Transmission electron microscopy (TEM).....	46
3.3.11.2	Field-emission scanning electron microscopy (FE-SEM).....	47
3.3.12	Determination of encapsulation efficiency (EE) and drug loading.....	47
3.4	<i>In vitro</i> drug release study.....	49
3.4.1	Topical delivery using inline vertical Franz diffusion cells.....	49
3.4.2	Oral delivery using dialysis tubing.....	50
3.4.3	Mathematics kinetics modelings.....	51
3.5	Data analysis.....	52

CHAPTER 4: RESULTS AND DISCUSSION.....	53
4.1 Modifications of chitosan.....	53
4.1.1 Depolymerization.....	53
4.1.2 Acylation.....	54
4.2 Characterizations of chitosan.....	55
4.2.1 Determination of average molecular weight.....	55
4.2.2 FTIR spectroscopy.....	56
4.2.3 ¹ H and ¹³ C NMR.....	58
4.2.4 Particle size and zeta potential.....	64
4.2.5 Powder X-ray diffraction (XRD).....	65
4.2.6 Thermogravimetric analysis (TGA).....	67
4.2.7 Determination of water solubility and critical aggregation concentration (CAC).	70
4.2.8 Kinematic viscosity measurement.....	73
4.2.9 Determination of swelling percentage.....	74
4.2.10 Transmission electron microscopy (TEM).....	75
4.2.11 Field-emission scanning electron microscopy (FE-SEM).....	77
4.3 Characterizations of drugs loaded ChA.....	79
4.3.1 Encapsulation efficiency and drug loading.....	79
4.3.2 FTIR spectroscopy.....	83
4.3.2.1 FTIR spectroscopy of SA loaded ChA.....	83
4.3.2.2 FTIR spectroscopy of LID loaded ChA.....	85
4.3.2.3 FTIR spectroscopy of ACE loaded ChA.....	86
4.3.2.4 FTIR spectroscopy of CAF loaded ChA.....	87
4.3.3 Particle size.....	90
4.3.4 Zeta potential.....	92
4.3.5 Transmission electron microscopy (TEM).....	93
4.3.5.1 TEM micrographs of SA loaded ChA.....	94
4.3.5.2 TEM micrographs of LID loaded ChA.....	95
4.3.5.3 TEM micrographs of ACE loaded ChA.....	96
4.3.5.4 TEM micrographs of CAF loaded ChA.....	97
4.4 <i>In vitro</i> drug release.....	99
4.4.1 Topical delivery using inline vertical Franz diffusion cells.....	99
4.4.1.1 <i>In vitro</i> release of SA.....	99
4.4.1.2 <i>In vitro</i> release of LID.....	103

4.4.1.3	<i>In vitro</i> release of ACE.....	106
4.4.1.4	<i>In vitro</i> release of CAF.....	110
4.4.2	Oral delivery using dialysis tubing.....	115
4.4.2.1	<i>In vitro</i> release of SA.....	115
4.4.2.2	<i>In vitro</i> release of LID.....	118
4.4.2.3	<i>In vitro</i> release of ACE.....	120
4.4.2.4	<i>In vitro</i> release of CAF.....	123
4.4.3	Drug release mechanism.....	126
4.4.4	Limitation of dialysis.....	128
CHAPTER 5: CONCLUSION.....		130
5.1	Conclusion.....	130
5.2	Future work.....	132
References.....		133
List of publications and papers presented.....		169

LIST OF FIGURES

Figure 1.1:	Examples of polysaccharides: (a) cellulose, (b) alginate, (c) dextran, (d) pullulan, (e) starch and (f) chitosan, where m and n are the repeating units of the monomers.....	4
Figure 1.2:	Publication number of Institute for Scientific Information (ISI) indexed publications on research of chitosan from 1980 – 2016.	6
Figure 2.1:	Resonance localization of amide via carbonyl π system.....	18
Figure 3.1:	The electrical double layer of a particle.....	41
Figure 3.2:	Electronic transitions of molecules from ground state to the excited state of the orbitals after light absorption.....	43
Figure 3.3:	The compartment of a Franz diffusion cell.....	50
Figure 3.4:	The apparatus set-up of <i>in vitro</i> drug release for oral delivery....	51
Figure 4.1:	Reaction mechanism of depolymerization of chitosan. Step 1: The reaction was initialized by the dissociation of sodium nitrite to sodium cation and nitrite ion. Step 2: Nitrite ion was protonated to form nitrosonium ion (NO^+). Step 3: Cleavage of β -glycosidic linkage to form reactive 2,5-anhydro- <i>D</i> -mannose unit at the new reducing end.....	53
Figure 4.2:	(i) The bond formation between the anhydride and chitosan and (ii) bond breaking of the leaving group during the acylation, where R is the alkyl chain of the acid anhydride, m and n is the number of <i>D</i> -glucosamine and <i>N</i> -acetyl- <i>D</i> -glucosamine units respectively.....	54
Figure 4.3:	FTIR spectra of (a) ChC4, (b) ChC6, (c) ChC8, (d) ChC10, (e) ChC12 from acylation of glucosamine units of chitosan to acid anhydrides at mole ratio of (i) 1:0.0 (Ch3), (ii) 1:0.2, (iii) 1:0.4, (iv) 1:0.6, (v) 1:0.8, (vi) 1:1.0 and (f) overall spectra of (i) Ch3, (ii) ChC4-M.8, (iii) ChC6-M.8, (iv) ChC8-M.8, (v) ChC10-M.8 and (vi) ChC12-M.8.....	57
Figure 4.4:	Degree of substitution (DS) of (i) ChC4, (ii) ChC6, (iii) ChC8, (iv) ChC10 and (v) ChC12 at different mole ratio of acylation...	58
Figure 4.5:	^1H NMR spectra of (a) Ch3, (b) ChC4, (c) ChC6, (d) ChC8, (e) ChC10 and (f) ChC12, the new CH_2 and CH_3 groups were plotted in red and pink colour respectively, where m and n in	

	the structure of chitosan represents the number of <i>D</i> -glucosamine and <i>N</i> -acetyl- <i>D</i> -glucosamine units respectively...	60
Figure 4.6:	¹³ C NMR spectra of (a) Ch3, (b) ChC4, (c) ChC6, (d) ChC8, (e) ChC10 and (f) ChC12. The new methylene and carbonyl carbons of ChA were highlighted in red colour, whereas methyl carbon was indicated by pink colour respectively.....	62
Figure 4.7:	(a) Zeta potential and (b) particle size of ChC4 (▨), ChC6 (▩), ChC8 (□), ChC10 (▨) and ChC12 (■) at different mole ratio of acylation.....	65
Figure 4.8:	XRD patterns of (a) ChC4, (b) ChC6, (c) ChC8, (d) ChC10 and (e) ChC12 from 2θ = 5 – 50°.....	66
Figure 4.9:	(a) Thermogravimetric and (b) derivate thermogravimetric thermogram of Ch3 (—), ChC4 (—), ChC6 (—), ChC8 (—), ChC10 (—) and ChC12 (—) from 35 to 900 °C.....	68
Figure 4.10:	Weight loss of Ch3, ChC4, ChC6, ChC8, ChC10 and ChC12 in the first stage (W ₁) which represented by solid symbol (■) and line (—) and second (W ₂) stage of decomposition in the TGA thermogram which indicated by hollow symbol (□) and dashed line (.....) respectively.....	68
Figure 4.11:	The linear relationship between water solubility and CAC of ChA.....	71
Figure 4.12:	(a) Plot of absorption at 350 nm as a function of logarithm of concentration of ChC4 (■), ChC6 (●), ChC8 (▲), ChC10 (▼) and ChC12 (★). (b) Schematic illustration of aggregates formation from ChA. (i) At low concentration, ChA appeared as individual polymer chains, (ii) as concentration increased, ChA started to associate among each other, (iii) aggregates formed from ChA at CAC, (iv) at higher concentration, more aggregates were formed.....	72
Figure 4.13:	Kinematic viscosity of Ch3 (◆), ChC4 (■), ChC6 (●), ChC8 (▲), ChC10 (▼) and ChC12 (★) as a function of temperature...	73
Figure 4.14:	Swelling of Ch3 and ChA in (■) deionised water and (□) 0.1 mol dm ⁻³ HCl solution at 37 °C.....	74

Figure 4.15:	TEM micrographs of (a) ChC4, (b) ChC6, under magnification of 10,000×, (c) ChC8, (d) ChC10 and (e) ChC12 under magnification of 8,000×. The scale shown was 200 nm. The arrow indicated in the micrographs was the diameter measured for the calculation of average particle size.....	76
Figure 4.16:	FE-SEM micrographs of (a) Ch3 (b) ChC4, (c) ChC6, (d) ChC8, (e) ChC10 and (f) ChC12 under magnification of 15k× at 5 kV voltage. The scale bar shown was 5 μm.....	78
Figure 4.17:	Schematic illustration of the drug encapsulation of ChA by precipitation. (a) ChA exist as individual chains when dispersed in THF containing drugs. (b) The addition of water into the dispersion promoted the hydrophobic association between the polymer chains of ChA. (c) The removal of THF facilitated the diffusion of ChA and drugs into the aqueous media and hence trapping the drug while ChA was precipitating.....	80
Figure 4.18:	(a) EE and (b) DL of (i) SA, (ii) LID, (iii) ACE and (iv) CAF using ChC4 (■), ChC6 (●), ChC8 (▲), ChC10 (▼) and ChC12 (★) by precipitation.....	82
Figure 4.19:	FTIR spectrum of (a) ChC4, (b) SA, (c) physical mixture of ChC4 and SA, SA loaded using (d) ChC4, (e) ChC6, (f) ChC8, (g) ChC10 and (h) ChC12.....	85
Figure 4.20:	FTIR spectrum of (a) ChC4, (b) LID, (c) physical mixture of ChC4 and LID, LID loaded using (d) ChC4, (e) ChC6, (f) ChC8, (g) ChC10 and (h) ChC12.....	86
Figure 4.21:	FTIR spectrum of (a) ChC4, (b) ACE, (c) physical mixture of ChC4 and ACE, ACE loaded using (d) ChC4, (e) ChC6, (f) ChC8, (g) ChC10 and (h) ChC12.....	87
Figure 4.22:	FTIR spectrum of (a) ChC4, (b) CAF, (c) physical mixture of ChC4 and CAF, CAF loaded using (d) ChC4, (e) ChC6, (f) ChC8, (g) ChC10 and (h) ChC12. (bi) is the FTIR spectrum of CAF with full label.....	89
Figure 4.23:	(a) Particle size and (b) zeta potential of (i) SA, (ii) LID, (iii) ACE, (iv) CAF after loading of ChC4 (■), ChC6 (●), ChC8 (▲), ChC10 (▼) and ChC12 (★) at different weight ratio.....	91

Figure 4.24:	The change of particle size of ChC4 (■), ChC6 (▨), ChC8 (■), ChC10 (▤) and ChC12 (□) correspond to the loading of drugs at 10:4 weight ratio.....	92
Figure 4.25:	Zwitterionic resonance structures of CAF with weakly basic properties.....	93
Figure 4.26:	TEM micrographs of (a) ChC4, (b) ChC6, (c) ChC8, (d) ChC10 and (e) ChC12 loaded with SA at weight ratio 10:4. The scale bar shown is 500 nm.....	94
Figure 4.27:	TEM micrographs of (a) ChC4, (b) ChC6, (c) ChC8, (d) ChC10 and (e) ChC12 loaded with LID at weight ratio 10:5. The scale bar shown is 500 nm.....	95
Figure 4.28:	TEM micrographs of (a) ChC4, (b) ChC6, (c) ChC8, (d) ChC10 and (e) ChC12 loaded with ACE at weight ratio 10:5. The scale bar shown is 500 nm.....	96
Figure 4.29:	TEM micrographs of (a) ChC4, (b) ChC6, (c) ChC8, (d) ChC10 and (e) ChC12 loaded with CAF at weight ratio 10:5. The scale bar shown in (a, b, e, f) is 500 nm, whereas is 1 μm in (c).....	97
Figure 4.30:	Schematic illustration of proposed position of SA (■), LID (●), ACE (▲) and CAF (◆) after encapsulation using ChA based on the correlation between solubility, encapsulation efficiency and particle size measured by DLS and TEM.....	99
Figure 4.31:	The cumulative release of SA in the absence (◆) and presence of ChC4 (■), ChC6 (●), ChC8 (▲), ChC10 (▼) and ChC12 (★) in PBS solution at 37 °C	100
Figure 4.32:	The cumulative release of LID in the absence (◆) and presence of ChC4 (■), ChC6 (●), ChC8 (▲), ChC10 (▼) and ChC12 (★) in PBS solution at 37 °C.....	104
Figure 4.33:	The cumulative release of ACE in the absence (◆) and presence of ChC4 (■), ChC6 (●), ChC8 (▲), ChC10 (▼) and ChC12 (★) in PBS solution at 37 °C	107
Figure 4.34:	The cumulative release of CAF in the absence (◆) and presence of ChC4 (■), ChC6 (●), ChC8 (▲), ChC10 (▼) and ChC12 (★) in PBS solution at 37 °C.....	110

Figure 4.35:	The cumulative release of free SA (■), LID (●), ACE (▲) and CAF (▼) solution in PBS solution at 37 °C	114
Figure 4.36:	The cumulative release of SA (■), LID (●), ACE (▲) and CAF (▼) from ChC12 in PBS solution at 37 °C.....	115
Figure 4.37:	The cumulative release of SA in the absence (◆) and presence of ChC4 (■), ChC6 (●), ChC8 (▲), ChC10 (▼) and ChC12 (★) in SGF for the first 2 hours and in SIF for the subsequent hours at 37 °C	116
Figure 4.38:	The cumulative release of LID in the absence (◆) and presence of ChC4 (■), ChC6 (●), ChC8 (▲), ChC10 (▼) and ChC12 (★) in SGF at 37 °C	119
Figure 4.39:	The cumulative release of ACE in the absence (◆) and presence of ChC4 (■), ChC6 (●), ChC8 (▲), ChC10 (▼) and ChC12 (★) in SGF for the first 2 hours and in SIF for the subsequent hours at 37 °C	121
Figure 4.40:	The cumulative release of CAF in the absence (◆) and presence of ChC4 (■), ChC6 (●), ChC8 (▲), ChC10 (▼) and ChC12 (★) in SGF for the first 2 hours and in SIF for the subsequent hours at 37 °C	123
Figure 4.41:	The cumulative release of SA (■), LID (●), ACE (▲) and CAF (▼) from ChC12 in SGF for the first 2 hours and in SIF for the subsequent hours at 37 °C	126
Figure 4.42:	Schematic illustration of drug release from donor chamber to the receptor chamber of vertical Franz diffusion cells which includes polymer swelling and diffusion, where k_1 and k_2 are the rate constant of polymer swelling and drug diffusion across the membrane respectively, k_0 is the rate constant of unencapsulated drug from donor to the receptor chamber.....	127
Figure 4.43:	Schematic illustration of drug release from internal to the external of dialysis tubing which includes polymer swelling and diffusion, where k_1 and k_2 are the rate constant of polymer swelling and drug diffusion across the tubing respectively, k_0 is the rate constant of unencapsulated drug from internal to the external of the dialysis tubing.....	127

LIST OF TABLES

Table 2.1:	Modifications of chitosan for different applications.....	9
Table 2.2:	The potentials of LMWC in drug delivery.....	13
Table 2.3:	Hydrophobically modified chitosan (HMC) in drug delivery.....	15
Table 3.1:	Volume of NaNO ₂ solution used in the depolymerization of chitosan.....	33
Table 3.2:	The equations used in the kinetic models, where M_t , M_0 and M_∞ are the amount of drug release at time t , initial and infinite time respectively, k is the release constant, t is the time and n is the release exponent.....	52
Table 3.3:	The release mechanism describes by the n release exponent in Korsmeyer-Peppas model.....	52
Table 4.1:	Average molecular weight and water solubility of the depolymerized chitosan at addition of different volume of sodium nitrite.....	55
Table 4.2:	Assignment of protons of (a) Ch3, (b) ChC4, (c) ChC6, (d) ChC8, (e) ChC10 and (f) ChC12 in ¹ H NMR.....	59
Table 4.3:	Assignment of carbons of (a) Ch3, (b) ChC4, (c) ChC6, (d) ChC8, (e) ChC10 and (f) ChC12 in ¹³ C NMR.....	63
Table 4.4:	The weight loss with the respective maximum temperature of Ch3 and ChA during first, second and third stage of decomposition from 35 – 900 °C.....	69
Table 4.5:	(a) Amount of solvent need for the dissolution of 1 g of solute. (b) Chemical structure, molecular formula and weight and also solubility of salicylic acid (SA), lidocaine (LID), acetaminophen (ACE) and caffeine (CAF) which were used to be encapsulated by ChA.....	79
Table 4.6:	Comparison of particle size of ChA after loading with drugs by mean of DLS and TEM measurement.....	98
Table 4.7:	Curve fitting of SA to different release kinetics models for 24 hours. R^2 is the coefficient correlation, k is constant (slope) and n is the exponent of Korsmeyer-Peppas model.....	101

Table 4.8:	Curve fitting of SA to different release kinetic models for 12 hours. R^2 is the coefficient correlation, k is constant (slope) and n is the exponent of Korsmeyer-Peppas model.....	102
Table 4.9:	Curve fitting of SA at different release period to Korsmeyer-Peppas model. R^2 is the coefficient correlation, k is constant (slope) and n is the release exponent.....	103
Table 4.10:	Curve fitting of LID release to different release kinetic models for 12 – 16 hours. R^2 is the coefficient correlation, k is constant (slope) and n is the exponent of Korsmeyer-Peppas model.....	105
Table 4.11:	Curve fitting of LID at different release period to Korsmeyer-Peppas model. R^2 is the coefficient correlation, k is constant (slope) and n is the release exponent.....	106
Table 4.12:	Curve fitting of ACE to different release kinetic models for 24 hours. R^2 is the coefficient correlation, k is constant (slope) and n is the exponent of Korsmeyer- Peppas model.....	108
Table 4.13:	Curve fitting of ACE to different release kinetic models for 12 hours. R^2 is the coefficient correlation, k is constant (slope) and n is the exponent of Korsmeyer- Peppas model.....	109
Table 4.14:	Curve fitting of ACE at different release period to Korsmeyer-Peppas model. R^2 is the coefficient correlation, k is constant (slope) and n is the release exponent.....	109
Table 4.15:	Curve fitting of CAF to different release kinetic models for 24 hours. R^2 is the coefficient correlation, k is constant (slope) and n is the exponent of Korsmeyer- Peppas model.....	111
Table 4.16:	Curve fitting of CAF to different release kinetic models for 12 hours. R^2 is the coefficient correlation, k is constant (slope) and n is the exponent of Korsmeyer- Peppas model.....	112
Table 4.17:	Curve fitting of CAF at different release period to Korsmeyer-Peppas model. R^2 is the coefficient correlation, k is constant (slope) and n is the release exponent.....	113
Table 4.18:	Curve fitting of release of SA to different release kinetic models for the first 120 minutes. R^2 is the coefficient correlation, k is constant (slope) and n is the exponent of Korsmeyer-Peppas model.....	117

Table 4.19: Curve fitting of release of SA to different release kinetic models for the first 60 minutes. R^2 is the coefficient correlation, k is constant (slope) and n is the exponent of Korsmeier-Peppas model.....	118
Table 4.20: Curve fitting of release of LID to different release kinetic models for the first 50 – 80 minutes. R^2 is the coefficient correlation, k is constant (slope) and n is the exponent of Korsmeier-Peppas model.....	120
Table 4.21: Curve fitting of release of ACE to different release kinetic models for the first 120 minutes. R^2 is the coefficient correlation, k is constant (slope) and n is the exponent of Korsmeier-Peppas model.....	122
Table 4.22: Curve fitting of release of ACE to different release kinetic models for the first 60 minutes. R^2 is the coefficient correlation, k is constant (slope) and n is the exponent of Korsmeier-Peppas model.....	122
Table 4.23: Curve fitting of release of CAF to different release kinetic models for the first 120 minutes. R^2 is the coefficient correlation, k is constant (slope) and n is the exponent of Korsmeier-Peppas model.....	124
Table 4.24: Curve fitting of release of CAF to different release kinetic models for the first 60 minutes. R^2 is the coefficient correlation, k is constant (slope) and n is the exponent of Korsmeier- Peppas model.....	125

LIST OF SYMBOLS AND ABBREVIATIONS

α	alpha
β	beta
ACE	Acetaminophen
CAF	Caffeine
^{13}C NMR	^{13}C Carbon nuclear magnetic resonance
CAC	Critical aggregation concentration
Ch1	Chitosan with average molecular weight of 5 kDa
Ch2	Chitosan with average molecular weight of 10 kDa
Ch3	Chitosan with average molecular weight of 25 kDa
Ch4	Chitosan with average molecular weight of 50 kDa
ChA	Acylated low molecular weight chitosan
ChC4	Butyryl low molecular weight chitosan
ChC6	Hexanoyl low molecular weight chitosan
ChC8	Octanoyl low molecular weight chitosan
ChC10	Decanoyl low molecular weight chitosan
ChC12	Lauroyl low molecular weight chitosan
cm^{-1}	Reciprocal centimeters (wavenumber)
COX	Cyclooxygenase
$^{\circ}\text{C}$	Degree celsius
$^{\circ}$	Degree
<i>D</i>	From Latin <i>Dexter</i> meaning "right"
DA	Degree of acylation
DL	Drug loading
DLS	Dynamic light scattering
DNA	Deoxyribonucleic acid
DS	Degree of substitution
EE	Encapsulation efficiency
FE-SEM	Field-emission scanning electron microscopy
FTIR	Fourier transform infrared
g	gram
^1H NMR	^1H Proton nuclear magnetic resonance
HMC	Hydrophobically modified chitosan

HPLC	High performance liquid chromatography
ISI	Institute for Scientific Information
k	Rate constant
kDa	kilo Dalton
L	Litre
L	From Latin <i>Laevo</i> meaning "left"
LID	Lidocaine
LMWC	Low molecular weight chitosan
m	Number of <i>D</i> -glucosamine units
MHz	Megahertz
μm	micro-meter
mL	millilitre
mM	millimolar
mol dm^{-3}	moles per cubic decimetre
N	At the amino group of chitosan
n	Number of <i>N</i> -acetyl- <i>D</i> -glucosamine units; release exponent in Korsmeyer-Peppas model
O	At the hydroxyl group of chitosan
Ω	Ohm
PBS	Phosphate buffered saline (pH 7.4)
PEG	Polyethylene glycol
pH	Potential of hydrogen
R^2	Linear regression
SA	Salicylic acid
SGF	Simulated gastric fluid (pH 1.2)
SIF	Simulated intestinal fluid (pH 6.8)
SLS	Static light scattering
T	Absolute temperature
TEM	Transmission electron microscopy
UV-Vis	Ultraviolet-visible
w/v	Weight per volume
XRD	X-ray diffraction
Z	Atomic number

CHAPTER 1: INTRODUCTION

1.1 Drug delivery

Drug delivery is widely defined as the art of formulation and administration of a pharmacologically active compound in the body to achieve desirable therapeutic effects (Ahmed & Aljaeid, 2016; Tiwari et al., 2012). Before 1950, drug was formulated in pill or capsule form which was easily or immediately released upon contact with water at burst amount and caused some undesirable consequences which provoked evolution to develop controlled drug delivery systems to manipulate drug release (Park, 2014). The advancements of present technologies attributed to continuous efforts of the researchers greatly recurred the traditional practice to more effective systems by delivering drug utilizing colloidal particle size of less than 1000 nm (Levine, 2008). It is not surprising that different colloidal particulate systems such as liposomes, nanolipids, microemulsion, inorganic particles and polymeric particles are receiving increased attention and have been extensively investigated in drug delivery.

The advantages of using colloidal particles in drug delivery is their smaller dimension compared to micro-sized carriers which can penetrate deeper into cells and tissues for better cellular uptake and drug efficacy, as reported in the previous study where the uptake of nanoparticles at 100 nm was 2.5 and 6 fold higher as compared to 1 μ m and 10 μ m microparticles respectively in the CaCo-2 cell line (Desai et al., 1997). Colloidal particles also have the ability to provide better protection of the drug from degradation within the matrix or adsorption onto the surface and subsequently prolong the drug release which not only reduce the drug intake frequency, but also help to decrease the side effects or toxicity of the drugs for better patient compliance (Liu et al. 2008; Panyam & Labhasetwar, 2003).

1.2 Polymeric particles in drug delivery

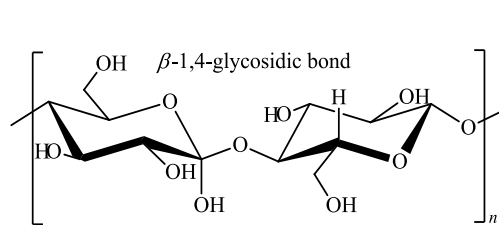
Polymeric particles are amongst prevalent colloidal particle systems drawing attention in healthcare related industries such as pharmaceuticals, cosmeceuticals and nutraceuticals (Nagavarma et al., 2012; Peer et al., 2007). Polymeric particles constructed from long chains of repeated monomers are not only able to load small molecule drugs but also bio-macromolecules such as nucleic acid and peptides by attaching, adsorbing, encapsulating or conjugating either onto the surface or within the matrix of the macromolecules (Jawahar & Meyyanathan, 2012; Singh & Lillard Jr., 2009). They possess the potential to co-deliver multiple drugs for synergistic effects as well (Zhang et al., 2007b). The merits of polymeric particles also included the flexibility of polymers for modifications to bring in different polymer derivatives for specific applications such as pH, temperature and light sensitive as well as active targeting delivery (Brewer et al., 2011; Liechty et al., 2010). Furthermore, polymer particles can also be easily fabricated at industrial scale at an effective cost by a multitude of methods and can be integrated with other modes of drug delivery for many potential medical applications, for instance biomedical engineering (Abhilash, 2010; Kayser et al., 2005).

The choice of polymeric particles as drug carriers is based on the biodegradability and biocompatibility of the polymers so that the polymer particles are safe and do not raise toxicity of the drug administered via topical, transdermal, oral, ocular, parenteral, nasal and even by intravenous routes (Liu et al., 2008; Panyam & Labhasetwar, 2003; Soppimath et al., 2001). Therefore, polymeric nanoparticles are preferably prepared from biocompatible and biodegradable natural polymers like polysaccharides and polypeptides or synthetic polymers such as polylactide (PLA), poly(lactide co-glycolic acid) (PLGA) and polycaprolactone (PCL) (Mora-Huertas et al., 2010).

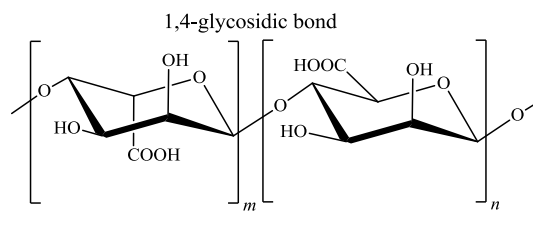
1.3 Polysaccharides in drug delivery

Polysaccharides are carbohydrates made up of a long chain of monosaccharide repeating units such as *D*-glucose, *D*-fructose, *D*-galactose, *D*-mannose, *D*-glucosamine, glucuronic and iduronic acids joined by glycosidic bonds (Sahoo et al., 2009). Polysaccharides are generally derived from natural resources including plants, microbial and animal origins as they are found abundantly as glycocalyx and extracellular matrices in biological systems for cellular adhesion, intercellular communication, lymphocyte-endothelium recognition, binding platform of pathogens, bacteria and virus and also control of cellular growth and differentiation (Sihorkar & Vyas, 2001; Abeygunawardana et al., 1991). This endows them the merits in terms of availability, safety and biocompatibility and thus propels the researches of drug carriers with polysaccharides based such as cellulose, starch, pullulan, dextran, alginate and chitosan (Figure 1.1) (Namazi, et al., 2012; Liu et al., 2008). In addition, polysaccharides have the tendency to be extremely bioactive and act as an excellent ‘biological response modifier’ with significant immunomodulatory activities (Ramesh & Tharanathan, 2003).

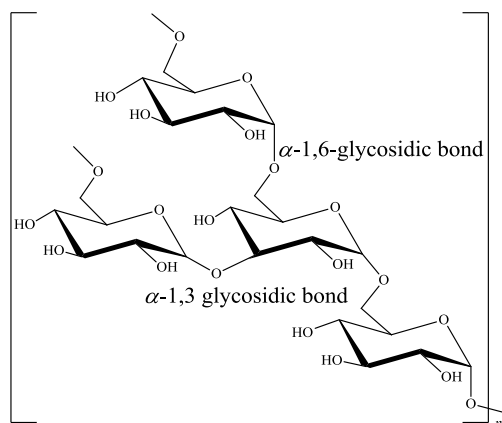
The presence of hydroxyl, carboxyl and amino groups on polysaccharides influence their charge in nature and categorized them as non-ionic (e.g. cellulose), cationic (e.g. chitosan) and anionic (e.g. alginate). In addition, the functional groups located on the polysaccharides backbone also offer room for reactions with other molecules. This also endows preparation of polysaccharides as particles can be accessed via different mechanisms, including self-assembly of hydrophobically modified polysaccharides, polyelectrolyte complexation, covalent and ionic crosslinking (Nitta & Numata, 2013; Janes et al., 2001).



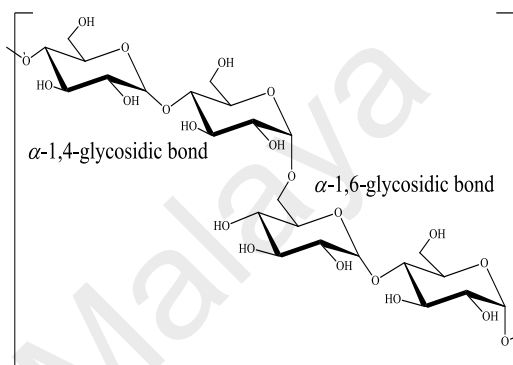
(a) Cellulose



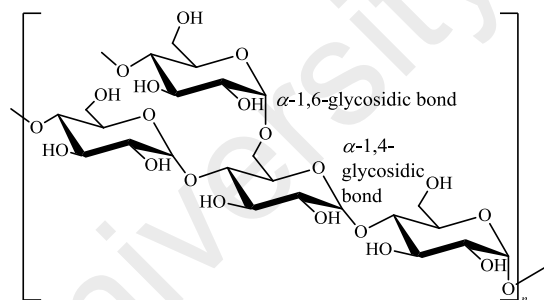
(b) Alginate



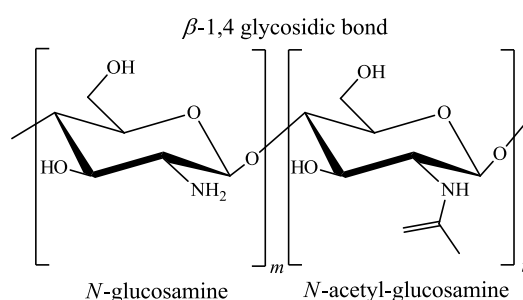
(c) Dextran



(d) Pullulan



(e) Starch



(f) Chitosan

Figure 1.1: Examples of polysaccharides: (a) cellulose, (b) alginate, (c) dextran, (d) pullulan, (e) starch and (f) chitosan, where m and n are the repeating units of the monomers.

1.4 Chitosan

Chitosan was first discovered as a water-soluble chitin compound by C. Rouget in 1859 while he was working on the chemical and thermal treatment of insoluble chitin which is the second most abundant resources worldwide after cellulose in the polysaccharides family. It was later named chitosan by F. Hopper-Seiler in 1894 (Tamura & Furuike, 2014; Novak et al., 2003; Rouget, 1859). Chitosan was left unattended at that time. Until the 1970s, chitosan became the subject of many researches and applications such as agriculture, textiles, construction, environmental protection and also bio-related fields including food, nutraceuticals, cosmeceuticals, pharmaceuticals, gene therapy, biomedicine and wound dressing as there was exploration of chitin as a renewable resources to solve the crustacean shells waste problems (Aranaz et al., 2009; Harish Prashanth & Tharanathan, 2007; Kumar, 2000). Chitosan comprised of random distribution of glucosamine at an extent of higher than 50% and *N*-acetyl glucosamine repeating units link by β -1,4-glycosidic bonds (Alves & Mano, 2008). Unlike the polysaccharides previously described, chitosan possesses amino groups in its molecular structure is cationic in nature.

Since chitosan is deacetylated from renewable and sustainable natural chitin such as the exoskeleton of crustaceans like crabs, shrimp, insects and cell walls of fungi and algae, and as such it is cost-effective. The biocompatibility, biodegradability, non-toxicity and low immunogenicity biological activities of chitosan (Sonia & Sharma, 2011; Senel & McClure, 2004) favored its versatile applications of drug delivery such as oral, ocular, parenteral and nasal (Tang et al., 2013; Bernkop-Schnurch & Dunnhaupt, 2012; Mourya & Inamdar, 2008).

1.4.1 Potentials of chitosan

Among the polysaccharides, chitosan was chosen as the subject of this study due to its abundance and excellent properties for drug delivery. The interest on the study of chitosan is gaining importance and developing tremendously, as can be reflected from the increasing number of Institute for Scientific Information (ISI) indexed publications on the research of chitosan from 1980 – 2017 which is presented in Figure 1.2.

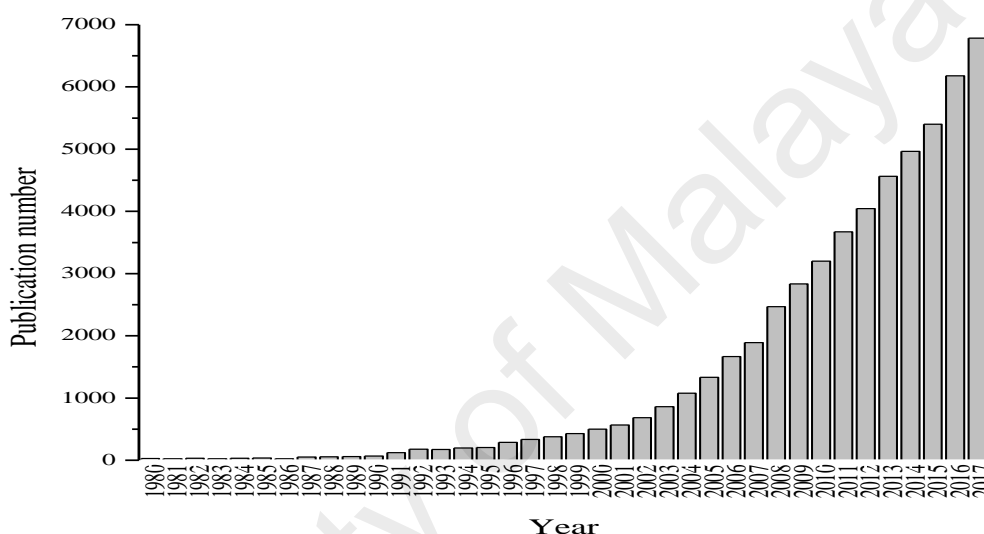


Figure 1.2: Publication number of Institute for Scientific Information (ISI) indexed publications on research of chitosan from 1980 – 2017.

Chitosan has been reported as being employed extensively for drug encapsulation (Prabaharan, 2015; Garcia-Fuentes & Alonso, 2012; Patel et al., 2010) and as carriers in the form of film, matrix, hydrogel, microgel, stent and graft (Chen et al., 2011a; Sahoo et al., 2009; Alves & Mano, 2008) as chitosan-based system have been described to have the unique polymeric character of gel forming properties and controlled delivery (Prabaharan & Mano, 2004; Hejazi & Amiji, 2003).

In addition, chitosan also exhibits desirable properties for topical delivery such as antibacterial, antioxidant, antifungal, antiviral, hemostasis and epidermal cell growth promotion (Ing et al., 2012; Yen et al., 2008; Tsai et al., 2002; Howling et al., 2001). Its

mucoadhesive property is attributed to the ability of its cationic amino groups to enhance cellular permeability and absorption in the gastrointestinal tract. This credits it as a popular material used in oral dosage formulation (Bowman & Leong, 2006; Hejazi & Amiji, 2003). Due to the versatile state of chitosan, it has been used for drug delivery in the macroscopic forms such as gel, beads, film, membrane and hydrogel, as well as micro- or nanosized carriers in the form of a microsphere, nanoparticle, nanosphere, nanocapsule, micelle and dendrimers (Duttagupta et al., 2015; Patel et al., 2010; Agnihotri et al., 2004).

1.4.2 Limitations of chitosan

Despite the promising advantages of chitosan, its application was limited by its insolubility in neutral aqueous media (Sinha et al., 2004; Singla & Chawla, 2001). Since the pKa of amino groups is 6.5, chitosan was only soluble in acid after the protonation of its amino groups into the NH_3^+ form as the electrostatic repulsion extends its chains. Above pH 6.5, deprotonation of chitosan occurs and causes aggregation and precipitation in the aqueous media which disfavored its utilisation onto humans.

In order to circumvent this limitation, the modifications of the chitosan were carried out to improve its properties and develop it as a drug carrier. In this study, the commercial chitosan was depolymerized into low molecular weight chitosan (25 kDa) for better solubility and acylated with short butyryl and hexanoyl groups and medium chain of alkyl groups included octanoyl, decanoyl and lauryl groups. The acylation on low molecular weight chitosan was confirmed via FTIR and NMR analyses. Physicochemical properties of acylated low molecular weight chitosan (ChA) such as particle size, zeta potential, structure crystallinity, water solubility, critical aggregation concentration (CAC),

kinematic viscosity and swelling were studied. The morphologies of ChA were observed by transmission electron microscope (TEM) and field-emission scanning electron microscope (FE-SEM). ChA was employed to encapsulate four types of analgesic drugs with different solubilities such as salicylic acid (SA), lidocaine (LID), acetaminophen (ACE) and caffeine (CAF). The interaction of ChA and drugs was investigated by FTIR analysis, whereas the particle size was obtained by dynamic light scattering (DLS) measurement and TEM microscopy. The *in vitro* drug release study was then carried out in phosphate buffered saline (PBS) pH 7.4 and simulated gastric fluid (SGF) pH1.2 to investigate the potential of ChA as drug carriers for topical and oral delivery.

1.5 Objectives

1. To prepare hydrophobically modified low molecular weight chitosan for drug delivery.
2. To characterize the physicochemical properties of the prepared hydrophobically modified low molecular weight chitosan.
3. To incorporate drugs into the hydrophobically modified low molecular weight chitosan.

CHAPTER 2: LITERATURE REVIEW

2.1 Modifications of chitosan

Since chitosan possesses good biological and biomedical properties, different modifications have been worked on the amino group at C2 of glucosamine subunits and hydroxyl groups at the C3 and C6 position of chitosan to manipulate or improve its properties for use in diversified applications (Table 2.1) (Mourya & Inamdar, 2008; Harish Prashanth & Tharanathan, 2007).

Table 2.1: Modifications of chitosan for different applications.

Modifications	Examples	Applications	References
Quaternization	<i>N, N, N</i> -trimethyl chitosan	Mucosal, drug, vaccine and gene delivery	(Verheul et al., 2008; Cano-Cebrian et al., 2005)
	<i>N-N</i> -propyl- <i>N,N</i> -dimethyl, <i>N</i> -furfuryl- <i>N,N</i> -dimethyl, C2,C6-trimethyl 6-amino-6-deoxy, C2,C6-triethyl 6-amino-6-deoxy chitosan	Antibacterial	(Sadeghi et al., 2008; Jia et al., 2001)
	<i>N</i> -alkylpyridinium chitosan salt	Antioxidant	(Li et al., 2017)
Alkylation	Butyl, octyl, dodecyl, hexadecyl chitosan	Gene Transfection	(Liu et al., 2003b)
	Isobutyl chitosan	Biomaterial	(Li et al., 2007a)
	<i>N</i> -dodecylated chitosan	Gene delivery	(Liu et al., 2001)
Hydroxyalkylation	Hydroxypropyl chitosan	Antifungal	(Peng et al., 2005)
	Hydroxybutyl chitosan	Temperature-responsive injectable carrier	(Dang et al., 2006)
	Ethylamine hydroxyethyl chitosan	Antibacterial	(Xie et al., 2007)
Carboxyalkylation	Carboxymethyl chitosan	Antimicrobial	(Farg & Mohamed, 2013)

Table 2.1 (continued)

Carboxyalkylation	<i>O</i> -carboxymethyl chitosan	Delivery of curcumin to cancer cells	(Anitha et al., 2011)
	<i>N</i> -(2-carboxyethyl) chitosan	Antioxidant, antimutagenic	(Kogan et al., 2004)
Sugar-modification	Lactose-modified chitosan	Repair of articular cartilage	(Donati et al., 2005)
	Galactosylated chitosan	Extracellular matrix for hepatocytes attachment	(Park et al., 2003)
	<i>L</i> -fucose, <i>D</i> -fucose, <i>N</i> -acetyl- <i>D</i> -glucosamine, <i>D</i> -mannose, <i>D</i> -lactose modified chitosan	Stimulate polymorphonuclear leukocyte cells for wound healing	(Morimoto et al., 2001)
Cyclodextrin links	β -cyclodextrin grafted chitosan	Mucoadhesive	(Venter et al., 2006)
	Tosylated β -cyclodextrin grafted chitosan	<i>In vivo</i> slow release of $^{131}\text{I}_2$	(Chen & Wang, 2001)
	β -cyclodextrin citrate grafted chitosan	Antimicrobial	(El-Tahlawy et al., 2006)
Thiolation	6-mercaptonicotinamide (6-MNA), 6,6'-dithionicotinamide (6,6-DTNA) thiolated chitosan conjugates	Controlled release of peptide	(Hauptstein et al., 2015)
	Chitosan-thioglycolic acid conjugates	Mucoadhesive	(Kast & Bernkop-Schnurch, 2001)
	Thiolated chitosan/DNA complex	Efficient and sustained gene delivery	(Lee et al., 2007)
Sulfation	Polysulphate chitosan	Anticoagulant	(Drozd et al., 2001)
	2-(4-acetamido-2 sulfanilamide), 2-(4-acetamido-2 sulfanilamide)-6-sulfo-chitosan	Antioxidant	(Zhong et al., 2007)
	<i>N</i> -octyl- <i>O</i> -sulfate chitosan	Delivery of taxol	(Zhang et al., 2003a)
Phosphorylation	Phosphorylated chitosan gel beads	Controlled release of ibuprofen	(Win et al., 2003)
	Phosphorylcholine modified chitosan	Hemocompatibility	(Meng et al., 2007)
	Phosphorylated chitosan membranes	Osteoconduction	(Amaral et al., 2005)

Table 2.1 (continued)

Thiourea modification	Thiourea chitosan–Ag ⁺ complex	Antibacterial, antifungal	(Chen et al., 2005)
	Acetyl, chloracetyl, benzoyl thiourea chitosan	Antifungal	(Zhong et al., 2008)
Graft copolymerization	PLA grafted chitosan	Cell biocompatibility	(Cai et al., 2002)
	Polyurethane grafted chitosan	Controlled and sustained drug release	(Mahanta et al., 2015)
	Carbon nanotubes grafted chitosan	Bone tissue engineering	(Carson et al., 2010)
Acylation	Urocanic acid acylated chitosan	Gene delivery	(Kim et al., 2003)
	Decanoyl, cinnamoyl, <i>p</i> -methoxybenzoyl, benzoyl, lauroyl, methoxy acetyl, methacryloyl, decanoyl chitosan	Antifungal	(Badawy et al., 2004)

2.1.1 Depolymerization

The attempts to enhance the solubility of chitosan in water include modification to water soluble derivatives and depolymerization to lower molecular weight. Chitosan can be modified to water-soluble derivatives via quaternization (methylation) as the cationic charge bearing on the quaternary chitosan derivatives facilitates its solubility over a wide range of pH. Quaternized chitosan not only exhibited higher aqueous solubility, but also demonstrated enhanced absorption to proteins and drugs such as busserelin, octreotide acetate, 9-desglycinamide-8-arginine vasopressin and fluorescein-isothiocyanate dextran (MW4400), as well as better mucoadhesive properties. This is due to the cationic charge of the derivatives promoting the interaction with the negatively charged mucin (Amidi et al., 2006; Cano-Cebrian et al., 2005; Xu et al., 2003).

Depolymerization of chitosan can be carried out by means of chemical, physical and enzymatic methods. Chemical treatment with acidic hydrolysis such as hydrochloric acid, working together with traditional heating caused some problems such as being not

specific, high cost, low product yield and possible residual acidity (Einbu et al., 2007; Kim & Rajapakse, 2005). These problems were improved by shortening the reaction time. The alternative deamination which uses nitrous acid was selective, rapid and easily controlled utilizing the stoichiometry on products as the nitrosating species from the nitrous acid only react on the glucosamine moieties without affecting the *N*-acetyl glucosamine subunits of chitosan (Allan & Peyron, 1995). Other chemicals like hydrogen peroxide (Lin et al., 2010; Tian et al., 2003), hot phosphoric acid (Hasegawa et al., 1993) and anhydrous hydrogen fluoride (Bosso et al., 1986) were also reported for the preparation of chitosan oligosaccharides as well.

Depolymerization via physical ways was employed using electromagnetic radiation (Hai et al., 2003), sonication (Liu et al., 2007b) and microwave technology with the aid of salts (Yin et al., 2009). For enzymatic depolymerization, several kinds of hydrolases including lysozyme, pectinase, cellulose, hemicellulose, lipases, amylases, papain and pronase showed the potentials as depolymerizing agents besides chitosanases and chitinases (Mourya & Inamdar, 2008).

2.1.1.1 Low molecular weight chitosan (LMWC)

Low molecular weight chitosan (LMWC) can provide better water solubility and can also biodegrade into oligosaccharides via enzymatic activities, which enables easier excretion from the body during physiological metabolism cycles. These are important parameters for safe *in vitro* and *in vivo* applications on humans. As compared to low molecular weight chitosan (less than 150 kDa), medium molecular weight chitosan (150 – 700 kDa) (Munmaya, 2015) are preferable as a drug carrier because preparation of low molecular weight chitosan involves laborious cost and time. Despite this, LMWC have been demonstrated to have better biological activities such as lower toxicity (Carreno-

Gomez & Duncan, 1997), higher antioxidant (Feng et al., 2008), being antimicrobial towards gram-negative bacteria (Fernandes et al., 2008; Zheng & Zhu, 2003) and having enhanced antitumor activity (Maeda & Kimura, 2004) compared to medium molecular weight chitosan. Previous studies on the potentials of LMWC in drug delivery were summarized in Table 2.2.

Table 2.2: The potentials of LMWC in drug delivery.

LMWC (kDa)	Study outcomes	References
1.3, 6, 13, 18, and 30 kDa	Oral delivery of insulin	(Al-Kurdi et al., 2015)
1–3 and 3–5 kDa	Antimutagenic	(Nam et al., 2001)
3–5 kDa	Combated 2,3,7,8-tetrachlorodibenzo- <i>p</i> -dioxin-induced pathogenesis	(Shon et al., 2002)
5–9.16 kDa	Antibacterial	(Liu et al., 2000)
<5 and 5–10 kDa	Decreased the growth of bifidobacteria	(Simunek et al., 2010)
20 and 5–50 kDa	Hyperglycemia, hyperinsulinemia and hypertriglyceridemia of diabetes mellitus	(Hayashi & Ito, 2002; Ikeda et al., 1993; Kondo et al., 2000)
25–50 kDa	Gastric cytoprotective and ulcer healing promotion	(Ito et al., 2000)
Chitosan oligomers	Stimulated murine peritoneal macrophage, antitumor, biocompatible, strong physiological activities in functional foods	(Jeon et al., 2000; Lim et al., 2007; Seo et al., 2000)
Trimethylated LMWC	Gene delivery vectors, decreased transepithelial electrical resistance (TEER) of tracheal epithelial cell monolayers	(Jonker-Venter et al., 2006; Thanou et al., 2002; Zheng et al., 2007)
<i>N</i> -2-hydroxypropyl trimethyl LMWC	Antioxidant	(Xing et al., 2008)
<i>N</i> -trimethyl chitosan (143–166 kDa), dicarboxymethyl LMWC (13.5 kDa), chitosan lactate oligomer (4 kDa)	Reduced TEER and enhanced transport of macromolecular compound across intestinal epithelial cell layer	(Enslin et al., 2008)

Table 2.2 (continued)

6–7 kDa LMWC modified with amino, carboxyl and sulfate groups	Anticancer	(Huang et al., 2006)
Sulfated LMWC (3–5 kDa)	Anticoagulant, anti-HIV-1	(Artan et al., 2010; Park et al., 2004)
5 kDa LMWC grafted with <i>N</i> -carboxymethyl group	Antioxidant	(Sun et al., 2008)
<i>N</i> -octyl- <i>N,O</i> carboxymethyl LMWC	Delivery of paclitaxel	(Zhang et al., 2009)
5 kDa LMWC grafted with oleic acid	Antibacterial, biocompatible antitumor drug carrier	(Huang et al., 2009; Zhang et al., 2012)
LMWC modified with doxorubicin and stearic acid	Antitumor	(Hu et al., 2009)
45 kDa LMWC grafted with linoleic acid	Delivery of doxorubicin	(Du et al., 2009)
18 and 28 kDa LMWC grafted with salicylic acid	Delivery of paclitaxel	(Wei et al., 2010)
3 kDa LMWC conjugated with all- <i>trans</i> -retinoic acid	Co-delivery of all- <i>trans</i> -retinoic acid and paclitaxel	(Zhang et al., 2015)
LMWC (4.6 kDa) and <i>N</i> -2(3)-(dodec-2-enyl) succinoyl-LMWC (5 kDa)	Nonviral vector, low cytotoxicity, good efficient transfection, antibacterial and antifungal	(Tikhonov et al., 2006; Zhang et al., 2008)
7.31 kDa LMWC <i>N</i> -acylated with maleoyl and succinyl groups	Antioxidant	(Sun et al., 2011)
18 kDa LMWC modified with ethoxy polyethylene glycol and cholesterol	Antitumor	(Jang et al., 2010)
Glycosylated chitosan oligomers	Higher gene transfer efficacy, lower cytotoxicity and improved serum compatibility	(Strand et al., 2008)
4 kDa LMWC grafted with pluronic copolymers	Temperature and pH responsive for release of doxorubicin	(Yang et al., 2010)
5 kDa LMWC grafted with stearic acid and PLGA	Enhanced solubility of 10-hydroxycamptothecin and antitumor	(Zhou et al., 2010b)

Table 2.2 (continued)

Hydrogel mixed with polyallylamine, oligochitosan, glycol chitosan and dextran	Promoted clotting <i>in vitro</i>	(Peng & Shek, 2009)
--	-----------------------------------	---------------------

2.1.2 Hydrophobic modifications

The introduction of hydrophobic alkyl groups onto the chitosan backbone can produce amphiphilic chitosan which can self-aggregate into a hydrophobic core in the physiological aqueous environment to minimize the interfacial energy with water. The hydrophobic core can serve as a nanocarrier of low water soluble drugs and protect them from easily leaking to the surrounding environment, hence prolonging drug sustainability and also to enhance drug efficacy in the body. Previous studies showed that the hydrophobically modified chitosan (HMC) such as cholesterol, glycol, tocopherol, galactosylated *O*-carboxymethyl grafting with stearic acid, *N*-octyl-*O*-sulfate-modified are among the potential carriers to deliver drugs, vitamins, steroids and proteins for sustainable release purposes (Table 2.3) as they are stable at very low concentration due to their low critical aggregation concentration (CAC) which prolong the circulation time within the body (Zhang et al., 2013a; Moazeni et al., 2012; Liu et al., 2008).

Table 2.3: Hydrophobically modified chitosan (HMC) in drug delivery.

Modified chitosans	Drugs	Purposes	Reference
Cholesterol modified chitosan	Epirubicin, bovine serum albumin, all- <i>trans</i> retinoic acid	Drug delivery, sustained release	(Li et al., 2012; Chen et al., 2011b; Wang et al., 2007)
Cholesteryl chloroformate chitosan	Deoxyribonucleic acid (DNA)	Gene delivery	(Son et al., 2004)
<i>N</i> , <i>O</i> 6-steroid-, tocopheryl-modified chitosan	Steroids, vitamin E	Sustained release	(Quinones et al., 2013)
Glycyrrhetic acid, cholic acid, stearic acid, lauric aldehyde modified sulphate chitosan	Doxorubicin	Liver-targeted delivery	(Wang et al., 2012)

Table 2.3 (continued)

Deoxycholic acid modified chitosan	Plasmid DNA, adriamycin	Gene delivery	(Bae, et al., 2005; Kim et al., 2001; Lee et al., 1998)
Deoxycholic acid modified carboxymethyl chitosan	Doxorubicin	Cancer therapy	(Jin et al., 2012)
Deoxycholic acid glycidol chitosan	Doxorubicin	Cancer therapy	(Zhou et al., 2010a)
<i>N</i> -deoxycholic acid- <i>N,O</i> -hydroxyethyl chitosan	Paclitaxel	Oral delivery of poorly water-soluble drugs	(Li et al., 2010)
5 β -cholanic acid glycol chitosan	Camptothecin, docetaxel, paclitaxel, DNA	Anticancer drugs and gene delivery	(Hwang et al., 2008; Min et al., 2008; Kim et al., 2006b; Yoo et al., 2005)
Bile acid modified glycol chitosans	Peptide, doxorubicin	Cancer therapy	(Kim et al., 2005)
<i>N</i> -octyl- <i>O</i> -glycol chitosan	Paclitaxel	Injectable delivery of paclitaxel	(Huo et al., 2010)
Quaternary ammonium palmitoyl glycol chitosan	Griseofulvin, cyclosporin A, ranitidine	Enhances oral absorption of hydrophobic and hydrophilic drugs	(Siew et al., 2012)
Phytosterol-fructose modified chitosan	Doxorubicin	Targeted delivery of anticancer drugs	(Qiu et al., 2013)
<i>N</i> -acetyl histidine and arginine grafted chitosan	Doxorubicin	Anticancer drug delivery	(Raja et al., 2017)
Stearic acid grafted galactosylated <i>O</i> -carboxymethyl chitosan	Doxorubicin	Chemotherapy	(Guo et al., 2013)
<i>N</i> -octyl- <i>N</i> -trimethyl chitosan	10-hydroxycamptothecin	Chemotherapy	(Zhang et al., 2007a)
<i>N</i> -octyl- <i>O</i> -sulfate chitosan	Paclitaxel	Nanocarrier of poor water soluble drugs	(Mo et al., 2011; Zhang et al., 2008; C. Zhang et al., 2004)
<i>N</i> -octyl- <i>N,O</i> -carboxymethyl chitosan	Paclitaxel	Anticancer delivery	(Zhang et al., 2009)

Table 2.3 (continued)

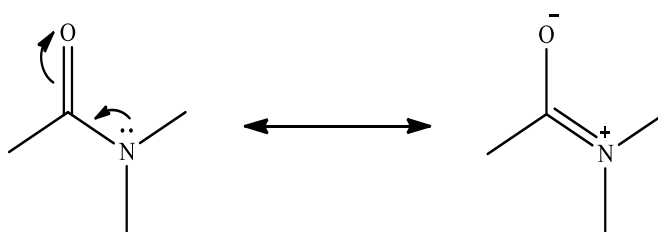
<i>N</i> -succinyl- <i>N</i> -octyl chitosan	Doxorubicin	Sustained release	(Xiangyang et al., 2007)
PEG conjugated <i>N</i> -octyl- <i>O</i> -sulfate chitosan	Paclitaxel	Chemotherapy	(Qu et al., 2009)
<i>N</i> -octyl/decyl/lauryl- <i>O</i> -sulfate chitosan	Taxol	Carrier of taxol	(Zhang et al., 2003a)
Butylated, octylated, dodecylated, hexadecylated chitosan	Vitamin B2, DNA	Vitamin B2 and gene delivery	(Liu et al, 2003a; Liu et al., 2003b)
Carboxymethyl hexanoyl chitosan	Doxorubicin	Sustained release	(Liu et al., 2006)
(3-aminopropyl) triethoxysilane modified carboxymethyl-hexanoyl chitosan	(<i>S</i>)-(+)-camptothecin	Controlled encapsulation and release	(Hsiao et al., 2012)
Propionyl, hexanoyl, nonanoyl, lauroyl, pentadecanoyl, stearyl chitosan	Bovine serum albumin, vitamin C	Drug and protein delivery, controlled release	(Cho et al., 2012a & 2012b)
Lauroyl chitosan	Naltrexone	Sustained delivery	(Calejo et al., 2014)
Lauroyl sulphated chitosan	Curcumin, insulin	Delivery of curcumin and insulin	(Shelma & Sharma, 2011b; Shelma et al., 2010)
<i>N</i> -lauryl-carboxymethyl-chitosan	Taxol	Delivery of taxol	(Miwa et al., 1998)
Lauric acid- <i>O</i> -carboxymethyl-transferrin chitosan	Paclitaxel	Sustained release and site-specific targeted delivery	(Nam et al., 2013)
Stearic acid grafted chitosan oligosaccharide	Doxorubicin, paclitaxel	Suppressed tumor growth, reduced toxicity, controlled release	(Hu et al., 2009; Hu et al, 2006)
Stearate grafted chitosan oligosaccharides	Paclitaxel	Cytoplasm targeting delivery	(You et al., 2007)

Table 2.3 (continued)

Stearyl chitosan, sulfated stearyl chitosan	Atorvastatin	Sustained release	(Mekhail et al., 2012)
<i>N</i> -palmitoyl chitosan	Ibuprofen	Drug carrier	(Jiang et al., 2006a)
Oleoyl carboxymethyl chitosan	Bacterial antigen	Carriers for oral administration of protein	(Liu et al., 2012)
Linoleic acid modified chitosan	Retinal acetate, doxorubicin	Encapsulation, sustained release	(Du, 2009; Chen et al., 2003)
Linoleic acid and poly (β -malic acid) grafted chitosan	Paclitaxel	Intravenous administration	(Zhao et al., 2009)
Linoleic acid modified carboxymethyl chitosan	Adriamycin	<i>In vitro</i> cancer	(Tan & Liu, 2009; Liu et al., 2007a)

2.1.2.1 Acylation

Among the hydrophobic modifications of chitosan, acylation is an interesting area of development due to the blood compatibility and biodegradability of acylated chitosan, which can be applied onto human by different routes even intravenously (Hirano et al., 1989; Hirano et al., 1976). Moreover, the amide obtained from the acylation also revealed higher stability compared to an acyl carbonyl due to the lone pair electrons on nitrogen being able to achieve stabilization via resonance of the carbonyl π system (Figure 2.1) (Shelma & Sharma, 2010a).

**Figure 2.1:** Resonance localization of amide via carbonyl π system.

Acylation can be carried out using acyl chlorides or anhydrides in aqueous acetic acid/methanol, pyridine, pyridine/chloroform, trichloroacetic acid/dichloroethane, ethanol/methanol, methanol/formamide and dimethylacetamide-lithium chloride (Shigemasa et al., 1999), however acyl anhydrides are more advantageous for reactions in protic solvents compared to acyl chlorides (Keisuke et al., 1988). The nucleophilic lone pairs on the amino and hydroxyl groups of chitosan were accessible to undergo acylation to form amide or ester, however acylation is more favorable at the amino groups due to its higher nucleophilicity. Reaction reagent and condition are very important to yield *N*-acyl (amide), *O*-acyl (ester) or both products (Shelma & Sharma, 2010a; Vasnev et al., 2006).

Products of acylation can be varied by using different acylating reagents. Acylation can be done by using chlorides and anhydrides, either in aliphatic saturated (C₂-C₁₈) or unsaturated derivatives (oleic, linoleic, linolenic, elaidic) and also in aromatic acyl forms such as benzoyl, *N*-benzylidene, phthaloyl and cinnamoyl to attach the acyl substituents randomly on the chitosan backbone (Hirano et al., 2002; Hirano et al., 1981; Hirano et al., 1976). Acylation using cyclic acid anhydrides such as succinic, citraconic, glutaric and maleic acid involve ring opening, yielding carboxyacyl chitosan which is a water soluble chitosan below pH 4 and above pH 7. This is attributed to the existence of protonated NH_3^+ ion in acidic media and negatively charged COO^- ion in basic condition. However, insolubility of chitosan takes place between pH 4 and 7 as a consequence of the equivalence molarity of both these charged groups at isoelectric point. Hydroxyacyl chitosan is produced via acylation with lactone. Another way to obtain acyl chitosan homologs is to carry out thermal treatment on the acylammonium salts with monocarboxylic acids, such as formic, propionic and butyric acids (Toffey & Glasser, 2001).

Despite the higher priority of acylation on amino groups, *O*-acylation can be performed by utilizing methane sulfonic acid (MeSO₃H) as a solvent. This is due to the salt formation of MeSO₃H with the amino group of chitosan results in the acylation is site specific on hydroxyl group. *O*-acylation via protection of the amino group by phthaloylation has also been successfully done to yield chitosan ester (*O*-acyl products) (Zhang et al., 2003b).

2.1.2.2 Physicochemical properties of HMC

The physicochemical properties of chitosan are mainly influenced by their molecular weight, hydrophobicity (chain length) and degree of acetylation (Dash et al., 2011; Sonam et al., 2013). For HMC, critical aggregation concentration (CAC) is an important criterion for the evaluation of aggregates as it indicates the minimum concentration at which formation of aggregates from the HMC occurs. CAC considers the balance between the gain in the interaction of associating groups and losses of Coulomb energy and entropy exist in HMC (Philippova & Korchagina, 2012). Thereby, the CAC value can also predict their stability in media. Higher molecular weight chitosan presented higher CAC value compared to those of lower ones in previous studies as a consequence of high rigidity and steric hindrance from the entangled junctions of long and less flexible polymer chains (Li et al., 2007b; Amiji, 1995). Molecular weight shall decrease to a certain extent for the consideration of solubility, toxicity and biological activities (Tian et al., 2015; Muzzarelli & Muzzarelli, 2005; Carreno-Gomez & Duncan, 1997).

Hydrophobicity was indicated by the chain length of the hydrophobes attached, in which the hydrophobicity was in direct proportional relation with chain length. Previous studies on the alkyl chain modified low molecular weight chitosan were focused on long chain length (Table 2.3) as longer hydrocarbon groups contributed to stronger hydrophobic interaction between polymer chains and therefore facilitated the self-

aggregation of polymers. Previous studies revealed that the increase in chain length of HMC led to a decline in CAC as a consequence of the gain of hydrophobic groups and energy of association between the attracting groups of HMC (Korchagina & Philippova, 2010; Ortona et al., 2008; Rinaudo et al., 2005). In addition, the increase in hydrophobic groups also contributed to the stability and drug protection from the external environment (Yoshioka, et al., 1995).

Nevertheless, long chain hydrophobes restrict the degree of substitution (DS) on the chitosan backbone and solubility of HMC in water which may cause precipitation as the hydrophobes disfavor the formation of hydrogen bonding with the water. For instance, the HMC with short chain up to eight carbon atoms at low to moderate DS were soluble in water and only exhibited little or no solubility when DS was further increased, however there was no solubility found in HMC with longer chain length regardless of the DS (Shelma & Sharma, 2010b). Duhem et al. (2012) found that glycol chitosan modified with α -tocopherol succinate at DS of 20% form large aggregates at phosphate buffer pH 7, this was in contrast to that with a DS of 6% which formed nanosized self-aggregate particles. High DS can also lower CAC because the substitution of hydrophobes can reduce the electrostatic repulsion between protonated amino groups and loss from the translational entropy of counterions, hence inducing the formation of aggregation in chitosan (Li et al., 2007b; Kim et al., 2001; Philippova et al., 2001). Therefore, low DS could weaken the stability of the aggregates in aqueous solution (Li et al., 2006). The gain in energy of interaction from high DS can contribute to the efficiency of HMC as drug carriers by enhancing the drug loading of poorly water-soluble drugs such as atorvastatin and cyclosporine A (Mekhail et al., 2012; Chen et al., 2008).

2.2 Chitosan for drug delivery

HMC attached with linear aliphatic groups, including propionyl, hexanoyl, nonanoyl, lauroyl, pentadecanoyl, lauryl, stearoyl, palmitoyl, oleoyl and linoleoyl chitosans demonstrated potential as carriers of vitamins, proteins and drugs such as doxorubicin, palitaxel, camptothecin, naltrexone, curcumin, taxol, adriamycin, atorvastatin, retinal acetate and ibuprofen (Table 2.3).

2.2.1 Chitosan for topical delivery

Chitosan is a good material for use in topical formulation due to its promising antimicrobial, antifungal, film forming, adhesive and moisturizing merits. Owing to these benefits, chitosan is always applied as a hemostatic agent in the form of a powder, film, filament composite, coated filament, hydrogel or fibre to heal bleeding and burn wounds. Such popular commercial products are HemCon®, Chitoflex®, Chitoseal®, Celox® and Syvek-Patch® (Pogorielov & Sikora, 2015; Whang et al., 2005; M et al., 2016). As a hemostatic material, chitosan can control bleeding via the mechanism of plasma sorption, coagulation of erythrocytes and platelets adhesion which results in fast clot formation. Chitosan also activates inflammatory cells such as polymorphonuclear leukocytes, macrophages and fibroblasts which can promote granulation and organization of skin cells and assist in wound healing (Ueno et al., 2001).

Chitosan is prepared in different macroscopic forms to deliver drugs for topical applications. For instance, hydrocortisone (Meler et al., 2013), alpha-hydroxy acid (Ribeiro et al., 2013), ferulic acid (Tsai et al., 2016), dihydroxyacetone (DHA) or 3-hydroxy-4-trimethylammonium butyrate (*L*-carnitine) (Sole et al., 2017) and latanoprost contain hydrogel (Cheng et al., 2016), silver sulfadiazine fill composite sponge (Shao et al., 2017), Plai (herbs) patches (Suksaeree et al., 2014), levofloxacin (Siafaka et al., 2016),

ferulic acid and resveratrol fill chitosan-polycaprolactone nanofiber wound dressings (Poornima & Korrapati, 2017), salvianic acid A sodium (Zhang et al., 2013b), ibuprofen (Morgado et al., 2017), gentamicin (da Silva et al., 2016) and citronella oil contain membrane (Tang & Ge, 2015), 5-aminolevulinic acid (Costa et al., 2014), chlorhexidine contain chitosan/montmorillonite composite films (Ambrogi et al., 2017).

In addition, chitosan was also developed as micro- and nanoparticles in line to the development of present technology. This was also due to the bountiful advantages of chitosan particles in topical delivery, including prolonged release, better drug permeation across the skin, reduced skin irritation and enhanced bioavailability of low solubility drugs. When compared to the chitosan gel and commercial cream containing clobetasol-17-propionate, lecithin-chitosan nanoparticles loaded with drug demonstrated drug accumulation in the epidermis without any significant permeation across the skin. This was remarkably important to reduce side effect and enhance the risk-benefit ratio of corticosteroids (Senyigit et al., 2010).

The reported studies on the micro-scaled particles for topical delivery included olive leaf extract (Acosta et al., 2015), acyclovir (Calderon et al., 2013; Genta et al., 1997), calendula oil (Lam et al., 2012b), miconazole nitrate and clotrimazole (Yuen et al., 2012), hydrocortisone succinic acid and 5-fluorouracil (Lam et al., 2012a) and also protein (Wassmer et al., 2013). For targeting delivery, the microencapsulation of minoxidil sulphate working synergistically with iontophoresis exhibited better local topical drug targeting to the hair follicles (Gelfuso et al., 2015). Chitosan is also studied in nanoparticles for topical drug delivery, for instance loading with lutein (Chaiyasan et al., 2015), minoxidil sulphate (Matos et al., 2015), hydroxytyrosol and hydrocortisone (Siddique et al., 2015), naringenin (Zhang et al., 2016), dexamethasone (Abul Kalam,

2016a & 2016b), ketorolac tromethamine (Fathalla et al., 2016), moxifloxacin (Kaskoos, 2014), ketoconazole (Namburi et al., 2014), tretinoin and clindamycin (Thakur et al., 2013), acyclovir (Calderon et al., 2013; Hasanovic et al., 2009), quercetin (Tan et al., 2011) and retinol (Kim et al., 2006a). Furthermore, chitosan nanoparticles are utilized to load macromolecules for skin delivery, such as antisense oligonucleotide (Ozbas-Turan et al., 2010) and plasmid DNA (Ozbas-Turan & Akbuga, 2011).

Some studies applied modified chitosan as the carriers in topical applications, these included chitosan acetate bandage for wound healing and burn infections (Dai et al., 2009; Burkatovskaya et al., 2008), hypromellose grafted chitosan for delivery of tetracycline chloride, methylene blue, mometasone furoate and metronidazole (Lai & Shum, 2016), carboxymethyl and *N,O*-carboxymethyl chitosan as a carrier of cimetidine (Divney & Di Schiena, 2014a & 2014b) and also chitosan succinate to deliver chlorhexidine (Lapenko et al., 2013) respectively. For hydrophobically modified chitosan, delivery of brimonidine tartrate using hexanoyl glycol chitosan demonstrated prolonged retention on the precocular surface and improved drug availability and efficacy (Cho et al., 2016). The cholesterol modified chitosan was also able to enhance the therapeutic effects of cyclosporine A at extraocular level (Yuan et al., 2006). Polymeric micelles from oleic or linoleic acid are able to increase the solubility of poor soluble clarithromycin to treat chronic wounds and burns (Bonferoni et al., 2014).

2.2.2 Chitosan for oral delivery

Chitosan is commonly used for oral applications due to its mucoadhesive properties as its cationic charge can bind well to the negatively charged sulphonated groups of cell mucin to prolong the permeation time and hence enhance the absorption (Shelma & Sharma, 2010b). Furthermore, the antacid and antiulcer properties of chitosan are

advantageous to prevent or weaken drug irritation in the stomach and hence relieve stomach discomfort (Kumar, 2000). For oral delivery, chitosan with pH-responsive was preferable for controlled released and this can be achieved via modification with carboxyalkyl, succinate and phthalate groups as anionic carboxylic groups exist in the non-ionized form in gastric acidic condition and are low hydrophilic but are ionized in the intestinal alkaline environment to release drugs (Sonia & Sharma, 2011; Cui et al., 2009; Ubaidulla, et al., 2007).

The benefit of introducing hydrophobic groups on chitosan for oral administration is reduced hydration by the hydrophilic amino or hydroxyl groups which can provide higher resistance to gastric enzymatic degradation (Shi & Caldwell, 2000). Le Tien et al. (2003) prepared caproyl, octanoyl, myristoyl and palmitoyl chitosan for drug dissolution study and concluded that palmitoyl chitosan exhibited the most sustained release which was suitable for oral application. Chitosan modified with lauroyl domains revealed higher mucoadhesion property compared to hexanoyl and oleoyl groups and also sustained release of curcumin at pH 1.2 and 7.4 (Shelma & Sharma, 2010b). Higher resistance was shown by longer chain oleoyl chitosan compared to octanoyl chitosan towards enzymatic degradation which improved its mucoadhesive, intestinal uptake of insulin and permeability, making it a suitable carrier for oral peptide applications (Sonia et al., 2011).

Chitosan phthalate has been reported for its ability to protect insulin and diclofenac sodium from the gastric enzyme degradation and potential to act as a carrier for oral administration purpose (Ubaidulla et al., 2007; Aiedeh & Taha, 1999). It also showed better intestinal mucoadhesive property compared to the unmodified chitosan (Rekha & Sharma, 2008). This attributed to the ability of the hydrophobic groups to interact with the hydrophobic peptide backbone segments of mucin (Varum et al., 2008). Lauryl succinyl chitosan has also been developed for oral insulin delivery where the hydrophobic

lauryl and hydrophilic succinyl moieties improved the mucoadhesiveness of the jejunum of rat intestine and also the permeability of insulin. This occurred by loosening the tight junctions and also through controlling the release of insulin at pH 7.4 (Rekha & Sharma, 2009). Anacardoylated chitosan demonstrated the release of orally administered insulin in the intestinal environment while retaining its conformation (Shelma et al., 2010). Nanoparticles prepared from chitosan diacetate and triacetate exhibited the efficient encapsulation of doxorubicin can prolong the drug release, as well as enhancing tumor cellular uptake and oral bioavailability of doxorubicin (Khdair et al., 2016).

2.3 Analgesic drugs

Due to the frequent pain and aches and also discomfort arisen from some disease disorders, analgesic drugs are amongst the most commonly prescribed and are highly demanded drugs worldwide. The analgesic drugs can be categorized into (1) para-aminophenol derivatives such as acetaminophen, (2) non-steroidal anti-inflammatory drugs (NSAIDs; for instance, salicylates and other organic acids (e.g. ibuprofen and piroxicam), and (3) opiates such as codeine (Paulose-Ram et al., 2003). It is expected that sales of prescription and non-prescription non-steroidal anti-inflammatory drugs (NSAID) can reach \$18 billion in the global pharmaceutical market annually (Petkova et al., 2014). They are used to reduce or relieve pain without losing consciousness as they are not blocking the conduction of nerve impulses and are therefore generally known as painkillers. They can be administered via oral, rectal, local, sublingual, inhalation or injection routes. They are divided into non-opioid analgesic drugs (non-narcotic analgesics) such as aspirin, opioid analgesic drugs (narcotic analgesics) such as morphine and adjuvant analgesic drugs or co-analgesic drugs such as antiepileptic drugs (AEDs).

Analgesic drugs act on the peripheral or central nervous systems to exert effects. For non-opioid analgesic drugs, the action mechanism is mainly on the inhibition of the

cyclooxygenase (COX) enzymes consists of COX-1 and COX-2 to block the synthesis of prostaglandin (Terzi et al., 2017; Rao & Knaus, 2008). COX-1 exists in normal tissues and is responsible for the synthesis of prostaglandins which regulate physiological functions in the gut, platelets, kidneys and vascular endothelium, such as blood flow regulation to the gastric mucosa and kidneys, manipulation of gastrointestinal secretion and motility and protection of gastric mucosa (Dey et al., 2006; Griswold & Adams, 1996). Unlike COX-1, COX-2 only induces during inflammation primarily producing prostaglandins that activate and sensitize nociceptors (sensory receptor at the end of a sensory neuron's axon which send pain signals to the spinal cord and brain upon responding to damaging or potentially damaging stimuli). Non-opioid analgesic drugs relieve mild and moderate level of pain. Examples of non-opioid analgesic drugs are ibuprofen, diclofenac, aspirin and indomethacin (The National Pharmaceutical Council & Joint Commission Accreditation of Healthcare Organization, 2001).

Opioid analgesic drugs, such as codeine, meperidine, methadone and fentanyl work more efficiently than non-opioid analgesic drugs as they bind to opioid receptors in the form of agonists (activators) or antagonists (blockers) in the central nervous system to perform the analgesic mechanism. These mechanisms include inhibition of transmission of nociceptive input from the periphery to the spinal cord, activation of descending inhibitory pathways and control of activities of the limbic system (Hoskin & Hanks, 1991; Stein, 1995). As such, opioid analgesic drugs were employed in moderate to severe pain, for instance, postoperative and cancer pain.

Adjuvant analgesic drugs or co-analgesic drugs treat neuropathic pain, such as episodic shooting, stabbing or knife-like pain from peripheral nerve syndromes by reducing membrane excitability and suppressing abnormal discharges in pathologically

altered neurons. This is due to the interaction with sodium (Na) or calcium (Ca) channels, as well as gamma-aminobutyric acid A (GABAA) receptors (Nicholson, 2000; Macdonald & Kelly, 1994; Swerdlow & Cundill, 1981). The examples of such drugs are barbiturate, benzodiazepines, gabapentin and phenytoin.

2.3.1 Examples of analgesic drugs

2.3.1.1 Salicylic acid (SA)

SA in ancient times was used to heal a headache, fever and pain, however due to causing stomach irritation and its unpleasant taste, it was modified to acetylsalicylic acid (aspirin) to perform same treatment effects by Felix Hoffmann in 1889 (Reger et al., 2009). In the present time, it is more commonly used to treat skin conditions including seborrhoeic dermatitis, acne, psoriasis, calluses, keratosis pilaris and warts due to its anti-inflammatory property. Its keratolytic potential can denature and deform bacteria by interacting with the membrane protein (Madan & Levitt, 2014; Tiwari et al., 2009). It is widely used as an exfoliating ingredient in skin care products as it can remove dead skin cells while soothing the skin. Due to the properties of SA as a monohydroxybenzoic acid, its overuse can cause dryness, erythema and skin irritation (Fabbrocini et al., 2010; Bhalerao & Raje Harshal, 2003).

2.3.1.2 Lidocaine (LID)

LID is an amide analgesic available in topical gel, dermal patch, oral gel, intravenous injection and nasal spray. It can act within a short onset time to treat not only neuropathic pain, but also headache, renal colic pain, postherpetic neuralgia, post-stroke pain syndrome and shoulder dislocation by blocking both peripheral and central voltage-dependent sodium channels (Derry et al., 2014; Golzari et al, 2014; Soltani & Aghadavoudi, 2002). Adverse effects of LID can be observed via the central nervous and

cardiovascular system, including nervousness, drowsiness, hypotension and respiratory depression (Lev & Rosen, 1994) and also mild skin reaction if applied topically (Gammaitoni et al., 2003).

2.3.1.3 Acetaminophen (ACE)

ACE is also known as paracetamol with the most well-known commercial medicine known as Panadol. ACE is an aniline analgesic widely used to relieve fever, headache, mild to moderate pain, osteoarthritis and low back pain, sometimes in combination with opioids analgesics for the treatment of postoperative pain (Machado et al., 2015; Hyllested et al., 2002; Moore et al., 1997). The usage of ACE is required to be controlled as the overdose can lead to acetaminophen toxicity and cause fatal liver damage (Hawkins et al., 2007; Fowler, 1987).

2.4.1.4 Caffeine (CAF)

CAF is a purine which consists of pyrimidine and an imidazole ring. As it is legal and unregulated, it is the most popularly used adjuvant analgesic or psychoactive drug (alterations brain functions in perception, mood, consciousness and behavior) compared to cocaine, barbiturates and nicotine (Goldstein, 2001). For medical purpose, CAF is used in prevention and treatment of bronchopulmonary dysplasia in premature infants (Kugelman & Durand, 2011; Schmidt, 2005), apnea of prematurity (Mathew, 2011) and orthostatic hypotension treatment (Gupta & Lipsitz, 2007). As CAF can block the binding of adenosine to its receptor to prevent drowsiness and also stimulate the autonomic nervous system to be alert, it is highly demanded in food and beverages to improve reaction time and motor coordination (Nehlig, 2010; Snel & Lorist, 2011). In addition, CAF is growing in its application in cosmetic products as well attributed to its numerous potentials. Its lipolytic activity on fatty cells through inhibition of the phosphodiesterase

activity makes it suitable to be formulated in anti-cellulite products. It can also increase blood microcirculation of skin to promote cell growth, which is very advantageous for reduction of dark eye circles and better skin appearance. Furthermore, it also acts as an antioxidant to protect cells from UV radiation and hence slows down skin aging (Herman & Herman, 2013; Velasco et al., 2008). Despite the advantages of CAF, its overdosing can cause vasoconstriction, anxiety, insomnia, caffeine addiction and dependence (McLella et al., 2016; Leonard et al., 1987).

2.3.2 Chitosan for delivery of analgesic drugs

Even though analgesic drugs can relieve pain symptoms, their adverse effects or overdosing especially longer term complications such as drug dependence, immunosuppression and possible organ damage are worrying and deteriorating health quality. Chitosan have been reported in the form of particles either in microparticles to encapsulate paracetamol (Bulut, 2016), ketoprofen (El-Kamel et al., 2003), mefenamic acid (Nair et al., 2011), aceclofenac (Mothilal et al., 2012; Umadevi et al., 2010), diclofenac (El-Leithy et al., 2010) or nanoparticles to deliver aspirin (Ajun et al., 2009), lidocaine (Choochottiros et al., 2009), indomethacin (Badawi et al., 2008), meloxicam (Fattahpour et al., 2015), diclofenac (Teixeira et al., 2016; Goncalves et al., 2015), aceclofenac and diclofenac sodium (Narayanan et al., 2014).

Previous studies have reported the potential of amphiphilic chitosan as carriers of analgesic drugs such as ibuprofen by methoxy polyethylene glycolated chitosan (Hassani Najafabadi et al., 2014), methyl acrylate, ethylene sulphide and cysteamine modified chitosan (Vieira et al., 2013), deoxycholic acid and leucine modified chitosan (Marques et al., 2014), ketoprofen by beta-cyclodextrin grafted chitosan (Yuan et al., 2013), meloxicam by *N*-phthaloylchitosan grafted poly(*N*-vinylcaprolactam) (Wang et al., 2016) and indomethacin by polyacrylamide grafted chitosan (Kumbar et al., 2003). The ability

of amphiphilic chitosan to sustain drug release, increase drug bioavailability for enhanced cellular uptake and reduce adverse effects of the analgesic drugs, endow them as promising drug carriers.

University of Malaya

CHAPTER 3: MATERIALS AND METHODS

3.1 Materials

Chitosan with molecular weight range 100 – 300 kDa was supplied by Acros Organics (New Jersey, USA). Hexanoic anhydride, acetic acid, deuterium oxide, hydrochloric acid (HCl) (37%), methanol, acetone and salicylic acid were purchased from Merck (Darmstadt, Germany). Phosphotungstic acid (PTA), sodium nitrite (NaNO_2) and sodium phosphate dibasic dihydrate ($\text{HNa}_2\text{OP}\cdot 2\text{H}_2\text{O}$) were obtained from Fluka (St. Louis, MO, USA), whereas butyric anhydride, caffeine, acetaminophen, lidocaine ($\geq 98\%$), deuterated acid and phosphate buffered saline (PBS) tablets were purchased from Sigma-Aldrich (St. Louis, MO, USA). Octanoic, decanoic and lauric anhydride were supplied by TCI America (Portland, Oregon, USA). Sodium hydroxide (NaOH) and tetrahydrofuran (THF) were obtained from Friedemann Schmidt Chemicals (Parkwood, WA, Australia). Sodium chloride (NaCl) and sodium dihydrogen phosphate (NaH_2PO_4) were supplied by System Chemicals (Shah Alam, Selangor, Malaysia). All the chemicals and reagents were used as received without further purification. Deionized water with a resistivity of $18.2 \Omega \text{ cm}^{-1}$ which processed from a Barnstead DiamondTM RO unit and further purified by Barnstead Diamond Nanopure water purification unit (Barnstead International, Iowa, USA) was used to prepare the samples and solutions throughout the experiments.

3.2 Sample preparation

3.2.1 Preparation of depolymerized chitosan

The different molecular weights of chitosan were prepared through depolymerization of commercially purchased chitosan by sodium nitrite, with some modifications on the previous work (Tan & Misran, 2013). Firstly, the experiment was started with the dissolution of 1% (w/v) chitosan in 1% acetic acid solution under magnetic stirring.

Different volumes of 0.1 mol dm^{-3} NaNO_2 solution at 5, 7, 10 and 12 mL were added dropwise into separate chitosan solutions and stirred at room temperature for 1 hour. The chitosan solutions were then named accordingly as shown in Table 3.1. The mixture was adjusted to pH 8 – 9 with 0.5 mol dm^{-3} NaOH solution to precipitate the undissolved chitosan. After removing the undissolved chitosan by filtration, the filtrate was neutralized with 0.5 mol dm^{-3} HCl solution. The water soluble chitosan was then collected via centrifugation (will be discussed in section 3.3.2) after precipitating with the aid of acetone. The chitosan was later dried in a vacuum oven at $30 \text{ }^\circ\text{C}$ over silica gels.

Table 3.1: Volume of NaNO_2 solution used in the depolymerization of chitosan.

Name	Volume of NaNO_2 solution added (mL)
Ch1	12
Ch2	10
Ch3	7
Ch4	5

3.2.2 Preparation of *N*-acylated chitosan (ChA)

Five types of acylated chitosan with different chain lengths were prepared by acylation with butyric (C4), hexanoic (C6), octanoic (C8) and decanoic (C10), lauric (C12) anhydrides. Water soluble chitosan with an average molecular weight of 25 kDa, which was indicated as Ch3 in section 3.2.1, was dissolved in a 1:1 mixture of 1% acetic acid solution and methanol to yield 1% (w/v) of chitosan solution. The solution was adjusted to pH 7 with 1 mol dm^{-3} NaOH solution before the dropwise addition of different acid anhydrides into chitosan solution at mole ratio of 0.2, 0.4, 0.6, 0.8, 1.0 to the *N*-glucosamine unit of chitosan under magnetic stirring, respectively. The acylated chitosan were labelled as ChC4, ChC6, ChC8, ChC10 and ChC12 accordingly. In order to indicate the mole ratio of acid anhydrides added, the suffix M was added after the chitosan name. For example, ChC4-M.2 designated as alkyl chain with four carbon atoms acylated to Ch3 at 0.2 mole. ChC4, ChC6, ChC8 and ChC10 were prepared at room temperature,

whereas ChC12 was pre-dissolved in methanol at 50 °C prior to reaction in a water-jacketed glass reactor with water bath circulation at constant temperature of 50 °C. The reaction was left to stir overnight and then neutralized with 1 mol dm⁻³ NaOH solution. The acylated chitosan (ChA) were collected by precipitating with excess acetone followed by the centrifugation which will be discussed in section 3.3.2. The collected ChA were washed with excess methanol to remove any unreacted fatty acid and then placed in a vacuum oven dehumidified over silica gels for evaporation of solvent.

3.2.3 Preparation of analgesic drugs loaded ChA

Four types of analgesic drugs with different solubilities which were salicylic acid (SA), lidocaine (LID), acetaminophen (ACE) and caffeine (CAF) were selected to be incorporated into ChA at different weight ratio of ChA to drug (^{w/w}) via the precipitation method. Drug loaded ChA was prepared at 5 g L⁻¹. Firstly, ChA was dispersed in THF. Then, the drug which was pre-dissolved in THF as well was added to the ChA dispersion and left to stir for 1 hour. It was followed by the removal of THF by nitrogen purging in a Buchi-480 water bath (Buchi Labortechnik AG, Flawil, Switzerland) at 50 °C. Deionized water was then added into the remaining THF. Agitation of nitrogen steam was continued to evaporate THF.

3.2.4 Preparation of buffer solutions

Buffer solutions were used as the mobile phase in high pressure liquid chromatography (HPLC) in section 3.3.12 and as the media in *in vitro* drug release in section 3.4. The mobile phase used in HPLC analysis was 10 mM phosphate buffer pH 6 which was prepared from sodium dihydrogen phosphate (NaH₂PO₄) and sodium phosphate dibasic dihydrate (HNa₂OP.2H₂O) and followed by adjustment with 1 mol dm⁻³ NaOH solution to pH 6 before topping up to the mark of the volumetric flask.

The buffer solutions prepared were then filtered with 0.2 μm nylon filter membrane to filter off any specks of dusts or suspended particles.

For the media of *in vitro* release for topical delivery (section 3.4.1), a 10 mM phosphate buffered saline (PBS) solution was prepared from the dissolution of five PBS tablets in 1 L deionized water, whereas simulated gastric fluid (SGF) and simulated intestinal fluid (SIF) without enzyme for oral delivery (section 3.4.2) were prepared following United States Pharmacopeia XXIV (United States Pharmacopeia and National Formulary, 2000) with slight modification. SGF was prepared by dissolving 2.0 g NaCl in deionized water and the pH was adjusted to pH 1.2 with 1 mol dm⁻³ HCl solution before topping up to the curve of the 1 L volumetric flask. For the preparation of SIF, 5.7 g HNa₂OP.2H₂O was dissolved in deionized water before the pH was adjusted to 6.8 with 1 mol dm⁻³ NaOH solution. It was then topped up to 1 L volumetric flask to be 50 mM.

3.3 Equipments and instrumentation

3.3.1 pH measurement

All pH measurements were conducted using a Cyberscan 510 pH meter (Eutech Instruments Pte Ltd, Ayer Rajah Crescent, Singapore) calibrated with standard buffer solutions of pH 4.01, 7.00 and 10.01 \pm 0.02 at 25 °C.

3.3.2 Centrifugation

Depolymerized and acylated chitosan mentioned in section 3.2.1 and 3.2.2 were collected by centrifugation using Velocity 18R Refrigerated Centrifuge (Dynamica Scientific Ltd, Newport Pagnell, UK) equipped with a 6 \times 50mL capacity TA15-6-50 angle rotor. Depolymerized and acylated chitosan were centrifuged at 5,000 rpm and 10,000 rpm respectively for 3 minutes at 25 °C.

3.3.3 Determination of average molecular weight

The average molecular weight of the depolymerized chitosan was determined based on the Static Light Scattering (SLS) theory. The working principle of SLS is based on the time averaged intensity of scattered light instead of scattering intensity with time dependent fluctuations as time averaging measurement can remove the inherent fluctuations in the signal. SLS describes the light scattering intensity from a particle as a function of few concentrations of the samples using Rayleigh equation as shown below.

$$\frac{KC}{R_{\theta}} = \left(\frac{1}{M} + 2A_2C \right) P_{\theta} \quad \text{Eq. 3.1}$$

R_{θ} : Rayleigh ratio which is the ratio of scattered light to incident light of the sample.

M : Molecular weight of the sample.

A_2 : Second virial coefficient which describes the interaction between the particles and the solvent.

C : Concentration of the sample.

P_{θ} : Angular dependence of the sample scattering intensity.

K : Optical constant which can be calculated from the equation below:

$$K = \frac{2\pi^2}{\lambda_0^4 N_A} \left(n_0 \frac{dn}{dc} \right)^2 \quad \text{Eq. 3.2}$$

N_A : Avogadro's constant.

λ_0 : Laser wavelength.

n_0 : Solvent refractive index.

$\frac{dn}{dc}$: The differential refractive index increment obtained from the difference in refractive index as a function of the change in concentration of the samples.

By assuming the particles in the samples are much smaller than the wavelength of the incident light, multiple photon scattering attributed from Mie scattering can be excluded. Since there is no angular dependence in the scattering intensity, P_θ is reduced to 1 and the Rayleigh equation can be rewritten to

$$\frac{KC}{R_\theta} = \left(\frac{1}{M} + 2A_2C \right) \quad \text{Eq. 3.3}$$

Rayleigh ratio (R_θ) of the sample in the equation 3.3 is obtained from the relative ratio of the sample scattering intensity to the scattering intensity of a standard pure liquid with a known Rayleigh ratio such as toluene which has its established wavelength and temperature, as calculated from the equation below:

$$R_\theta = \frac{I_A n_0^2}{I_T n_T^2} R_T \quad \text{Eq. 3.4}$$

I_A : Residual scattering intensity of the sample (sample intensity – solvent intensity).

I_T : Toluene scattering intensity.

n_0 : Solvent refractive index.

n_T : Toluene refractive index.

R_T : Rayleigh ratio of toluene.

The intensity of the scattered light of a particle detected as a function of various sample concentrations which is compared to the respective scattering from the toluene is represented in a Debye plot. The average molecular weight (M) was then determined from the intercept at zero concentration $\frac{K}{CR_\theta}$, as $\frac{K}{CR_\theta}$ is equals to $\frac{1}{M}$.

A series concentrations of depolymerized chitosan were prepared and observed under the Abbe Refractometer NAR-2T (ATAGO Co., Ltd, Tokyo, Japan) at 25 °C to obtain

their refractive indices of which the differential refractive indices calculated were used as the input in acquiring the scattered light intensity by Malvern Nano ZS Zetasizer (Malvern Instruments Ltd, Worcestershire, UK). As mentioned in the SLS theory above, the scattered light intensity of the particle is proportional to the product of the average molecular weight and the concentration of the macromolecules, hence the molecular weight of the chitosan can then be determined.

3.3.4 Structural analysis of chitosan

3.3.4.1 Fourier-transform infrared spectroscopy (FTIR) spectroscopy

FTIR is a useful technique for qualitative and quantitative analysis of molecules. Every type of bond in a molecule has a different dipole moment that absorbs at different frequencies of infrared radiation energy to excite to higher energy when the infrared radiation matches their vibrational frequency. This characterized absorption infrared spectrum is important to determine the structures of a molecule based on the absorption wavenumber. Moreover, the energy absorbed can increase the amplitude of the vibrational frequencies like stretching and bending vibration modes and hence is useful to quantify the intensity of the absorption peaks.

All the samples in this study were acquired with the Frontier FTIR spectrometer (Perkin Elmer, Massachusetts, USA) in transmittance mode. The samples were mixed with potassium bromide and dried in an oven overnight at 100 °C prior to usage at a 1:100 ratio before being compressing into pellet form and then examined at a resolution of 4 cm^{-1} with 32 scans from 400 – 4000 cm^{-1} for triplicates. The degree of acylation (DA) and degree of substitution (DS) of chitosan were obtained from the FTIR spectra using the following equation (Kasaai, 2008):

$$DA (\%) = \left(\frac{A_{1655}/A_{3450}}{1.33} \right) \times 100\% \quad \text{Eq. 3.5}$$

$$DS (\%) = DA_{\text{ChA}} - DA_{\text{Ch3}} \quad \text{Eq. 3.6}$$

A_{1655} : Peak intensity at 1655 cm^{-1} (carbonyl absorption of secondary amide).

A_{3450} : Peak intensity at 3450 cm^{-1} (hydroxyl absorption).

1.33 : Ratio of $A_{1655/3450}$ for fully *N*-acylated chitosan (Khan et al., 2002).

3.3.4.2 ^1H and ^{13}C Nuclear magnetic resonance (NMR) spectroscopy

NMR is a non-destructive technique to investigate the magnetic properties of atomic nuclei. Since many nuclei have spin and are electrically charged, they absorb electromagnetic radiation in order to excite to a higher energy level at a frequency corresponding to their radio frequencies when subjected to the external magnetic field. Energy is liberated at the same radio frequencies as well when the spin return to its base state. This signal is measured and processed into a NMR spectrum based on the nucleus chemical environment derived from its resonant frequency.

Depolymerized chitosans and ChA were prepared at 20 g L^{-1} in 2% $\text{CD}_3\text{COOD}/\text{D}_2\text{O}$ solution for NMR analyses by JNM-ECX500 spectrometer (JEOL Ltd, Tokyo, Japan) at $20 \text{ }^\circ\text{C}$. ^1H and ^{13}C NMR were acquired at 500 MHz and 125.77 MHz operating frequencies respectively.

3.3.5 Particle size and zeta potential analysis

Particle size measurement is working on the principle of dynamic light scattering (DLS) which also known as photon correlation spectroscopy (PCS) or quasi-elastic light scattering. This technique measures the size of the particles using the velocity of random collisions of the particles with the surrounding liquid molecules known as the Brownian motion by employing Stokes-Einstein equation.

$$D_h = \frac{k_B T}{3\pi\eta D_t} \quad \text{Eq. 3.7}$$

D_h : Hydrodynamic diameter.

k_B : Boltzmann's constant.

T : Absolute temperature.

η : Viscosity.

D_t : Translational diffusion coefficient (velocity of Brownian motion).

Particles at different size fluctuate at different intensity fluctuation rates. For instance, smaller particles are able to fluctuate more rapidly than those of larger ones. The scattered light intensity at successive times detected is correlated to derive the rate at which the intensity is varying in order to derive the information of the particle size.

Zeta potential is the electrostatic repulsion between the adjacent particles in the system, which is determined from the potential between the boundary of the slipping plane of the particles and the dispersing media (Figure 3.1). Each particle is surrounded by an electrical double layer, which is the inner Stern layer and outer diffuse layer. The ions are strongly bound in the Stern layer, but less firmly attached in the diffuse layer. For those ions located within the slipping plane of the diffuse layer, they move with the particles. On the other hand, the ions do not move with the particles if they are beyond the slipping plane. The zeta potential is calculated from the Henry equation using the electrophoretic mobility of the particle which can be obtained through the Laser Doppler Velocimetry (LDV) technique in an electrophoresis experiment.

$$U_E = \frac{2\varepsilon z f(k_a)}{3\eta} \quad \text{Eq. 3.8}$$

U_E : electrophoretic mobility.

ϵ : dielectric constant.

z : zeta potential.

$f(Ka)$: Henry's function.

η : viscosity.

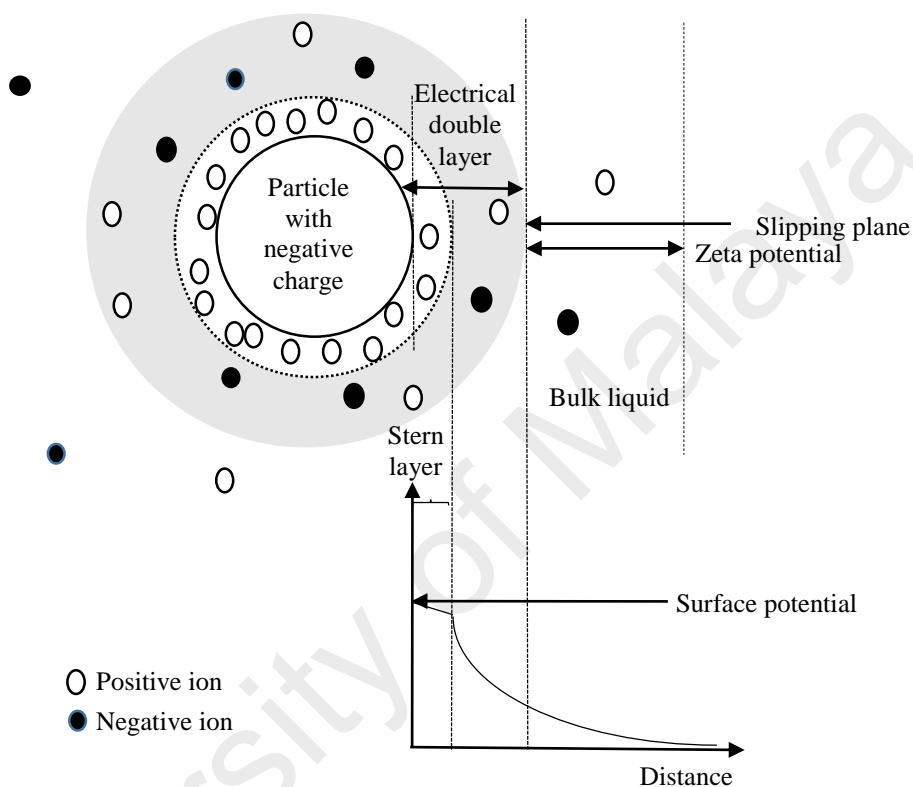


Figure 3.1: The electrical double layer of a particle.

The average particle size and zeta potential of ChA and drugs loaded ChA were measured with Malvern Nano ZS Zetasizer Zen 3600 (Malvern Instruments Ltd, Worcestershire, UK) at laser light of 633 nm and measurement angle of 173° with respect to the scattered light. The analyses were performed at 25°C and automatic attenuator was selected. The reported value was calculated based on the average of three measurements.

3.3.6 Powder X-ray diffraction (XRD)

Powder X-ray diffraction is a non-destructive and powerful analytical technique to study the structures and atomic spacing of crystalline materials. After the X-ray is

projected from an X-ray tube, the wavelength of the X-ray is filtered to obtain monochromatic X-ray and collimate to concentrate before directing onto the samples. When the incident beam interfaces with the crystalline samples, the X-ray is diffracted and formed constructive interference based on Bragg's Law ($n\lambda = 2d \sin \theta$, where the integer n is the order of the diffracted beam, λ is the wavelength of the incident X-ray beam, d is the distance between adjacent planes of atoms (d -spacings). The X-ray signal was then recorded and measured by the detector.

The X-ray diffraction patterns of ChA samples were recorded using Panalytical Empyrean diffractometer (Almelo, The Netherlands) by exposing the samples to Cu K α radiation ranged $2\theta = 5^\circ - 50^\circ$.

3.3.7 Thermogravimetry analysis (TGA)

TGA monitors the mass gain or loss of a sample as a function of temperature or time in a controlled atmosphere of nitrogen, helium, air, other gas, or in a vacuum. TGA is commonly used to study physical phenomena, such as vaporization, sublimation, absorption, adsorption and desorption, as well as chemical phenomena including chemisorptions, dehydration, decomposition and solid-gas reactions (for instance oxidation or reduction).

Pyris 6 Thermogravimetric Analyzer (Perkin-Elmer, Massachusetts, USA) equipped with Pyris software was used to study the thermal decomposition and moisture content of chitosan based on the percentage of weight loss from the thermogram. Approximately 2 – 3mg of the sample was loaded into a ceramic pan and heated from 35 °C to 900 °C at a heating rate of 10 °C min⁻¹ under a constant nitrogen purging of 20 mL min⁻¹.

3.3.8 Determination of water solubility and critical aggregation concentration (CAC) using ultraviolet-visible (UV-Vis) spectroscopy

Ultraviolet-Visible (UV-Vis) is the measurement of attenuation of light beam after it passes through a sample or reflects from the sample surface over the ultraviolet (200 – 400 nm) and visible (400 – 800 nm) spectral region. When the electrons-filled chromophores of light absorbing molecules are exposed to light having an energy which matches the electronic transition of the molecule, the molecules can absorb the energy to excite the electrons from ground state to the orbital of higher energy state (Figure 3.2).

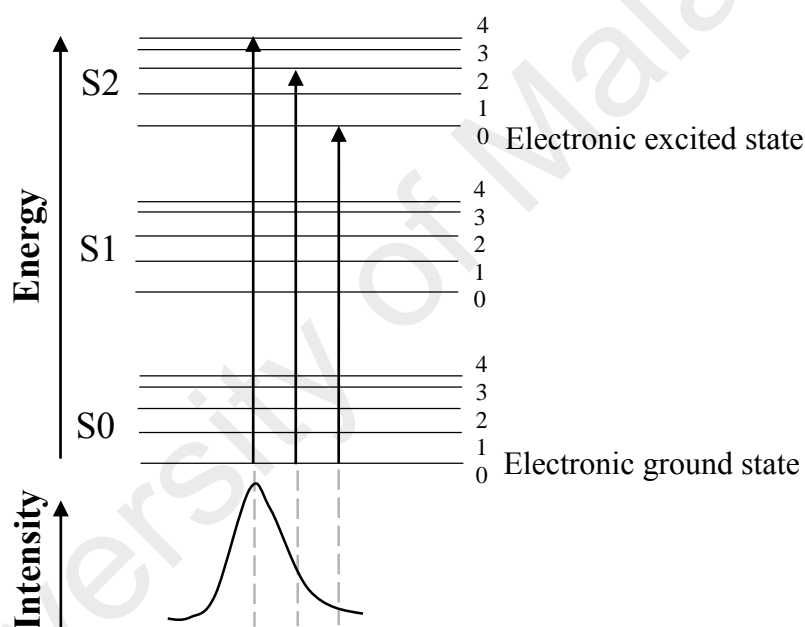


Figure 3.2: Electronic transitions of molecules from ground state to the excited state of the orbitals after light absorption.

The UV-Vis spectrum characterized the electronic transition of the molecules as a continuous absorption band as it consists of a superimposition of electronic levels as the consequence of combinations of different excited modes of vibration and rotation of molecules. Since the intensity of the light absorption at a certain wavelength corresponds to the number of molecules capable of absorbing light, the concentration of the samples can be quantified using Beer's Law as shown in Eq. 3.9 with known molar absorption:

$$A = \epsilon bc$$

Eq. 3.9

A : absorbance.

ϵ : molar absorptivity.

c : sample concentration in mole/liter.

b : length of light path through the sample in cm.

The water solubility of depolymerized and acylated chitosan (ChA) and also drugs was determined by UV-Visible spectroscopy using Varian Cary 50 UV-Visible spectrophotometer (Agilent Technologies, California, USA) at 25 °C. Depolymerized chitosan and ChA were prepared as a series of soluble concentrations to construct a calibration curve at 270 nm and 283 nm respectively, whereas the UV absorption of SA, LID, ACE and CAF were measured at 296 nm, 263 nm, 244 nm and 273 nm respectively. The solubility of the samples was determined from the extrapolation of a saturated sample from the calibration curve.

Determination of CAC of ChA was carried out using Varian Cary 50 UV-Visible spectrophotometer (Agilent Technologies, California, USA) at 25 °C as well. Hydrophobically modified chitosan (HMC) form aggregates with their amphiphilic structures. The point at which the hydrophobic parts of the polymers interact with each other to form aggregates is called the critical aggregation concentration (CAC), which can be investigated by turbidity method as the change in intensity of light scattering arising from the HMC can be a qualitative parameter to indicate the formation of the aggregates. ChA samples were prepared at a series of different concentrations for the absorption measurement at 350 nm using a quartz cuvette with optical path length of 10 mm which was later reported as a function of the natural logarithm of ChA

concentrations. The CAC value of ChA was hence estimated from the first sight of absorption increment from the flat region of the plot.

3.3.9 Kinematic viscosity measurement

Kinematic viscosity is the ratio of the dynamic viscosity of a fluid to its density (Eq. 3.10). Dynamic viscosity also known as absolute viscosity measures the internal resistance of the fluid to flow.

$$\nu = \frac{\mu}{\rho} \quad \text{Eq. 3.10}$$

ν : kinematic viscosity ($\text{m}^2 \text{s}^{-1}$).

μ : absolute or dynamic viscosity (N s m^{-2}).

ρ : density (kg m^{-3}).

Kinematic viscosity of Ch3 and ChA was measured using Cannon Ubbelohde Capillary No 1c and Lauda S5 measuring stand in Lauda E200 water bath (Lauda Scientific GmbH, Lauda-Konigshofen, Germany) at 20, 30, 40, 50, 60, 70 and 80 °C. The time for the samples to flow from the upper etched mark to lower mark of the viscometer was recorded by the Lauda PVS 1/4 software as the average of three measurements and was input into the following equation to obtain kinematic viscosity:

$$\nu = K (t - \theta) \quad \text{Eq. 3.11}$$

ν : kinematic viscosity.

K : viscometer constant.

t : time flow between two etched marks of viscometer.

θ : kinetic energy correction of viscometer.

3.3.10 Determination of swelling percentage

Swelling is the increase of the volume of material as a result of absorption of a solvent. ChA were weighted as w_1 before immersing in deionized water for 24 hours and 0.1 mol dm⁻³ HCl solution for 2 hours respectively at 37 °C. ChA were then blotted on the filter paper to remove excess water and recorded as weight w_2 . The percentage of swelling was calculated from the average of triplicates, using the equation 3.12 as shown:

$$\text{Percentage of swelling (\%)} = \frac{w_2 - w_1}{w_1} \times 100\% \quad \text{Eq. 3.12}$$

w_1 : Weight of ChA before swelling.

w_2 : Weight of ChA after swelling.

3.3.11 Morphology observations

3.3.11.1 Transmission electron microscopy (TEM)

In TEM imaging, electron beam ejected from the electron gun is focused into a small, thin, coherent beam by a condenser lens to exclude high angle electrons. The electron beam strikes the sample and was partially transmitted through the sample depending on the electron transparency and thickness of the sample. The transmitted electrons were then captured by the objective lens onto an image recording system such as a fluorescent screen, photographic film or charge-coupled device to convert the electrons to images.

LEO-Libra 120 transmission electron microscope (Carl Zeiss SMT AG, Oberkochen, Germany) with operating voltage of 120 kV working along with Soft Imaging Viewer software was employed to observe the morphology of the ChA with and without drugs. A sample drop was carefully dropped onto a 400 mesh copper grid (Electron Microscopy Sciences, Pennsylvania, USA). The excess water drop was removed using filter paper, followed by a small drop of 1% (w/v) phosphotungstic acid solution. Excess media was

wiped off with filter paper before keeping the samples in the desiccator prior to examination under microscope.

3.3.11.2 Field-emission scanning electron microscopy (FE-SEM)

Similar to the working principles of TEM, FE-SEM utilizes the electrons instead of light to visualize the surface topography and morphology of a sample. These primary electrons emitted from the field emitter source are accelerated in the high vacuum column chamber of the microscope and is focused before being deflected by electronic lenses to produce a narrow scan beam that bombarded the samples. The secondary electrons with different angle and velocity generated based on the surface structure of the sample was then detected by the detector to produce an electrical signal which can be further processed into images.

Ch3 and ChA were firstly spray dried using a Mini Spray Dryer, Model 290 (BÜCHI Labortechnik AG, Flawil, Switzerland) at an inlet temperature of 150°C in the Faculty of Food Science and Technology, Universiti Putra Malaysia (UPM), Malaysia prior to FE-SEM observation. The chitosan powder was put on the double sided adhesive tape fixed on a metal stub and deposited with gold before being observed under FEI Quanta 450 field-emission scanning electron microscope (Hillsboro, Oregon, USA) under magnification of 10,000×.

3.3.12 Determination of encapsulation efficiency (EE) and drug loading (DL)

High performance liquid chromatography (HPLC) is a powerful instrument to separate, identify and quantify each component in a mixture by pumping a sample mixture under a stream of mobile phase at high pressure through a column with a chromatographic packing material referred to as the stationary phase. As the samples passes through the column, every component in the sample interacts differently with the stationary phase due

to differences in polarities of the components, resulting in the separation of components at different elution rates. The components that interact strongly with the stationary phase of the column exit the column slower than those components that exhibited the least amount of interaction.

After removal of THF, ChA loaded with drugs were topped up with deionised water to prepare acylated chitosan suspension at 5 g L⁻¹ which were then filtered with 0.2 µm syringe filter and diluted with pre-filtered mobile phase as mentioned in section 3.2.4 at an appropriate dilution factor prior to analyzing with a Shimadzu HPLC system (Shimadzu Corporation, Kyoto, Japan) including a LC-20AT pump, DGU-20A5 degasser, SIL-20AC autosampler, CTO-20AC column oven and SPD-M20A photodiode array detector (PDA). The samples were passed through a Chromolith RP-18e (1.3×10 – 2×10³ nm pore size, 3×100 mm) column fitted with a Chromolith RP-18e of 5×3 mm internal diameter (i.d) guard cartridge and then processed by the LabSolutions software.

The composition of the acetonitrile and 10 mM phosphate buffer pH 6 for HPLC analysis of SA, LID, ACE and CAF were 6:94 at 0.5 mL min⁻¹, 25:75 at 1 mL min⁻¹, 5:95 at 0.5 mL min⁻¹, 7:93 at 1 mL min⁻¹ respectively and detected at 245 nm, 247 nm, 243 nm and 272 nm respectively. The calibration curve was constructed from the graph of absorption peak area versus a series of diluted concentrations of drug solutions. The EE and DL of ChA onto the drugs were calculated based on the equation below by taking the dilution factor into account:

$$EE (\%) = \frac{D_T - D_F}{D_T} \times 100\% \quad \text{Eq. 3.13}$$

$$DL (\%) = \frac{D_T - D_F}{ChA_T} \times 100\% \quad \text{Eq.3.14}$$

D_T : Total amount of drugs loaded.

D_F : Free amount of drugs detected.

ChA_T : Total amount of ChA used.

3.4 *In vitro* drug release study

3.4.1 Topical delivery using inline vertical Franz diffusion cells

Franz diffusion cell system is a common method for *in vitro* drug release study by employing a membrane of known diameter as a barrier sandwich between the donor and receptor compartments. The membrane is used to separate the donor compartment containing the loading sample from the receptor compartment filled with a medium like phosphate buffered saline (PBS) (Figure 3.3). The automatic sampling operation of the cells can ease the sampling operation simultaneously during withdrawing and replenishing of the receptor media at a particular time to obtain a consistent and reproducible reading. The drug release across the membrane was determined by collecting the medium from the receptor chamber at a certain time interval and replenishing it with fresh medium to maintain the sink condition of the system.

Automated Franz Diffusion Cell System (Microette Autosampling System, Hanson Research Co., California, USA) with three individual Franz diffusion cells was used to study the *in vitro* release of drugs in the absence and presence of ChA for topical delivery. The regenerated cellulose membranes of 5000 Da molecular weight cut-off (MWCO) were washed with deionized water and saturated with 10 mM phosphate buffered saline (PBS) solution pH 7.4 overnight before mounting onto the diffusion cells. Air bubbles of the diffusion cells system were removed before the loading of each sample at approximately 500 μ g onto the donor chamber of the diffusion cells with a chamber volume of 4 mL 10 mM PBS solution under magnetic stirring at 400 rpm and jacketed water circulation at 37 ± 0.1 °C. The sample was automatically withdrawn at particular time for UV-Vis measurement and replenished with the equal amount of PBS solution.

The release of SA, LID, ACE and CAF were determined using Varian Cary 50 UV-Visible spectrophotometer (Agilent Technologies, California, USA) at 296 nm, 263 nm, 244 nm and 273 nm respectively and calculated as the average of three measurements.

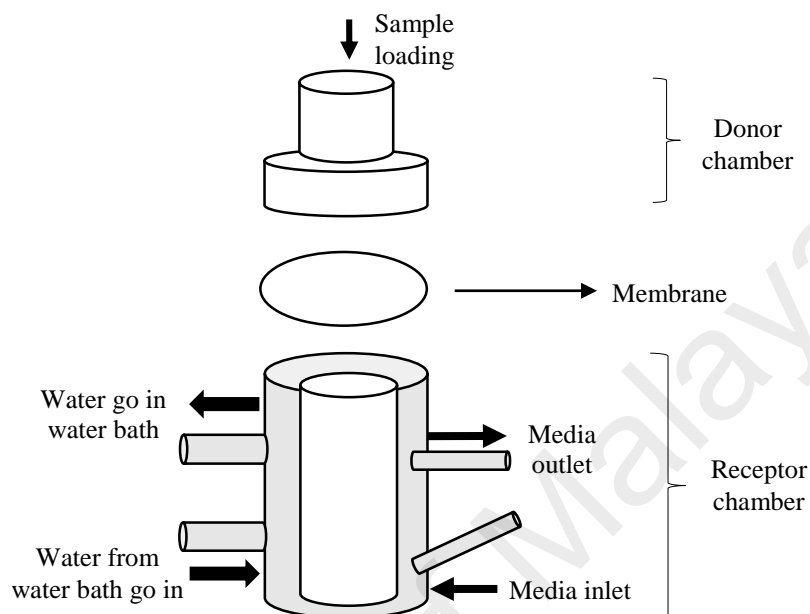


Figure 3.3: The compartments of a Franz diffusion cell.

3.4.2 Oral delivery using dialysis tubing

For the *in vitro* drug release for oral delivery, dialysis tubing was employed and immersed in the simulated media of stomach and intestine at 37 °C to mimic the environment of the drugs intake orally.

The cellulose dialysis tubing of MWCO 5000 kDa was cut at the similar length and washed with deionized water, followed by pre-saturation in SGF pH 1.2 prior to usage. Approximately 500 µg of drug was loaded into the dialysis tubing and tied before putting into a test tube containing SGF which was pre-equilibrium at 37 °C. The experiment was carried out in a water-jacketed beaker at 37 °C under magnetic stirring at 100 rpm (Figure 3.4). The sample was withdrawn at a certain time interval and replenished with the same volume of SGF to maintain the sink condition. After 2 hours, the dialysis tubing was

transferred to another test tube filled with SIF at pH 6.8. The drug release was analyzed by UV-Vis spectrophotometer and the average absorption value of triplicates was reported.

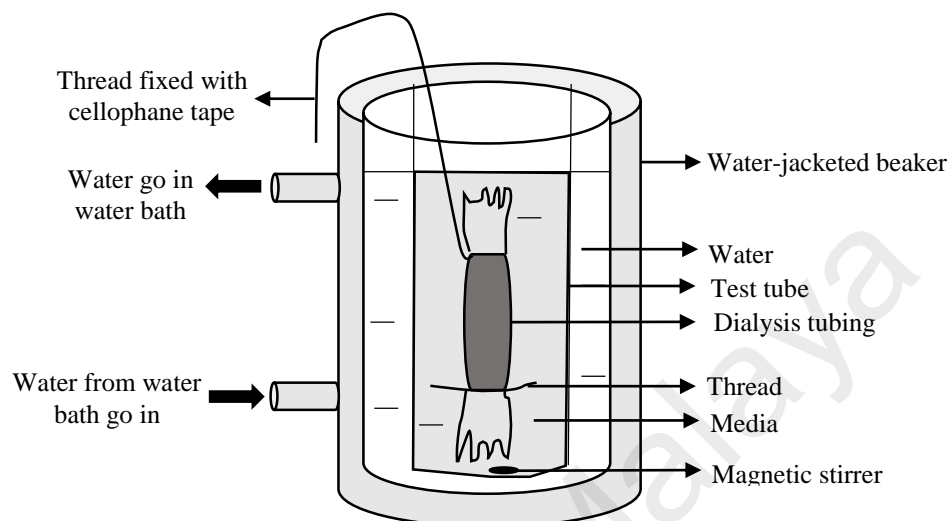


Figure 3.4: The apparatus set-up of *in vitro* drug release for oral delivery.

3.4.3 Mathematical kinetic modelings

Drug release kinetics in section 3.4.1 and 3.4.2 were studied by fitting the data into different kinetic equations of the models using DDSolver software (Zhang et al., 2010) to evaluate the best model to describe the drug release. The models to be investigated were zero, first order, Higuchi model, Hixson model and Korsmeyer-Peppas models, which are based on cumulative drug release against time, logarithm of cumulative drug release percentage against time, cumulative drug release percentage against square root of time, cube root of drug percentage remaining in matrix against time and logarithm-logarithm plot $-\ln(1 - \text{cumulative drug release percentage})$ against time respectively (Table 3.2) (Costa & Sousa Lobo, 2001). For Korsmeyer-Peppas model, n which is the release exponent describes the drug release mechanism of the carriers based on the shape properties (Table 3.3) (Carbinatto et al., 2014).

Table 3.2: The equations used in the kinetic models, where M_t , M_0 and M_∞ are the amount of drug release at time t , initial and infinite time respectively, k is the release constant, t is the time and n is the release exponent.

Kinetic model	Equation	
Zero order	$M_t = M_0 + kt$	Eq. 3.15
First order	$\ln (1-M_t) = kt$	Eq. 3.16
Higuchi	$M_t = kt^{1/2}$	Eq. 3.17
Korsmeyer-Peppas	$\frac{M_t}{M_\infty} = kt^n$	Eq. 3.18
Hixson	$M_t^{1/3} = M_i^{1/3} - kt$	Eq. 3.19

Table 3.3: The release mechanism describes by the n release exponent in Korsmeyer-Peppas model.

Thin film	n		Drug transport mechanism	Rate as a function of time
	cylindrical	sphere		
< 0.5	< 0.45	< 0.43	Fickian diffusion	$t^{-0.5}$
$0.5 < n < 1.0$	$0.45 < n < 0.89$	$0.43 < n < 0.85$	Anomalous transport	t^{n-1}
1.0	0.89	0.85	Case-II transport	Zero order release
> 1.0			Super Case-II transport	t^{n-1}

3.5 Data analysis

The data analysis and calculations were done by using Microsoft Excel and graphs were plotted with the Origin programme (OriginLab Corporation, Massachusetts, USA). GraphPad Prism 6 (GraphPad Software, California, USA) was employed for the analysis of the significance level of data by accessing the differences of the data using one-way or two ways analysis of variance (ANOVA) with Bonferroni post doc test. The differences in means were considered statistically significant when $P < 0.05$.

CHAPTER 4: RESULTS AND DISCUSSION

4.1 Modifications of chitosan

4.1.1 Depolymerization

Commercial chitosan was depolymerized into several chitosan of lower molecular weight by using different volumes of sodium nitrite. The depolymerization mechanism of chitosan was mainly dependent on the volume of sodium nitrite used as it influenced the amount of nitrosonium ion (NO^+) generated to cleave the β -glycosidic linkage, as illustrated in step 1 – 3 in Figure 4.1.

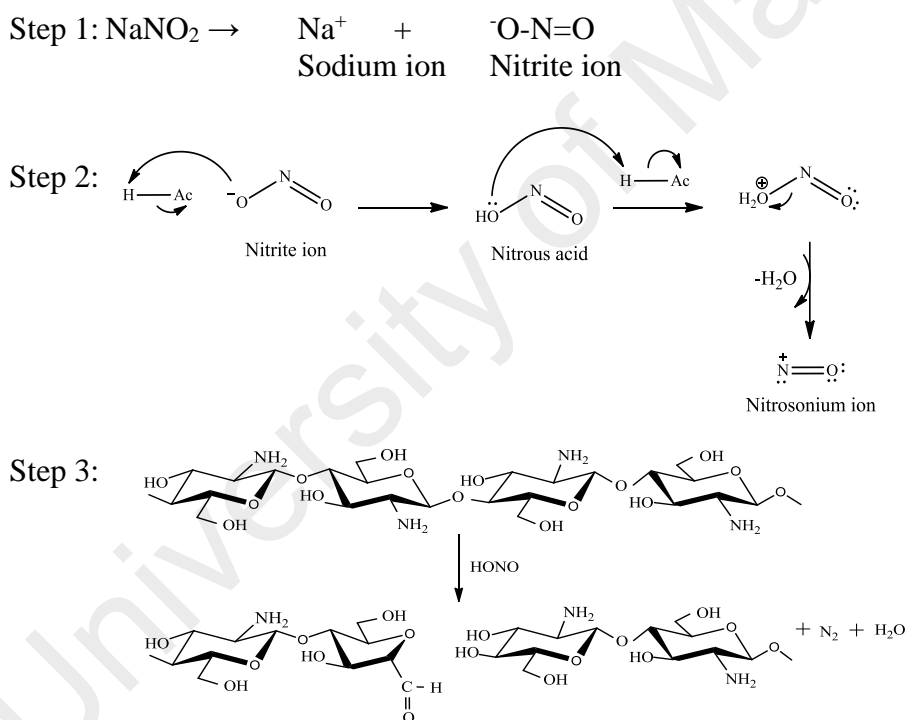


Figure 4.1: Reaction mechanism of depolymerization of chitosan.

Step 1: The reaction was initialized by the dissociation of sodium nitrite to sodium cation and nitrite ion.

Step 2: Nitrite ion was protonated to form nitrosonium ion (NO^+).

Step 3: Cleavage of β -glycosidic linkage to form reactive 2,5-anhydro-*D*-mannose unit at the new reducing end.

Sodium nitrite was dissociated into sodium cation (Na^+) and nitrite anion (NO_2^-) when dissolved in water. The nitrite ions were then protonated in the chitosan solution

containing acetic acid and converted to nitrous acid (HONO), followed by the removal of water molecules to form nitrosonium ion (Clayden et al., 2012) which then attacks the amino group of *D*-glucosamine unit of chitosan to cleave the adjacent β -glycosidic linkage, forming a reactive 2,5-anhydro-*D*-mannose unit at the new reducing end (Allan & Peyron, 1995; Tommeraas et al., 2001).

4.1.2 Acylation

The nucleophilic acyl substitution or simply known as acylation was carried out in the presence of methanol to mix the reaction mixture containing the polar aqueous solution and non-polar acid anhydrides homogenously to prevent phase separation (Keisuke et al., 1988). The reaction is favored at the amino group of chitosan attributed to the higher reactivity of amino group at C2 atom of the *D*-glucosamine subunits as compared to the hydroxyl groups at C3 and C6. The reaction mechanism involved the bond formation between the nucleophilic amino group of chitosan with the electrophilic carbon of the carbonyl of anhydride, followed by the bond breaking of the carboxylate ion leaving group, as shown in Figure 4.2.

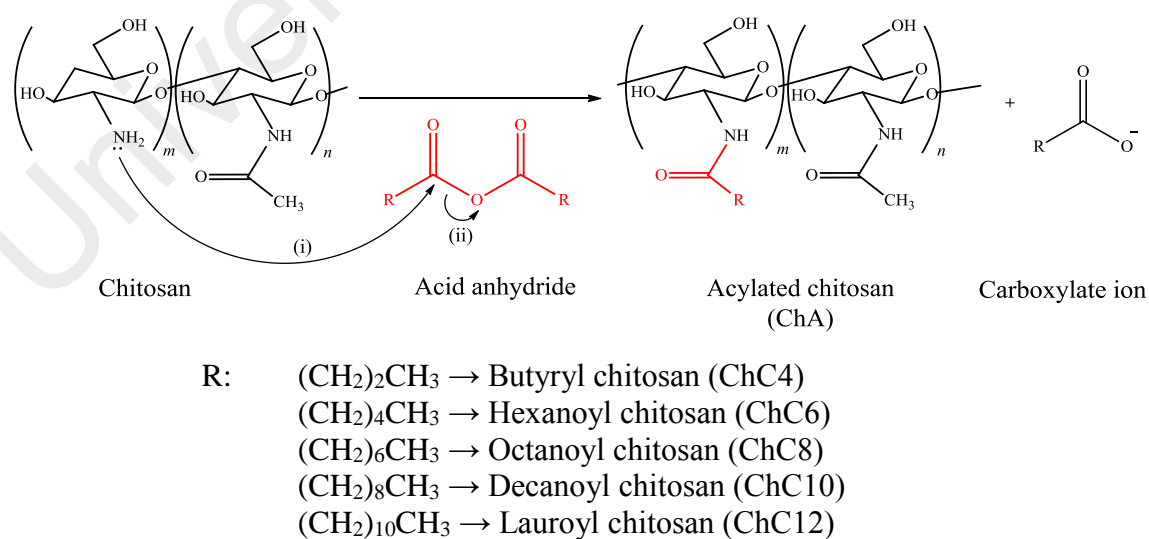


Figure 4.2: (i) The bond formation between the anhydride and chitosan and (ii) bond breaking of the leaving group during the acylation, where R is the alkyl chain of the acid anhydride, *m* and *n* is the number of *D*-glucosamine and *N*-acetyl-*D*-glucosamine units respectively.

4.2 Characterizations of chitosan

4.2.1 Determination of average molecular weight

Table 4.1 showed that the average molecular weight of the depolymerized chitosan was decreased corresponding to the increase of added sodium nitrite volume, as the higher volume of sodium nitrite provided more NO^+ ions for the cleavage of glycosidic linkage and resulted in lower molecular weight, as discussed in section 4.1.1.

Table 4.1: Average molecular weight and water solubility of the depolymerized chitosan at addition of different volumes of sodium nitrite.

Chitosan	Volume of NaNO_2 solution added (mL)	Average molecular weight, M_w (kDa)	Water solubility (g L^{-1})
Ch1	12	5	21.31
Ch2	10	10	9.41
Ch3	7	25	5.60
ChC4		33	3.75
ChC6		32	3.68
ChC8		31	3.63
ChC10		30	3.43
ChC12		35	3.24
Ch4	5	50	3.65

Chitosan with an average molecular weight of 25 kDa (Ch3) was chosen as the main subject in this study. From the preliminary screening, it was found that the chitosan with 50 kDa (Ch4) acylated with lauric anhydride was hardly soluble in water ($< 1\text{g L}^{-1}$) because the water solubility of the chitosan decreased as the hydrophobic interaction between polymer chains became more significant, whereas the DS of chitosan with 10 kDa (Ch2) with lauric anhydride at 1:1 ratio was low at 5%, this may result in high critical aggregation concentration (CAC) and is more challenging to the drug encapsulation. From Table 4.1, the molecular weight of Ch3 was increased after acylation as the introduction of hydrophobic alkyl carbon group contributed to the molecular weight. The water solubility decreased as the molecular weight increased in the sequence of Ch1, Ch2, Ch3 and Ch4, this was plausibly explained by the stronger steric hindrance effect of longer polymer chain to the formation of hydrogen bonding with water (Holowka & Bhatia, 2014).

4.2.2 FTIR spectroscopy

FTIR analyses was carried out to characterize the changes in functional groups and quantification of DA of chitosan before and after acylation. The FTIR spectra of Ch3 and acylated chitosan include ChC4, ChC6, ChC8, ChC10 and ChC12 prepared from acylation of acid anhydrides of different chain length on Ch3 at different mole ratio to the *N*-glucosamine of chitosan were presented in Figure 4.3(a-e) and the overall spectra of Ch3 and acylated chitosan were summarized in Figure 4.3(f). In terms of qualitative analysis by functional groups, Ch3 and ChA showed a typical C–O stretching of chitosan backbone at 1068 cm^{-1} and 1033 cm^{-1} and also an asymmetric stretching of C–O–C bridge of the molecule at 1154 cm^{-1} (Shelma & Sharma, 2011a). The N–H stretching in both Ch3 and ChA at 3108 cm^{-1} and 3270 cm^{-1} were ascribed to the intramolecular and intermolecular vibration within the chitosan (Rumengan et al., 2014), whereas the O–H vibration at $3436 - 3431\text{ cm}^{-1}$ was ascribed to the hydroxyl groups at C3 and C6 (Focher et al., 1992).

The prominent change after acylation shown in Figure 4.3 was the disappearance of the absorption peak at 1570 cm^{-1} attributed to the bending of the primary amino group of chitosan at C2 in Ch3 and substituted with 1558 cm^{-1} corresponding to –NH bending of amide II (in combination with C–N stretching) in ChA (Lao et al., 2010; Le Tien et al., 2003). The absence of absorption peak above 1700 cm^{-1} characterized for *O*-acyl ester chitosan in the spectrum (Chiandotti et al., 2010) revealed that no *O*-acylation occurred on the Ch3 in the reaction. All these observations showed the successful *N*-acylation of acid anhydrides onto the Ch3.

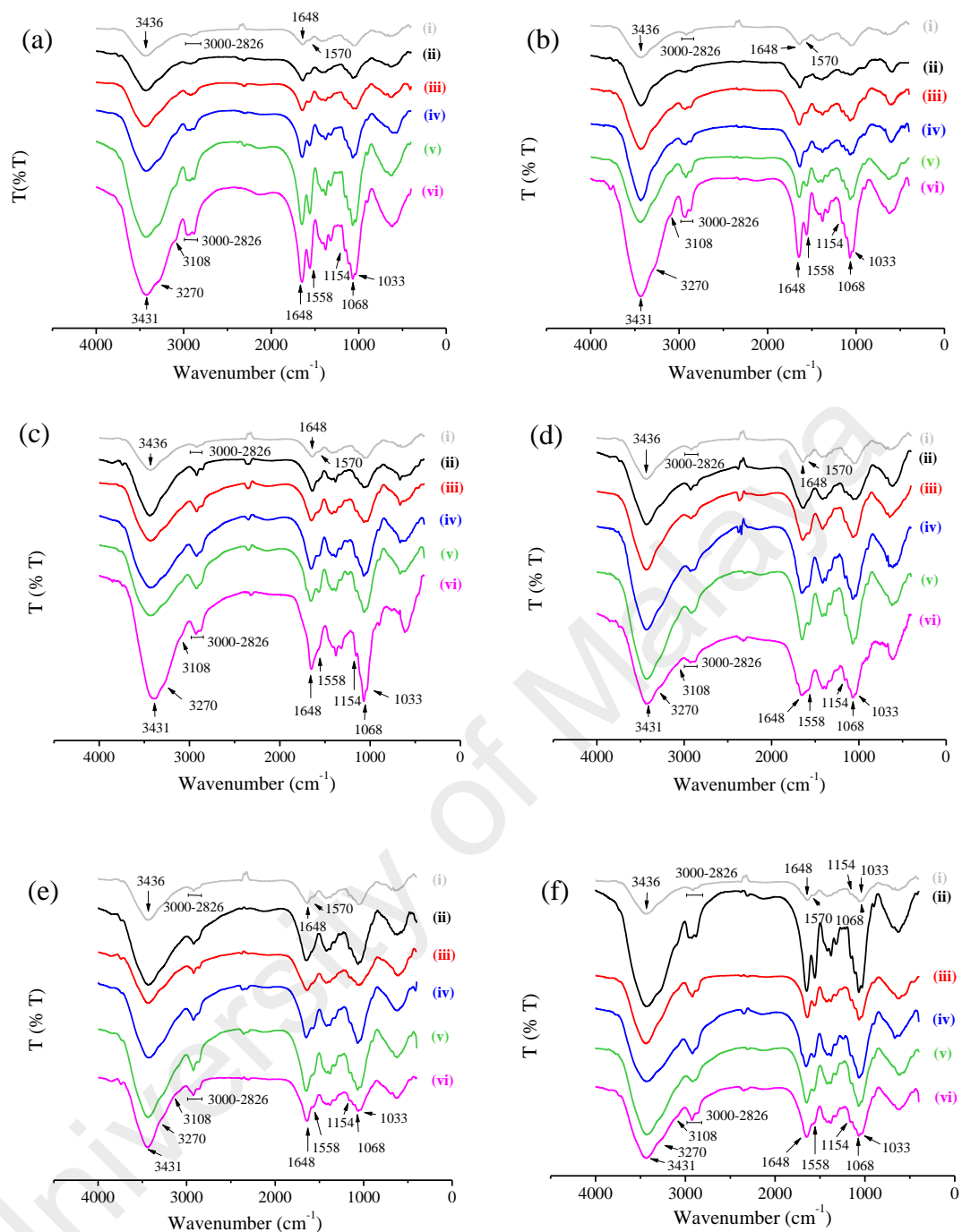


Figure 4.3: FTIR spectra of (a) ChC4, (b) ChC6, (c) ChC8, (d) ChC10, (e) ChC12 from acylation of glucosamine units of chitosan to acid anhydrides at mole ratio of (i) 1:0.0 (Ch3), (ii) 1:0.2, (iii) 1:0.4, (iv) 1:0.6, (v) 1:0.8, (vi) 1:1.0 and (f) overall spectra of (i) Ch3, (ii) ChC4-M.8, (iii) ChC6-M.8, (iv) ChC8-M.8, (v) ChC10-M.8 and (vi) ChC12-M.8.

For quantitative analysis, the peak intensity at a certain wavelength number was measured to determine the effect of the acylating agent on the DA as well as on the DS. For instance, the intensity of carbonyl stretching of the secondary amide at 1648 cm^{-1} was

increased as DS increased. The same observation was also displayed by the peak intensity of CH₂ and CH₃ around the region 3000 – 2826 cm⁻¹ as more alkyl groups were acylated on the amino group of the chitosan (Liu et al., 2010). The DA of ChA increased as the mole ratio of Ch3 to acid anhydrides increased regardless of alkyl chain length (Figure 4.4). The increment of DS of the ChA increased inversely proportional to the alkyl chain length, in the sequence of ChC4 > ChC6 > ChC8 > ChC12 > ChC10, the trend was similar to the study obtained by Mi et al. (2005) who worked on acylation of C2, C3 and C4. Longer carbon chain was harder to be acylated as long alkyl chain induced more steric hindrance to nucleophilic substitution. Despite the longer chain length of ChC12, its DS was slightly higher than ChC10 as it was pre-heated prior to its addition to chitosan solution and reacted at 50 °C. This revealed that heat could promote acylation.

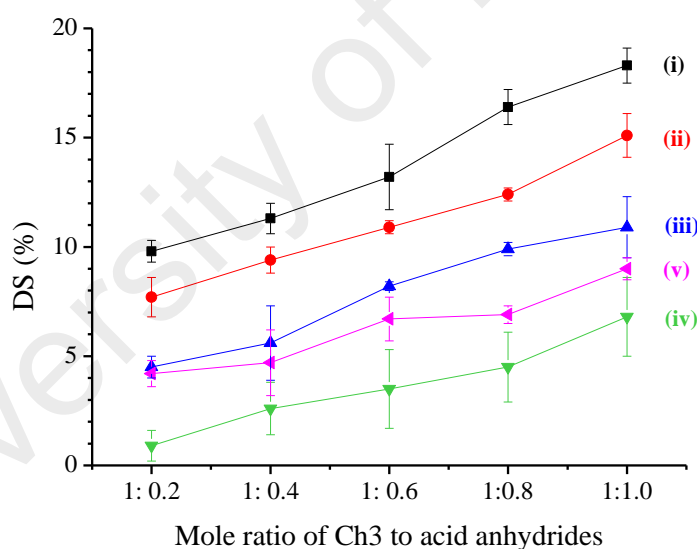


Figure 4.4: Degree of substitution (DS) of (i) ChC4, (ii) ChC6, (iii) ChC8, (iv) ChC10 and (v) ChC12 at different mole ratio of acylation.

4.2.3 ¹H and ¹³C NMR analysis

The ¹H NMR spectra of Ch3 and ChA was shown in Figure 4.5. The intense solvent protons of deuterium oxide (HOD) and acetic acid (CD₂HCOOD) appeared at 4.85 – 4.41 ppm and 2.14 – 2.06 ppm for Ch3 and 4.84 – 4.50 ppm and 2.06 – 1.80 ppm for ChA respectively. The proton assignments for Ch3 and ChA were done based on the previous

literature values (Balan et al., 2015; Al-Sou'od et al., 2013; Tan & Misran, 2013; Jiang et al., 2006b; Zhang et al., 2003a) and summarized in Table 4.2. From Figure 4.5, the confirmation of the successful acylation was shown by the newly existing CH₂ protons peaks which indicated by (a-b) in ChC4, (a-d) in ChC6, (a-f) in ChC8, (a-h) in ChC10, (a-j) in ChC12 respectively around 1.25 – 1.03 ppm, 1.49 – 1.35 ppm and 2.24 – 2.00 ppm. The appearance of CH₃ protons peaks were observed around 0.78 – 0.65 ppm which represented by (c) in ChC4, (e) in ChC6, (g) in ChC8, (i) in ChC10 and (k) in ChC12 respectively.

Table 4.2: Assignment of protons of (a) Ch3, (b) ChC4, (c) ChC6, (d) ChC8, (e) ChC10 and (f) ChC12 in ¹H NMR.

(a) Ch3		(b) ChC4		(c) ChC6	
Chemical shift (δ)	H assignment	Chemical shift (δ)	H assignment	Chemical shift (δ)	H assignment
		0.78 - 0.70	HNCOCH ₂ CH ₂ CH ₃	0.78 - 0.65	HNCO(CH ₂) ₄ CH ₃
				1.22 - 1.05	HNCO(CH ₂) ₂ (CH ₂) ₂ CH ₃
		1.49 - 1.39	HNCOCH ₂ CH ₂ CH ₃	1.49 - 1.36	HNCOCH ₂ CH ₂ (CH ₂) ₂ CH ₃
1.94	HNCOCH ₃	1.77	HNCOCH ₃	1.77	HNCOCH ₃
2.14 - 2.06	CD ₂ HCOOD	1.94 - 1.80	CD ₂ HCOOD	2.06 - 1.82	CD ₂ HCOOD
		2.15 - 2.05	HNCOCH ₂ CH ₂ CH ₃	2.24 - 2.06	HNCOCH ₂ (CH ₂) ₃ CH ₃
3.06 - 3.02	CH of carbon 2	3.00 - 2.94	CH of carbon 2	3.04 - 2.92	CH of carbon 2
4.09 - 3.32	CH of carbon 3 - 6	4.01 - 3.17	CH of carbon 3 - 6	3.87 - 3.24	CH of carbon 3 - 6
4.44 - 4.32	CH of carbon 1	4.44 - 4.32	CH of carbon 1	4.44 - 4.32	CH of carbon 1
4.85 - 4.41	HOD	4.73 - 4.62	HOD	4.82 - 4.56	HOD

(d) ChC8		(e) ChC10		(f) ChC12	
Chemical shift (δ)	H assignment	Chemical shift (δ)	H assignment	Chemical shift (δ)	H assignment
0.74 - 0.63	HNCO(CH ₂) ₆ CH ₃	0.72 - 0.65	HNCO(CH ₂) ₈ CH ₃	0.77 - 0.67	HNCO(CH ₂) ₁₀ CH ₃
1.19 - 1.03	HNCO(CH ₂) ₂ (CH ₂) ₄ CH ₃	1.15 - 1.05	HNCO(CH ₂) ₂ (CH ₂) ₆ CH ₃	1.25 - 1.04	HNCO(CH ₂) ₂ (CH ₂) ₈ CH ₃
1.48 - 1.35	HNCOCH ₂ CH ₂ (CH ₂) ₄ CH ₃	1.45 - 1.37	HNCOCH ₂ CH ₂ (CH ₂) ₆ CH ₃	1.47 - 1.38	HNCOCH ₂ CH ₂ (CH ₂) ₈ CH ₃
1.76	HNCOCH ₃	1.75	HNCOCH ₃	1.76	HNCOCH ₃
1.97 - 1.82	CD ₂ HCOOD	1.96 - 1.81	CD ₂ HCOOD	1.97 - 1.80	CD ₂ HCOOD
2.20 - 2.01	HNCOCH ₂ (CH ₂) ₅ CH ₃	2.15 - 2.00	HNCOCH ₂ (CH ₂) ₇ CH ₃	2.18 - 2.01	HNCOCH ₂ (CH ₂) ₉ CH ₃
3.05 - 2.92	CH of carbon 2	3.03 - 2.91	CH of carbon 2	3.05 - 2.92	CH of carbon 2
3.87 - 3.24	CH of carbon 3 - 6	3.84 - 3.24	CH of carbon 3 - 6	3.87 - 3.25	CH of carbon 3 - 6
4.46 - 4.32	CH of carbon 1	4.44 - 4.31	CH of carbon 1	4.45 - 4.32	CH of carbon 1
4.80 - 4.57	HOD	4.80 - 4.50	HOD	4.84 - 4.58	HOD

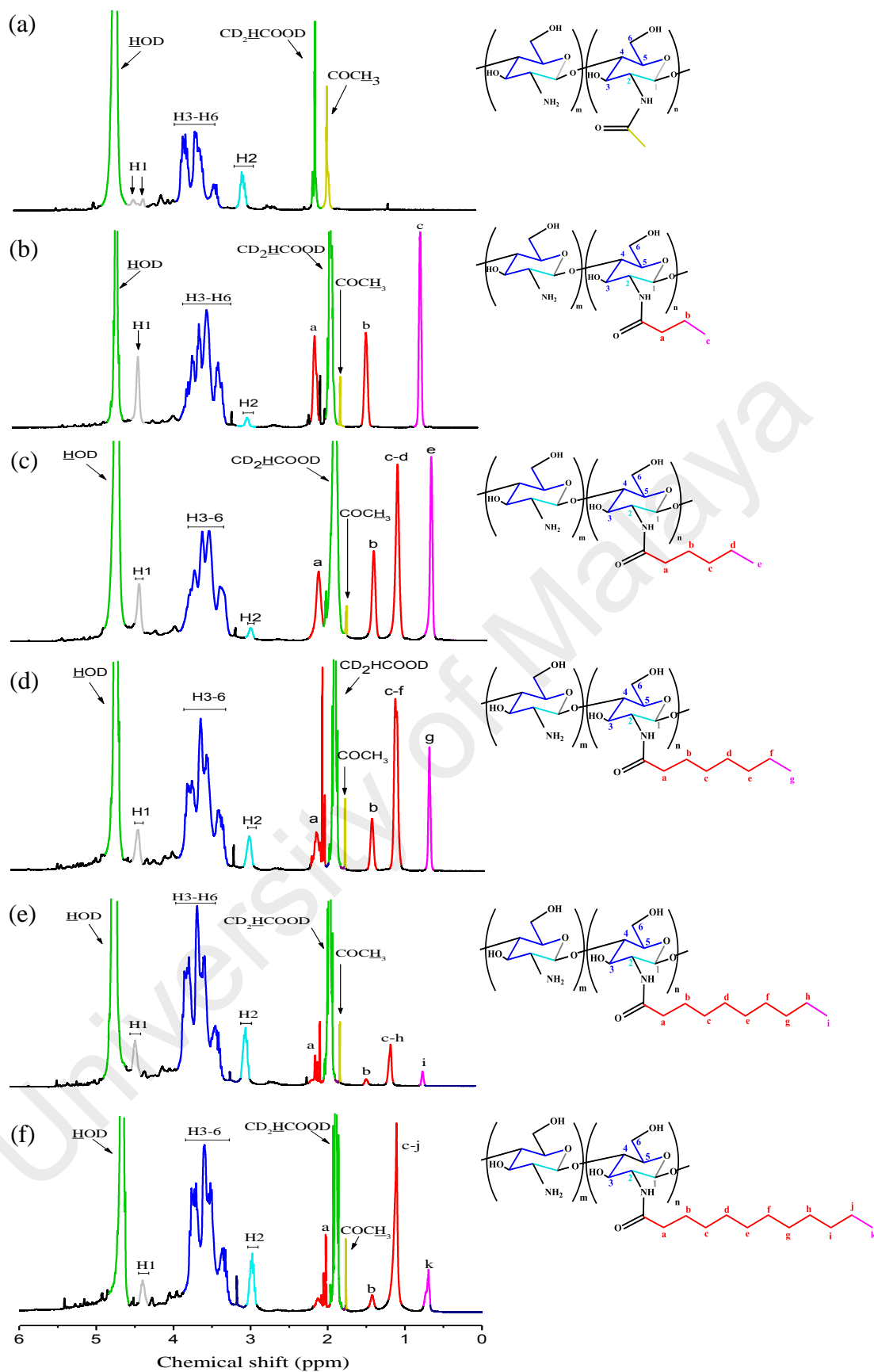


Figure 4.5: ^1H NMR spectra of (a) Ch3, (b) ChC4, (c) ChC6, (d) ChC8, (e) ChC10 and (f) ChC12, the new CH₂ and CH₃ groups were plotted in red and pink colour respectively, where m and n in the structure of chitosan represent the number of *D*-glucosamine and *N*-acetyl-*D*-glucosamine units respectively.

^{13}C NMR was carried out as well to further confirm the successful acylation of ChA, as presented in Figure 4.6. The carbon assignments were done by referring to literature (Zhang et al., 2003a) and tabulated in Table 4.3. As compared to Ch3, ChA showed new carbon peaks for methyl carbon ($\text{NHCO}(\text{CH}_2)_n\text{CH}_3$) at 13.5 – 12.7 ppm, methylene carbon at 18.9 ppm, 37.9 – 22.0 ppm ($\text{NHCO}(\text{CH}_2)_n\text{CH}_3$) as well as carbonyl carbon at 177.8 – 177.6 ppm ($\text{NHCO}(\text{CH}_2)_n\text{CH}_3$), where n is 2, 4, 6, 8 and 10. This proved that the alkyl carbon chain have been acylated to Ch3. Carbonyl carbons were not observed in ChC10 and ChC12, this may be caused by low DS incurred low intensity of carbon peak and is hard to be detected.

It can be found that the protons of Ch3 in Figure 4.5 showed higher chemical shift compared to ChA in ^1H NMR spectra, this can be explained by the better dissolution of Ch3 with higher degree of protonation with its more available amino group of glucosamine in acidic medium compared to ChA which is restricted by the hydrophobic alkyl group (Kadokawa et al., 2015).

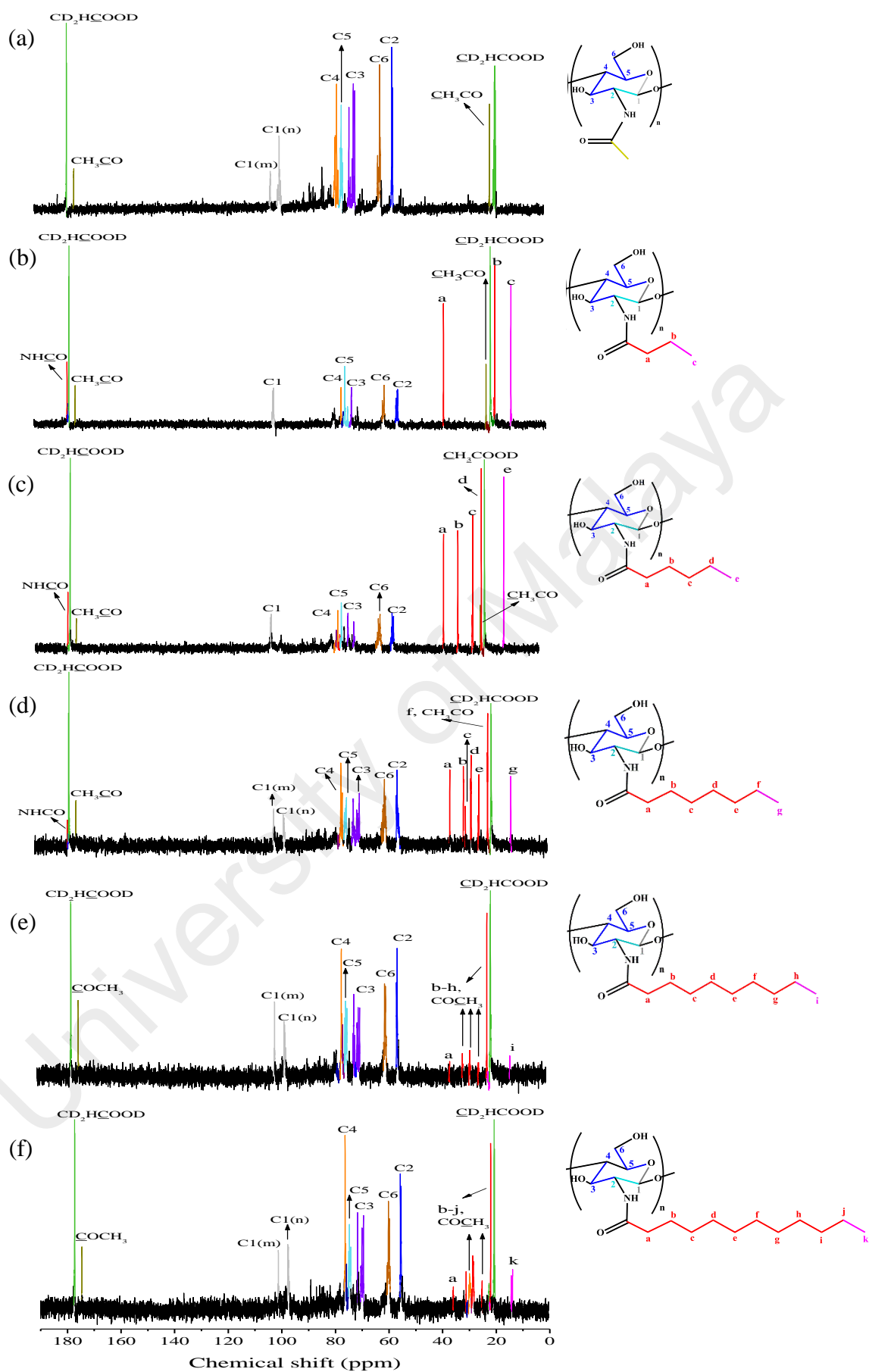


Figure 4.6: ^{13}C NMR spectra of (a) Ch3, (b) ChC4, (c) ChC6, (d) ChC8, (e) ChC10 and (f) ChC12. The new methylene and carbonyl carbons of ChA were highlighted in red colour, whereas methyl carbon was indicated by pink colour.

Table 4.3: Assignment of carbons of (a) Ch3, (b) ChC4, (c) ChC6, (d) ChC8, (e) ChC10 and (f) ChC12 in ^{13}C NMR.

(a) Ch3		(b) ChC4		(c) ChC6	
Chemical shift (δ)	Carbon assignment	Chemical shift (δ)	Carbon assignment	Chemical shift (δ)	Carbon assignment
		12.7	NHCOCH ₂ CH ₂ CH ₃	13.3	NHCO(CH ₂) ₄ C H ₃
21.6-20.4	CD ₂ HCOOD	18.9	NHCOCH ₂ CH ₂ CH ₃	20.7-20.0	CD ₂ HCOOD
22.7	COCH ₃	20.7-20.0	CD ₂ HCOOD	20.7-20.1	NHCO(CH ₂) ₃ C H ₂ CH ₃
		22.0	COCH ₃	21.7	COCH ₃
				22.1	NHCO(CH ₂) ₂ C H ₂ CH ₂ CH ₃
				24.9	NHCOCH ₂ CH ₂ (CH ₂) ₂ CH ₃
		37.9	NHCOCH ₂ CH ₂ CH ₃	30.6	NHCOCH ₂ (CH ₂) ₃ CH ₃
56.8-56.0	C2	55.8-54.4	C2	36.0	NHCOCH ₂ (CH ₂) ₃ CH ₃
62.0-60.3	C6	60.8-59.6	C6	55.8-54.6	C2
72.8-70.2	C3	72.3-69.3	C3	61.1-59.4	C6
76.0-74.8	C5	74.9-74.2	C5	72.2-69.4	C3
78.3-76.4	C4	76.0-75.6	C4	74.7-74.1	C5
99.2-97.7, 102.1-101.6	C1 (n), C1 (m)	101.6-100.6	C1	76.5-75.6	C4
175.0	COCH ₃	174.6	COCH ₃	101.6-100.4	C1
177.9-177.6	CD ₂ HCOOD	177.2-176.7	CD ₂ HCOOD	174.5	COCH ₃
		177.6	NHCOCH ₂ CH ₂ CH ₃	177.1-176.5	CD ₂ HCOOD
				177.8	NHCO(CH ₂) ₄ C H ₃

(d) ChC8		(e) ChC10		(f) ChC12	
Chemical shift (δ)	Carbon assignment	Chemical shift (δ)	Carbon assignment	Chemical shift (δ)	Carbon assignment
13.5	NHCO(CH ₂) ₆ C H ₃	13.5	NHCO(CH ₂) ₈ C H ₃	13.4	NHCO(CH ₂) ₁₀ C H ₃
20.8-20.3, 22.2-21.8	CD ₂ HCOOD NHCO(CH ₂) ₅ CH ₂ CH ₃ , COCH ₃	21.1-20.4, 22.0,25.1, 28.4, 31.2	CD ₂ HCOOD NHCO(CH ₂) ₈ C H ₃ , COCH ₃	21.0 -20.4 22.1,25.2, 30.2-28.2, 32.0	CD ₂ HCOOD NHCO(CH ₂) ₁₀ CH ₃ , COCH ₃
25.2	NHCO(CH ₂) ₄ CH ₂ CH ₂ CH ₃				
28.1	NHCO(CH ₂) ₃ CH ₂ (CH ₂) ₂ CH ₃				
30.2	NHCO(CH ₂) ₂ CH ₂ (CH ₂) ₃ CH ₃				
30.9	NHCOCH ₂ CH ₂ (CH ₂) ₄ CH ₃				
36.0	NHCOCH ₂ (CH ₂) ₅ CH ₃	35.9	NHCOCH ₂ (CH ₂) ₇ CH ₃	36.0	NHCOCH ₂ (CH ₂) ₉ CH ₃
55.9-54.6	C2	55.9-54.9	C2	56.2-55.0	C2
61.5-59.5	C6	60.8-59.4	C6	60.8-59.5	C6
72.3-69.4	C3	72.1-69.5	C3	72.1-69.4	C3
75.2-74.2	C5	75.2-74.2	C5	75.4-74.3	C5
76.7-75.8	C4	76.7-75.6	C4	76.8-75.9	C4
97.9-97.0, 101.6-100.6	C1 (n), C1 (m)	97.8-97.1, 101.0-101.5	C1 (n), C1 (m)	97.9-97.0, 101.6-101.0	C1 (n), C1 (m)
174.7	COCH ₃	174.6	COCH ₃	174.6	COCH ₃
177.4-176.9	CD ₂ HCOOD	177.6-177.1	CD ₂ HCOOD	177.7-177.2	CD ₂ HCOOD
177.7	NHCO(CH ₂) ₆ C H ₃				

4.2.4 Particle size and zeta potential

The Z-average particle size of the ChA obtained by dynamic light scattering (DLS) measurement decreased as feed mole ratio of acid anhydrides increased, as presented in Figure 4.7(b). This was attributed to the increased substitution of alkyl chain which can be explained in two ways. First was the presence of the hydrophobic alkyl chain which can provide stronger Van der Waals forces to pull the polymer chains closer and hence form smaller particles. Second was the substitution of the hydrophobic moieties on the nucleophilic amino group reducing the hydrophilicity of ChA to interact with aqueous water molecules and led to lower swelling. The result was in agreement with the previous studies that higher degree of substitution by highly hydrophobic groups such as octyl, stearoyl and palmitoyl chains formed smaller chitosan micelles (Mekhail et al., 2012; Jiang et al., 2006b). As shown in Figure 4.7(b), the decrease of particle size was more pronounced in short chain acylated ChC4 and ChC6 with the particle size dramatically decreased from 600 – 800 nm at 1:0.2 mole ratio of Ch3 to acid anhydride to < 300 nm at 1:1.0. This is presumably due to their loose network as a consequence of weak hydrophobic effect between short alkyl chains. The size of ChA was marginally different from 1:0.8 onwards, as the substituting groups may trigger aggregation to form compact particles, hence further increase of DS did not significantly reduce the size. Therefore, the ChA prepared at 1:0.8 was chosen for further analysis and drug encapsulation.

In addition, the effect of the modification on the amino groups of chitosan was also observed from the change of zeta potential as observed from Figure 4.7(a). The zeta potential of Ch3 was changed from +10.4 mV to -1.29, -0.462, +1.24, +1.97, +3.6 mV with respect to ChC4-M.2, ChC6-M.2, ChC8-M.2, ChC10-M.2 and ChC12-M.2 after acylation. Since the free amino group which can be protonated in the water was

substituted after acylation, the cationic charge of chitosan was reduced and thus shifted the zeta potential to a more negative value as DS of ChA increased (Wei et al., 2010).

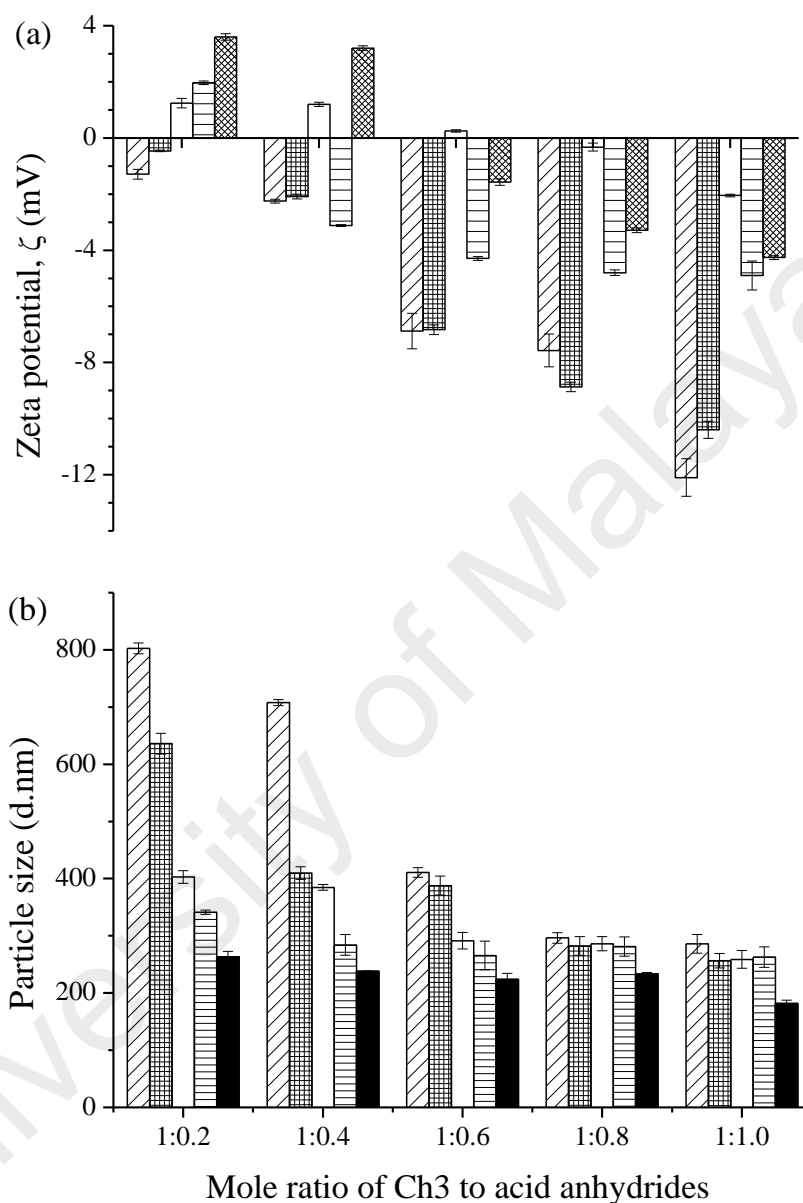


Figure 4.7: (a) Zeta potential and (b) particle size of ChC4 (▨), ChC6 (▩), ChC8 (□), ChC10 (▧) and ChC12 (■) at different mole ratio of acylation.

4.2.5 Powder X-ray diffraction (XRD)

XRD is useful to investigate the phase identification such as crystallinity of crystalline materials. As shown from the XRD patterns of ChA in Figure 4.8, there was a prominent peak observed at $2\theta = 19 - 20^\circ$ which was characterized as crystal form I of chitosan (Samuels, 1981). This was attributed to the formation of intermolecular hydrogen

bonding of the amino and hydroxyl groups of the chitosan chain (Abdel Aziz et al., 2015). Nevertheless, the peak intensity was significantly decreased and became broader in ChC10, due to the low crystallinity of ChC10 with the substitution of long alkyl chain at low DS. Unlike ChC10, ChC12 showed a sharp peak at $2\theta = 19 - 20^\circ$ despite attaching with the longest alkyl groups, presumably owing to its higher DS thus contributing to a more stable organization with stronger hydrophobic interaction, which was corroborated with the study of Le Tien et al. (2003) stating that hydrophobic interaction can enhance stability via organization of self-assembly arrangement.

In addition, there was also a peak appearing at $2\theta = 5.7^\circ$ and 6.8° in ChC4 and ChC6 respectively. The shift from higher diffraction angle in ChC4 to lower diffraction angle in ChC6 indicated the increase in d -spacing according to Bragg's Law (Reddy et al., 2016). The presence of peaks at $2\theta = 5.7^\circ$ and 6.8° endowed ChC4 and ChC6 possessing higher crystallinity compared to longer chain acylated ChC8, ChC10 and ChC12 because the random distribution of longer alkyl groups disordered their network bonding. The space hindrance of alkyl groups may also weaken the hydrogen bonding and rigidity of the chitosan (Feng et al., 2012).

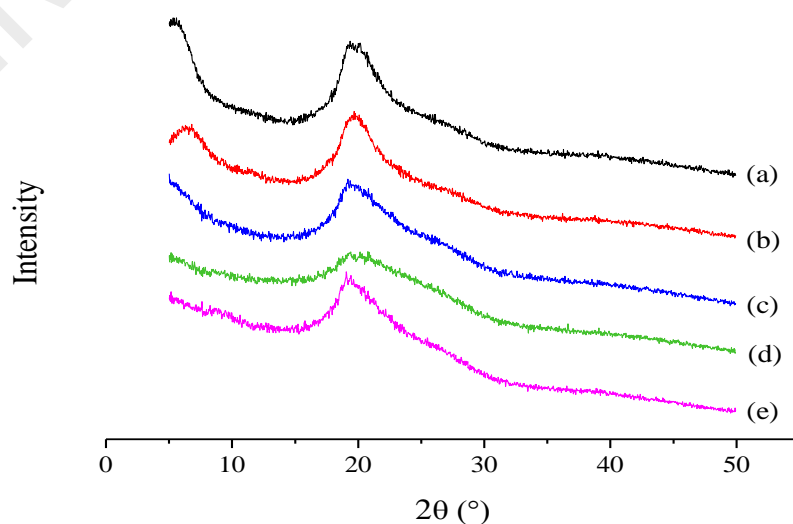


Figure 4.8: XRD patterns of (a) ChC4, (b) ChC6, (c) ChC8, (d) ChC10 and (e) ChC12 from $2\theta = 5 - 50^\circ$.

4.2.6 Thermogravimetric analysis (TGA)

The TGA results of Ch3 and ChA were presented as the percentage of weight loss with the derivative plot as shown in Figure 4.9(a) and (b) respectively. There were three main weight losses occurring during the heating from 35 – 900 °C. The first weight loss (W_1) of Ch3 and ChA from 35 °C to 140 – 150 °C was attributed to the evaporation of water molecules from moisture. From Figure 4.9(a), the weight loss of ChA at 8.0 – 13.0% was higher as Ch3 trapped lower water moisture at 3.6%. This was due to the random distribution of alkyl groups onto chitosan which disrupted the hydrogen bonding of the more organized and rigid structure of Ch3 by changing the distance between polymer chains and hence loosen the arrangement of chitosan (Feng et al., 2012). This disordered structure in turns facilitated the water penetration in an easier way. Hence, Ch3 with higher rigidity showed higher thermal stability towards moisture and maximum degradation temperature at 97 °C as compared to ChA around 59 – 65 °C (Table 4.4). Among the ChA, chitosan acylated with ChC10 and ChC12 demonstrated higher weight loss at 10 – 12% moisture than those of shorter chain such as ChC4, ChC6 and ChC8 (around 8 – 10%), presumably caused by the longer carbon chain of ChC10 and ChC12 distorting the structure of Ch3 to a higher extent (Figure 4.10). The higher moisture absorption of ChC10 and ChC12 could be further triggered by higher availability of amino group to bind moisture due to their lower DS. It can be deduced that the structure of ChC10 and ChC12 were more disordered with their higher moisture sensitivity as compared to ChC4, ChC6 and ChC8. The result supported the observation in XRD analysis (section 4.2.5) that the long chain acylated chitosan was less crystalline than those of short chain, as well as in agreement with the study of Ioelovich (2014) that water vapor sorption ability of chitosan was increased as the crystallinity was decreased because the loose packing arrangement eases the water penetration and holds higher water capacity.

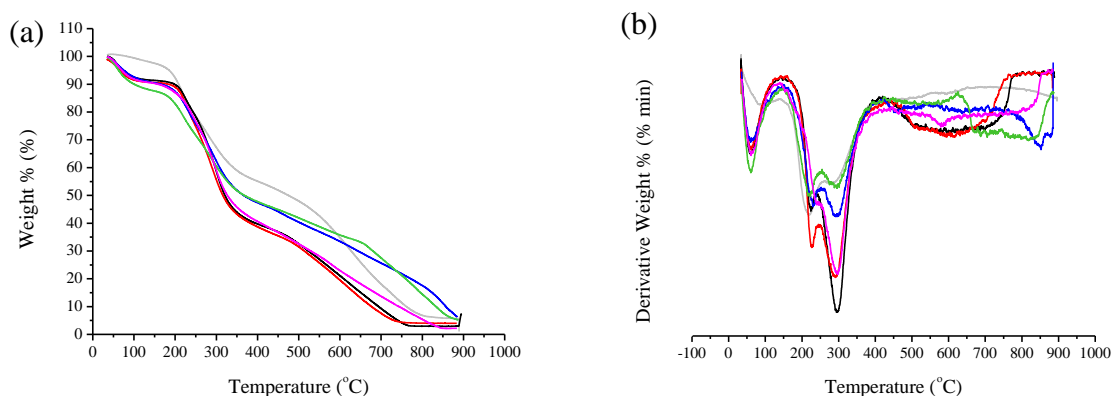


Figure 4.9: (a) Thermogravimetric and (b) derivatize thermogravimetric thermogram of Ch3 (—), ChC4 (—), ChC6 (—), ChC8 (—), ChC10 (—) and ChC12 (—) from 35 to 900 °C.

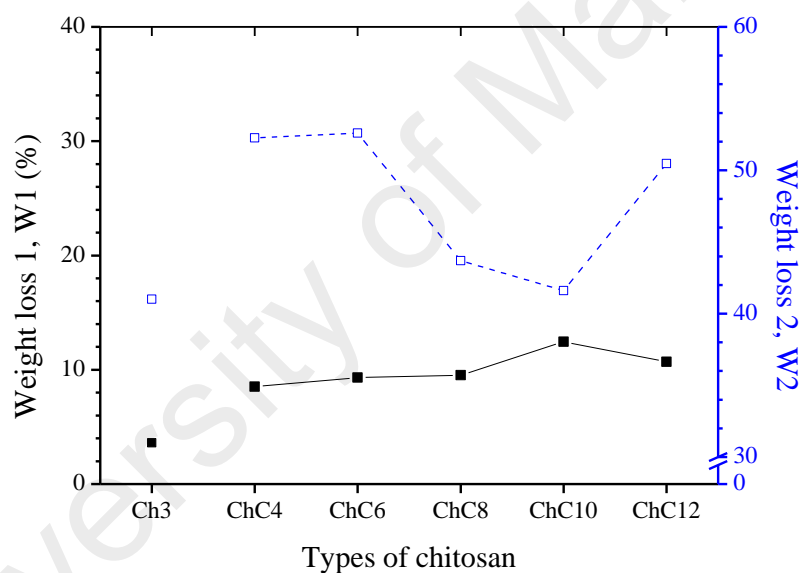


Figure 4.10: Weight loss of Ch3, ChC4, ChC6, ChC8, ChC10 and ChC12 in the first stage (W_1) which represented by solid symbol (■) and line (—) and second (W_2) stage of decomposition in the TGA thermogram which indicated by hollow symbol (□) and dashed line (.....) respectively.

The second thermal degradation was the major weight loss (W_2) of chitosan occurring in the steep region around 141 – 151 °C to 400 – 410 °C (Figure 4.9(a) and (b)). This significant weight loss of chitosan was due to the decomposition of chitosan main chains (Chen et al., 2013; El-Hefian et al., 2010). From Figure 4.10, as compared to the weight loss of Ch3 at 41.0% during this stage, ChC4, ChC6 and ChC8 and ChC12 showed a

higher amount of weight loss at 43 – 53% as more chitosan constituents including glucosamine, *N*-acetyl-glucosamine and *N*-acyl-glucosamine were decomposed as compared to Ch3 consisting of only glucosamine and *N*-acetyl-glucosamine subunits. ChC10 showed the lowest weight loss at 41.6% among ChA due to its low DS. Figure 4.9(b) presented two obvious differential peaks in the thermogram of derivative of weight loss percentage for the second phase of decomposition from 141 – 151 °C to 400 – 410 °C. It was found that ChC4 with the highest DS demonstrated the deepest depression at the second peak around 261 – 271 °C to 400 – 410 °C as compared to the first peak around 141 – 151 °C to 260 – 270 °C, this suggests that the first differential peak indicates the decomposition of glucosamine subunits whereas the second differential peak reflects the decomposition of *N*-acyl-glucosamine monomers of chitosan respectively. This suggestion is consistent with the DSC study by Guinesi and Cavalheiro (2006) in which the decomposition of *N*-acetyl-glucosamine occurred after the decomposition of glucosamine of chitosan. The weight loss observed above 400 – 410 °C was resulted from the decomposition of the inorganic complex comprised of carbon, nitrogen and oxygen (Figure 4.9(a) and (b) (El-Hefian et al., 2012). The weight loss with the respective maximum temperature of Ch3 and ChA during first, second and third stage of decomposition from 35 – 900 °C were summarized in Table 4.4.

Table 4.4: The weight loss with the respective maximum temperature of Ch3 and ChA during first, second and third stage of decomposition from 35 – 900 °C.

Samples	Weight loss 1, W ₁ (%)	Weight loss 2, W ₂ (%)	Weight loss 3, W ₃ (%)	Maximum temperature (T _{max1})	Maximum temperature (T _{max2})	Maximum temperature (T _{max3})
Ch3	3.6	41.0	50.4	96.6	213.6	280.4
ChC4-M.8	8.5	52.3	42.0	60.1	227.9	296.6
ChC6-M.8	9.4	52.6	34.4	60.3	225.4	288.2
ChC8-M.8	9.5	46.7	46.6	64.2	231.8	297.2
ChC10-M.8	12.4	41.6	40.5	59.9	218.0	287.9
ChC12-M.8	10.7	50.5	38.3	60.6	241.3	295.3

4.2.7 Determination of critical aggregation concentration (CAC) and water solubility

The CAC value of ChC12 determined from the plot of absorption at 350 nm as a function of the logarithm of concentration (Figure 4.12(a)) was presented in Figure 4.11, which was $30 \mu\text{g mL}^{-1}$, it was lower than ChC6, ChC8 and ChC10 which was approximately $40 \mu\text{g mL}^{-1}$ and also ChC4 at $50 \mu\text{g mL}^{-1}$. This was due to longer alkyl chain of ChC12 providing stronger hydrophobic interaction between polymer chains to form aggregates at lower concentration, it was in agreement with the previous studies by Jiang et al. (2006b) and Wang et al. (2011). Even though ChC6 possessed shorter chain as compared to ChC8 and ChC10, the CAC of ChC6 was similar to ChC8 and ChC10 as high DS of ChC6 contributed to its hydrophobicity and gain in the energy of association which in turn promoted aggregate formation (Mekhail et al., 2012; Chen et al., 2011b). Hence, it can be deduced that both high DS and long alkyl chain can facilitate the formation of aggregates and lower the CAC value.

The water solubility of Ch3, ChC4, Ch6, ChC8, ChC10 and ChC12 were 5.60, 3.75, 3.68, 3.63, 3.43 and 3.24 g L^{-1} , respectively (Table 4.1 in section 4.2.1 and Figure 4.11). The water solubility of Ch3 was improved after acylation as the attachment of alkyl group on the chitosan backbone disrupts the crystalline structure of chitosan constructed from extensive intramolecular and intermolecular hydrogen bonding (Sogias et al., 2010). The introduction of alkyl chain on chitosan changes the directional and horizontal order of chitosan which affects their spatial arrangement and extension, this in turn exposes the amino and hydroxyl groups for the formation of hydrogen bonding with water (Zhang et al., 2014). Nevertheless, the substitution of longer alkyl group resulted in higher hydrophobicity of ChA which disfavored their interaction with water molecules and promoted the hydrophobic interaction between chitosan chains (Hirano et al., 2002). As

a consequence, the CAC value of ChA was directly proportional to the water solubility (Figure 4.11).

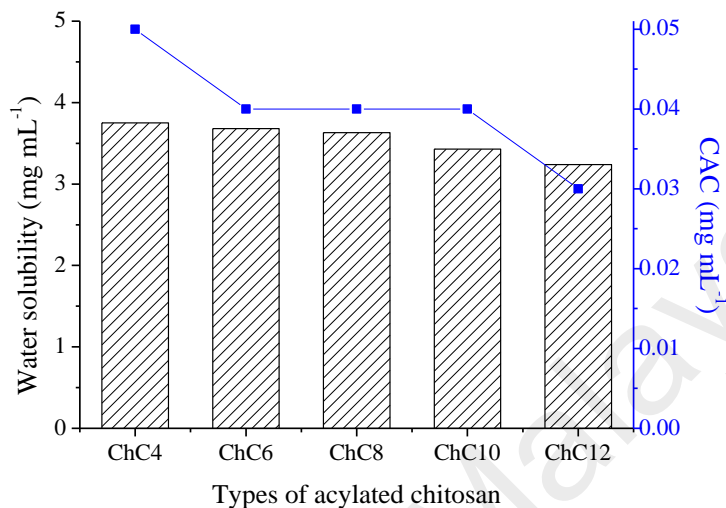


Figure 4.11: The linear relationship between water solubility and CAC of ChA.

The schematic illustration of ChA to form aggregates was presented in Figure 4.12(b). As illustrated in Figure 4.12(bi), ChA were unassociated at low concentration, thus no scattering was detected. As more polymer chains were introduced into the media as the concentration of ChA increased, the energetically unfavourable interaction with the aqueous environment facilitated the ease of the hydrophobic group of the polymer chain to approach closer and associate among each other (Figure 4.12(bii)). At a certain concentration as shown in Figure 4.12(biii), the hydrophobic interaction of ChA was adequate to induce the formation of aggregates and this concentration was called as critical aggregation concentration (CAC). Once CAC was achieved, the turbidity arised from the light scattering of the aggregates, which can be found from the point where the absorption near flat region started to increase. Further increase in concentration can increase the number of aggregates formed and resulted in higher light scattering as well as turbidity (Figure 4.12(biv)).

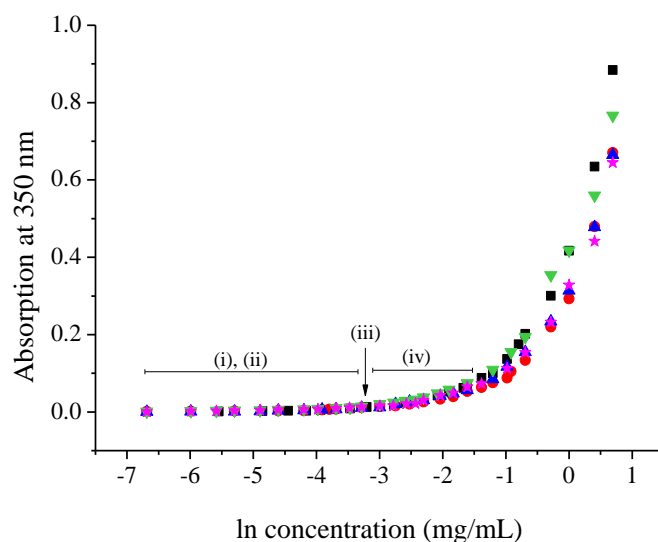


Figure 4.12: (a) Plot of absorption at 350 nm as a function of logarithm of concentration of ChC4 (■), ChC6 (●), ChC8 (▲), ChC10 (▼) and ChC12 (★).

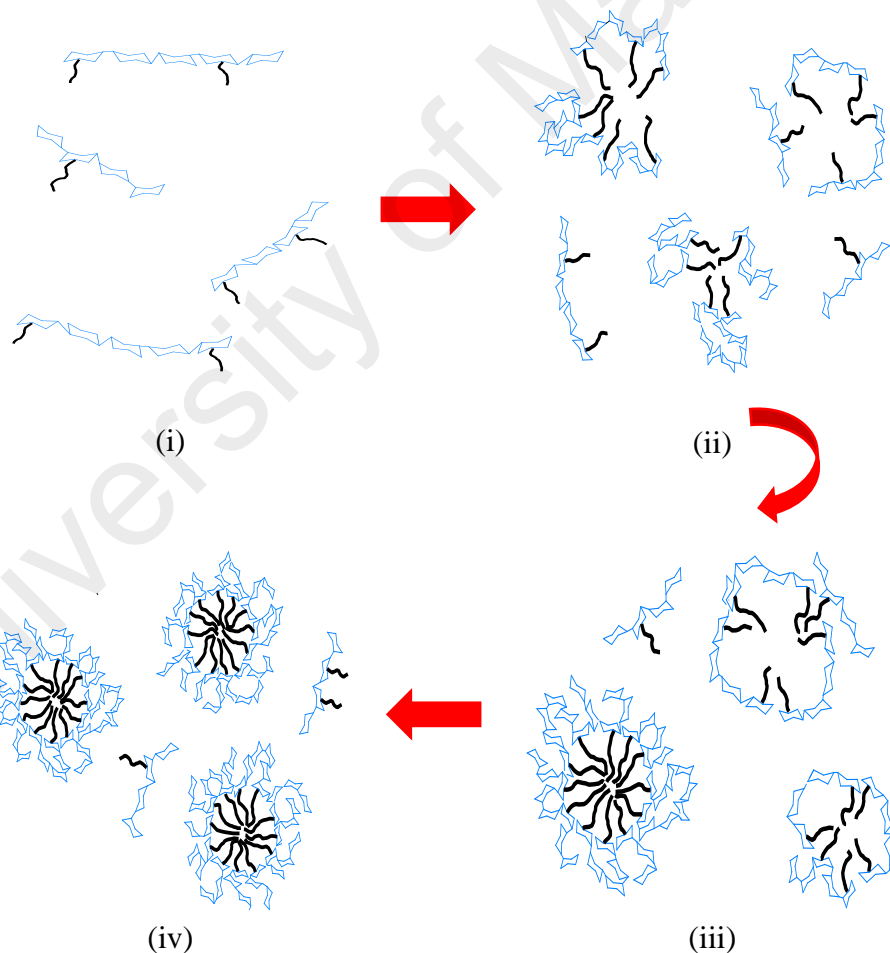


Figure 4.12(b): Schematic illustration of aggregates formation from ChA. (i) At low concentration, ChA appeared as individual polymer chains, (ii) as concentration increased, ChA started to associate among each other, (iii) aggregates formed from ChA at CAC, (iv) at higher concentration, more aggregates were formed.

4.2.8 Kinematic viscosity

The kinematic viscosity of the pure water in this study was $1.005 \text{ mm}^2 \text{ s}^{-1}$ and $0.366 \text{ mm}^2 \text{ s}^{-1}$ at $20 \text{ }^\circ\text{C}$ and $80 \text{ }^\circ\text{C}$, respectively, this result was close to the value obtained by Crittenden et al. (2012), which was $1.003 \text{ mm}^2 \text{ s}^{-1}$ ($20 \text{ }^\circ\text{C}$) and $0.364 \text{ mm}^2 \text{ s}^{-1}$ ($80 \text{ }^\circ\text{C}$), respectively. The kinematic viscosity values which presented in Figure 4.13 increased to $1.020 - 1.030 \text{ mm}^2 \text{ s}^{-1}$ at $20 \text{ }^\circ\text{C}$ and $0.480 - 0.540 \text{ mm}^2 \text{ s}^{-1}$ at $80 \text{ }^\circ\text{C}$, respectively after the addition of small amounts of Ch3 and ChA (1 g L^{-1}). It was found that the kinematic viscosity of Ch3 was slightly higher than ChA, this result did not coincide with the previous findings of Li et al. (2007b) and Rinaudo et al. (2005) in which dramatic increase of solution viscosity or gelation was observed in the hydrophobically modified high molecular weight chitosan which was attributed to the intermolecular aggregation of chitosan. As discussed in the aforementioned TGA analysis (section 4.2.6), ChA exhibited lower stability and resistance towards heat due to the disruption of hydrogen bonding between polymer chains by the alkyl group, this in turns decreased the hydrodynamic volume of polymer in the solvent as it became less polar and thus led to a reduction in viscosity and higher flexibility (Zhang et al., 2014).

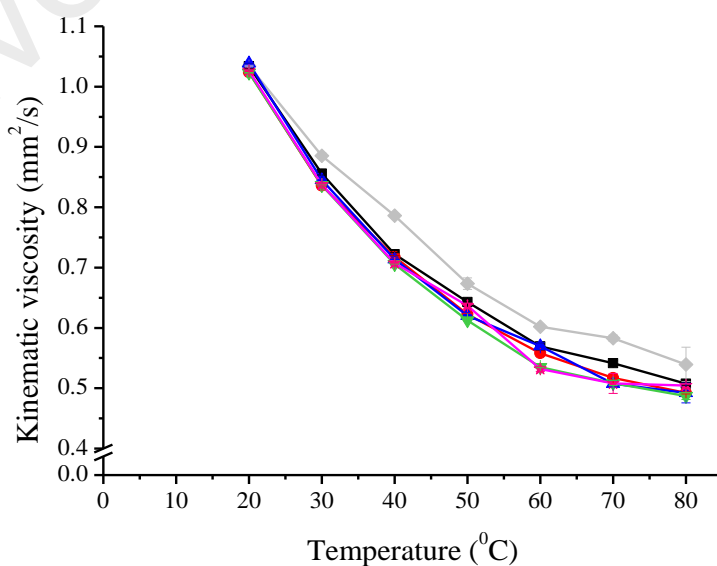


Figure 4.13: Kinematic viscosity of Ch3 (\diamond), ChC4 (\blacksquare), ChC6 (\bullet), ChC8 (\blacktriangle), ChC10 (\blacktriangledown) and ChC12 (\star) as a function of temperature.

4.2.9 Determination of swelling percentage

The swelling of Ch3 and ChA in deionised water and 0.1 mol dm^{-3} HCl solution were plotted in Figure 4.14. The ability of chitosan to absorb solvent to gain in volume are greatly influenced by the charged ions in the chitosan network. This explained chitosan showed higher swelling in 0.1 mol dm^{-3} HCl as compared to in deionized water as the protonation of amino group of chitosan as NH_3^+ ion in the acidic medium endowed the chitosan stronger polarity and hence showing higher affinity to bind water. Moreover, the charged amino group also led to the dissociation of hydrogen bonding which in turns can promote the hydration of chitosan by allowing more entrapment of water into the polymer network. As compared to Ch3, ChA demonstrated lower swelling ability in both water and acidic media. This observation was mainly attributed to the substitution of an alkyl group at the amino group of Ch3 reducing the hydrophilicity and hydrating capacity of acylated chitosan (Le Tien et al., 2003). Furthermore, the steric hindrance effect of the long alkyl chain of ChA disfavored the binding of chitosan with the polar medium, thereby the swelling of ChA decreased and exhibited the lowest weight gain in long chain acylated ChC12.

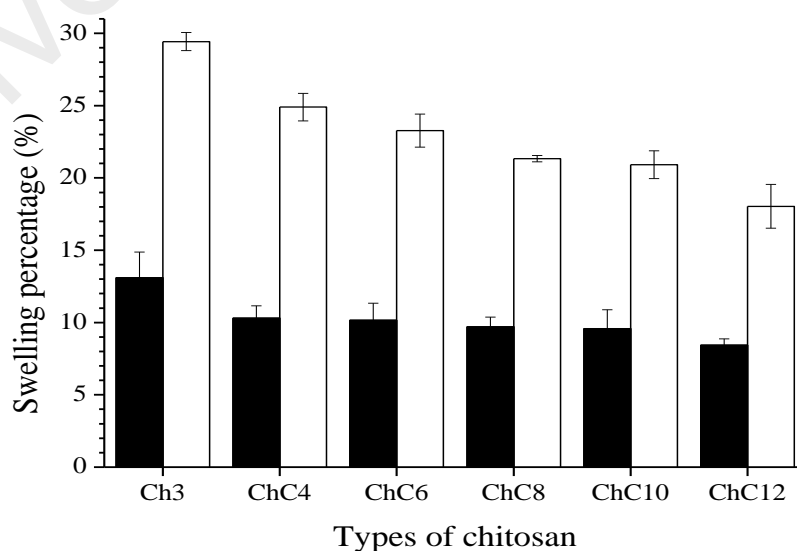


Figure 4.14: Swelling of Ch3 and ChA in (■) deionised water and (□) 0.1 mol dm^{-3} HCl solution at 37°C .

4.2.10 Transmission electron microscopy (TEM)

The backbones of chitosan consisting of carbon, hydrogen, nitrogen and oxygen atoms have low Z atomic number and resulting low contrast is observed under TEM as images produced by TEM are electrons dependence. Thus, staining agents containing high atomic number elements could be used to improve the image quality and contrast as their high charge can deflect the electrons towards the core and produce higher scattering intensity in the sample, for instance phosphotungstic acid (PTA, Z of tungsten = 74), gold ($Z = 79$) and uranyl acetate (Z of uranium = 92) (Monnier et al., 2015). This resulted in the area deposited with sample appearing dark, whereas those areas without sample appeared bright as more transmitted electrons was detected on the fluorescent imaging screen. In this study, PTA comprised of twelve high atomic number tungsten ($Z = 74$) was chosen for not only its electrostatic interaction between its negative charge with the cationic amino group of ChA (Quintarelli et al., 1971), but also its cost-effectiveness and availability.

The average particle size reported was measured from 30 particles of several micrographs and measured from the diameter of the particles as the arrows indicated in the micrographs in Figure 4.15(a-e). From Figure 4.15(a-b), the average particle size of ChC4 and ChC6 depicted was 180 – 200 nm and 170 – 240 nm respectively, it was smaller than those obtained by DLS, which were 296 nm for ChC4 and 282 nm and ChC6 respectively. This can be explained by the state of ChC4 and ChC6 exist during the sample analysis. For DLS measurement, the size was measured from the hydrodynamic radius of all the swollen particles in the sample after solvent penetration included aggregated particles. On the other hand, TEM presented the geometric size of the particles in dry form.

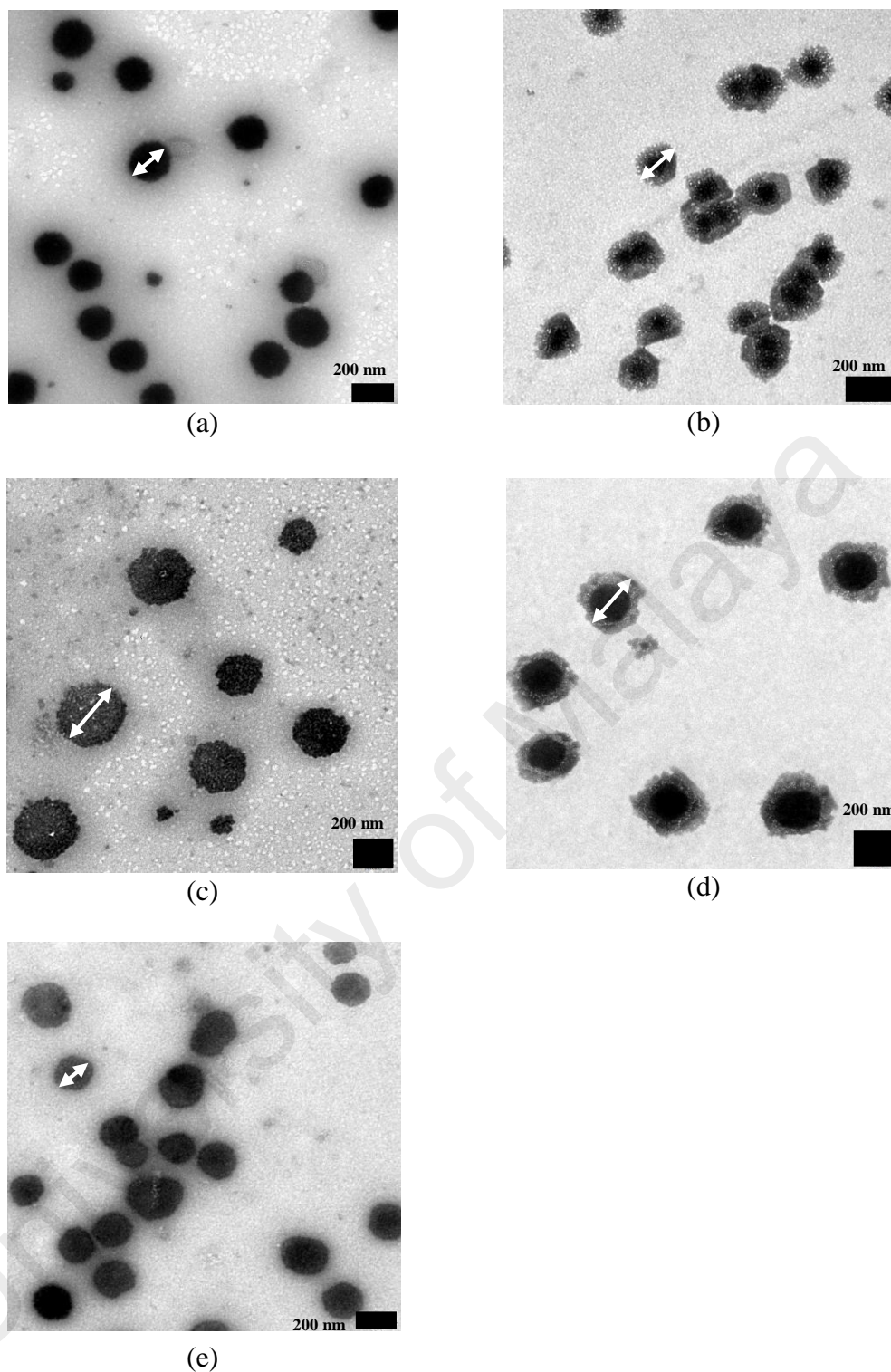


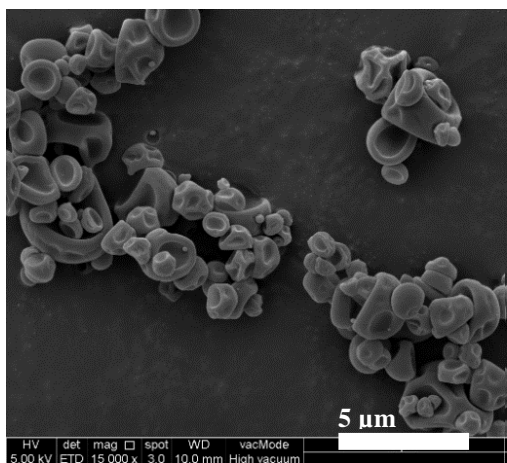
Figure 4.15: TEM micrographs of (a) ChC4, (b) ChC6, under magnification of 10,000 \times , (c) ChC8, (d) ChC10 and (e) ChC12 under magnification of 8,000 \times . The scale shown was 200 nm. The arrow indicated in the micrographs was the diameter measured for the calculation of average particle size.

Unlike ChC4 and ChC6, the particle size of longer chain acylated ChC8, ChC10 and ChC12 in TEM micrographs were 280 – 320 nm, 270 – 330 nm and 200 – 260 nm respectively (Figure 4.15(c-e)). This was close to the value obtained by DLS, which were

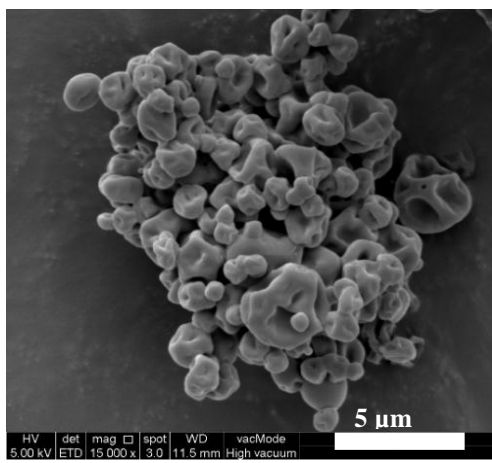
286 nm, 281 nm and 234 nm for ChC8, ChC10 and ChC12 respectively. This was plausibly explained by the larger space occupancy of longer alkyl groups in the core which could resist shrinkage better during drying. The particles in Figure 4.15(b) and (d) exhibited colour contrast in the core and peripheral region, this could be due to thickness contrast. The electron scattering intensity was increased as the electrons travelled in a longer distance and had more interaction in the thicker area at the centre, thereby reducing the amount of transmitted electrons. This resulted in the thick central area of the particles appearing darker than the thinner area at the peripheral.

4.2.11 Field-emission scanning electron microscopy (FE-SEM)

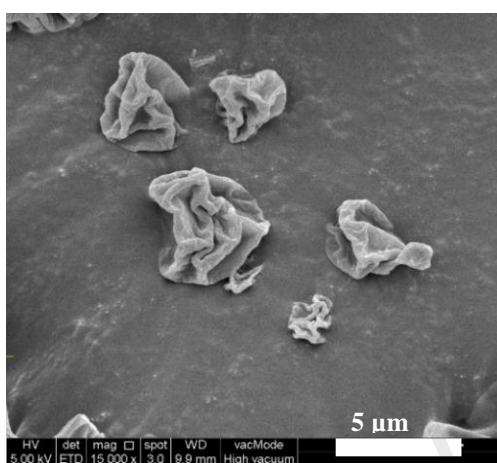
Figure 4.16(a-f) depicted Ch3 and ChA as spherical in shape with a smooth but indented surface. During spray drying, heating caused the water to be removed from the particles rapidly and hence led to indented particles, this was consistent with the morphology of spray-dried chitosan microspheres in previous studies (Harris et al., 2011; He et al., 1999). There were at least 30 particles taken into consideration to calculate the average size of the particles. The diameter of Ch3 as presented in Figure 4.16(a) was approximately 1 – 2 μm , the size was similar to ChC4 in Figure 4.16(b). The average particle size increased to 4 – 5 μm after acylation with hexanoyl group (Figure 4.16(c), whereas ChC8, ChC10 and ChC12 showed average particle size of 5 – 6 μm (Figure 4.16(d-f). It can be deduced that the longer hydrophobic domain of longer chain ChA possessed higher resistance strength towards shrinkage during heating, similar to the observations in TEM (section 4.2.10). The coalescence between particles was observed in smaller particles of Ch3 and ChC4 (Figure 4.16(a) and (b) which was presumably caused by the smaller hydrodynamic volume promoted layer adhesion when susceptible to heat during spray drying as described in the aforementioned kinematic viscosity analysis (section 4.2.8). The hollow capacity inside the core of ChA revealed the capability of the spherical particles for drug encapsulation within it.



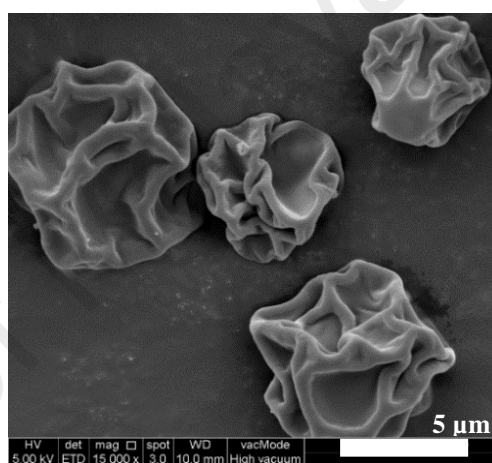
(a)



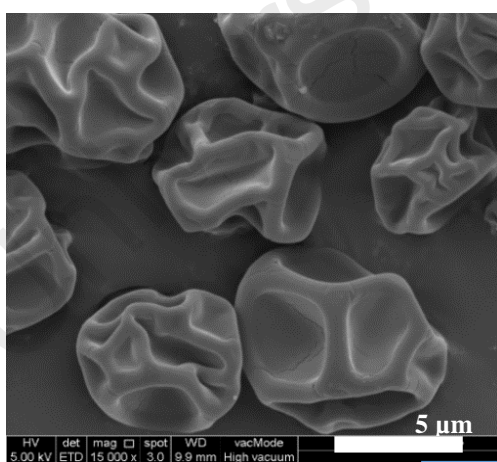
(b)



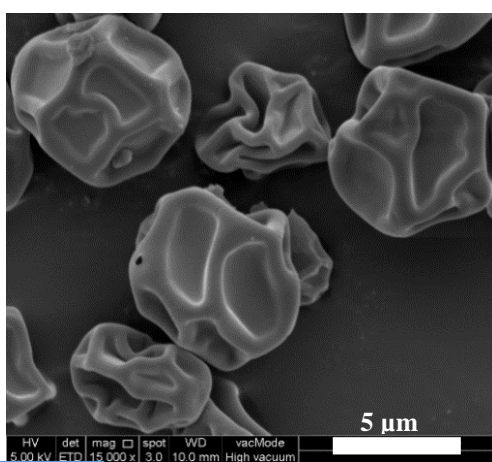
(c)



(d)



(e)



(f)

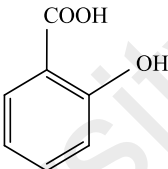
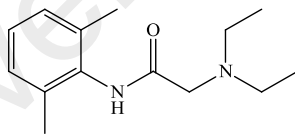
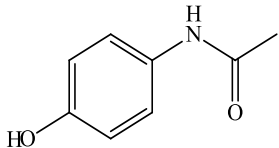
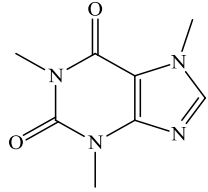
Figure 4.16: FE-SEM micrographs of (a) Ch3 (b) ChC4, (c) ChC6, (d) ChC8, (e) ChC10 and (f) ChC12 under magnification of 15k \times at 5 kV voltage. The scale bar shown was 5 μ m.

4.3 Characterizations of drugs loaded ChA

4.3.1 Encapsulation efficiency (EE) and drug loading (DL)

The four analgesic drugs with different solubilities namely salicylic acid (SA: 2.0 g L⁻¹), lidocaine (LID: 3.0 g L⁻¹), acetaminophen (ACE: 10.8 g L⁻¹), caffeine (CAF: 20.5 g L⁻¹) were employed to be encapsulated by ChA via precipitation, where the drug solubilities are categorized following United States Pharmacopeia (USP) and British Pharmacopeia (BP) (Table 4.5(a), which is based on the amount of solvent need for the dissolution of 1 g of solute (Table 4.5(b) (Savjani et al., 2012). The encapsulation of the slightly soluble SA and LID was carried out at their respective maximum solubilities.

Table 4.5(a): Chemical structure, molecular formula and weight and also solubility of salicylic acid (SA), lidocaine (LID), acetaminophen (ACE) and caffeine (CAF) which were used to be encapsulated by ChA.

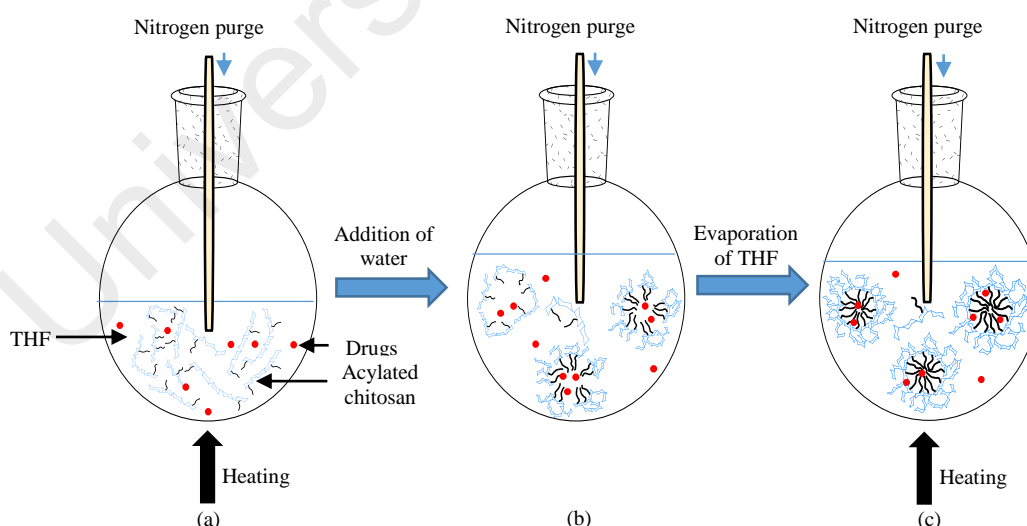
Drugs	Chemical Structure	Molecular formula	Molecular weight (g mol ⁻¹)	Experimental solubility (g L ⁻¹)	*Literature solubility (g L ⁻¹)
Salicylic acid (SA)		C ₇ H ₆ O ₃	138.12	2.0 (slightly soluble)	2.24
Lidocaine (LID)		C ₁₄ H ₂₂ N ₂ O	234.34	3.0 (slightly soluble)	4.1 (at 30 °C)
Acetaminophen (ACE)		C ₈ H ₉ NO ₂	151.16	10.8 (sparingly soluble)	14.0
Caffeine (CAF)		C ₈ H ₁₀ N ₄ O ₂	194.19	20.5 (sparingly soluble)	21.6

*The literature solubility value was determined at 25 °C (unless mentioned) by Wishart et al. (2016).

Table 4.5 (continued)**Table 4.5(b):** Amount of solvent need for the dissolution of 1 g of solute.

Solubility	Amount of solvent need (mL)
Very soluble	Less than 1
Freely soluble	1 to 10
Soluble	10 to 30
Sparingly soluble	30 to 100
Slightly soluble	100 to 1000
Very slightly soluble	1000 to 10000
Practically soluble	More than 10000

The dielectric constant (ϵ) of THF and water are 7.39 and 78.48 at 25 °C respectively. As more water was added into the ChA containing drug which is dispersed in THF, the dielectric constant of the binary solvents mixture increased (ϵ_{mix}) to 71.76 when the water added is 90% of the mixture, as previously studied by Critchfield et al. (1953). This results in the destruction of the hydrophobic interaction between THF and alkyl groups of ChA, and instead promoted the hydrophobic association between the polymer chains of ChA (Patnaik, 2012). THF removal via heating and nitrogen agitation facilitated the diffusion of ChA and drugs into the aqueous media, therefore trapping the drug while ChA was precipitating (Figure 4.17).

**Figure 4.17:** Schematic illustration of the drug encapsulation of ChA by precipitation.

- ChA exist as individual chains when dispersed in THF containing drugs.
- The addition of water into the dispersion promoted the hydrophobic association between the polymer chains of ChA.
- The removal of THF facilitated the diffusion of ChA and drugs into the aqueous media and hence trapping the drug while ChA was precipitating.

Among the four types of drugs chosen, SA exhibited the highest EE in ChA at 92 – 95%, followed by LID (62 – 73%), ACE (36 – 39%) and CAF (30 – 32%) (Figure 4.18(a-d) at weight ratio of ChA to drugs at 10:1. Even though the solubility of LID was slightly lower than SA, LID showed at least 20% lower EE than SA. This was presumably due to the positive charge of LID being electrostatically repelled by the cationic chitosan. The higher EE of SA and LID compared to sparingly soluble drugs like ACE and CAF was conferred to the lower solubility of SA and LID compared to ACE and CAF, thus SA and LID tend to reside in the hydrophobic core of ChA during removal of THF. On the contrary, sparingly soluble ACE and CAF prefer to move along with water and is not encapsulated at high efficiency (Govender et al., 1999; Lince et al., 2011). The EE of SA by different ChA in Figure 4.18(ai) were similar and decreased from 92 – 95% to 33 – 36% as the weight ratio of ChA to SA was increased from 10:1 to 10:4. This decrease in EE could plausibly be explained by the close solubility value of SA and ChA at 2.0 g L^{-1} and $3.24 - 3.75 \text{ g L}^{-1}$ respectively, limiting the ability of ChA to take up SA in their matrix. Similar results on the decrease in EE followed by the loading of high amounts of the hydrophobic drugs into HMC were also reported in the previous studies (Chen et al., 2011b; Kim et al., 2006b; Wang et al., 2007). The maximum DL of SA was achieved at 10:2 weight ratio and then decreased as more SA was added (Figure 4.18(bi)).

EE of LID as shown in Figure 4.18(aii) was also decreased as the weight ratio increased, but the decrease was not as dramatic as exhibited by SA. For instance, as the weight ratio varied from 10:1 to 10:4, the difference of EE of SA using ChC4 at 55% was higher than the decrease of EE for LID at 12%. For sparingly soluble ACE and CAF, EE of ChC4 and ChC6 decreased from 39% to 34% for ACE (Figure 4.18(aiii)) and 32% to 27% for CAF (Figure 4.18(aiv)) respectively from 10:1 to 10:7. ChC8 demonstrated highest EE of ACE and CAF at 10:3 and 10:4 respectively, whereas longer chain acylated ChC10 and ChC12 achieved highest EE at higher weight ratio of ChA to drugs, which

were at 10:5 for ACE (Figure 4.18(aiii)) and around 10:4 and 10:5 for CAF (Figure 4.18(aiv)) individually. This was attributed to their less compact packing structure which was more flexible to accommodate higher amount of drugs as a consequence of higher extent of hydrogen bonding disruption by the longer chain as discussed in XRD (section 4.2.5) and TGA (section 4.2.6). Previous studies also found that the longer chain length of acylated chitosan which possessed stronger hydrophobic interaction and higher partition coefficient revealed higher loading efficiency on both hydrophobic cyclosporine A and hydrophilic vitamin C (Chen et al., 2008; Cho et al., 2012b). Unlike hydrophobic SA, the DL of LID, ACE and CAF were increased for increased addition of drugs (Figure 4.18(bii), (biii) and (biv)) as their higher solubility may enhance their interaction with polar THF and water during precipitation of ChA.

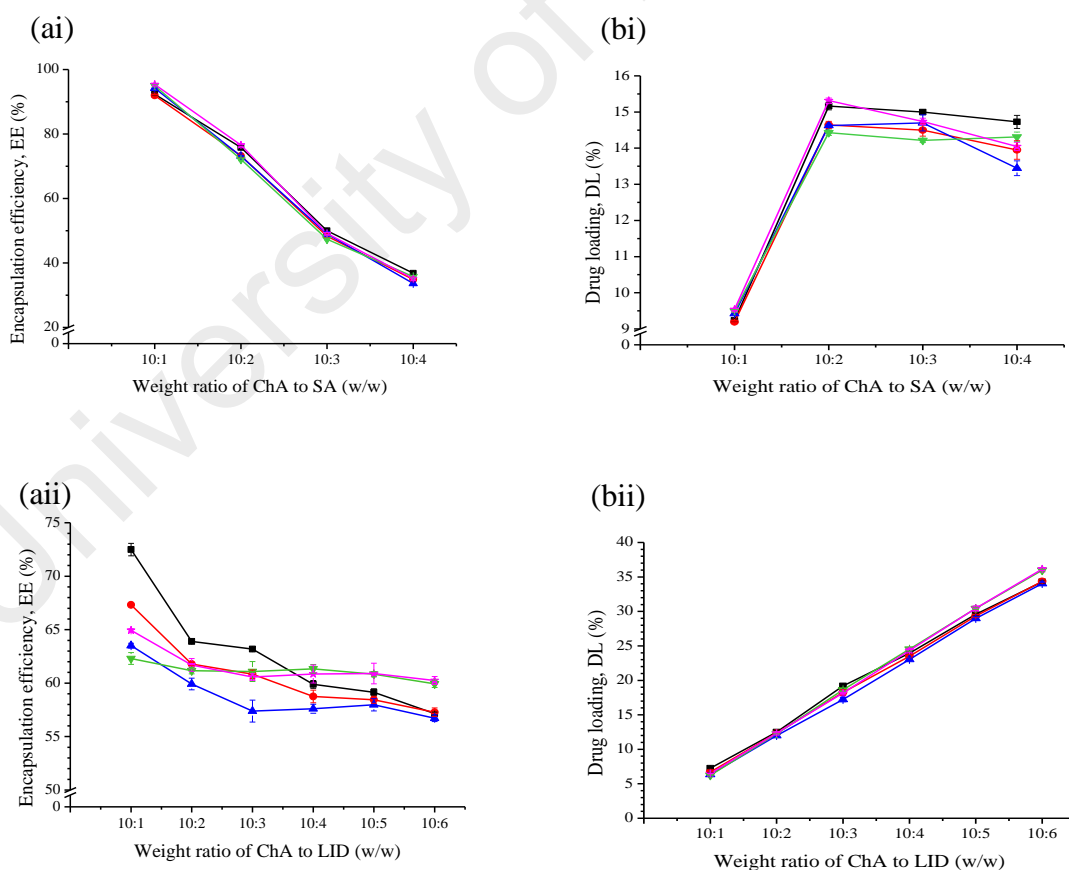
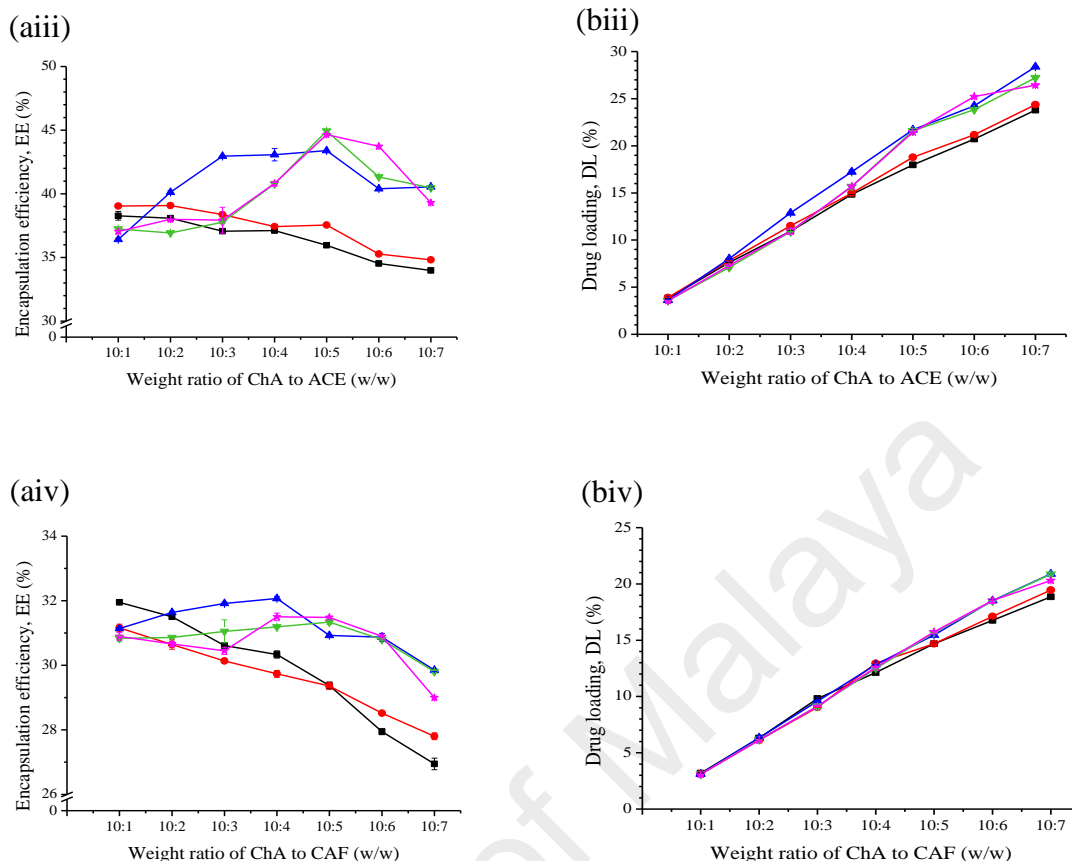


Figure 4.18: (a) EE and (b) DL of (i) SA, (ii) LID, (iii) ACE and (iv) CAF using ChC4 (■), ChC6 (●), ChC8 (▲), ChC10 (▼) and ChC12 (★) by precipitation

Figure 4.18 (continued)



4.3.2 FTIR spectroscopy

FTIR was employed to study the interaction between ChA and drugs prepared via precipitation by examining the shift or intensity change in peak absorption, as discussed in the following subtopics 4.3.2.1 – 4.3.2.4 for ChA loaded with SA, LID, ACE and CAF respectively, together with a physical mixture of ChA and drug for comparison.

4.3.2.1 FTIR spectroscopy of SA loaded ChA

The spectra of SA, ChA and physical mixture of ChA and SA was present in Figure 4.19. The characterized peaks of SA included OH stretching and C=O bond of carboxylic acid at 3435 cm^{-1} and 1659 cm^{-1} respectively. The out-of-plane CH vibration of the phenol of SA appeared around $900 - 650\text{ cm}^{-1}$ (Figure 4.19(b) (He et al., 2011)).

As compared to the physical mixture of ChA and SA at 1655 cm^{-1} , SA loaded ChA showed wavenumber shifted to a lower frequency at 1633 cm^{-1} which is attributed to the formation of hydrogen bonding between amide I of ChA and the carbonyl stretching of SA (Figure 4.19(d-h)) (Peniche et al., 1998; Barry et al., 1976). The decrease of the peak intensity of SA loaded ChA around 1556 cm^{-1} possibly due to the formation of hydrogen bonding from the interaction of NH of amide II stretching of ChA with carbonyl of SA ($\text{C}=\text{O}\cdots\text{N}-\text{HCOCH}_2\text{CH}_2\text{CH}_3$) decreased the availability of the NH of amide II to be scanned. On the contrary, physical mixture of ChA and SA in Figure 4.19(c) showed a peak at 1569 cm^{-1} which can be plausibly explained by the electrostatic forces between positively charged amino groups of ChA and negatively charged carboxylate ions of SA (Peniche et al., 1998). The vibration band of phenol-OH of SA at 1384 cm^{-1} was observed to be higher in SA loaded ChA than in the physical mixture as the intermolecular interaction between ChA and phenol in SA loaded ChA was stronger. The interruption of hydrogen bonding between chitosan chains after loading of SA resulted in the region around $3435 - 3431\text{ cm}^{-1}$ in SA loaded ChA being more narrow as the availability of hydroxyl groups of ChA to form hydrogen bonding with air moisture was reduced (Jiang et al., 2012). Unlike the physical mixture which exhibited clear individual peaks close to the spectrum of SA, the peaks of SA were partially shielded in the observed spectrum of SA loaded ChA as SA was presumably incorporated inside ChA. The result from FTIR revealed that hydrogen bonding was the main interaction formed between SA and ChA using precipitation.

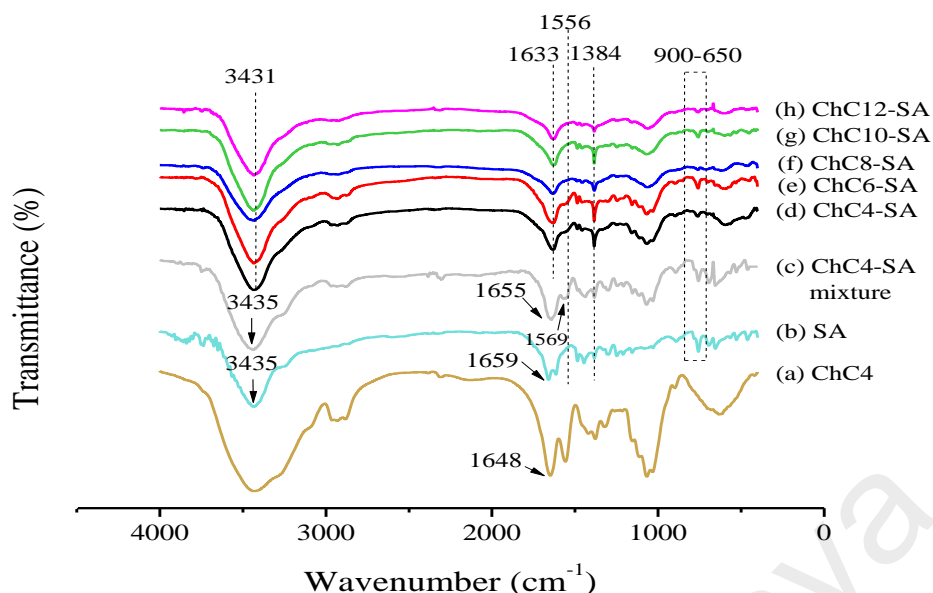


Figure 4.19: FTIR spectrum of (a) ChC4, (b) SA, (c) physical mixture of ChC4 and SA, SA loaded using (d) ChC4, (e) ChC6, (f) ChC8, (g) ChC10 and (h) ChC12.

4.3.2.2 FTIR spectroscopy of LID loaded ChA

The assignment of the LID peaks in FTIR spectrum in Figure 4.20(b) were as follow: 3248 cm^{-1} as NH stretching of secondary amide, 3022 cm^{-1} as CH stretching of benzene ring, 3003 – 2769 cm^{-1} as CH_2 and CH_3 stretching, 1666 cm^{-1} as C=O stretching of amide, 1597 cm^{-1} and 1497 cm^{-1} as C=C stretching and bending of aromatic ring, 1208 cm^{-1} as C–N stretching of amide and 765 cm^{-1} as CH_3 wagging (Badawi et al., 2015). As presented in Figure 4.20(c), the physical mixture appeared similar to the spectrum of superimposition of ChA (Figure 4.20(a) and LID (Figure 4.20(b). Unlike the physical mixture of ChA and LID which showed the carbonyl stretching of free LID at 1666 cm^{-1} , the peak was shifted to 1629 cm^{-1} in ChC4 and ChC6 (Figure 4.20(d-e), this suggests that there are some interaction between ChA and LID. Additionally, the frequency was shifted to a higher value at 1630 cm^{-1} in ChC8, 1634 cm^{-1} in ChC10 and 1637 cm^{-1} in ChC12 (Figure 4.20 (f-h). The shift to a lower frequency from the initial 1666 cm^{-1} after encapsulation by ChA could be due to the change of electronegativity of neighbouring atoms for possible formation of hydrogen bonding, in which the interaction between the

highly electronegative oxygen atoms of carbonyl group of LID and amide I of ChA decrease the bond length and hence lower the wavenumber.

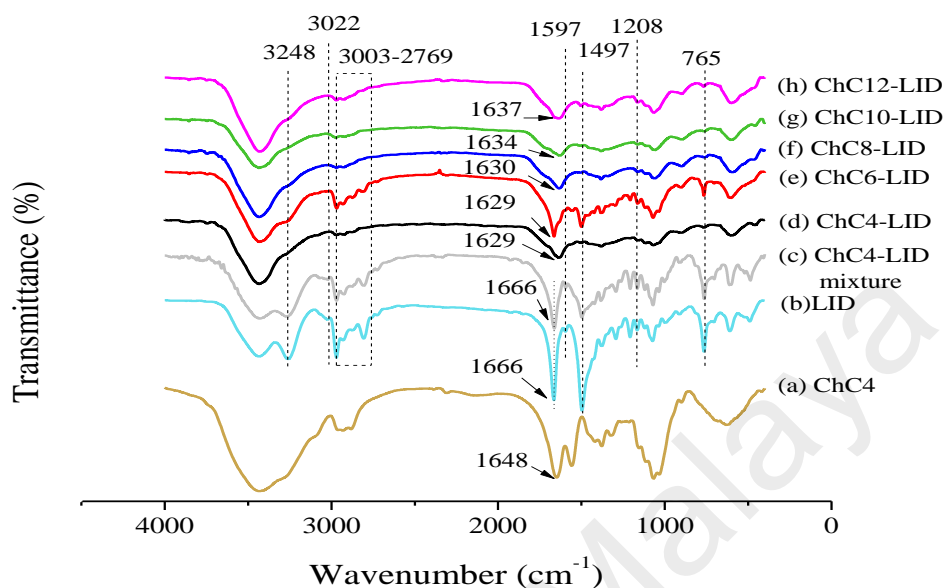


Figure 4.20: FTIR spectrum of (a) ChC4, (b) LID, (c) physical mixture of ChC4 and LID, LID loaded using (d) ChC4, (e) ChC6, (f) ChC8, (g) ChC10 and (h) ChC12.

4.3.2.3 FTIR spectroscopy of ACE loaded ChA

As described by “para-” in paracetamol which is the common name of ACE, ACE possessed substituents at the 1,4 position of the aromatic ring. The featured absorption peaks of ACE in Figure 4.21(b) are O–H stretching at 3432 cm^{-1} , N–H stretching at 3328 cm^{-1} , C=O at 1653 cm^{-1} , N–H amide bending at 1564 cm^{-1} , C=C stretching of aromatic ring at 1613 cm^{-1} , 1508 cm^{-1} and 1440 cm^{-1} , C–O and C–N at $1259 - 1226\text{ cm}^{-1}$, CH bend of para-di-substituted at 837 cm^{-1} (Burgina et al., 2004; Wang et al., 2002). After ACE was encapsulated by ChA via precipitation, the most pronounced change was the shift of ACE from 1653 cm^{-1} to a lower frequency at 1635 cm^{-1} in ChC4, 1632 cm^{-1} in ChC6, 1639 cm^{-1} in ChC8, 1637 cm^{-1} in ChC10 and 1636 cm^{-1} in ChC12 (Figure 4.21(d-h)) as a possible consequence of the hydrogen bonding between the carbonyl of ACE and amide I of ChA. The peak at 1564 cm^{-1} which was presented in the physical mixture of ACE and ChA (Figure 4.21(c)) disappeared in the ACE loaded ChA, this may be attributed to

the disappearance of intermolecular N–H amide bonding of ACE molecules as ACE was incorporated into ChA. The physical mixture presented some peaks at the same wavenumber as the overlapping of the peaks of ACE and ChA. On the contrary, these peaks were shifted in ACE loaded ChA via precipitation, for instance, 1508 cm^{-1} of ACE (C=C of benzene ring) shifted to 1513 cm^{-1} , proposing some hydrophobic Van der Waals interaction between the benzene ring and alkyl groups of ChA. The peaks around 1259 – 1226 cm^{-1} of ACE (C–O, C–N) which appeared as a few small peaks in the physical mixture were observed as a broad peak around region 1260 – 1237 cm^{-1} in ACE loaded ChA prepared via precipitation technique. This suggests that the C–O and C–N of ACE were involved in the interaction with ChA for drug encapsulation.

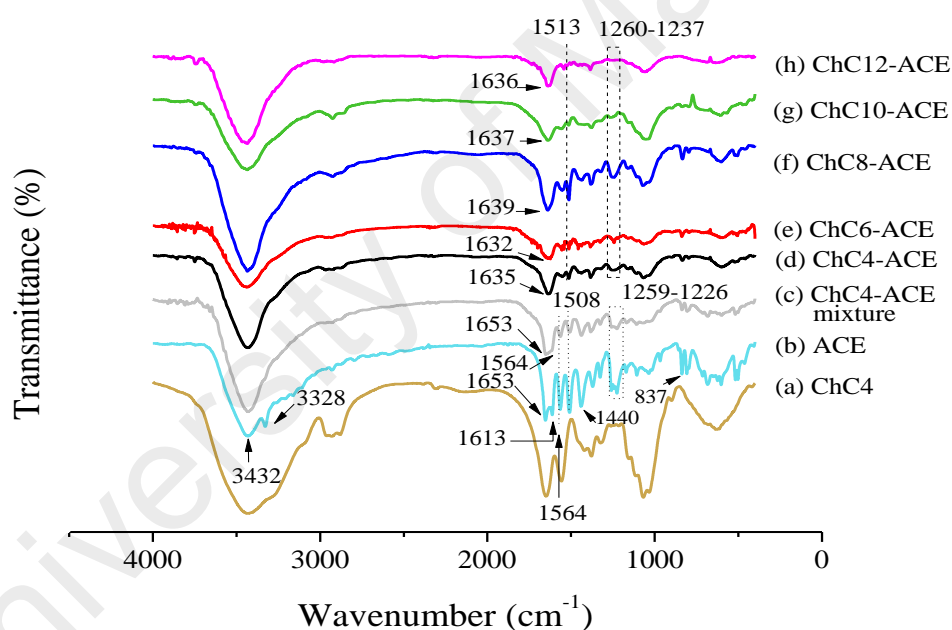


Figure 4.21: FTIR spectrum of (a) ChC4, (b) ACE, (c) physical mixture of ChC4 and ACE, ACE loaded using (d) ChC4, (e) ChC6, (f) ChC8, (g) ChC10 and (h) ChC12.

4.3.2.4 FTIR spectroscopy of CAF loaded ChA

CAF is an alkaloid which consisting of aromatic five-membered imidazole and six-membered pyrimidine containing two nitrogen atoms each. The assignments of CAF vibrations in the FTIR spectrum in Figure 4.22(bi) were CH stretching at 3111 cm^{-1} , symmetric CH_3 stretching at 2957 cm^{-1} , asymmetric and symmetric C=O stretching at

1701 cm^{-1} and 1658 cm^{-1} , C=N stretching at 1549 cm^{-1} , C=C stretching at 1484 cm^{-1} , CH_3 bend at 1455 cm^{-1} , N- CH_3 stretching at 1358 cm^{-1} , C-C stretching at 1285 cm^{-1} , CH_3 rocking at 1186 cm^{-1} , in-plane CH_3 rocking at 1024, CH wagging at 898 cm^{-1} , N-C-N stretching at 758 cm^{-1} and N- CH_3 at 745 cm^{-1} (Figure 4.21(bi)) (Prabu et al., 2015; Silverstein et al., 2014; Paradkar & Irudayaraj, 2002).

There were some peaks of CAF shown in both the physical mixture and when encapsulated by the precipitation after the addition of ChC4, these peaks appeared at 3111 cm^{-1} as CH stretching, 1549 cm^{-1} as C=N stretching, 1484 cm^{-1} as C=C stretching and 1285 cm^{-1} as C-C stretching in Figure 4.22(c-h). The shift observed in physical mixture was 1658 cm^{-1} of asymmetric and symmetric C=O stretching of CAF to 1652 cm^{-1} . Similarly, ChC4 loaded with CAF demonstrated a more profound shift of the same peak to a lower wavenumber at 1650 cm^{-1} in ChC4 and ChC6, 1641 cm^{-1} in ChC8 and ChC10, 1644 cm^{-1} in ChC12 (Figure 4.22(d-h), which may be attributed to the hydrogen bonding of C=O of CAF and amide I of ChA. The absorption peak at 1701 cm^{-1} of CAF also shifted to 1704 cm^{-1} in CAF loaded ChA. In addition, van der Waals forces could contribute to the entrapment of CAF by ChA as there were some wavenumber shifts in the peaks of non-polar groups. First was the CH_3 stretching of CAF at 2957 cm^{-1} shifted to 2963 cm^{-1} in ChA loaded CAF, the second was 1024 cm^{-1} assigned to in-plane CH_3 rocking of CAF shifted to 1067 – 1062 cm^{-1} in ChA. This suggests that CAF was encapsulated by ChA via formation of hydrogen bonding between the carbonyl of CAF and amide I of ChA and also van der Waals forces between the hydrophobic methyl groups of CAF and alkyl chains of ChA.

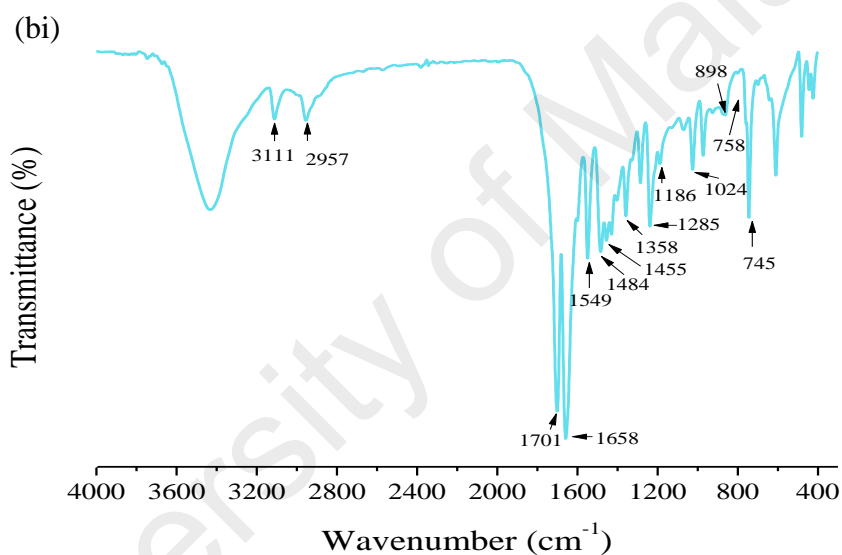
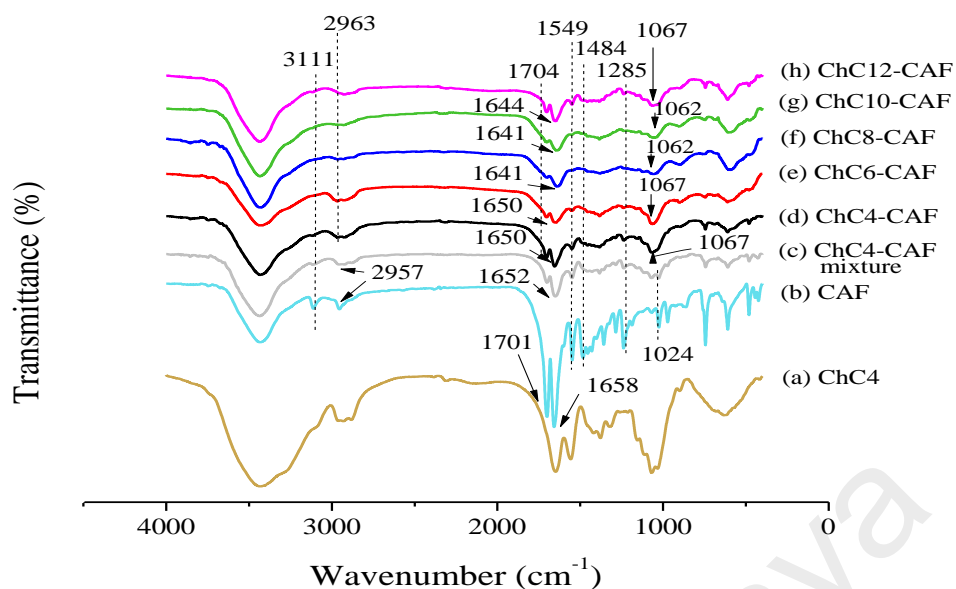


Figure 4.22: FTIR spectrum of (a) ChC4, (b) CAF, (c) physical mixture of ChC4 and CAF, CAF loaded using (d) ChC4, (e) ChC6, (f) ChC8, (g) ChC10 and (h) ChC12. (bi) is the FTIR spectrum of CAF with full label.

From the FTIR spectra of the four drugs and ChA by solvent-aid entrapment (precipitation) and physical mixture, the physical mixture showed the peaks as the overlapping of ChA and drugs without wavenumber change or less shift in wavenumber. The peak appeared less intense in drugs loaded ChA compared to the physical mixture as the drugs were entrapped by ChA and shielded from being scanned. In addition, the most prominent change in solvent-aid entrapment was the wavenumber shift of the carbonyl

stretching of drug to lower frequency. This proposes that the formation of hydrogen bonding of ChA and drugs change the electronegativity of the neighbouring atoms and hence shorten the bond length. Besides the hydrogen bonding, Van der Waals may also form between ChA and drugs, as observed in neutral ACE and CAF. The presence of solvent could promote the interaction between the drugs and ChA during precipitation, in which such interaction is important and could contribute to their release behavior in *in vitro* drug release study which will be discussed in section 4.4.

4.3.3 Particle size

The particle size of drugs loaded ChA was plotted in Figure 4.23(ai)-(aiv) and the change of particle size of ChA after loading at 10:4 were presented in Figure 4.24. As shown in Figure 4.24, the particle size of ChA was increased after loading with SA and LID, whereas the size of ChA loaded with ACE and CAF was slightly increased or was smaller than the unencapsulated ChA. The particle size of ChC4 after drug loading was decreased in the order of SA, LID, ACE and CAF at 540 nm, 471 nm, 379 nm and 292 nm respectively at weight ratio of 10:4. There were two possibilities to explain the observations, first was due to the higher EE of hydrophobic drugs such as SA and LID, second was possibly explained by the hydrophobic drugs loaded within the core of the ChA, resulting in higher volume expansion of ChA. The increment of particle size of SA and LID was higher in ChC4 and ChC6 compared to the longer chain ChC10 and ChC12 as the chitosan of shorter chain length was less flexible to load drugs with stronger hydrogen bonding, thus the incorporation of the drug molecules led to higher volume expansion.

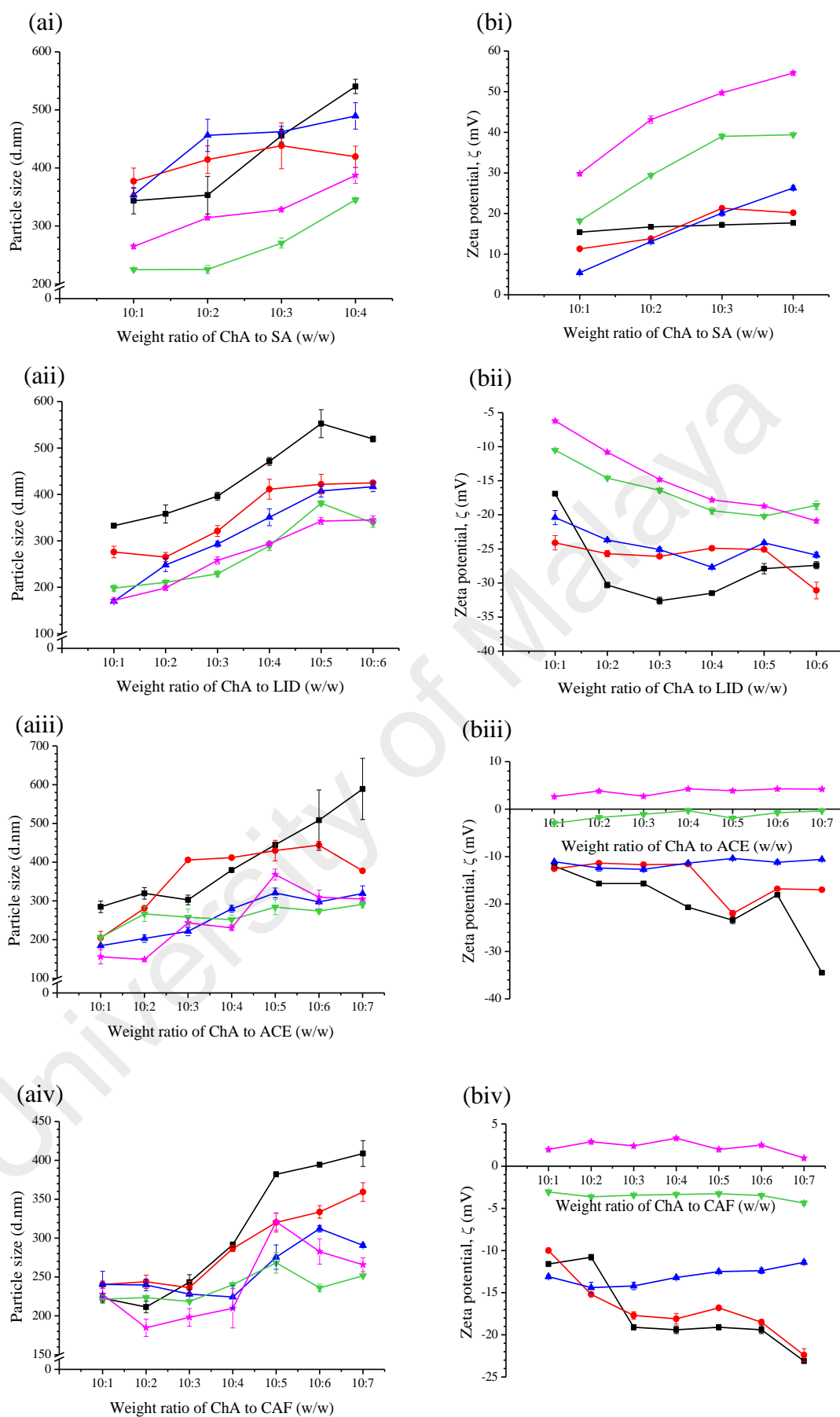


Figure 4.23: (a) Particle size and (b) zeta potential of (i) SA, (ii) LID, (iii) ACE, (iv) CAF after loading using ChC4 (■), ChC6 (●), ChC8 (▲), ChC10 (▼) and ChC12 (★) at different weight ratio.

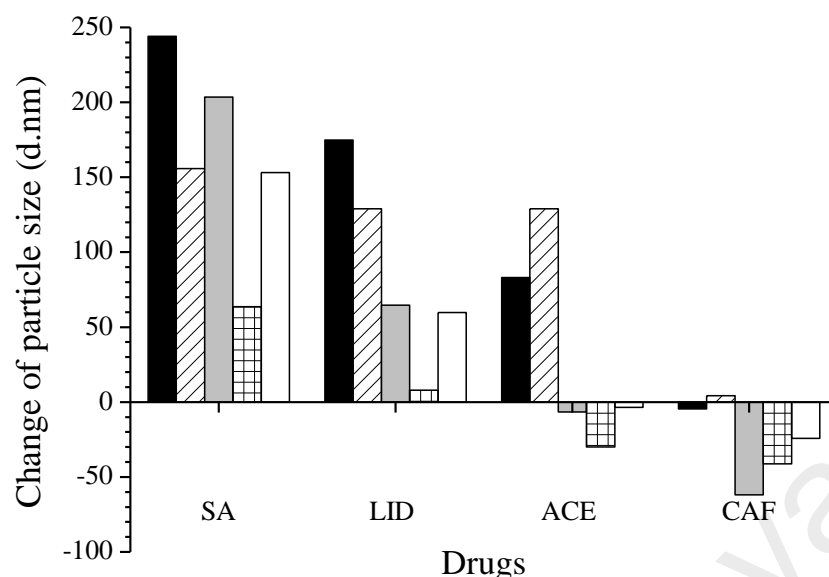


Figure 4.24: The change of particle size of ChC4 (■), ChC6 (▨), ChC8 (■), ChC10 (▤) and ChC12 (□) correspond to the loading of drugs at 10:4 weight ratio.

4.3.4 Zeta potential

Zeta potential which measures the electrostatic potential of the particle was changed after drug loading, as presented in Figure 4.23(bi)-(biv). ChA (-7.57 to -0.324 mV) shifted to positive zeta potential value after loading with SA and became more positive as the amount of SA was increased. This is presumably attributed to the protons from the dissociation of the excess SA in the solution as the pKa of SA is 2.97 (Wishart et al., 2006). On the contrary, the zeta potential of ChA was shifted to more negative value (-6.21 to -24.1 mV) for the encapsulation of LID and to even more negative potential at a higher amount of LID. As the pKa of LID is 8.01, excessive LID exists as the basic compound gives negative zeta potential (Wishart et al., 2006). Despite the equal amount of cations and anions on the ACE imparting it as a zero net charge molecule, anions are more strongly adsorbed than cations as they have greater polarizability as well as lower hydration (Popiel, 1978). As a result, the zeta potential of ACE loaded ChA was negative. The double bond between N and C atoms in planar aromatic sp^2 hybridization orbital in CAF resulted in the two amide groups existing predominately as zwitterionic resonance structure (Figure 4.25) and weakly basic at pKa around 0.6 when ionized in water

(Yaneva et al., 2015), thereby giving negative zeta potential value. The zeta potential of medium chain acylated ChC8, ChC10 and ChC12 do not differ significantly for the drug loading with zero net charge ACE and CAF as the added drugs were increased. This could be attributed to their looser structure to accommodate drugs without causing much change in zeta potential.

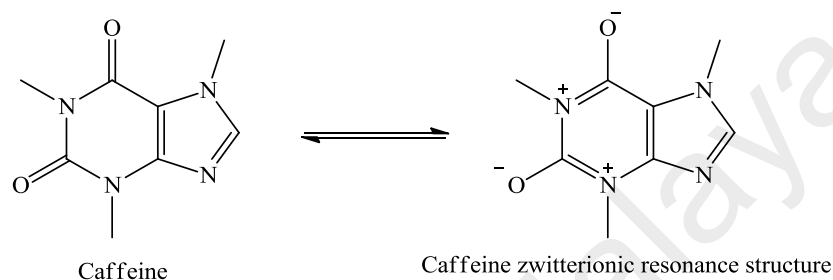


Figure 4.25: Zwitterionic resonance structures of CAF with weakly basic properties.

4.3.5 Transmission electron microscopy (TEM)

ChA loaded with SA, LID, ACE and CAF were observed under transmission electron microscope to study their morphology and particle size. The TEM micrographs of ChA loaded with SA, LID, ACE and CAF were presented in Figure 4.26, 4.27, 4.28 and 4.29 respectively. As shown in Figure 4.26 – 4.29, ChA maintained their spherical shape after loading with both slightly and sparingly water soluble drugs. Due to the thickness contrast as discussed in section 4.2.10, ChA appeared darker in the core compared to the area at the peripheral.

4.3.5.1 TEM micrographs of SA loaded ChA

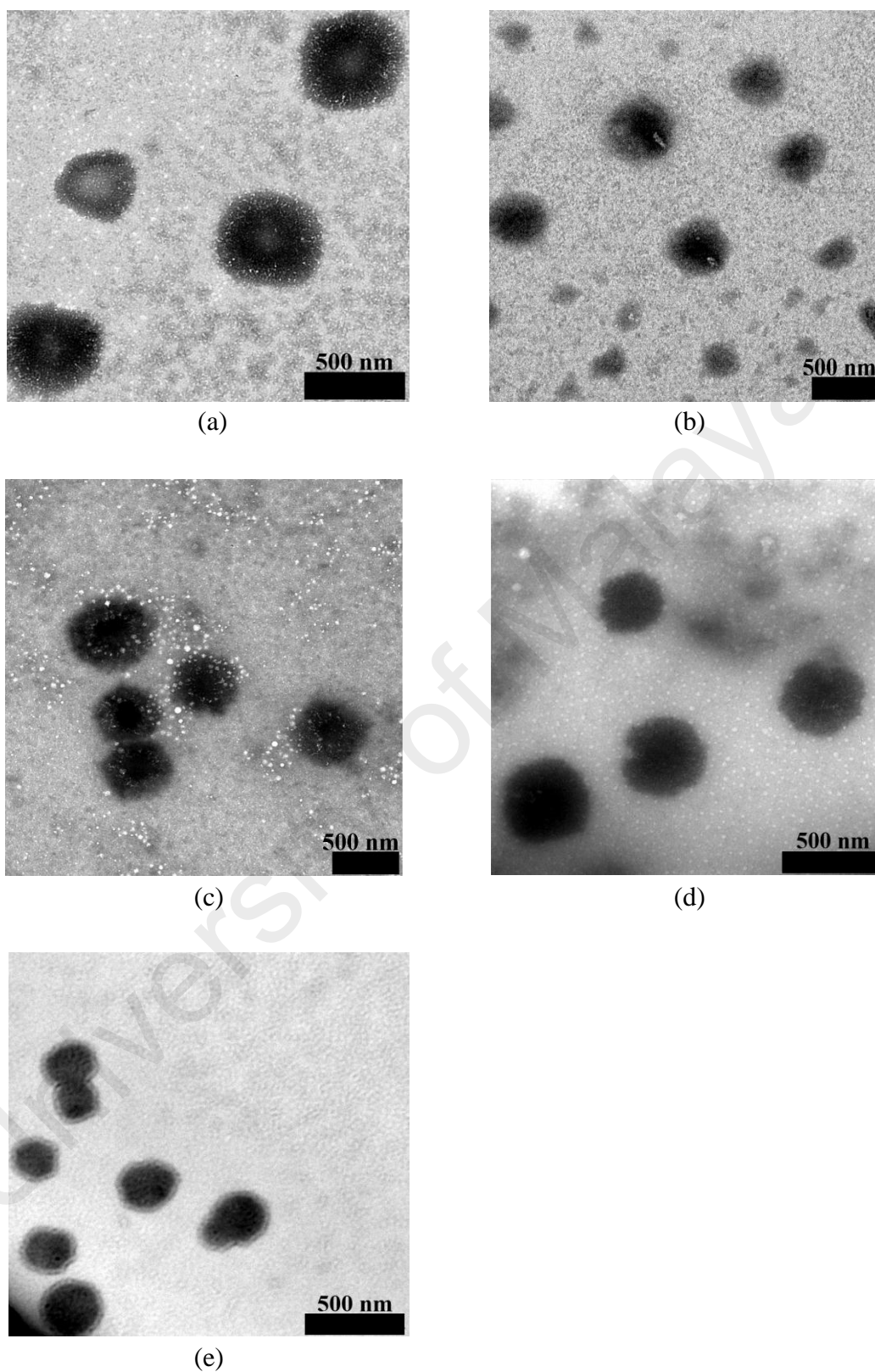
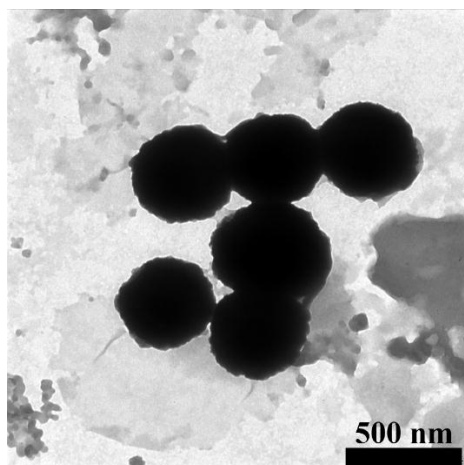
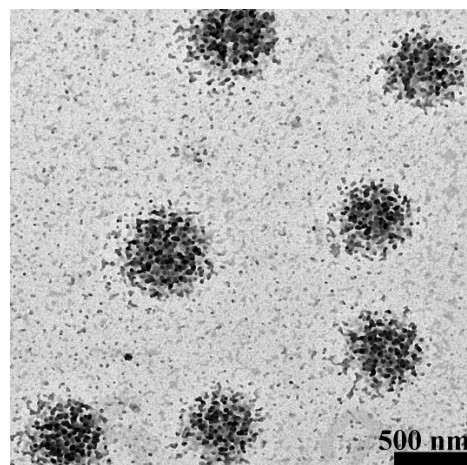


Figure 4.26: TEM micrographs of (a) ChC4, (b) ChC6, (c) ChC8, (d) ChC10 and (e) ChC12 loaded with SA at weight ratio 10:4. The scale bar shown is 500 nm.

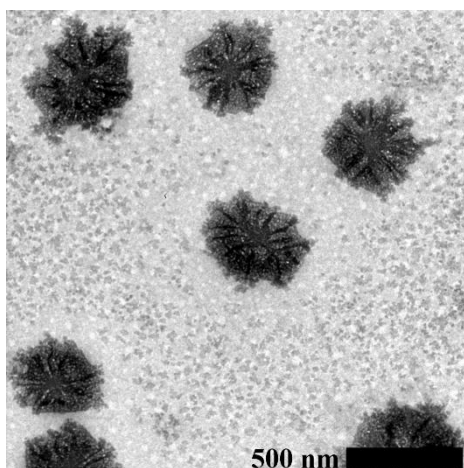
4.3.5.2 TEM micrographs of LID loaded ChA



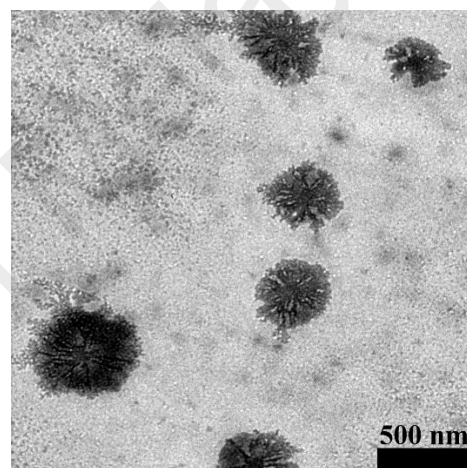
(a)



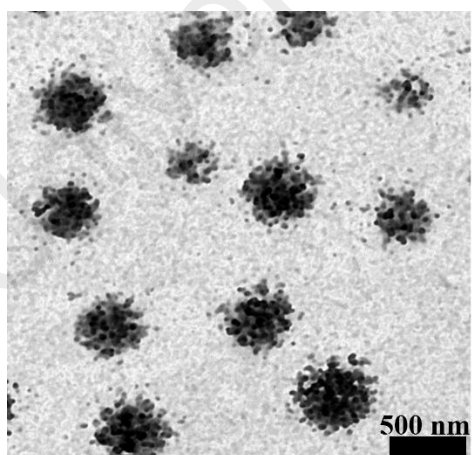
(b)



(c)



(d)



(e)

Figure 4.27: TEM micrographs of (a) ChC4, (b) ChC6, (c) ChC8, (d) ChC10 and (e) ChC12 loaded with LID at weight ratio 10:5. The scale bar shown is 500 nm.

4.3.5.3 TEM micrographs of ACE loaded ChA

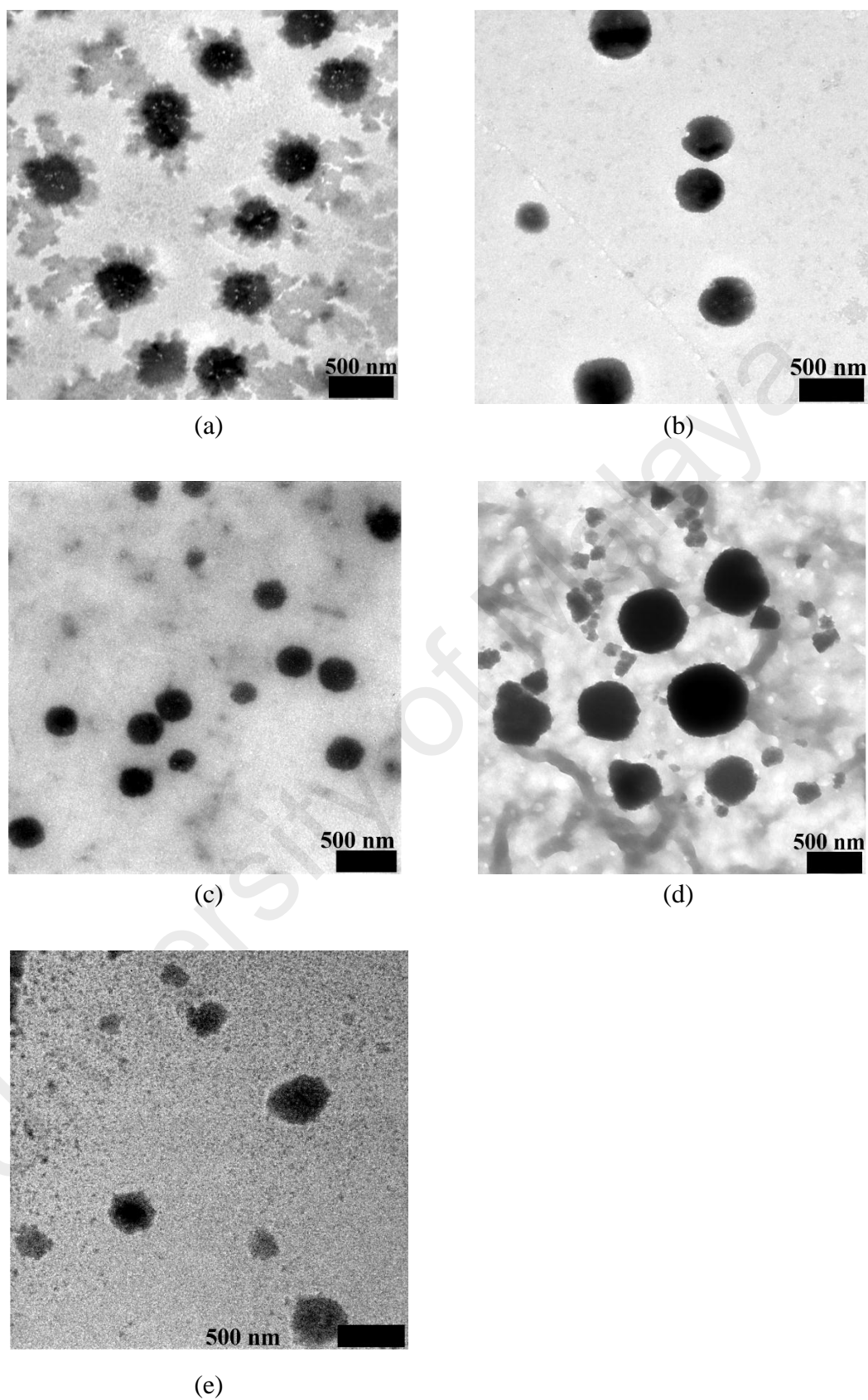


Figure 4.28: TEM micrographs of (a) ChC4, (b) ChC6, (c) ChC8, (d) ChC10 and (e) ChC12 loaded with ACE at weight ratio 10:5. The scale bar shown is 500 nm.

4.3.5.4 TEM micrographs of CAF loaded ChA

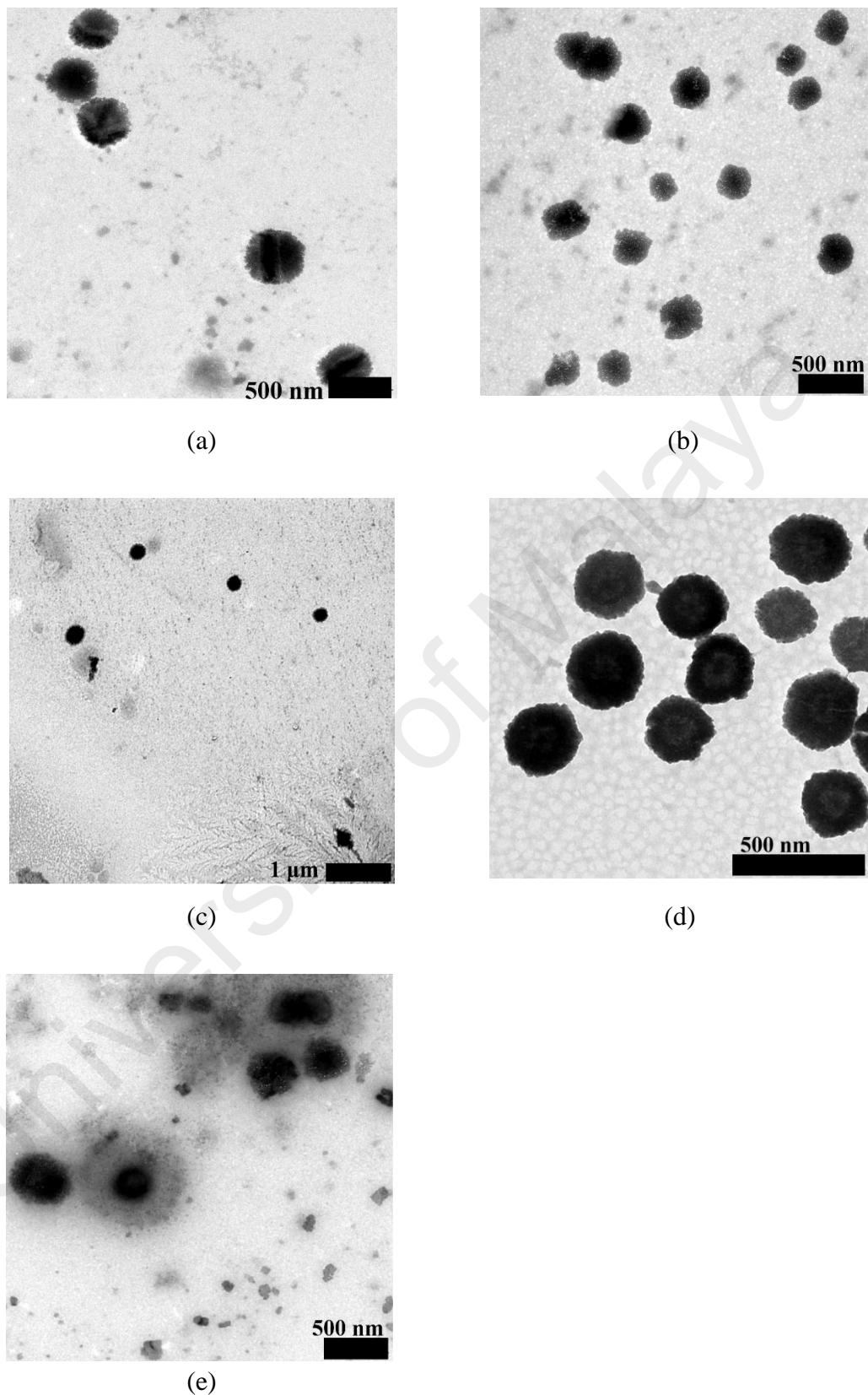


Figure 4.29: TEM micrographs of (a) ChC4, (b) ChC6, (c) ChC8, (d) ChC10 and (e) ChC12 loaded with CAF at weight ratio 10:5. The scale bar shown in (a, b, e, f) is 500 nm, whereas is 1 μm in (c).

The average particle size reported for drugs loaded ChA was obtained from at least 20 particles and presented together with the average value measured by DLS method, as shown in Table 4.6. As compared to the particle size of unencapsulated ChA from measurement of TEM micrographs, ChA showed pronounced increment after loading with slightly soluble drugs such as SA and LID, the result was in agreement with those obtained by DLS measurement. The average particle size in TEM microscopy was smaller than measured by the DLS method, the difference was based on the different working principle of these two methods, as previously discussed for unencapsulated ChA in section 4.1.10. It was found that the difference in particle size from DLS calculation and TEM viewing was slightly higher in short chain acylated ChC4 and ChC6 than those in ChC8, ChC10 and ChC12. Bigger occupancy volume of longer acyl chain in aforementioned TEM microscopy of unencapsulated ChA (section 4.1.10) can be applied to explain this observation in drugs loaded ChA.

Table 4.6: Comparison of particle size of ChA after loading with drugs by mean of DLS and TEM measurement.

Drugs	Particle size (d.nm)							
	SA		LID		ACE		CAF	
Method	DLS	TEM	DLS	TEM	DLS	TEM	DLS	TEM
ChC4	540 ± 13	417 ± 98	552 ± 30	448 ± 60	445 ± 5	379 ± 53	382 ± 2	362 ± 38
ChC6	419 ± 18	380 ± 92	421 ± 21	422 ± 92	430 ± 26	405 ± 101	320 ± 12	294 ± 22
ChC8	490 ± 23	498 ± 53	408 ± 13	361 ± 71	321 ± 13	320 ± 90	276 ± 16	272 ± 61
ChC10	344 ± 3	326 ± 75	381 ± 5	392 ± 43	284 ± 19	247 ± 88	268 ± 13	236 ± 43
ChC12	387 ± 14	360 ± 76	343 ± 7	371 ± 53	368 ± 14	337 ± 82	321 ± 11	275 ± 43

From this, we could propose the position of drugs encapsulated using ChA, where slightly soluble SA is in the hydrophobic core of ChA, LID locates within the inner non-polar alkyl groups of ChA, whereas sparingly soluble ACE and CAF may reside around the region between hydrophobic alkyl groups and hydrophilic polar head of ChA (Figure 4.30).

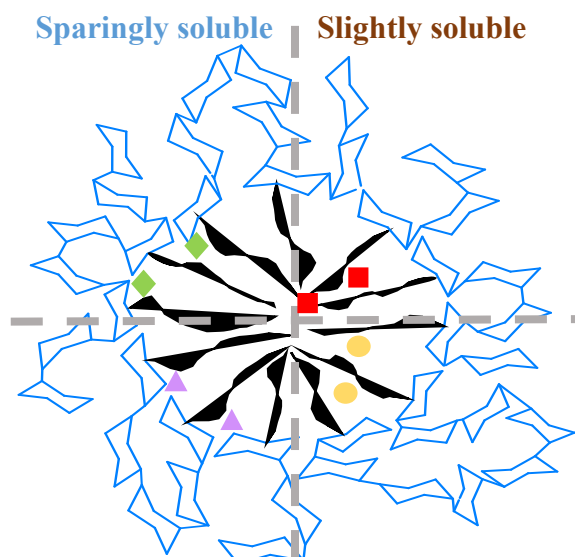


Figure 4.30: Schematic illustration of proposed position of SA (■), LID (●), ACE (▲) and CAF (◆) after encapsulation using ChA based on the correlation between solubility, encapsulation efficiency and particle size measured by DLS and TEM.

4.4 *In vitro* drug release

4.4.1 Topical delivery using inline vertical Franz diffusion cells

In vitro drug release study is an evaluation of efficiency and performance of the drug carrier as well as to predict the mechanism or route of drug release from the carrier. The release study of free drugs and encapsulated form with ChA at weight ratio of ChA: drugs at 10:1 was carried out in phosphate buffered saline pH 7.4 using vertical Franz diffusion cells at 37 °C and curve fitted to five types of kinetic models using DDSolver software to obtain the rate constant (k), linear regression (R^2) and release exponent (n) in each model in order to determine the most suitable model describing the release profile of the drugs.

4.4.1.1 *In vitro* release of SA

The cumulative release of SA in PBS solution at 37 °C over 24 hours was plotted in Figure 4.31. It was observed that free SA solution reached 100% release after 16 hours. The encapsulation of SA using ChA at encapsulation efficiency of 92 – 95% slowed down the release of SA significantly to 82 – 94% after 24 hours, especially ChC12 exhibited

prominently slower SA release from the fourteenth hour onwards compared to the other ChA ($P < 0.05$).

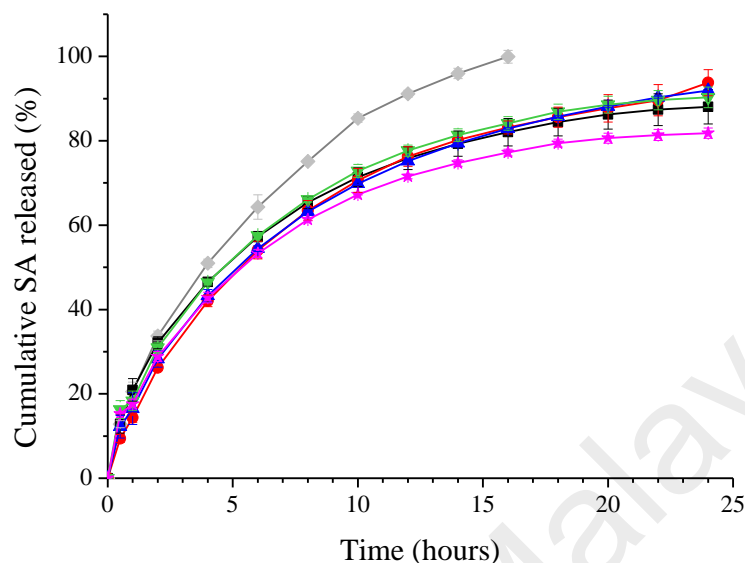


Figure 4.31: The cumulative release of SA in the absence (◆) and presence of ChC4 (■), ChC6 (●), ChC8 (▲), ChC10 (▼) and ChC12 (★) in PBS solution at 37 °C.

The release profile of SA was curve fitted into different kinetics models to evaluate the release mechanism of SA, as tabulated in Table 4.7. Free SA solution showed higher R^2 in first order (0.993) and Korsmeyer-Peppas model (0.994). The release exponent n in the Korsmeyer-Peppas model describes the release mechanism of the carrier. If the n value is lower than 0.43, it indicates the occurrence of Fickian diffusion, meanwhile non-Fickian diffusion occurs when the n is between 0.43 and 0.85 (section 3.4.3). For this reason, the first order model is a more suitable model to describe the Fickian diffusion of SA following the concentration gradient as the combined release mechanism indicated by $n = 0.533$ in Korsmeyer-Peppas model is not suitable to explain the release mechanism of merely free drug solution. Instead, Korsmeyer-Peppas model was more appropriate to apply on the release behaviour of polymeric ChA which showing high R^2 at ≥ 0.978 as shown in Table 4.7. The same model was also employed by Yang et al. (2016) to describe the release of SA from freeze-dried chitosan microcapsules.

Table 4.7: Curve fitting of SA to different release kinetics models for 24 hours. R^2 is the coefficient correlation, k is constant (slope) and n is the exponent of Korsmeyer-Peppas model.

Sample		Zero order	First order	Higuchi	Hixson-Crowell	Korsmeyer-Peppas
SA	R^2	0.826	0.993	0.992	0.989	0.994
	k	7.555	0.190	25.763	0.050	23.904
	n	-	-	-	-	0.533
ChC4-SA	R^2	0.585	0.966	0.962	0.917	0.978
	k	4.794	0.126	20.250	0.033	25.676
	n	-	-	-	-	0.411
ChC6-SA	R^2	0.720	0.993	0.980	0.967	0.981
	k	4.868	0.122	20.379	0.032	21.852
	n	-	-	-	-	0.474
ChC8-SA	R^2	0.691	0.986	0.983	0.955	0.986
	k	4.852	0.122	20.352	0.033	23.006
	n	-	-	-	-	0.454
ChC10-SA	R^2	0.594	0.974	0.966	0.933	0.981
	k	4.908	0.132	20.712	0.035	26.122
	n	-	-	-	-	0.413
ChC12-SA	R^2	0.563	0.937	0.959	0.874	0.979
	k	4.488	0.105	18.972	0.028	24.608
	n	-	-	-	-	0.403

In order to study the possibility of kinetic difference at the earlier stage of release, the release data of SA was also curve fitted to different kinetics models using release data during the first twelve hours as presented in Table 4.8. Similar to the release kinetics of SA for the duration of 24 hours, the linear regression of free SA solution was higher in first order ($R^2 = 0.994$) and Korsmeyer-Peppas model ($R^2 = 0.998$) as compared to other models. The first order model is chosen to describe the release of free SA as the diffusion of SA from the donor chamber to the receptor chamber was mainly governed by the concentration gradient. The Korsmeyer-Peppas model with the highest linear regression was selected to describe the release of SA in the presence of ChA ($R^2 = 0.995 - 0.996$), same as the observation to the SA release from ChA for 24 hours. Nevertheless, the release exponent for the release of SA from ChC4, ChC10 and ChC12 for 24 hours

reflected diffusion process ($n < 0.430$), whereas it demonstrated combined release mechanism when the curve fitting was considered for the first 12 hours ($0.43 < n < 0.85$).

Table 4.8: Curve fitting of SA to different release kinetic models for 12 hours. R^2 is the coefficient correlation, k is constant (slope) and n is the exponent of Korsmeyer-Peppas model.

Sample		Zero order	First order	Higuchi	Hixson-Crowell	Korsmeyer-Peppas
SA	R^2	0.876	0.994	0.990	0.984	0.998
	k	8.849	0.186	26.086	0.050	22.311
	n	-	-	-	-	0.578
ChC4-SA	R^2	0.796	0.963	0.996	0.929	0.996
	k	7.580	0.141	22.581	0.039	22.281
	n	-	-	-	-	0.507
ChC6-SA	R^2	0.899	0.994	0.981	0.978	0.995
	k	7.374	0.129	21.648	0.036	17.293
	n	-	-	-	-	0.611
ChC8-SA	R^2	0.859	0.981	0.992	0.958	0.996
	k	7.351	0.130	21.724	0.036	19.224
	n	-	-	-	-	0.561
ChC10-SA	R^2	0.816	0.969	0.995	0.940	0.996
	k	7.690	0.144	22.849	0.039	21.923
	n	-	-	-	-	0.521
ChC12-SA	R^2	0.807	0.955	0.996	0.923	0.996
	k	7.107	0.124	21.137	0.035	20.571
	n	-	-	-	-	0.514

Therefore, the SA release from ChA from 12 – 24 hours was further curved fitted to different release period using Korsmeyer-Peppas model to investigate the change in release mechanism over the time. From Table 4.9, Korsmeyer-Peppas model was suitable to describe up to 20 hours for SA release from ChA ($n = 0.438 – 0.583$) which included the occurrence of both diffusion and swelling phenomena as the n value of 0.428 and 0.420 obtained from more than 20 hours drug release of ChC4 and ChC12 respectively only governed by diffusion process.

Table 4.9: Curve fitting of SA at different release period to Korsmeyer-Peppas model. R^2 is the coefficient correlation, k is constant (slope) and n is the release exponent.

Sample		Korsmeyer-Peppas model				
		0-14 h	0-16 h	0-18 h	0-20 h	0-22 h
ChC4-SA	R^2	0.991	0.989	0.986	0.984	0.981
	k	22.083	22.799	23.478	24.205	24.930
	n	0.502	0.481	0.462	0.444	0.428
ChC6-SA	R^2	0.993	0.990	0.987	0.984	0.981
	k	18.058	18.885	19.720	20.540	21.311
	n	0.583	0.555	0.530	0.507	0.487
ChC8-SA	R^2	0.995	0.994	0.992	0.990	0.988
	k	19.810	20.434	21.073	21.725	22.363
	n	0.540	0.520	0.502	0.485	0.469
ChC10-SA	R^2	0.994	0.992	0.990	0.988	0.985
	k	22.534	23.218	23.883	24.585	25.332
	n	0.501	0.481	0.464	0.447	0.430
ChC12-SA	R^2	0.994	0.992	0.990	0.994	0.983
	k	21.155	21.794	22.432	23.129	23.853
	n	0.493	0.474	0.456	0.438	0.420

4.4.1.2 *In vitro* release of LID

Free LID solution exhibited 100% release in PBS solution after 12 hours, as displayed in Figure 4.32. The drug sustainability of ChA played role on the release of LID starting from first hour onward with the statistically significant P value ($P < 0.05$), hence it was observed that the encapsulation of LID using ChC4, ChC6, ChC8 and ChC10 prolonged the release to 14 hours, whereas the LID release from ChC12 was completed after 16 hours. No significant differences were found on the release of LID from ChC4 and ChC6 during the first six hours compared to ChC8, ChC10 and ChC12 ($P > 0.05$), however, the differences in the amount of drug released after six hours were statistically significant ($P < 0.05$).

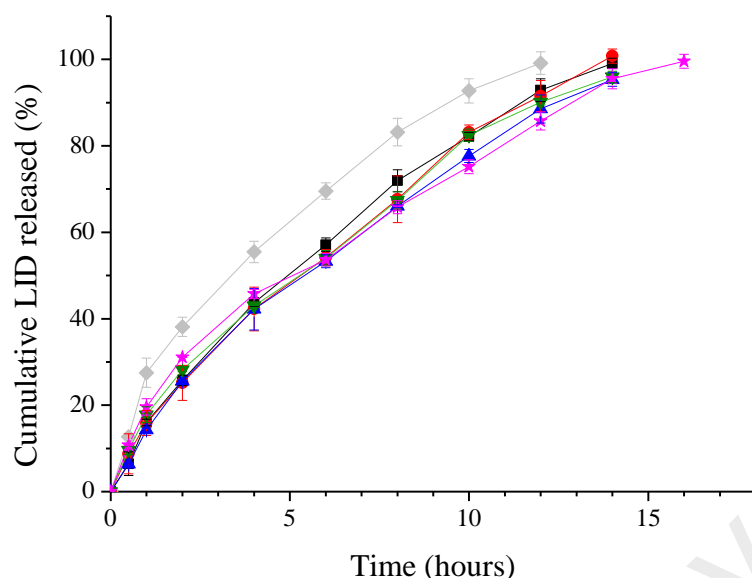


Figure 4.32: The cumulative release of LID in the absence (◇) and presence of ChC4 (■), ChC6 (●), ChC8 (▲), ChC10 (▼) and ChC12 (★) in PBS solution at 37 °C.

Table 4.10 displayed the curve fitting of LID release profile to different kinetics models. The linear regression of free LID solution to the first order, Higuchi and Korsmeyer-Peppas model were high at 0.986, 0.991 and 0.998 respectively. The first order model was chosen to describe the release mechanism for free LID solution due to the rational of the phenomenon of free drug solution release that LID diffused from high concentration region in donor chamber to the lower concentration region in receptor chamber. In order to apply Higuchi model, certain conditions shall be fulfilled, these include initial drug concentration is much higher than drug solubility, drug diffusion occurs in one dimension only to avoid edge effect, the size of the drug particles are much smaller than the thickness of the system, matrix swelling and dissolution are not significant, constant drug diffusivity and perfect sink conditions are maintained throughout the experiment (Dash et al., 2010). For these reasons, Higuchi model is mostly applied to the system with semi-solid or solid based matrix. Since the sample was prepared within the solubility limit, the release mechanism of free LID solution was not well represented by Higuchi model. In Korsmeyer-Peppas model, the $n = 0.577$ obtained

from the release of free LID solution indicates the combined release mechanism, thereby this model was not suitable to describe the release of free LID solution as well.

For the ChA, Korsmeyer-Peppas model with the highest R^2 (0.995 – 0.999) among all the models in Table 4.10 was undoubtedly selected to describe the release mechanism of LID from ChA, where diffusion occurred concomitantly with swelling as indicated by $n = 0.606 – 0.722$. Additionally, this mechanism is valid for the release from 0 to 6, 8, 10, 12 and 14 hours (Table 4.11).

Table 4.10: Curve fitting of LID release to different release kinetic models for 12 – 16 hours. R^2 is the coefficient correlation, k is constant (slope) and n is the exponent of Korsmeyer- Peppas model.

Sample		Zero order	First order	Higuchi	Hixson Crowell	Korsmeyer- Peppas
LID	R^2	0.878	0.986	0.991	0.983	0.998
	k	9.500	0.215	27.998	0.057	23.990
	n	-	-	-	-	0.577
ChC4-LID	R^2	0.957	0.978	0.960	0.991	0.999
	k	8.095	0.166	25.305	0.045	15.988
	n	-	-	-	-	0.710
ChC6-LID	R^2	0.957	0.977	0.961	0.961	0.999
	k	7.879	0.157	24.630	0.043	15.552
	n	-	-	-	-	0.710
ChC8-LID	R^2	0.962	0.979	0.957	0.990	0.999
	k	7.692	0.150	24.014	0.041	14.771
	n	-	-	-	-	0.722
ChC10-LID	R^2	0.950	0.973	0.966	0.985	0.998
	k	7.962	0.161	24.940	0.044	16.466
	n	-	-	-	-	0.690
ChC12-LID	R^2	0.897	0.978	0.987	0.980	0.995
	k	7.134	0.155	24.093	0.041	18.717
	n	-	-	-	-	0.606

Table 4.11: Curve fitting of LID at different release period to Korsmeyer-Peppas model. R^2 is the coefficient correlation, k is constant (slope) and n is the release exponent.

Sample		Korsmeyer- Peppas model				
		0-6h	0-8h	0-10 h	0-12 h	0-14 h
ChC4-LID	R^2	0.996	0.999	0.998	0.998	0.999
	k	15.049	15.044	15.440	15.747	15.988
	n	0.752	0.752	0.732	0.719	0.710
ChC6- LID	R^2	0.990	0.999	0.998	0.998	0.999
	k	15.607	15.525	14.929	15.419	15.552
	n	0.701	0.706	0.737	0.715	0.710
ChC8- LID	R^2	0.995	0.997	0.998	0.998	0.999
	k	14.590	14.783	14.857	15.014	14.771
	n	0.737	0.723	0.759	0.712	0.722
ChC10- LID	R^2	0.998	0.998	0.997	0.998	0.998
	k	17.533	17.323	16.588	16.274	16.466
	n	0.635	0.649	0.684	0.697	0.690
ChC12- LID	R^2	0.993	0.992	0.993	0.993	0.994
	k	19.753	20.256	19.707	19.091	18.536
	n	0.575	0.543	0.569	0.593	0.612

4.4.1.3 *In vitro* release of ACE

Figure 4.33 presented the *in vitro* release profile of ACE in PBS solution at 37 °C. The encapsulation of ACE using ChC4 has effectively slowed down the release of ACE from 10 hours to 24 hours, with ChA contributed their pronounced positive effect on the drug sustainability from 0.5 hour onward ($P < 0.05$). The release was further slowed down as longer chain ChA was employed in the sequence of ChC6 (98%), ChC8 (93%), ChC10 (91.5%) and ChC12 (85%). ChC12 exhibited profoundly slower release of ACE as compared to ChC4, ChC6, ChC8 and ChC10 starting at the eighth, twelfth, twentieth and twenty-second hour of release respectively ($P < 0.05$).

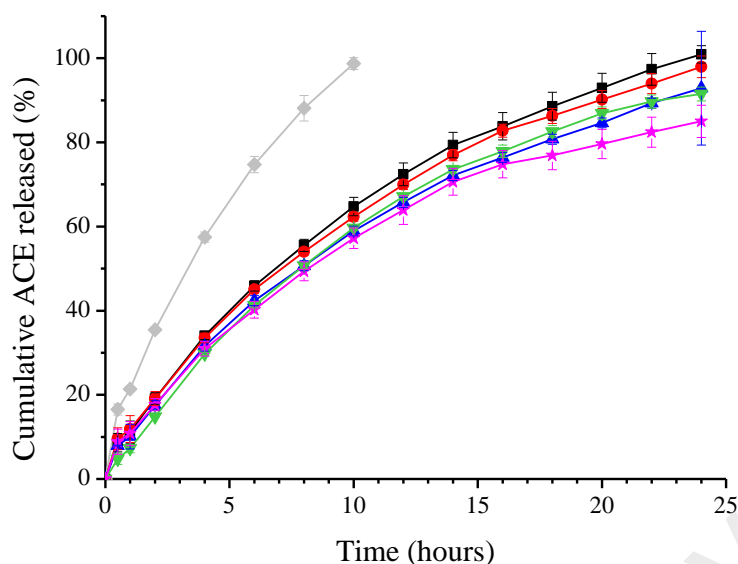


Figure 4.33: The cumulative release of ACE in the absence (◆) and presence of ChC4 (■), ChC6 (●), ChC8 (▲), ChC10 (▼) and ChC12 (★) in PBS solution at 37 °C.

The rate constant and linear regression of the release of ACE to the different kinetics models were calculated and tabulated in Table 4.12. It showed that the linear regression of free ACE solution was high in all models ($R^2 \geq 0.981$) except zero order model. Higuchi model was not applicable to the release of the free ACE solution as the prepared drug concentration does not exceed its solubility. Korsmeyer-Peppas model was not rational to be employed to the release of free ACE solution as $n = 0.628$ obtained indicates non-Fickian drug transport. For Hixson-Crowell model, it explains the occurrence of the change in surface area of tablet or particles is proportional to the cube root of its volume during the release process, hence it is mostly applicable to the surface erosion or diminish of tablets in a proportional manner when the dissolution happens in the plane of drug surface (Dash et al., 2010). Therefore, the best model for the release of free ACE solution was the first order model where the diffusion of ACE across the membrane was driven by the concentration difference between the donor and receptor chambers.

From Table 4.12, R^2 calculated from the first order, Hixson-Crowell and Korsmeyer-Peppas model for the release of ACE from ChA were comparable to each other. Hixson-

Crowell is related the drug release to the surface erosion of carrier, whereas the first order model describes the drug release based on the concentration gradient of the sample, hence Korsmeyer-Peppas model was the best model to describe ACE release from ChA as the n value of 0.568 – 0.633 describes the release mechanism as non-Fickian transport (Table 4.12), which is more suitable employed on the polymer based carrier which can swell.

Table 4.12: Curve fitting of ACE to different release kinetic models for 24 hours. R^2 is the coefficient correlation, k is constant (slope) and n is the exponent of Korsmeyer-Peppas model.

Sample		Zero order	First order	Higuchi	Hixson-Crowell	Korsmeyer-Peppas
ACE	R^2	0.914	0.987	0.981	0.991	0.998
	k	11.167	0.241	29.923	0.065	23.657
	n	-	-	-	-	0.628
ChC4-ACE	R^2	0.889	0.991	0.982	0.997	0.994
	k	4.958	0.112	20.397	0.030	15.411
	n	-	-	-	-	0.603
ChC6-ACE	R^2	0.883	0.993	0.985	0.995	0.995
	k	4.817	0.106	19.836	0.028	15.355
	n	-	-	-	-	0.595
ChC8-ACE	R^2	0.891	0.997	0.983	0.993	0.995
	k	4.531	0.092	18.638	0.025	14.047
	n	-	-	-	-	0.604
ChC10-ACE	R^2	0.903	0.998	0.969	0.998	0.988
	k	4.569	0.093	18.744	0.025	13.061
	n	-	-	-	-	0.633
ChC12-ACE	R^2	0.854	0.996	0.969	0.980	0.990
	k	4.292	0.085	18.744	0.023	14.744
	n	-	-	-	-	0.568

The curve fitting of release kinetics was also calculated based on the release of ACE for 12 hours to study the possible kinetics deviation during the initial part of drug release (Table 4.13). The R^2 of ACE release in the first order, Higuchi, Hixson-Crowell and Korsmeyer-Peppas model were higher than 0.980. The first order model was employed for the release of free ACE solution, the justifications were the same as the explanations as previously discussed in the release of ACE for 24 hours. For ACE loaded ChA, both

first order and Korsmeyer-Peppas models demonstrated high R^2 with a minimum of 0.992. Instead of merely Fickian diffusion process following the first order model, the Korsmeyer-Peppas model with combined processes of diffusion and swelling showed a better illustration of the overall release mechanism ($n = 0.685 - 0.801$) of ACE release from polymeric ChA. Furthermore, these phenomena were valid for release from 0 hour to 12 – 24 hours (Table 4.14).

Table 4.13: Curve fitting of ACE to different release kinetic models for 12 hours. R^2 is the coefficient correlation, k is constant (slope) and n is the exponent of Korsmeyer-Peppas model.

Sample		Zero order	First order	Higuchi	Hixson-Crowell	Korsmeyer-Peppas
ACE	R^2	0.914	0.987	0.981	0.991	0.998
	k	11.167	0.241	29.923	0.065	23.657
	n	-	-	-	-	0.628
ChC4-ACE	R^2	0.958	0.997	0.959	0.993	0.999
	k	6.643	0.104	19.255	0.030	12.493
	n	-	-	-	-	0.713
ChC6-ACE	R^2	0.946	0.994	0.967	0.987	0.998
	k	6.444	0.100	18.738	0.029	12.884
	n	-	-	-	-	0.685
ChC8-ACE	R^2	0.954	0.996	0.961	0.990	0.998
	k	6.061	0.091	17.585	0.027	11.604
	n	-	-	-	-	0.705
ChC10-ACE	R^2	0.980	0.999	0.931	0.999	0.997
	k	6.063	0.090	17.403	0.026	9.414
	n	-	-	-	-	0.801
ChC12-ACE	R^2	0.947	0.992	0.967	0.984	0.999
	k	5.886	0.087	17.112	0.026	11.750
	n	-	-	-	-	0.685

Table 4.14: Curve fitting of ACE at different release period to Korsmeyer-Peppas model. R^2 is the coefficient correlation, k is constant (slope) and n is the release exponent.

Sample		Korsmeyer- Peppas model				
		0-14 h	0-16 h	0-18 h	0-20 h	0-22 h
ChC4-ACE	R^2	0.999	0.997	0.996	0.995	0.995
	k	12.816	13.366	13.918	14.451	14.928
	n	0.698	0.674	0.653	0.634	0.618
ChC6-ACE	R^2	0.999	0.999	0.998	0.996	0.995
	k	13.077	13.356	13.862	14.400	14.910

Table 4.14 (continued)

ChC6-ACE	<i>n</i>	0.676	0.664	0.644	0.625	0.608
ChC8-ACE	R^2	0.998	0.997	0.996	0.995	0.995
	<i>k</i>	11.89	12.365	12.838	13.315	13.683
	<i>n</i>	0.690	0.668	0.648	0.630	0.617
ChC10-ACE	R^2	0.996	0.995	0.993	0.992	0.991
	<i>k</i>	9.906	10.556	11.162	11.726	12.352
	<i>n</i>	0.771	0.737	0.708	0.684	0.659
ChC12-ACE	R^2	0.999	0.998	0.996	0.994	0.992
	<i>k</i>	11.887	12.256	12.904	13.560	14.174
	<i>n</i>	0.678	0.661	0.634	0.609	0.587

4.4.1.4 *In vitro* release of CAF

Similar to ACE, the cumulative release of sparingly soluble CAF as shown in Figure 4.34 was 100% at the tenth hour. Free CAF was released at a higher amount compared to the release profile of CAF from ChA starting from the first hour onward with statistical significant P value greater than 0.05. After encapsulation of CAF was carried out using ChA, the release of CAF was slowed down by 1.6 to 2.2 times. The time taken to release all CAF from ChC4 was 16 hours, from ChC6, ChC8 and ChC10 was 20 hours and from ChC12 was 22 hours respectively. ChC12 exhibited significant lower CAF release at the tenth hour as compared to ChC4, ChC6, ChC8 and ChC10 ($P < 0.05$).

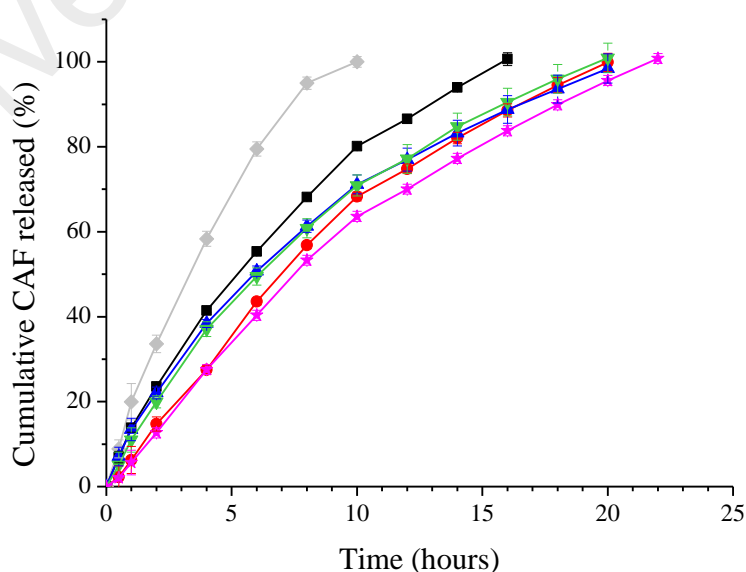


Figure 4.34: The cumulative release of CAF in the absence (\diamond) and presence of ChC4 (\blacksquare), ChC6 (\bullet), ChC8 (\blacktriangle), ChC10 (\blacktriangledown) and ChC12 (\star) in PBS solution at 37 °C.

The curve fitting of CAF release for 24 hours to different kinetic models was done to calculate the linear regression and rate constant (Table 4.15). Free CAF solution in Table 4.15 demonstrated high R^2 to first order (0.980), Hixson-Crowell (0.996) and Korsmeyer-Peppas model (0.990). The Hixson-Crowell and Korsmeyer-Peppas models were not suitably applied to describe the release of free CAF solution, as the Hixson-Crowell model predicts surface erosion of CAF while the Korsmeyer-Peppas model describes non-Fickian drug transport ($n = 0.689$). Hence, the free CAF solution following the first order model was released based on the difference in concentration gradient between donor and receptor chambers. From Table 4.15, the R^2 obtained from the release of CAF from ChA using the Hixson-Crowell model (0.994 – 0.997) was comparable to Korsmeyer-Peppas model (0.990 – 0.995). As compared to the Hixson-Crowell model which describes the erosion of carriers during dissolution, the Korsmeyer-Peppas model was a better model to depict the release of CAF from polymeric carriers like ChA over 24 hours, in which $n = 0.605 – 0.746$ indicated that the release was anomalous diffusion controlled.

Table 4.15: Curve fitting of CAF to different release kinetic models for 24 hours. R^2 is the coefficient correlation, k is constant (slope) and n is the exponent of Korsmeyer-Peppas model.

Sample		Zero order	First order	Higuchi	Hixson Crowell	Korsmeyer- Peppas
CAF	R^2	0.936	0.980	0.956	0.996	0.990
	k	11.578	0.251	30.794	0.068	21.741
	n	-	-	-	-	0.689
ChC4-CAF	R^2	0.935	0.986	0.940	0.997	0.995
	k	7.188	0.153	24.094	0.041	16.272
	n	-	-	-	-	0.670
ChC6-CAF	R^2	0.958	0.977	0.940	0.994	0.990
	k	5.650	0.113	20.943	0.031	11.186
	n	-	-	-	-	0.746
ChC8-CAF	R^2	0.892	0.995	0.982	0.996	0.994
	k	5.764	0.127	21.700	0.034	16.662
	n	-	-	-	-	0.605

Table 4.15 (continued)

ChC10-CAF	R^2	0.920	0.989	0.971	0.996	0.994
	k	5.840	0.127	21.879	0.034	15.030
	n	-	-	-	-	0.648
ChC12-CAF	R^2	0.957	0.978	0.945	0.995	0.991
	k	5.163	0.104	20.070	0.028	10.711
	n	-	-	-	-	0.738

The curve fitting of CAF release data to different kinetics models for 12 hours tabulated in Table 4.16 showed that the linear regression in the first order, Hixson-Crowell and Korsmeyer-Peppas model was high ($R^2 \geq 0.980$). Among the models, the Korsmeyer-Peppas model was chosen to describe the release of CAF from ChA as the release mechanism of polymeric carrier mostly involved combined processes instead of merely diffusion as indicated in first order model.

Table 4.16: Curve fitting of CAF to different release kinetic models for 12 hours. R^2 is the coefficient correlation, k is constant (slope) and n is the exponent of Korsmeyer-Peppas model.

Sample		Zero order	First order	Higuchi	Hixson-Crowell	Korsmeyer-Peppas
CAF	R^2	0.936	0.980	0.956	0.996	0.990
	k	11.578	0.251	30.794	0.068	21.741
	n	-	-	-	-	0.689
ChC4-CAF	R^2	0.959	0.994	0.955	0.999	0.997
	k	8.071	0.145	23.372	0.041	14.890
	n	-	-	-	-	0.722
ChC6-CAF	R^2	0.991	0.984	0.895	0.994	0.995
	k	6.690	0.102	18.994	0.030	8.230
	n	-	-	-	-	0.906
ChC8-CAF	R^2	0.945	0.999	0.965	0.994	0.997
	k	7.241	0.122	21.052	0.035	14.392
	n	-	-	-	-	0.688
ChC10-CAF	R^2	0.963	0.999	0.948	0.999	0.996
	k	7.173	0.118	20.728	0.034	12.731
	n	-	-	-	-	0.740
ChC12-CAF	R^2	0.991	0.988	0.896	0.995	0.995
	k	6.261	0.093	17.778	0.027	7.747
	n	-	-	-	-	0.904

Unlike the CAF release for 24 hours, super case II transport described the relaxational release controlled from polymer swelling was observed in ChC6 and ChC12 ($n > 0.890$). Hence, the release profile of CAF was further curve fitted to different release period from 0 to 14, 16, 18 and 20 hours to study the change in the release mechanism over the time (Table 4.17). It was found that the mechanism calculated from CAF release from ChC6 and ChC12 during 0 – 14 hours was showing super case II transport where the polymer relaxation during swelling upon water penetration into polymer matrix was the key factor of rate-determining step (Soni et al., 2017). Considering unencapsulated CAF diffused across the membrane at the initial stage of release was high due to the low EE of CAF (30 – 32%) while the release of CAF from the network of ChA was occurred at a later period during swelling, so CAF release from ChA shall be considered for longer duration in fitting to the kinetics models. As observed from Table 4.17, the release of CAF from ChA was combined processes of diffusion and swelling ($0.43 < n < 0.89$) when the kinetics was counted for 0 – 16 and more hours, which was more suitable to describe the release of CAF from ChA as compared to the swelling dependent mechanism shown by kinetics which only considered 0 – 14 hours. It is suggested that longer duration of release shall be taken into consideration to curve fitting for drug release with low EE.

Table 4.17: Curve fitting of CAF at different release period to Korsmeyer-Peppas model. R^2 is the coefficient correlation, k is constant (slope) and n is the release exponent.

Sample		Korsmeyer- Peppas model				
		0-14 h	0-16 h	0-18 h	0-20 h	0-22 h
ChC4-CAF	R^2	0.996	0.995	-	-	-
	k	15.613	16.272	-	-	-
	n	0.693	0.670	-	-	-
ChC6-CAF	R^2	0.993	0.991	0.990	0.990	-
	k	9.075	9.841	10.536	11.186	-
	n	0.852	0.809	0.775	0.746	-
ChC8-CAF	R^2	0.996	0.995	0.995	0.640	-
	k	15.000	15.583	16.154	15.583	-
	n	0.662	0.640	0.620	0.640	-

Table 4.17 (continued)

ChC10-CAF	R ²	0.995	0.995	0.994	0.995	-
	k	13.295	13.900	14.477	13.295	-
	n	0.713	0.688	0.667	0.713	-
ChC12-CAF	R ²	0.993	0.992	0.992	0.992	0.991
	k	8.477	9.124	9.700	10.223	10.711
	n	0.854	0.815	0.784	0.759	0.738

Free drugs SA, LID, ACE and CAF were released at 100% after 16, 12, 10 and 10 hours respectively, as presented in Figure 4.35. It was found that the drug release across the cellulose dialysis membrane was hydrophilicity dependent with the sparingly water soluble drugs being easier to diffuse through the membrane compared to those of lower water solubility.

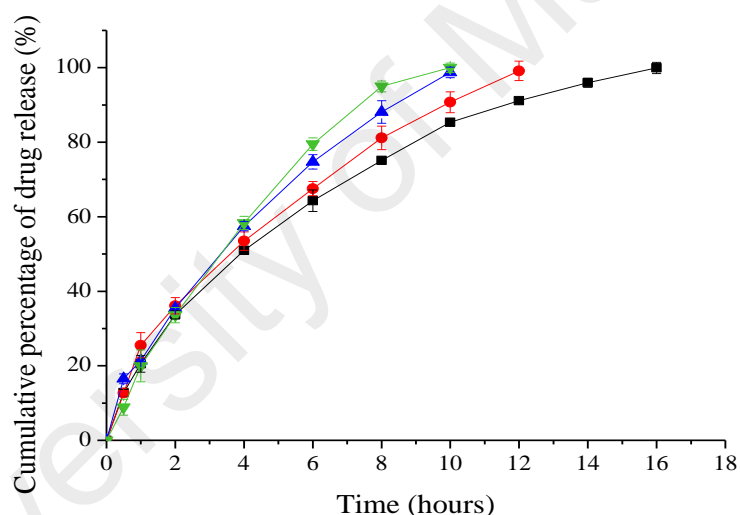


Figure 4.35: The cumulative release of free SA (■), LID (●), ACE (▲) and CAF (▼) solution in PBS solution at 37 °C.

The encapsulation of drugs using ChA was able to sustain the drug release for a longer period at a lower release rate due to the interactions such as hydrogen bonding and Van der Waals force as discussed in section 4.3.2. Among the ChA, longer chain acylated ChC12 exhibited the slowest release for these four types of drugs as the release of SA, LID, ACE and CAF from ChC12 at 16th, 12th, 10th and 10th hour (time required for the complete release of free drug solution) were 77%, 86%, 57% and 64% respectively (Figure 4.36). This was attributed to the stronger hydrophobic interaction between longer

alkyl groups of polymer chains and between polymer chains and drugs to prolong the drug release.

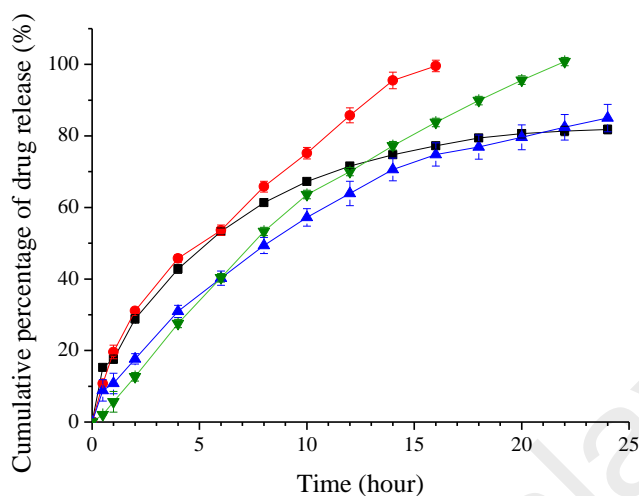


Figure 4.36: The cumulative release of SA (■), LID (●), ACE (▲) and CAF (▼) from ChC12 in PBS solution at 37 °C.

4.4.2 Oral delivery using dialysis tubing

Dialysis is a common approach to study drug release owing to its easy setup and no involvement of expensive equipment. The utilization of dialysis tubing or sac with the semi-permeable membrane with suitable molecular weight cut-off (MWCO) only allows drugs smaller than MWCO to permeate across the membrane while impeding the diffusion of the carrier, hence eliminating the labor and cost to separate the released drug from the carrier.

4.4.2.1 *In vitro* release of SA

The release of SA in simulated gastric fluid (SGF) pH 1.2 for the first 120 minutes followed by simulated intestinal fluid (SIF) pH 6.8 at 37 °C was displayed in Figure 4.37. SA exhibited complete diffusion after 80 minutes and showed a plateau release, whereas SA loaded in ChA demonstrated significant slower release ($P < 0.05$) and extended release until 120 minutes. The burst release at the initial stage was driven by the higher amount of SA in the inner dialysis tubing compared to the external dialysis media, the

release was slowed down as the concentration decreased and did not exhibit apparent diffusion despite transferring to SIF after 120 minutes. Among the ChA, ChC4 was almost completely released (98%) after 120 minutes, whereas the release of ChC6 and ChC8 at the same duration was around 89 – 91%. The lowest amount of released SA was found in ChC10 and ChC12 at approximate 85%.

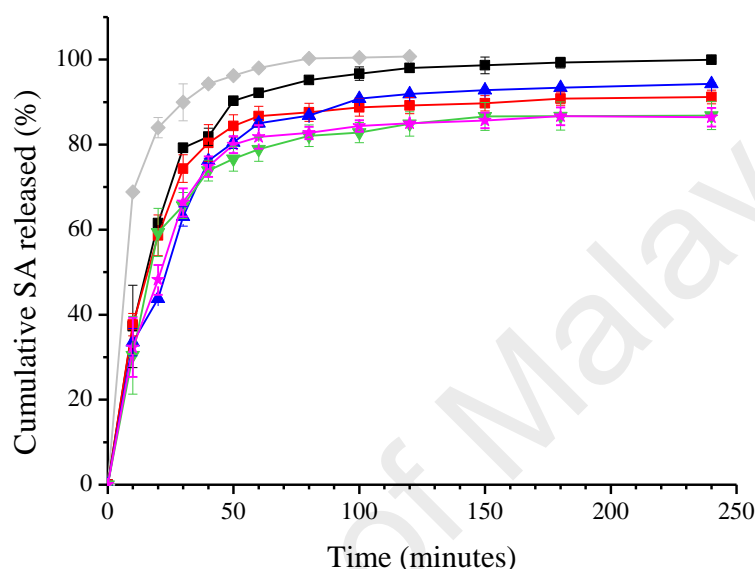


Figure 4.37: The cumulative release of SA in the absence (◇) and presence of ChC4 (■), ChC6 (●), ChC8 (▲), ChC10 (▼) and ChC12 (★) in SGF for the first 2 hours and in SIF for the subsequent hours at 37 °C.

The release of SA for the first 120 minutes was curved fitted to different kinetics models, as presented in Table 4.18. The R^2 of free SA solution in both the first order and Korsmeyer-Peppas model was high at the value of 0.989 and 0.988 respectively. The first order model describes the release of free SA solution as concentration gradient dependent following the Fick's first law, in accordance to the Fickian diffusion as reflected by the release exponent $n = 0.134$ in the Korsmeyer-Peppas model. Since it is a release of drug solution without any carrier, the first order model is more suitable to describe the release of the free SA solution. The release of SA from ChA presented R^2 was higher than 0.930 in Korsmeyer-Peppas model. Similar to the free SA solution, the n value of SA loaded ChA was lower than 0.43, this followed release mechanism with is merely diffusion control.

In order to study the difference in release kinetics, the SA release was also curve fitted to a shorter release duration for the first 60 minutes (Table 4.19). As observed from Table 4.19, the n value of ChA in the Korsmeyer-Peppas model increased to a value close to or higher than 0.43 ($n = 0.418 - 0.544$) suggesting that the swelling process might be responsible for the drug release mechanism of ChA as well as the diffusion process previously mentioned. Since the matrix of ChA is made up of polymeric material, the Korsmeyer-Peppas model is more rational to describe the release of SA from ChA as compared to the first order model as swelling of ChA presumably played a role in the release mechanism of SA as well. During swelling, the penetration of water induces the chain loosening of ChA, hence facilitating the release of SA which is proposed to be encapsulated within the hydrophobic core of ChA to the surrounding medium in the inner tubing and then to the outside of the tubing.

Table 4.18: Curve fitting of release of SA to different release kinetic models for the first 120 minutes. R^2 is the coefficient correlation, k is constant (slope) and n is the exponent of Korsmeyer-Peppas model.

Sample		Zero order	First order	Higuchi	Hixson-Crowell	Korsmeyer-Peppas
SA	R^2	-0.872	0.989	0.496	0.734	0.988
	k	1.245	0.101	12.015	0.013	55.289
	n	-	-	-	-	0.134
ChC4-SA	R^2	0.0233	0.996	0.830	0.970	0.949
	k	1.162	0.047	10.959	0.012	26.540
	n	-	-	-	-	0.290
ChC6-SA	R^2	-0.226	0.957	0.779	0.908	0.943
	k	1.078	0.041	10.224	0.011	27.903
	n	-	-	-	-	0.261
ChC8-SA	R^2	0.296	0.981	0.905	0.953	0.953
	k	1.061	0.032	9.900	0.009	18.183
	n	-	-	-	-	0.356
ChC10-SA	R^2	-0.0212	0.903	0.810	0.825	0.941
	k	1.003	0.032	9.480	0.009	23.866
	n	-	-	-	-	0.280

Table 4.18 (continued)

ChC12-SA	R^2	0.0803	0.903	0.839	0.880	0.938
	k	1.014	0.032	9.548	0.009	21.744
	n	-	-	-	-	0.304

Table 4.19: Curve fitting of release of SA to different release kinetic models for the first 60 minutes. R^2 is the coefficient correlation, k is constant (slope) and n is the exponent of Korsmeyer-Peppas model.

Sample		Zero order	First order	Higuchi	Hixson-Crowell	Korsmeyer-Peppas
SA	R^2	0.2175	0.988	0.832	0.950	0.997
	k	2.147	0.101	14.869	0.023	46.651
	n	-	-	-	-	0.187
ChC4-SA	R^2	0.7206	0.996	0.830	0.970	0.949
	k	1.901	0.047	10.959	0.012	26.540
	n	-	-	-	-	0.290
ChC6-SA	R^2	-0.226	0.957	0.977	0.980	0.981
	k	1.078	0.041	12.844	0.013	15.917
	n	-	-	-	-	0.442
ChC8-SA	R^2	0.690	0.990	0.975	0.958	0.983
	k	1.804	0.042	12.218	0.011	16.507
	n	-	-	-	-	0.418
ChC10-SA	R^2	0.8439	0.990	0.986	0.978	0.988
	k	1.679	0.033	11.224	0.009	9.545
	n	-	-	-	-	0.544
ChC12-SA	R^2	0.681	0.962	0.960	0.916	0.968
	k	1.647	0.034	11.154	0.009	14.824
	n	-	-	-	-	0.423

4.4.2.2 *In vitro* release of LID

From the release of LID in SGF at 37 °C as shown in Figure 4.38, LID with a cationic charge was protonated in the acidic environment and completely released within 50 minutes. The differences in the amount of LID released with and without ChA during first 10 minutes were not statistically significant ($P > 0.05$). Nevertheless, the release of LID in the presence of ChA was slowed down where ChC4, ChC6, ChC8 and ChC10 reached 100% of LID release within 70 minutes, whereas ChC12 took around 80 minutes to release all LID.

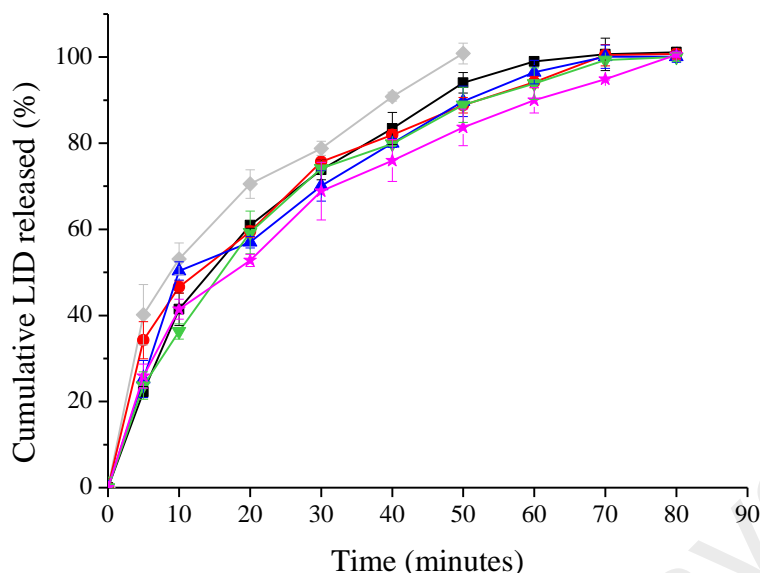


Figure 4.38: The cumulative release of LID in the absence (◇) and presence of ChC4 (■), ChC6 (●), ChC8 (▲), ChC10 (▼) and ChC12 (★) in SGF at 37 °.

The curve fitting of LID release to different kinetics models was carried out and tabulated in Table 4.20. The R^2 of free LID solution in both the first order (0.965) and Korsmeyer-Peppas model (0.999) were higher as compared to other models. The first order model was chosen to describe the release of free LID solution from the inner to the outer medium across the dialysis tubing following the difference of chemical potential in the media between internal and external of the tubing. For the release of LID from ChA, the first order model, Higuchi and Korsmeyer-Peppas models were comparable at R^2 higher than 0.970. Since the prepared drug was within the drug solubility, the Higuchi model was not suitable to describe the release of LID from ChA. In the Korsmeyer-Peppas model, the n value close to or higher than 0.43 revealed anomalous transport of LID from ChA, this predicts that both diffusion and chain relaxation occur, in which LID which was proposed to have resided in the hydrophobic area of ChA is released from ChA and then diffused across the dialysis tubing.

Table 4.20: Curve fitting of release of LID to different release kinetic models for the first 50 – 80 minutes. R^2 is the coefficient correlation, k is constant (slope) and n is the exponent of Korsmeier-Peppas model.

Sample		Zero order	First order	Higuchi	Hixson-Crowell	Korsmeier-Peppas
LID	R^2	0.635	0.965	0.981	0.929	0.999
	k	2.386	0.069	14.788	0.018	21.26
	n	-	-	-	-	0.395
ChC4-LID	R^2	0.750	0.993	0.988	0.989	0.988
	k	1.784	0.049	12.853	0.013	13.537
	n	-	-	-	-	0.486
ChC6-LID	R^2	0.608	0.970	0.980	0.938	0.998
	k	1.747	0.051	12.704	0.013	18.559
	n	-	-	-	-	0.400
ChC8-LID	R^2	0.691	0.970	0.984	0.948	0.989
	k	1.737	0.048	12.561	0.012	15.507
	n	-	-	-	-	0.444
ChC10-LID	R^2	0.751	0.996	0.989	0.984	0.989
	k	1.720	0.045	12.389	0.012	13.055
	n	-	-	-	-	0.486
ChC12-LID	R^2	0.698	0.980	0.992	0.960	0.996
	k	1.517	0.041	11.685	0.011	14.210
	n	-	-	-	-	0.450

4.4.2.3 *In vitro* release of ACE

The release of ACE in the absence and presence of ChA in SGF and transferred to SIF at 37 °C was shown in Figure 4.39. The free ACE solution was totally released in SGF within first two hours, whereas the ACE encapsulated by ChA exhibited slower release in SGF and extended the remaining drug release in SIF. The release of ACE from ChC10 and ChC12 were significantly lower than ChC4, ChC6 and ChC8 starting from 30 minutes onward ($P < 0.05$). Unlike ChC10 which released around 78% in SGF for the first two hours, the sustainability performance of ChC12 towards ACE was better as it released approximate 71.6% of ACE.

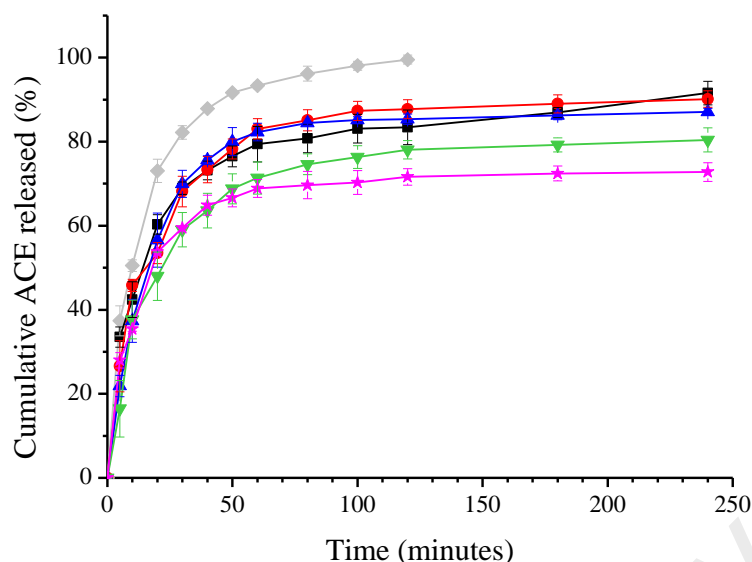


Figure 4.39: The cumulative release of ACE in the absence (◇) and presence of ChC4 (■), ChC6 (●), ChC8 (▲), ChC10 (▼) and ChC12 (★) in SGF for the first 2 hours and in SIF for the subsequent hours at 37 °C.

The curve fitting of ACE for the first 120 minutes was tabulated in Table 4.21. As shown in Table 4.21, the first order model with the highest R^2 at 0.981 was undoubtedly chosen as the model to describe the flux of ACE moved from higher concentration region to lower concentration region by obeying Fick's first law. Meanwhile, the R^2 of the Korsmeyer-Peppas model was the highest among the models (> 0.930) for the release of ACE from ChA during 120 minutes (Table 4.21) and 60 minutes (Table 4.22), however different mechanisms were described for different release duration. The release exponent of $n = 0.251 - 0.330$ for the first 120 minutes reflected diffusion of ACE from ChA (Table 4.21), whereas the n value increased to 0.337 to 0.457 (Table 4.22) when the release kinetics of ACE was limited for the first 60 minutes, indicating the combined release processes occurred instead of diffusion only. By taking consideration that the ChA are carriers made up of polymers and saturation of outside media (will be discussed in section 4.4.4) greatly influenced the drug release from inner to external tubing as time is prolonged, the release kinetics is preferable to count for the first 60 minutes duration where combined processes of diffusion and polymeric swelling were involved during drug release.

Table 4.21: Curve fitting of release of ACE to different release kinetic models for the first 120 minutes. R^2 is the coefficient correlation, k is constant (slope) and n is the exponent of Korsmeyer-Peppas model.

Sample		Zero order	First order	Higuchi	Hixson Crowell	Korsmeyer- Peppas
ACE	R^2	-0.247	0.981	0.746	0.880	0.961
	k	1.196	0.066	11.414	0.013	31.632
	n	-	-	-	-	0.255
ChC4-ACE	R^2	-0.2814	0.616	0.728	0.4327	0.954
	k	0.867	0.023	8.283	0.006	23.373
	n	-	-	-	-	0.251
ChC6-ACE	R^2	0.0269	0.911	0.839	0.844	0.965
	k	1.042	0.036	9.850	0.010	22.7778
	n	-	-	-	-	0.299
ChC8-ACE	R^2	0.059	0.928	0.825	0.868	0.932
	k	1.029	0.036	9.740	0.010	21.451
	n	-	-	-	-	0.311
ChC10-ACE	R^2	0.173	0.842	0.870	0.733	0.952
	k	0.912	0.024	8.585	0.006	17.459
	n	-	-	-	-	0.330
ChC12-ACE	R^2	-0.2615	0.816	0.745	0.711	0.967
	k	1.006	0.036	9.596	0.010	26.904
	n	-	-	-	-	0.252

Table 4.22: Curve fitting of release of ACE to different release kinetic models for the first 60 minutes. R^2 is the coefficient correlation, k is constant (slope) and n is the exponent of Korsmeyer-Peppas model.

Sample		Zero order	First order	Higuchi	Hixson Crowell	Korsmeyer- Peppas
ACE	R^2	0.459	0.977	0.937	0.938	0.985
	k	2.007	0.066	11.414	0.018	24.061
	n	-	-	-	-	0.344
ChC4-ACE	R^2	0.476	0.828	0.941	0.741	0.985
	k	1.470	0.028	10.024	0.008	17.251
	n	-	-	-	-	0.350
ChC6-ACE	R^2	0.061	0.930	0.971	0.969	0.989
	k	1.703	0.038	11.523	0.010	16.672
	n	-	-	-	-	0.398
ChC8-ACE	R^2	0.699	0.976	0.977	0.933	0.980
	k	1.718	0.038	11.556	0.010	13.532
	n	-	-	-	-	0.457

Table 4.22 (continued)

ChC10-ACE	R^2	0.679	0.921	0.970	0.866	0.975
	k	1.474	0.027	9.931	0.008	12.091
	n	-	-	-	-	0.446
ChC12-ACE	R^2	0.449	0.880	0.937	0.792	0.991
	k	1.686	0.039	11.512	0.010	20.717
	n	-	-	-	-	0.337

4.4.2.4 *In vitro* release of CAF

The release of CAF in SGF reached 100% at the 60th minute and became constant after that, as shown in Figure 4.40. Owing to the encapsulation by ChA, the CAF release in SGF was slower and prolonged over the time. For instance, ChC4 released 91% CAF at the first hour compared to the release of CAF completed in one hour. ChC6 and ChC8 significantly slowed down the CAF release to 86% and 84% respectively after 2 hours. Longer chain ChC10 and ChC12 further extended the CAF release to 73 – 74% for the first two hours in SGF. Insignificant differences on the release of CAF among ChA was observed during early five minutes, however, the drug sustainability of ChC10 and ChC12 contributed significantly to the release of CAF from 50 minutes onward ($P < 0.05$).

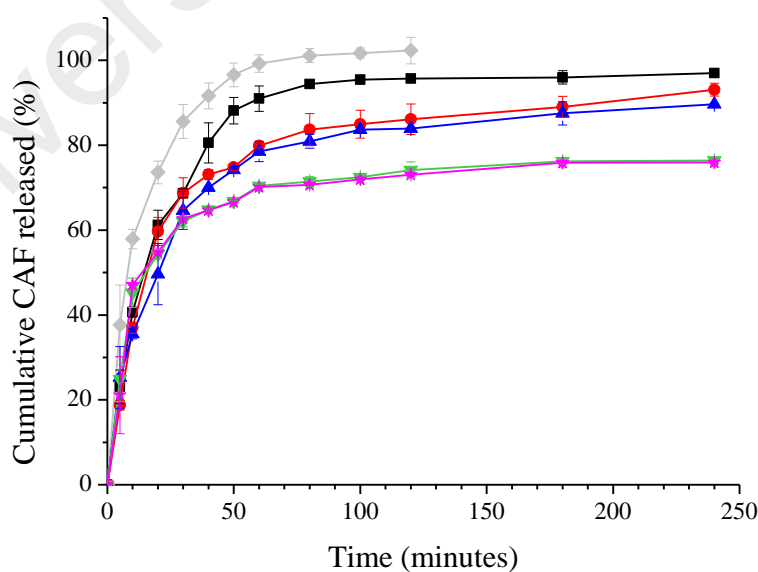


Figure 4.40: The cumulative release of CAF in the absence (\diamond) and presence of ChC4 (\blacksquare), ChC6 (\bullet), ChC8 (\blacktriangle), ChC10 (\blacktriangledown) and ChC12 (\star) in SGF for the first 2 hours and in SIF for the subsequent hours at 37 °C.

The release kinetics of CAF from the curve fitting to different models was presented in Table 4.23. The release of free CAF solution was described using the first order model ($R^2 = 0.987$) where the driving force of drug transport was mainly attributed to the concentration gradient of inner and outer media of the dialysis tubing, whereas the Korsmeyer-Peppas model with $R^2 \geq 0.930$ was chosen for the release of CAF in the presence of ChA. As indicated by $n = 0.243 - 0.338$ in this model, Fickian diffusion was used to explain the release of CAF from ChA for 120 minutes. When the same model is employed for the release of CAF loaded ChA for 60 minutes, the release was not simply diffusion transport, but also possibly include swelling where the polymer network expanded and disentangled to release the drug ($n = 0.324 - 0.478$) (Table 4.24). Owing to the effect of media saturation outside the tubing, the release mechanism with combined transport which only considered the first 60 minutes was more suitable to describe CAF release from ChA.

Table 4.23: Curve fitting of release of CAF to different release kinetic models for the first 120 minutes. R^2 is the coefficient correlation, k is constant (slope) and n is the exponent of Korsmeyer-Peppas model.

Sample		Zero order	First order	Higuchi	Hixson-Crowell	Korsmeyer-Peppas
CAF	R^2	0.466	0.987	0.941	0.958	0.989
	k	2.110	0.076	14.403	0.020	25.281
	n	-	-	-	-	0.344
ChC4-CAF	R^2	0.202	0.990	0.878	0.963	0.950
	k	1.139	0.044	10.710	0.011	21.055
	n	-	-	-	-	0.338
ChC6-CAF	R^2	0.127	0.920	0.847	0.853	0.937
	k	1.020	0.034	9.620	0.009	20.175
	n	-	-	-	-	0.323
ChC8-CAF	R^2	-0.328	0.598	0.690	0.417	0.930
	k	0.884	0.024	8.466	0.007	24.619
	n	-	-	-	-	0.244
ChC10-CAF	R^2	-0.328	0.614	0.709	0.434	0.954
	k	0.890	0.025	8.516	0.007	24.827
	n	-	-	-	-	0.243
ChC12-CAF	R^2	0.155	0.908	0.875	0.832	0.964
	k	0.991	0.030	9.322	0.008	19.341
	n	-	-	-	-	0.325

Table 4.24: Curve fitting of release of CAF to different release kinetic models for the first 60 minutes. R^2 is the coefficient correlation, k is constant (slope) and n is the exponent of Korsmeyer- Peppas model.

Sample		Zero order	First order	Higuchi	Hixson-Crowell	Korsmeyer-Peppas
CAF	R^2	0.466	0.987	0.941	0.958	0.989
	k	2.110	0.076	14.403	0.020	25.281
	n	-	-	-	-	0.344
ChC4-CAF	R^2	0.746	0.990	0.988	0.964	0.989
	k	1.852	0.044	12.409	0.012	13.440
	n	-	-	-	-	0.478
ChC6-CAF	R^2	0.659	0.953	0.957	0.900	0.962
	k	1.663	0.036	11.221	0.010	13.772
	n	-	-	-	-	0.444
ChC8-CAF	R^2	0.402	0.788	0.895	0.691	0.950
	k	1.499	0.030	10.272	0.008	18.712
	n	-	-	-	-	0.334
ChC10-CAF	R^2	0.392	0.788	0.909	0.688	0.973
	k	1.500	0.030	10.277	0.008	19.380
	n	-	-	-	-	0.324
ChC12-CAF	R^2	0.692	0.949	0.987	0.899	0.992
	k	1.604	0.032	10.794	0.009	13.340
	n	-	-	-	-	0.442

As observed in Figure 4.37 – 4.40, the release of drugs were slowed down after encapsulation using ChA by solvent entrapment, this showed that hydrogen bonding and Van der Waals forces between polymer chains and drugs as discussed previously in section 4.3.2 were involved in the sustained release of drugs. Among the ChA, ChC12 demonstrated highest ability to slow down the drug release with its longest chain length relative to the hydrophobic interaction between the polymer chains and between polymer and drug. The release of SA, LID, ACE and CAF in SGF took around 80, 50, 120 and 60 minutes to achieve 100% respectively. After encapsulation was carried out using ChC12, the release of SA, LID, ACE and CAF was slowed down by 17%, 24%, 30% and 33% as the release was suppressed to 83%, 76%, 70% and 67% at the respective release time. Even though the encapsulation of ACE and CAF by ChC12 was lower compared to SA and LID, ChC12 demonstrated better drug sustainability towards neutral ACE and CAF in SGF (Figure 4.41). This may be due to the chain extension of chitosan in acidic SGF

exposed the cationic chitosan to ionic interaction with the negatively charged SA and positively charged LID, especially the charge repulsion between the similar charge of chitosan and LID resulted in faster release of LID than SA. The hydrophobic interaction between alkyl groups of ChA can retain the neutral drugs ACE and CAF better compared to ionic drugs.

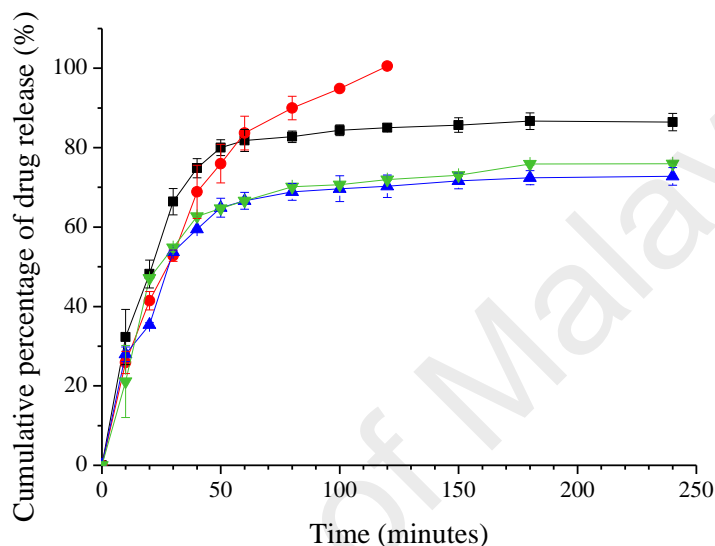


Figure 4.41: The cumulative release of SA (■), LID (●), ACE (▲) and CAF (▼) from ChC12 in SGF for the first 2 hours and in SIF for the subsequent hours at 37 °C.

4.4.3 Drug release mechanism

The proposed kinetic model for the release of four drugs from ChA for topical and oral delivery was the Korsmeyer-Peppas model, which not only described diffusion, but also involved swelling, as illustrated in Figure 4.42 using vertical Franz diffusion cells for topical delivery and in Figure 4.43 using dialysis tubing for oral delivery. During water penetration to the chitosan network, the chitosan swells and hence leads to the disentanglement and loosening of chitosan chains. The swelling percentage of ChA in 0.1 mol dm⁻³ HCl solution in the range of 18 – 25% was higher than those in deionized water due to the charged ions in the surrounding (8.43 – 10.31%) (section 4.2.9), chitosan chains were expanding faster and in a larger extent. Hence, the drugs were more flexible to move in a less dense network and diffused from the carrier to the surrounding media in the

donor compartment or inner of the dialysis tubing. This was followed by the diffusion of the drug across the membrane to the receptor compartment in vertical Franz diffusion cells or outside of the dialysis tubing.

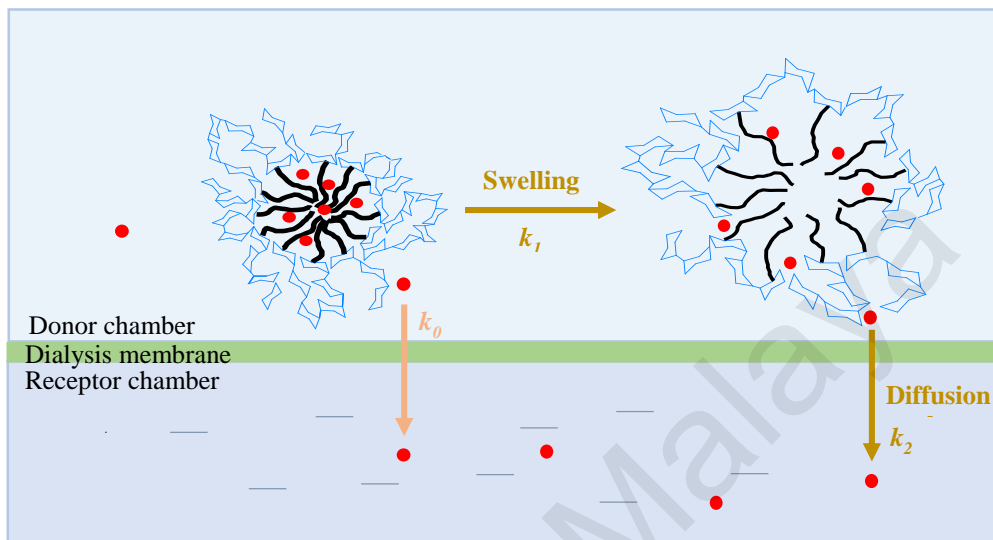


Figure 4.42: Schematic illustration of drug release from donor chamber to the receptor chamber of vertical Franz diffusion cells which includes polymer swelling and diffusion, where k_1 and k_2 are the rate constant of polymer swelling and drug diffusion across the membrane respectively, k_0 is the rate constant of unencapsulated drug from donor to the receptor chamber.

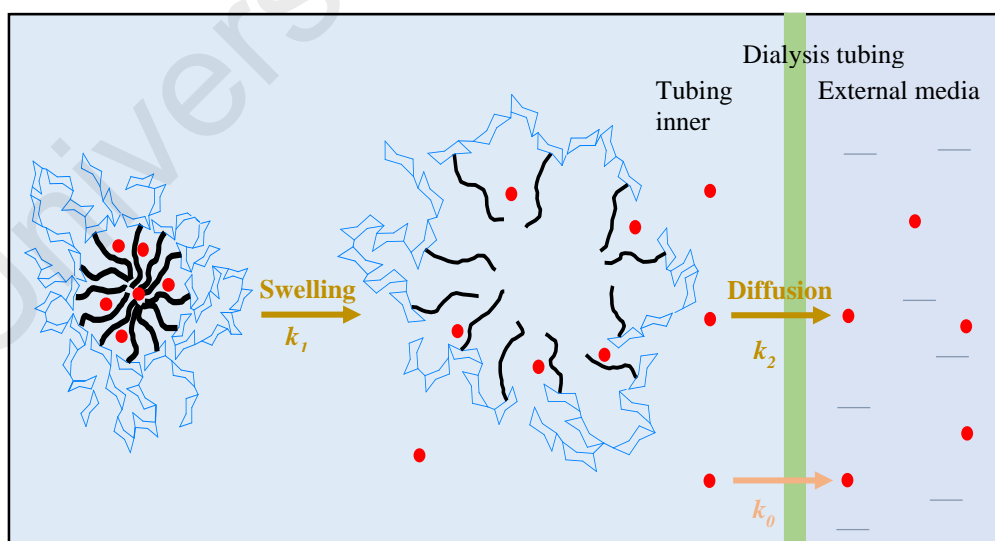


Figure 4.43: Schematic illustration of drug release from internal to the external of dialysis tubing which includes polymer swelling and diffusion, where k_1 and k_2 are the rate constant of polymer swelling and drug diffusion across the tubing respectively, k_0 is the rate constant of unencapsulated drug from internal to the external of the dialysis tubing.

For an anomalous non-Fickian transport system ($0.43 < n < 0.85$), the release kinetics was governed by the diffusion and swelling processes. As the swelling occurs throughout the polymer matrix continuously, the loosening of polymer chains triggers the release of drug from the system as the time passes, therefore the release kinetics was mainly dependent on the diffusion process. For a swelling controlled system, the polymeric system shows an interface to differentiate the swollen gel area from the inner glassy core, as spatial discontinuous swelling happens. The release initial from the gel region by diffusion, the interface extend to the inner matrix as gelatinization proceeds. Since the diffusivity is determined by time-dependent relaxation of polymer chains in this gel region during the transition process, thus the release rate was swelling dependent (Fan & Singh, 1989). There is no clear cut between diffusion and swelling as these two processes mostly occur synergistically.

Drug release in acidic SGF was fast using dialysis tubing as the surface area of totally immersed dialysis tubing exposed to media for diffusion was larger. Secondly, the low pH of acidic SGF protonated the cationic chitosan to extend the polymer chains and weaken the chain association, facilitated the release of drugs from the tubing at much easier and faster manner.

4.4.4 Limitation of dialysis

Limited permeability of the dialysis membrane or tubing sometimes occurs, especially to the poorly water soluble drugs such as paclitaxel (Abouelmagd et al., 2015). Nevertheless, this phenomenon presumably did not occur in this study as the release of pure drug was completed within 16 hours for topical delivery or within 120 minutes for oral delivery. Unlike the gravitational force driven in nature for the drug diffusion from donor compartment to receptor compartment in vertical Franz diffusion cells (Figure

4.41), the inner drug solution across the dialysis tubing to the external media for oral delivery was in a parallel horizontal direction (Figure 4.42). As time passes, the drug accumulation outside the tubing is gaining while those in the inner was decreasing, resulting in the drug permeation across the tubing slowing down until equilibrium of both sides was achieved, this giving rise to media saturation outside the tubing problem. Hence, the drug release reached a plateau where no significant drug release was observed as the driving force is too weak. The effect was more obvious when it was further delayed by the interaction between drugs and ChA. This explained that the drug release from ChA in Figure 4.36 – 4.39 reached plateau after certain time of release. This drawback also affected the calculation of the release exponent in the Korsmeyer-Peppas model for the first 120 and 60 minutes. When the release was counted for 120 minutes, diffusion was the only process to describe the drug release. However, swelling is also included as well as the diffusion when the release duration was only considered for the first 60 minutes. This showed that the media saturation at the external of the tubing as a consequence of long duration of dialysis greatly influenced the diffusion process from the inner to the external of the tubing and may mislead the release mechanism.

CHAPTER 5: CONCLUSION

5.1 Conclusion

In order to improve solubility of chitosan in water for drug delivery in a physiological environment, low molecular weight chitosan with 25 kDa chitosan was prepared via depolymerization with sodium nitrite, which was further hydrophobically modified with low and medium alkyl chain to produce acylated chitosan (ChA) such as butyryl (ChC4), hexanoyl (ChC6), octanoyl (ChC8), decanoyl (ChC10) and lauryl chitosan (ChC12). The appearance of amide II peak and the increase of peak intensity of amide carbonyl stretching of ChA after acylation shown in the FTIR spectrum which further enhanced as the degree of substitution increased provided confidence on the successful acylation of chitosan. Furthermore, the successful acylation of chitosan was also confirmed by the presence of new CH₂ and CH₃ peaks in ¹H NMR and new carbon peaks in ¹³C NMR respectively.

Both long chain length and a high degree of substitution of ChA contributed to the decrease in the particle size as the hydrophobic interaction of ChA was enhanced. The zeta potential of ChA shifted from positive value to negative value after acylation because the neutralization of cationic amino group of chitosan by the substitution of alkyl groups. The water solubility and critical aggregation concentration (CAC) of ChA were decreased as the chain length increased, as well as their swelling in deionized water and acidic media, nevertheless the viscosity of ChA was marginally different. Both X-ray diffraction (XRD) and thermogravimetric analysis (TGA) showed that longer chain acylated chitosan were less crystalline and more susceptible to water sorption. The micrographs from transmission electron microscopy (TEM) and field-emission scanning electron microscopy (FE-SEM) showed that ChA formed spherical particles.

After the successful confirmation of modifications and characterization studies of ChA, the ChA prepared was loaded with four model analgesic drugs with different solubilities by the precipitation technique. The encapsulation efficiency of ChA decreased as the drug solubility increased in the sequence of salicylic acid (SA), lidocaine (LID), acetaminophen (ACE) and caffeine (CAF). From the FTIR spectrum, the suggested interaction between ChA and drugs were hydrogen bonding or together with Van der Waals forces. ChA still maintained a spherical shape after drug loading from the observation in TEM micrographs. The increment of particle size of SA was higher than LID and ACE, whereas the size was decreased after loading of CAF, hence this proposes that slightly water soluble SA and LID was entrapped in the hydrophobic region of ChA whereas sparingly water soluble ACE and CAF resides at the region between the hydrophobic core and hydrophilic corona of ChA. Particle size of drugs loaded ChA was not only dependent on the drug solubility, but was also influenced by the chain length of ChA.

The *in vitro* release using inline vertical Franz diffusion cells in phosphate buffered saline solution pH 7.4 and in simulated gastric fluid pH 1.2 using dialysis tubing showed that the release of drugs was slower after incorporation using ChA as compared to free drug solution. The best model to describe the drug release from ChA was the Korsmeyer-Peppas model, with the release exponent (n) calculated proposing that the drug release mechanism of ChA was the swelling of ChA chains followed by the drug diffusion across the membrane. The drug sustainability of ChA suggested that ChA are potential drug carriers for topical delivery and possibly for oral delivery with further pH responsive modifications, particularly the longest chain length of ChC12 can prolong drug release to the longest period among the ChA due to its strongest hydrophobic interaction between polymer chains and between polymer chains and drugs.

5.2 Future Work

We have proposed the position of drugs with different solubilities in acylated chitosan after encapsulation by taking considerations on drugs solubility, particle size and interaction between ChA and drugs in section 4.3.5. For future study, the work can be investigated by other methods such as computational simulation to compare with the proposed hypothesis, as the outcome may contribute to further studies on the pharmacology and pharmacokinetics of drugs loaded ChA with the cell lines and animals. For topical delivery in details, the acylated chitosan can be incorporated into cream or gel for drug release study and also to carry out some biological assays such as skin irritation, cytotoxicity tests, *ex vivo* and *in vivo* animal studies, whereas for oral applications, the acylated chitosan can be further modified with carboxyl groups to be pH sensitive so that it can control release in acidic stomach and stimulate release in the intestinal environment.

REFERENCES

- Abdel Aziz, M. S., Naguib, H. F., & Saad, G. R. (2015). Nanocomposites based on chitosan-graft-poly(*N*-vinyl-2-pyrrolidone): Synthesis, characterization, and biological activity. *International Journal of Polymeric Materials and Polymeric Biomaterials*, 64(11), 578-586.
- Abeygunawardana, C., Bush, C. A., & Cisar, J. O. (1991). Complete structure of the cell surface polysaccharide of *Streptococcus oralis* ATCC 10557: a receptor for lectin-mediated interbacterial adherence. *Biochemistry*, 30(26), 6528-6540.
- Abhilash, M. (2010). Potential applications of nanoparticles. *International Journal of Pharma and Bio Sciences*, 1(1), 1-12.
- Abouelmagd, S. A., Sun, B., Chang, A. C., Ku, Y. J., & Yeo, Y. (2015). Release kinetics study of poorly water-soluble drugs from nanoparticles: Are we doing it right? *Molecular Pharmaceutics*, 12(3), 997-1003.
- Abul Kalam, M. (2016a). Development of chitosan nanoparticles coated with hyaluronic acid for topical ocular delivery of dexamethasone. *International Journal of Biological Macromolecules*, 89, 127-136.
- Abul Kalam, M. (2016b). The potential application of hyaluronic acid coated chitosan nanoparticles in ocular delivery of dexamethasone. *International Journal of Biological Macromolecules*, 89, 559-568.
- Acosta, N., Sanchez, E., Calderon, L., Cordoba-Diaz, M., Cordoba-Diaz, D., Dom, S., & Heras, A. (2015). Physical stability studies of semi-solid formulations from natural compounds loaded with chitosan microspheres. *Marine Drugs*, 13(9), 5901-5919.
- Agnihotri, S. A., Mallikarjuna, N. N., & Aminabhavi, T. M. (2004). Recent advances on chitosan-based micro- and nanoparticles in drug delivery. *Journal of Controlled Release*, 100(1), 5-28.
- Ahmed, T. A., & Aljaeid, B. M. (2016). Preparation, characterization, and potential application of chitosan, chitosan derivatives, and chitosan metal nanoparticles in pharmaceutical drug delivery. *Drug Design, Development and Therapy*, 10, 483-507.
- Aiedeh, K., & Taha, M. O. (1999). Synthesis of chitosan succinate and chitosan phthalate and their evaluation as suggested matrices in orally administered, colon-specific drug delivery systems. *Archiv der Pharmazie*, 332(3), 103-107.

- Ajun, W., Yan, S., Li, G., & Huili, L. (2009). Preparation of aspirin and probucol in combination loaded chitosan nanoparticles and *in vitro* release study. *Carbohydrate Polymers*, 75(4), 566-574.
- Al-Kurdi, Z. I., Chowdhry, B. Z., Leharne, S. A., Al Omari, M. M., & Badwan, A. A. (2015). Low molecular weight chitosan-insulin polyelectrolyte complex: Characterization and stability studies. *Marine Drugs*, 13(4), 1765-1784.
- Al-Sou'od, K., Abu-Falaha, R., & Al-Remawi, M. (2013). Surface activity of some low molecular weight chitosan derivatives. *Jordan Journal of Chemistry*, 8(1), 1-17.
- Allan, G. G., & Peyron, M. (1995). Molecular weight manipulation of chitosan I: Kinetics of depolymerization by nitrous acid. *Carbohydrate Research*, 277(2), 257-272.
- Alves, N. M., & Mano, J. F. (2008). Chitosan derivatives obtained by chemical modifications for biomedical and environmental applications. *International Journal of Biological Macromolecules*, 43(5), 401-414.
- Amaral, I. F., Granja, P. L., & Barbosa, M. A. (2005). Chemical modification of chitosan by phosphorylation: an XPS, FT-IR and SEM study. *Journal of Biomaterials Science, Polymer Edition*, 16(12), 1575-1593.
- Ambroggi, V., Pietrella, D., Nocchetti, M., Casagrande, S., Moretti, V., De Marco, S., & Ricci, M. (2017). Montmorillonite-chitosan-chlorhexidine composite films with antibiofilm activity and improved cytotoxicity for wound dressing. *Journal of Colloid and Interface Science*, 491, 265-272.
- Amidi, M., Romeijn, S. G., Borchard, G., Junginger, H. E., Hennink, W. E., & Jiskoot, W. (2006). Preparation and characterization of protein-loaded *N*-trimethyl chitosan nanoparticles as nasal delivery system. *Journal of Controlled Release*, 111(1-2), 107-116.
- Amiji, M. M. (1995). Pyrene fluorescence study of chitosan self-association in aqueous solution. *Carbohydrate Polymers*, 26(3), 211-213.
- Anitha, A., Maya, S., Deepa, N., Chennazhi, K. P., Nair, S. V., Tamura, H., & Jayakumar, R. (2011). Efficient water soluble *O*-carboxymethyl chitosan nanocarrier for the delivery of curcumin to cancer cells. *Carbohydrate Polymers*, 83(2), 452-461.
- Aranaz, I., Mengibar, M., Harris, R., Panos, I., Miralles, B., Acosta, N., Galed, G., Heras, A. (2009). Functional characterization of chitin and chitosan. *Current Chemical Biology*, 3, 203-230.
- Artan, M., Karadeniz, F., Karagozlu, M. Z., Kim, M. M., & Kim, S. K. (2010). Anti-HIV-1 activity of low molecular weight sulfated chitoooligosaccharides. *Carbohydrate Research*, 345(5), 656-662.

- Badawi, A. A., El-Laithy, H. M., El Qidra, R. K., El Mofty, H., & El dally, M. (2008). Chitosan based nanocarriers for indomethacin ocular delivery. *Archives of Pharmacal Research*, 31(8), 1040-1049.
- Badawi, H. M., Forner, W., & Ali, S. A. (2015). The conformational stability, solvation and the assignments of the experimental infrared, Raman, ¹H and ¹³C NMR spectra of the local anesthetic drug lidocaine. *Spectrochimica Acta Part A: Molecular and Biomolecular Spectroscopy*, 142, 382-391.
- Badawy, M. E. I., Rabea, E. I., Rogge, T. M., Stevens, C. V., Smagghe, G., Steurbaut, W., & Hofte, M. (2004). Synthesis and fungicidal activity of new *N,O*-acyl chitosan derivatives. *Biomacromolecules*, 5(2), 589-595.
- Bae, M. S., Kwon, I. C., Jeong, S. Y., & Lee, K. Y. (2005). Nano-structured chitosan self-aggregates as a drug delivery carrier. Technical Proceedings of the 2005 NSTI Nanotechnology Conference and Trade Show. In *Chapter 3 Drug delivery* (pp. 164-167). Austin, USA: Nano Science and Technology Institute.
- Balan, V., Dodi, G., Tudorachi, N., Ponta, O., Simon, V., Butnaru, M., & Verestiuc, L. (2015). Doxorubicin-loaded magnetic nanocapsules based on *N*-palmitoyl chitosan and magnetite: Synthesis and characterization. *Chemical Engineering Journal*, 279, 188-197.
- Barry, J. E., Finkelstein, M., & Ross, S. D. (1976). The amide-phenol ratios and structures in amide-picric acid complexes. *Tetrahedron*, 32(2), 223-227.
- Bernkop-Schnurch, A., & Dunnhaupt, S. (2012). Chitosan-based drug delivery systems. *European Journal of Pharmaceutics and Biopharmaceutics*, 81(3), 463-469.
- Bhalerao, S. S., & Raje Harshal, A. (2003). Preparation, optimization, characterization, and stability studies of salicylic acid liposomes. *Drug Development and Industrial Pharmacy*, 29(4), 451-467.
- Bonferoni, M. C., Sandri, G., Delleria, E., Rossi, S., Ferrari, F., Mori, M., & Caramella, C. (2014). Ionic polymeric micelles based on chitosan and fatty acids and intended for wound healing. Comparison of linoleic and oleic acid. *European Journal of Pharmaceutics and Biopharmaceutics*, 87(1), 101-106.
- Bosso, C., Defaye, J., Domard, A., Gadelle, A., & Pedersen, C. (1986). The behavior of chitin towards anhydrous hydrogen fluoride. Preparation of β -(1 \rightarrow 4)-linked 2-acetamido-2-deoxy-*D*-glucopyranosyl oligosaccharides. *Carbohydrate Research*, 156, 57-68.
- Bowman, K., & Leong, K. W. (2006). Chitosan nanoparticles for oral drug and gene delivery. *International Journal of Nanomedicine*, 1(2), 117-128.

- Brewer, E., Coleman, J., & Lowman, A. (2011). Emerging technologies of polymeric nanoparticles in cancer drug delivery. *Journal of Nanomaterials*, 408675, 10 pages.
- Bulut, E. (2016). Controlled delivery of the popular nonsteroidal anti-inflammatory drug, paracetamol, from chitosan-g-polyacrylamide microspheres prepared by the emulsion crosslinking technique. *Artificial Cells, Nanomedicine, and Biotechnology*, 44(6), 1482-1490.
- Burgina, E. B., Baltakhinov, V. P., Boldyreva, E. V., & Shakhtschneider, T. P. (2004). IR Spectra of paracetamol and phenacetin. 1. Theoretical and experimental studies. *Journal of Structural Chemistry*, 45(1), 64-73.
- Burkatovskaya, M., Castano, A. P., Demidova-Rice, T. N., Tegos, G. P., & Hamblin, M. R. (2008). Effect of chitosan acetate bandage on wound healing in infected and noninfected wounds in mice. *Wound repair and regeneration : official publication of the Wound Healing Society [and] the European Tissue Repair Society*, 16(3), 425-431.
- Cai, K., Yao, K., Cui, Y., Lin, S., Yang, Z., Li, X., Xie, H., Qing, T., & Luo, J. (2002). Surface modification of poly (*D,L*-lactic acid) with chitosan and its effects on the culture of osteoblasts *in vitro*. *Journal of Biomedical Materials Research Part A*, 60(3), 398-404.
- Calderon, L., Harris, R., Cordoba-Diaz, M., Elorza, M., Elorza, B., Lenoir, J., Adriaens, E., Remon, J. P., Heras, A., & Cordoba-Diaz, D. (2013). Nano and microparticulate chitosan-based systems for antiviral topical delivery. *European Journal of Pharmaceutical Sciences*, 48(1-2), 216-222.
- Calejo, M. T., Kjoniksen, A. L., Maleki, A., Nystrom, B., & Sande, S. A. (2014). Microparticles based on hydrophobically modified chitosan as drug carriers. *Journal of Applied Polymer Science*, 131(7), 40055, 11 pages.
- Cano-Cebrian, M. J., Zornoza, T., Granero, L., & Polache, A. (2005). Intestinal absorption enhancement via the paracellular route by fatty acids, chitosans and others: A target for drug delivery. *Current Drug Delivery*, 2(1), 9-22.
- Carbinatto, F. M., de Castro, A. D., Evangelista, R. C., & Cury, B. S. F. (2014). Insights into the swelling process and drug release mechanisms from cross-linked pectin/high amylose starch matrices. *Asian Journal of Pharmaceutical Sciences*, 9, 27-34.
- Carreno-Gomez, B., & Duncan, R. (1997). Evaluation of the biological properties of soluble chitosan and chitosan microspheres. *International Journal of Pharmaceutics*, 148(2), 231-240.

- Carson, L., Kelly-Brown, C., Stewart, M., Oki, A., Regisford, G., Stone, J., Traisawatwong, P., Durand-Rougely, C., & Luo, Z. (2010). Grafting of chitosan and chitosantrimethoxysilylpropyl methacrylate on single walled carbon nanotubes-synthesis and characterization. *Journal of Chemistry and Chemical Engineering*, 4(9), 6-13.
- Chaiyasan, W., Srinivas, S. P., & Tiyaboonchai, W. (2015). Crosslinked chitosan-dextran sulfate nanoparticle for improved topical ocular drug delivery. *Molecular Vision*, 21, 1224-1234.
- Chen, C., Tao, S., Qiu, X., Ren, X., & Hu, S. (2013). Long-alkane-chain modified *N*-phthaloyl chitosan membranes with controlled permeability. *Carbohydrate Polymers*, 91(1), 269-276.
- Chen, M. C., Mi, F. L., Liao, Z. X., & Sung, H. W. (2011a). Chitosan: Its applications in drug-eluting devices. In Jayakumar, R., Prabakaran, M., & Muzzarelli, R. A. A. (Eds.), *Chitosan for biomaterials I* (pp. 185-230). Berlin, Heidelberg: Springer-Verlag GmbH.
- Chen, M., Liu, Y., Yang, W., Li, X., Liu, L., Zhou, Z., Wang, Y., Li, R., & Zhang, Q. (2011b). Preparation and characterization of self-assembled nanoparticles of 6-*O*-cholesterol-modified chitosan for drug delivery. *Carbohydrate Polymers*, 84(4), 1244-1251.
- Chen, S., & Wang, Y. (2001). Study on β -cyclodextrin grafting with chitosan and slow release of its inclusion complex with radioactive iodine. *Journal of Applied Polymer Science*, 82(10), 2414-2421.
- Chen, S., Wu, G., & Zeng, H. (2005). Preparation of high antimicrobial activity thiourea chitosan-Ag⁺ complex. *Carbohydrate Polymers*, 60(1), 33-38.
- Chen, X., Ding, S., Qu, G., & Zhang, C. (2008). Synthesis of novel chitosan derivatives for micellar solubilization of cyclosporine A. *Journal of Bioactive and Compatible Polymers*, 23(6), 563-578.
- Chen, X. G., Lee, C. M., & Park, H. J. (2003). O/W emulsification for the self-aggregation and nanoparticle formation of linoleic acid-modified chitosan in the aqueous system. *Journal of Agricultural and Food Chemistry*, 51(10), 3135-3139.
- Cheng, Y. H., Tsai, T. H., Jhan, Y. Y., Chiu, A. W. H., Tsai, K. L., Chien, C. S., Chiou, S. H., & Liu, C. J. L. (2016). Thermosensitive chitosan-based hydrogel as a topical ocular drug delivery system of latanoprost for glaucoma treatment. *Carbohydrate Polymers*, 144, 390-399.
- Chiandotti, R. S., Rodrigues, P. C., & Akcelrud, L. (2010). Grafting of chitosan with fatty acyl derivatives. *Journal of the Brazilian Chemical Society*, 21, 1910-1916.

- Cho, I. S., Park, C. G., Huh, B. K., Cho, M. O., Khatun, Z., Li, Z., Kang, S. W., Choy, Y. B., & Huh, K. M. (2016). Thermosensitive hexanoyl glycol chitosan-based ocular delivery system for glaucoma therapy. *Acta Biomaterialia*, 39, 124-132.
- Cho, Y., Kim, J. T., & Park, H. J. (2012a). Preparation, characterization, and protein loading properties of *N*-acyl chitosan nanoparticles. *Journal of Applied Polymer Science*, 124, 1366-1371.
- Cho, Y., Kim, J. T., & Park, H. J. (2012b). Size-controlled self-aggregated *N*-acyl chitosan nanoparticles as a vitamin C carrier. *Carbohydrate Polymers*, 88(3), 1087-1092.
- Choochottiros, C., Yoksan, R., & Chirachanchai, S. (2009). Amphiphilic chitosan nanospheres: Factors to control nanosphere formation and its consequent pH responsive performance. *Polymer*, 50(8), 1877-1886.
- Clayden, J., Greeves, N., & Warren, S. (2012). *Organic Chemistry* (pp. 521). Oxford, UK: Oxford University Press.
- Costa, I. d. S. M., Abranches, R. P., Garcia, M. T. J., & Pierre, M. B. R. (2014). Chitosan-based mucoadhesive films containing 5-aminolevulinic acid for buccal cancer's treatment. *Journal of Photochemistry and Photobiology B: Biology*, 140, 266-275.
- Costa, P., & Sousa Lobo, J. M. (2001). Modeling and comparison of dissolution profiles. *European Journal of Pharmaceutical Sciences*, 13(2), 123-133.
- Critchfield, F. E., Gibson, J. A., & Hall, J. L. (1953). Dielectric constant and refractive index from 20 to 35° and density at 25° for the system tetrahydrofuran-water. *Journal of the American Chemical Society*, 75(23), 6044-6045.
- Crittenden, J. C., Trussell, R. R., Hand, D. W., Howe, K. J., & Tchobanoglous, G. (2012). Appendix C: Physical properties of water. In *MWH's water treatment: Principles and design, Third Edition* (pp. 1861-1862). New Jersey, USA: John Wiley & Sons, Inc.
- Cui, F., Qian, F., Zhao, Z., Yin, L., Tang, C., & Yin, C. (2009). Preparation, characterization, and oral delivery of insulin loaded carboxylated chitosan grafted poly(methyl methacrylate) nanoparticles. *Biomacromolecules*, 10(5), 1253-1258.
- da Silva, D. S., Canafistula, F. V. C., & Fernandes, F. P. (2016). Preparation and characterization of membranes based on chitosan for topical drug delivery. *Indo American Journal of Pharmaceutical Research*, 6(2), 4436-4443.
- Dai, T., Tegos, G. P., Burkatovskaya, M., Castano, A. P., & Hamblin, M. R. (2009). Chitosan acetate bandage as a topical antimicrobial dressing for infected burns. *Antimicrobial Agents and Chemotherapy*, 53(2), 393-400.

- Dang, J. M., Sun, D. D. N., Shin-Ya, Y., Sieber, A. N., Kostuik, J. P., & Leong, K. W. (2006). Temperature-responsive hydroxybutyl chitosan for the culture of mesenchymal stem cells and intervertebral disk cells. *Biomaterials*, 27(3), 406-418.
- Dash, M., Chiellini, F., Ottenbrite, R. M., & Chiellini, E. (2011). Chitosan-A versatile semi-synthetic polymer in biomedical applications. *Progress in Polymer Science*, 36(8), 981-1014.
- Dash, S., Murthy, P. N., Nath, L., & Chowdhury, P. (2010). Kinetic modeling on drug release from controlled drug delivery systems. *Acta Polonica Pharmaceutica*, 67(3), 217-223.
- Derry, S., Wiffen, P. J., Moore, R. A., & Quinlan, J. (2014). Topical lidocaine for neuropathic pain in adults. *Cochrane Database of Systematic Reviews*, (7), CD010958, 50 pages.
- Desai, M. P., Labhsetwar, V., Walter, E., Levy, R. J., & Amidon, G. L. (1997). The mechanism of uptake of biodegradable microparticles in Caco-2 cells is size dependent. *Pharmaceutical Research*, 14(11), 1568-1573.
- Dey, I., Lejeune, M., & Chadee, K. (2006). Prostaglandin E2 receptor distribution and function in the gastrointestinal tract. *British Journal of Pharmacology*, 149(6), 611-623.
- Divney, S., & Di Schiena, M. (2014a). *U.S. Patent No. WO2014085421A1*. Washington, United States: United States Patent and Trademark Office. Retrieved on January 5, 2015, from <https://patents.google.com/patent/WO2014085421A1/en>
- Divney, S., & Di Schiena, M. G. (2014b). *U.S. Patent No. EP2737902A1*. Washington, United States: United States Patent and Trademark Office. Retrieved on January 5, 2015, from <https://patents.google.com/patent/EP2737902A1/en>
- Donati, I., Stredanska, S., Silvestrini, G., Vetere, A., Marcon, P., Marsich, E., Mozetic, P., Gamini, A., Paoletti, S., & Vittur, F. (2005). The aggregation of pig articular chondrocyte and synthesis of extracellular matrix by a lactose-modified chitosan. *Biomaterials*, 26(9), 987-998.
- Drozd, N. N., Sher, A. I., Makarov, V. A., Galbraikh, L. S., Vikhoreva, G. A., & Gorbachiova, I. N. (2001). Comparison of antithrombin activity of the polysulphate chitosan derivatives in *in vivo* and *in vitro* system. *Thrombosis Research*, 102(5), 445-455.
- Du, Y. Z., Wang, L., Yuan, H., Wei, X. H., & Hu, F. Q. (2009). Preparation and characteristics of linoleic acid-grafted chitosan oligosaccharide micelles as a carrier for doxorubicin. *Colloids and Surfaces B: Biointerfaces*, 69(2), 257-263.

- Duhem, N., Rolland, J., Riva, R., Guillet, P., Schumers, J. M., Jerome, C., Gohy, J.F., & Preat, V. (2012). Tocol modified glycol chitosan for the oral delivery of poorly soluble drugs. *International Journal of Pharmaceutics*, 423(2), 452-460.
- Duttagupta, D. S., Jadhav, V. M., & Kadam, V. J. (2015). Chitosan: A propitious biopolymer for drug delivery. *Current Drug Delivery*, 12(4), 369-381.
- Einbu, A., Grasdalen, H., & Varum, K. M. (2007). Kinetics of hydrolysis of chitin/chitosan oligomers in concentrated hydrochloric acid. *Carbohydrate Research*, 342(8), 1055-1062.
- El-Hefian, E. A., Elgannoudi, E. S., Mainal, A., & Yahaya, A. H. (2010). Characterization of chitosan in acetic acid: rheological and thermal studies. *Turkish Journal of Chemistry*, 34(1), 47-56.
- El-Hefian, E. A., Nasef, M. M., & Yahaya, A. H. (2012). Preparation and characterization of chitosan/agar blended films: Part 2. Thermal, mechanical, and surface properties. *E-Journal of Chemistry*, 9(2), 510-516.
- El-Kamel, A. H., Sokar, M. S., Al Gamal, S. S., & Naggar, V. F. (2003). Evaluation of stomach protective activity of ketoprofen floating microparticles. *Indian Journal of Pharmaceutical Sciences*, 65(4), 399-401.
- El-Leithy, E. S., Shaker, D. S., Ghorab, M. K., & Abdel-Rashid, R. S. (2010). Evaluation of mucoadhesive hydrogels loaded with diclofenac sodium-chitosan microspheres for rectal administration. *AAPS PharmSciTech*, 11(4), 1695-1702.
- El-Tahlawy, K., Gaffar, M. A., & El-Rafie, S. (2006). Novel method for preparation of β -cyclodextrin-grafted chitosan and its application. *Carbohydrate Polymers*, 63(3), 385-392.
- Enslin, G. M., Hamman, J. H., & Kotze, A. F. (2008). Intestinal drug absorption enhancers: synergistic effects of combinations. *Drug Development and Industrial Pharmacy*, 34(12), 1343-1349.
- Fabbrocini, G., Annunziata, M. C., D'Arco, V., De Vita, V., Lodi, G., Mauriello, M. C., Pastore, F., & Monfrecola, G. (2010). Acne scars: Pathogenesis, classification and treatment. *Dermatology Research and Practice*, 2010, 893080, 13 pages.
- Fan, L. T., & Singh, S. K. (1989). Swelling-Controlled Release. In *Controlled release: A quantitative treatment* (pp. 110-156). Berlin, Heidelberg: Springer-Verlag GmbH.
- Farag, R. K., & Mohamed, R. R. (2013). Synthesis and characterization of carboxymethyl chitosan nanogels for swelling studies and antimicrobial activity. *Molecules*, 18, 190-203.

- Fathalla, Z. M. A., Khaled, K. A., Hussein, A. K., Alany, R. G., & Vangala, A. (2016). Formulation and corneal permeation of ketorolac tromethamine-loaded chitosan nanoparticles. *Drug Development and Industrial Pharmacy*, 42(4), 514-524.
- Fattahpour, S., Shamanian, M., Tavakoli, N., Fathi, M., Sheykhi, S. R., & Fattahpour, S. (2015). Design and optimization of alginate-chitosan-pluronic nanoparticles as a novel meloxicam drug delivery system. *Journal of Applied Polymer Science*, 132(28), 42241, 12 pages.
- Feng, F., Liu, Y., Zhao, B., & Hu, K. (2012). Characterization of half *N*-acetylated chitosan powders and films. *Procedia Engineering*, 27, 718-732.
- Feng, T., Du, Y., Li, J., Hu, Y., & Kennedy, J. F. (2008). Enhancement of antioxidant activity of chitosan by irradiation. *Carbohydrate Polymers*, 73(1), 126-132.
- Fernandes, J. C., Tavaría, F. K., Soares, J. C., Ramos, O. S., Joao Monteiro, M. J., Pintado, M. E., & Malcata, F. X. (2008). Antimicrobial effects of chitosans and chitooligosaccharides, upon *Staphylococcus aureus* and *Escherichia coli*, in food model systems. *Food Microbiology*, 25(7), 922-928.
- Focher, B., Naggi, A., Torri, G., Cosani, A., & Terbojevich, M. (1992). Chitosans from *Euphausia superba*. 2: Characterization of solid state structure. *Carbohydrate Polymers*, 18(1), 43-49.
- Fowler, P. D. (1987). Aspirin, paracetamol and non-steroidal anti-inflammatory drugs. A comparative review of side effects. *Medical Toxicology and Adverse Drug Experience*, 2(5), 338-366.
- Gammaitoni, A. R., Alvarez, N. A., & Galer, B. S. (2003). Safety and tolerability of the lidocaine patch 5%, a targeted peripheral analgesic: A review of the literature. *The Journal of Clinical Pharmacology*, 43(2), 111-117.
- Garcia-Fuentes, M., & Alonso, M. J. (2012). Chitosan-based drug nanocarriers: Where do we stand? *Journal of Controlled Release*, 161(2), 496-504.
- Gelfuso, G. M., Barros, M. A. d. O., Delgado-Charro, M. B., Guy, R. H., & Lopez, R. F. V. (2015). Iontophoresis of minoxidil sulphate loaded microparticles, a strategy for follicular drug targeting? *Colloids and Surfaces B: Biointerfaces*, 134, 408-412.
- Genta, I., Conti, B., Perugini, P., Pavanetto, F., Spadaro, A., & Puglisi, G. (1997). Bioadhesive microspheres for ophthalmic administration of acyclovir. *Journal of Pharmacy and Pharmacology*, 49(8), 737-742.

- Goldstein, J. (2001). Caffeine as an analgesic adjuvant. *Inflammopharmacology*, 9(1), 51-61.
- Golzari, S. E. J., Soleimanpour, H., Mahmoodpoor, A., Safari, S., & Ala, A. (2014). Lidocaine and pain management in the emergency department: A review article. *Anesthesiology and Pain Medicine*, 4(1), e15444, 6 pages.
- Goncalves, R. M., Pereira, A. C. L., Pereira, I. O., Oliveira, M. J., & Barbosa, M. A. (2015). Macrophage response to chitosan/poly-(γ -glutamic acid) nanoparticles carrying an anti-inflammatory drug. *Journal of Materials Science: Materials in Medicine*, 26(4), 1-12.
- Govender, T., Stolnik, S., Garnett, M. C., Illum, L., & Davis, S. S. (1999). PLGA nanoparticles prepared by nanoprecipitation: drug loading and release studies of a water soluble drug. *Journal of Controlled Release*, 57(2), 171-185.
- Griswold, D. E., & Adams, J. L. (1996). Constitutive cyclooxygenase (COX-1) and inducible cyclooxygenase (COX-2): Rationale for selective inhibition and progress to date. *Medical Research Reviews*, 16(2), 181-206.
- Guinesi, L. S., & Cavalheiro, E. T. G. (2006). The use of DSC curves to determine the acetylation degree of chitin/chitosan samples. *Thermochimica Acta*, 444(2), 128-133.
- Guo, H., Zhang, D., Li, C., Jia, L., Liu, G., Hao, L., Zheng, D., Shen, J., Li, T., Guo, Y., & Zhang, Q. (2013). Self-assembled nanoparticles based on galactosylated *O*-carboxymethyl chitosan-graft-stearic acid conjugates for delivery of doxorubicin. *International Journal of Pharmaceutics*, 458(1), 31-38.
- Gupta, V., & Lipsitz, L. A. (2007). Orthostatic hypotension in the elderly: Diagnosis and treatment. *American Journal of Medicine*, 120(10), 841-847.
- Hai, L., Bang Diep, T., Nagasawa, N., Yoshii, F., & Kume, T. (2003). Radiation depolymerization of chitosan to prepare oligomers. *Nuclear Instruments and Methods in Physics Research Section B: Beam Interactions with Materials and Atoms*, 208, 466-470.
- Harish Prashanth, K. V., & Tharanathan, R. N. (2007). Chitin/chitosan: modifications and their unlimited application potential-an overview. *Trends in Food Science & Technology*, 18(3), 117-131.
- Harris, R., Lecumberri, E., Mateos-Aparicio, I., Mengibar, M., & Heras, A. (2011). Chitosan nanoparticles and microspheres for the encapsulation of natural antioxidants extracted from *Ilex paraguariensis*. *Carbohydrate Polymers*, 84(2), 803-806.

- Hasanovic, A., Zehl, M., Reznicek, G., & Valenta, C. (2009). Chitosan-tripolyphosphate nanoparticles as a possible skin drug delivery system for aciclovir with enhanced stability. *Journal of Pharmacy and Pharmacology*, 61(12), 1609-1616.
- Hasegawa, M., Isogai, A., & Onabe, F. (1993). Preparation of low-molecular-weight chitosan using phosphoric acid. *Carbohydrate Polymers*, 20(4), 279-283.
- Hassani Najafabadi, A., Abdouss, M., & Faghihi, S. (2014). Synthesis and evaluation of PEG-O-chitosan nanoparticles for delivery of poor water soluble drugs: ibuprofen. *Material Science and Engineering C: Materials for Biological Applications*, 41, 91-99.
- Hauptstein, S., Dezorzi, S., Prufert, F., Matuszczak, B., & Bernkop-Schnurch, A. (2015). Synthesis and *in vitro* characterization of a novel S-protected thiolated alginate. *Carbohydrate Polymers*, 124, 1-7.
- Hawkins, L. C., Edwards, J. N., & Dargan, P. I. (2007). Impact of restricting paracetamol pack sizes on paracetamol poisoning in the United Kingdom: A review of the literature. *Drug Safety*, 30(6), 465-479.
- Hayashi, K., & Ito, M. (2002). Antidiabetic action of low molecular weight chitosan in genetically obese diabetic KK-A^y mice. *Biological & Pharmaceutical Bulletin*, 25(2), 188-192.
- He, G., Chen, X., Yin, Y., Zheng, H., Xiong, X., & Du, Y. (2011). Synthesis, characterization and antibacterial activity of salicyloyl chitosan. *Carbohydrate Polymers*, 83(3), 1274-1278.
- He, P., Davis, S. S., & Illum, L. (1999). Chitosan microspheres prepared by spray drying. *International Journal of Pharmaceutics*, 187(1), 53-65.
- Hejazi, R., & Amiji, M. (2003). Chitosan-based gastrointestinal delivery systems. *Journal of Controlled Release*, 89(2), 151-165.
- Herman, A., & Herman, A. P. (2013). Caffeine's mechanisms of action and its cosmetic use. *Skin Pharmacology and Physiology*, 26(1), 8-14.
- Hirano, S., Ohe, Y., & Ono, H. (1976). Selective *N*-acylation of chitosan. *Carbohydrate Research*, 47(2), 315-320.
- Hirano, S., Tobetto, K., & Noishiki, Y. (1981). SEM ultrastructure studies of *N*-acyl- and *N*-benzylidene-chitosan and chitosan membranes. *Journal of Biomedical Materials Research Part A*, 15(6), 903-911.

- Hirano, S., Tsuchida, H., & Nagao, N. (1989). *N*-acetylation in chitosan and the rate of its enzymic hydrolysis. *Biomaterials*, 10(8), 574-576.
- Hirano, S., Yamaguchi, Y., & Kamiya, M. (2002). Novel *N*-saturated-fatty-acyl derivatives of chitosan soluble in water and in aqueous acid and alkaline solutions. *Carbohydrate Polymers*, 48(2), 203-207.
- Holowka, E. P., & Bhatia, S. K. (2014). *Drug Delivery: Materials Design and Clinical Perspective* (pp. 27). Berlin, Heidelberg: Springer-Verlag GmbH.
- Hoskin, P. J., & Hanks, G. W. (1991). Opioid agonist-antagonist drugs in acute and chronic pain states. *Drugs*, 41(3), 326-344.
- Howling, G. I., Dettmar, P. W., Goddard, P. A., Hampson, F. C., Dornish, M., & Wood, E. J. (2001). The effect of chitin and chitosan on the proliferation of human skin fibroblasts and keratinocytes *in vitro*. *Biomaterials*, 22(22), 2959-2966.
- Hsiao, M. H., Tung, T. H., Hsiao, C. S., & Liu, D. M. (2012). Nano-hybrid carboxymethyl-hexanoyl chitosan modified with (3-aminopropyl)triethoxysilane for camptothecin delivery. *Carbohydrate Polymers*, 89(2), 632-639.
- Hu, F. Q., Liu, L. N., Du, Y. Z., & Yuan, H. (2009). Synthesis and antitumor activity of doxorubicin conjugated stearic acid-g-chitosan oligosaccharide polymeric micelles. *Biomaterials*, 30(36), 6955-6963.
- Hu, F. Q., Ren, G. F., Yuan, H., Du, Y. Z., & Zeng, S. (2006). Shell cross-linked stearic acid grafted chitosan oligosaccharide self-aggregated micelles for controlled release of paclitaxel. *Colloids and Surfaces B: Biointerfaces*, 50(2), 97-103.
- Huang, L., Cheng, X., Liu, C., Xing, K., Zhang, J., Sun, G., Li, X., & Chen, X. (2009). Preparation, characterization, and antibacterial activity of oleic acid-grafted chitosan oligosaccharide nanoparticles. *Frontiers of Biology in China*, 4(3), 321-327.
- Huang, R., Mendis, E., Rajapakse, N., & Kim, S. K. (2006). Strong electronic charge as an important factor for anticancer activity of chitoooligosaccharides (COS). *Life Sciences*, 78(20), 2399-2408.
- Huo, M., Zhang, Y., Zhou, J., Zou, A., Yu, D., Wu, Y., Li, Y., & Li, H. (2010). Synthesis and characterization of low-toxic amphiphilic chitosan derivatives and their application as micelle carrier for antitumor drug. *International Journal of Pharmaceutics*, 394(1-2), 162-173.
- Hwang, H. Y., Kim, I. S., Kwon, I. C., & Kim, Y. H. (2008). Tumor targetability and antitumor effect of docetaxel-loaded hydrophobically modified glycol chitosan nanoparticles. *Journal of Controlled Release*, 128(1), 23-31.

- Hyllested, M., Jones, S., Pedersen, J. L., & Kehlet, H. (2002). Comparative effect of paracetamol, NSAIDs or their combination in postoperative pain management: A qualitative review. *British Journal of Anaesthesia*, 88(2), 199-214.
- Ikeda, I., Sugano, M., Yoshida, K., Sasaki, E., Iwamoto, Y., & Hatano, K. (1993). Effects of chitosan hydrolyzates on lipid absorption and on serum and liver lipid concentration in rats. *Journal of Agricultural and Food Chemistry*, 41(3), 431-435.
- Ing, L. Y., Zin, N. M., Sarwar, A., & Katas, H. (2012). Antifungal activity of chitosan nanoparticles and correlation with their physical properties. *International Journal of Biomaterials*, 2012, 632698, 9 pages.
- Ioelovich, M. (2014). Crystallinity and hydrophilicity of chitin and chitosan. *Research & Reviews: Journal of Chemistry*, 3(3), 7-14.
- Ito, M., Ban, A., & Ishihara, M. (2000). Anti-ulcer effects of chitin and chitosan, healthy foods, in rats. *Japanese Journal of Pharmacology*, 82(3), 218-225.
- Janes, K. A., Calvo, P., & Alonso, M. J. (2001). Polysaccharide colloidal particles as delivery systems for macromolecules. *Advanced Drug Delivery Reviews*, 47(1), 83-97.
- Jang, M. K., Jeong, Y. I., & Nah, J. W. (2010). Characterization and preparation of core-shell type nanoparticle for encapsulation of anticancer drug. *Colloids and Surfaces B: Biointerfaces*, 81(2), 530-536.
- Jawahar, N., & Meyyanathan, S. N. (2012). Polymeric nanoparticles for drug delivery and targeting: A comprehensive review. *International Journal of Health & Allied Sciences*, 1(4), 217-223.
- Jeon, Y. J., Shahidi, F., & Kim, S. K. (2000). Preparation of chitin and chitosan oligomers and their applications in physiological functional foods. *Food Reviews International*, 16(2), 159-176.
- Jia, Z., Shen, D., & Xu, W. (2001). Synthesis and antibacterial activities of quaternary ammonium salt of chitosan. *Carbohydrate Research*, 333(1), 1-6.
- Jiang, G. B., Lin, Z. T., Xu, X. J., Hai, Z., & Song, K. (2012). Stable nanomicelles based on chitosan derivative: *In vitro* antiplatelet aggregation and adhesion properties. *Carbohydrate Polymers*, 88(1), 232-238.
- Jiang, G. B., Quan, D., Liao, K., & Wang, H. (2006a). Novel polymer micelles prepared from chitosan grafted hydrophobic palmitoyl groups for drug delivery. *Molecular Pharmaceutics*, 3(2), 152-160.

- Jiang, G. B., Quan, D., Liao, K., & Wang, H. (2006b). Preparation of polymeric micelles based on chitosan bearing a small amount of highly hydrophobic groups. *Carbohydrate Polymers*, 66(4), 514-520.
- Jin, Y. H., Hu, H. Y., Qiao, M. X., Zhu, J., Qi, J. W., Hu, C. J., Zhang, Q., & Chen, D. W. (2012). pH-sensitive chitosan-derived nanoparticles as doxorubicin carriers for effective anti-tumor activity: preparation and *in vitro* evaluation. *Colloids and Surfaces B: Biointerfaces*, 94, 184-191.
- Jonker-Venter, C., Snyman, D., Janse van Rensburg, C., Jordaan, E., Schultz, C., Steenekamp, J. H., Hamman, J. H., & Kotze, A. F. (2006). Low molecular weight quaternised chitosan (11): *In vitro* assessment of absorption enhancing properties. *Die Pharmazie*, 61(4), 301-305.
- Kadokawa, J., Shimohigoshi, R., Yamashita, K., & Yamamoto, K. (2015). Synthesis of chitin and chitosan stereoisomers by thermostable α -glucan phosphorylase-catalyzed enzymatic polymerization of α -D-glucosamine 1-phosphate. *Organic & Biomolecular Chemistry*, 13(14), 4336-4343.
- Kasaai, M. R. (2008). A review of several reported procedures to determine the degree of N-acetylation for chitin and chitosan using infrared spectroscopy. *Carbohydrate Polymers*, 71(4), 497-508.
- Kaskoos, R. A. (2014). Investigation of moxifloxacin loaded chitosan-dextran nanoparticles for topical instillation into eye: *in-vitro* and *ex-vivo* evaluation. *International Journal of Pharmaceutical Investigation*, 4(4), 164-173.
- Kast, C. E., & Bernkop-Schnurch, A. (2001). Thiolated polymers-thiomers: development and *in vitro* evaluation of chitosan-thioglycolic acid conjugates. *Biomaterials*, 22(17), 2345-2352.
- Kayser, O., Lemke, A., & Hernandez-Trejo, N. (2005). The impact of nanobiotechnology on the development of new drug delivery systems. *Current Pharmaceutical Biotechnology*, 6(1), 3-5.
- Keisuke, K., Satoyuki, C., Mami, K., & Yoshiyuki, K. (1988). Studies on chitin. 14. N-acetylation behavior of chitosan with acetyl chloride and acetic anhydride in a highly swelled state. *Bulletin of the Chemical Society of Japan*, 61(3), 927-930.
- Khan, T. A., Peh, K. K., & Ch'ng, H. S. (2002). Reporting degree of deacetylation values of chitosan: the influence of analytical methods. *Journal of Pharmacy and Pharmaceutical Sciences*, 5(3), 205-212.
- Khdaif, A., Hamad, I., Alkhatib, H., Bustanji, Y., Mohammad, M., Tayem, R., & Aiedeh, K. (2016). Modified-chitosan nanoparticles: Novel drug delivery systems

improve oral bioavailability of doxorubicin. *European Journal of Pharmaceutical Sciences*, 93, 38-44.

Kim, D. G., Jeong, Y. I., Choi, C., Roh, S. H., Kang, S. K., Jang, M. K., & Nah, J. W. (2006a). Retinol-encapsulated low molecular water-soluble chitosan nanoparticles. *International Journal of Pharmaceutics*, 319(1-2), 130-138.

Kim, J. H., Kim, Y. S., Kim, S., Park, J. H., Kim, K., Choi, K., Chung, H., Jeong, S. Y., Park, R. W., Kim, I. S. & Kwon, I. C. (2006b). Hydrophobically modified glycol chitosan nanoparticles as carriers for paclitaxel. *Journal of Controlled Release*, 111(1-2), 228-234.

Kim, K., Kim, J. H., Kim, S., Chung, H., Choi, K., Kwon, I. C., Park, J. H., Kim, Y. S., Park, R. W., Kim, I. S., & Jeong, S. Y. (2005). Self-assembled nanoparticles of bile acid-modified glycol chitosans and their applications for cancer therapy. *Macromolecular Research*, 13(3), 167-175.

Kim, S. K., & Rajapakse, N. (2005). Enzymatic production and biological activities of chitosan oligosaccharides (COS): A review. *Carbohydrate Polymers*, 62(4), 357-368.

Kim, T. H., Ihm, J. E., Choi, Y. J., Nah, J. W., & Cho, C. S. (2003). Efficient gene delivery by urocanic acid-modified chitosan. *Journal of Controlled Release*, 93(3), 389-402.

Kim, Y. H., Gihm, S. H., Park, C. R., Lee, K. Y., Kim, T. W., Kwon, I. C., Chung, H., & Jeong, S. Y. (2001). Structural characteristics of size-controlled self-aggregates of deoxycholic acid-modified chitosan and their application as a DNA delivery carrier. *Bioconjugate Chemistry*, 12(6), 932-938.

Kogan, G., Skorik, Y. A., Zitnanova, I., Krizkova, L., Durackova, Z., Gomes, C. A. R., Yatluk, Y. G., Krajcovic, J. (2004). Antioxidant and antimutagenic activity of N-(2-carboxyethyl) chitosan. *Toxicology and Applied Pharmacology*, 201(3), 303-310.

Kondo, Y., Nakatani, A., Hayashi, K., & Ito, M. (2000). Low molecular weight chitosan prevents the progression of low dose streptozotocin-induced slowly progressive diabetes mellitus in mice. *Biological and Pharmaceutical Bulletin*, 23(12), 1458-1464.

Korchagina, E. V., & Philippova, O. E. (2010). Multichain aggregates in dilute solutions of associating polyelectrolyte keeping a constant size at the increase in the chain length of individual macromolecules. *Biomacromolecules*, 11(12), 3457-3466.

Kugelman, A., & Durand, M. (2011). A comprehensive approach to the prevention of bronchopulmonary dysplasia. *Pediatric Pulmonology*, 46(12), 1153-1165.

- Kumar, M. N. V. R. (2000). A review of chitin and chitosan applications. *Reactive and Functional Polymers*, 46(1), 1-27.
- Kumbar, S. G., Soppimath, K. S., & Aminabhavi, T. M. (2003). Synthesis and characterization of polyacrylamide-grafted chitosan hydrogel microspheres for the controlled release of indomethacin. *Journal of Applied Polymer Science*, 87(9), 1525-1536.
- Lai, W. F., & Shum, H. C. (2016). U. S. Patent No. *US20160310440A1*. Washington: United States Patent and Trademark Office. Retrieved on January 5, 2015, from <https://patents.google.com/patent/WO2016173492A1/en>
- Lam, P. L., Lee, K. K. H., Wong, R. S. M., Cheng, G. Y. M., Cheng, S. Y., Yuen, M. C. W., Lam, K. H., Gambari, R., Kok, S. H. L., & Chui, C. H. (2012a). Development of hydrocortisone succinic acid/and 5-fluorouracil/chitosan microcapsules for oral and topical drug deliveries. *Bioorganic & Medicinal Chemistry Letters*, 22(9), 3213-3218.
- Lam, P. L., Yuen, M. C. W., Kan, C. W., Wong, R. S. M., Cheng, G. Y. M., Lam, K. H., Gambari, R., Kok, S. H. L., & Chui, C. H. (2012b). Development of calendula oil/chitosan microcapsules and their biological safety evaluation. *Australian Journal of Chemistry*, 65(1), 72-80.
- Lao, S. B., Zhang, Z. X., Xu, H. H., & Jiang, G. B. (2010). Novel amphiphilic chitosan derivatives: Synthesis, characterization and micellar solubilization of rotenone. *Carbohydrate Polymers*, 82(4), 1136-1142.
- Lapenko, V. L., Pavlyuchenko, S. V., Popov, V. N., Parkhisenko, Y. A., Slivkin, D. A., Bychuk, A. I., & Bulynin, V. V. (2013). *Russia Patent No. RU2471477C1*. Moscow, Russia: Federal Service for Intellectual Property. Retrieved on January 9, 2015, from <http://russianpatents.com/patent/247/2471477.html>
- Le Tien, C., Lacroix, M., Ispas-Szabo, P., & Mateescu, M. A. (2003). *N*-acylated chitosan: hydrophobic matrices for controlled drug release. *Journal of Controlled Release*, 93(1), 1-13.
- Lee, D., Zhang, W., Shirley, S. A., Kong, X., Hellermann, G. R., Lockey, R. F., & Mohapatra, S. S. (2007). Thiolated chitosan/DNA nanocomplexes exhibit enhanced and sustained gene delivery. *Pharmaceutical Research*, 24(1), 157-167.
- Lee, K. Y., Kwon, I. C., Kim, Y. H., Jo, W. H., & Jeong, S. Y. (1998). Preparation of chitosan self-aggregates as a gene delivery systems. *Journal of Controlled Release*, 51, 213-220.

- Leonard, T. K., Watson, R. R., & Mohs, M. E. (1987). The effects of caffeine on various body systems: A review. *Journal of the American Dietetic Association*, 87(8), 1048-1053.
- Lev, R., & Rosen, P. (1994). Prophylactic lidocaine use preintubation: A review. *The Journal of Emergency Medicine*, 12(4), 499-506.
- Levine, I. N. (2008). *Physical Chemistry* (6th ed.) (pp. 234). Boston, Massachusetts: McGraw-Hill.
- Li, D. H., Liu, L. M., Tian, K. L., Liu, J. C., & Fan, X. Q. (2007a). Synthesis, biodegradability and cytotoxicity of water-soluble isobutylchitosan. *Carbohydrate Polymers*, 67(1), 40-45.
- Li, H., Huo, M., Zhou, J., Dai, Y., Deng, Y., Shi, X., & Masoud, J. (2010). Enhanced oral absorption of paclitaxel in *N*-deoxycholic acid-*N,O*-hydroxyethyl chitosan micellar system. *Journal of Pharmaceutical Sciences*, 99(11), 4543-4553.
- Li, Q., Zhang, C., Tan, W., Gu, G., & Guo, Z. (2017). Novel amino-pyridine functionalized chitosan quaternary ammonium derivatives: Design, synthesis, and antioxidant activity. *Molecules*, 22(1), 156, 1-10.
- Li, X., Chen, M., Yang, W., Zhou, Z., Liu, L., & Zhang, Q. (2012). Interaction of bovine serum albumin with self-assembled nanoparticles of 6-*O*-cholesterol modified chitosan. *Colloids and Surfaces B: Biointerfaces*, 92, 136-141.
- Li, Y. Y., Chen, X. G., Yu, L. M., Wang, S. X., Sun, G. Z., & Zhou, H. Y. (2006). Aggregation of hydrophobically modified chitosan in solution and at the air–water interface. *Journal of Applied Polymer Science*, 102(2), 1968-1973.
- Li, Y. Y., Chen, X. G., Liu, C. S., Cha, D. S., Park, H. J., & Lee, C. M. (2007b). Effect of the molecular mass and degree of substitution of oleoylchitosan on the structure, rheological properties, and formation of nanoparticles. *Journal of Agricultural and Food Chemistry*, 55(12), 4842-4847.
- Liechty, W. B., Kryscio, D. R., Slaughter, B. V., & Peppas, N. A. (2010). Polymers for drug delivery systems. *Annual Review of Chemical and Biomolecular Engineering*, 1, 149-173.
- Lim, C. K., Halim, A. S., Lau, H. Y., Ujang, Z., & Hazri, A. (2007). *In vitro* cytotoxicology model of oligo-chitosan and *N, O*-carboxymethyl chitosan using primary normal human epidermal keratinocyte cultures. *Journal of Applied Biomaterials and Biomechanics*, 5(2), 82-87.

- Lin, H. R., Yu, S. P., Lin, Y. J., & Wang, T. S. (2010). High pH tolerance of a chitosan-PAA nanosuspension for ophthalmic delivery of pilocarpine. *Journal of Biomaterials Science, Polymer Edition*, 21(2), 141-157.
- Lince, F., Bolognesi, S., Stella, B., Marchisio, D. L., & Dosio, F. (2011). Preparation of polymer nanoparticles loaded with doxorubicin for controlled drug delivery. *Chemical Engineering Research and Design*, 89(11), 2410-2419.
- Liu, C., Fan, W., Chen, X., Liu, C., Meng, X., & Park, H. J. (2007a). Self-assembled nanoparticles based on linoleic-acid modified carboxymethyl-chitosan as carrier of adriamycin (ADR). *Current Applied Physics*, 7, Supplement 1, e125-e129.
- Liu, G., Gan, J., Chen, A., Liu, Q., & Zhao, X. (2010). Synthesis and characterization of an amphiphilic chitosan bearing octyl and methoxy polyethylene glycol groups. *Natural Science*, 2(7), 707-712.
- Liu, H., Du, Y. M., & Kennedy, J. F. (2007b). Hydration energy of the 1,4-bonds of chitosan and their breakdown by ultrasonic treatment. *Carbohydrate Polymers*, 68(3), 598-600.
- Liu, T. Y., Chen, S. Y., Lin, Y. L., & Liu, D. M. (2006). Synthesis and characterization of amphiphatic carboxymethyl-hexanoyl chitosan hydrogel: Water-retention ability and drug encapsulation. *Langmuir*, 22(23), 9740-9745.
- Liu, W. G., Sun, S. J., Zhang, X., & Yao, K. D. (2003a). Self-aggregation behavior of alkylated chitosan and its effect on the release of a hydrophobic drug. *Journal of Biomaterials Science, Polymer Edition*, 14(8), 851-859.
- Liu, W. G., Kang, D. Y., & Liu, Q. G. (2001). Formation of a DNA/*N*-dodecylated chitosan complex and salt-induced gene delivery. *Journal of Applied Polymer Science*, 82(14), 3391-3395.
- Liu, W. G., Zhang, X., Sun, S. J., Sun, G. J., Yao, K. D., Liang, D. C., Guo, G., Zhang, J. Y. (2003b). *N*-alkylated chitosan as a potential nonviral vector for gene transfection. *Bioconjugate Chemistry*, 14(4), 782-789.
- Liu, X. F., Guan, Y. L., Yang, D. Z., Li, Z., & De Yao, K. (2000). Antibacterial action of chitosan and carboxymethylated chitosan. *Journal of Applied Polymer Science*, 79(7), 1324-1335.
- Liu, Y., Cheng, X. J., Dang, Q. F., Ma, F. K., Chen, X. G., Park, H. J., & Kim, B. K. (2012). Preparation and evaluation of oleoyl-carboxymethyl-chitosan (OCMCS) nanoparticles as oral protein carriers. *Journal of Materials Science: Materials in Medicine*, 23(2), 375-384.

- Liu, Z., Jiao, Y., Wang, Y., Zhou, C., & Zhang, Z. (2008). Polysaccharides-based nanoparticles as drug delivery systems. *Advanced Drug Delivery Reviews*, 60(15), 1650-1662.
- M, N. S., Mony, U., & Jayakumar, R. (2016). Chitin and chitosan as hemostatic agents. In Mark, H. F. & Seidel, A., *Encyclopedia of Polymer Science and Technology* (pp. 1-12). New York, USA: John Wiley & Sons Incorporation.
- Macdonald, R. L., & Kelly, K. M. (1994). Mechanisms of action of currently prescribed and newly developed antiepileptic drugs. *Epilepsia*, 35 Suppl 4, S41-50.
- Machado, G. C., Maher, C. G., Ferreira, P. H., Pinheiro, M. B., Lin, C. W. C., Day, R. O., McLachlan, A., & Ferreira, M. L. (2015). Efficacy and safety of paracetamol for spinal pain and osteoarthritis: systematic review and meta-analysis of randomised placebo controlled trials. *British Medical Journal*, 350, h1225.
- Madan, R. K., & Levitt, J. (2014). A review of toxicity from topical salicylic acid preparations. *Journal of American Academy of Dermatology*, 70(4), 788-792.
- Maeda, Y., & Kimura, Y. (2004). Antitumor effects of various low-molecular-weight chitosans are due to increased natural killer activity of intestinal intraepithelial lymphocytes in sarcoma 180-bearing mice. *Journal of Nutrition*, 134(4), 945-950.
- Mahanta, A. K., Mittal, V., Singh, N., Dash, D., Malik, S., Kumar, M., & Maiti, P. (2015). Polyurethane-grafted chitosan as new biomaterials for controlled drug delivery. *Macromolecules*, 48(8), 2654-2666.
- Marques, J. G., Gaspar, V. M., Costa, E., Paquete, C. M., & Correia, I. J. (2014). Synthesis and characterization of micelles as carriers of non-steroidal anti-inflammatory drugs (NSAID) for application in breast cancer therapy. *Colloids and Surfaces B: Biointerfaces*, 113, 375-383.
- Mathew, O. P. (2011). Apnea of prematurity: Pathogenesis and management strategies. *Journal of Perinatology*, 31(5), 302-310.
- Matos, B. N., Reis, T. A., Gratieri, T., & Gelfuso, G. M. (2015). Chitosan nanoparticles for targeting and sustaining minoxidil sulphate delivery to hair follicles. *International Journal of Biological Macromolecules*, 75, 225-229.
- McLellan, T. M., Caldwell, J. A., & Lieberman, H. R. (2016). A review of caffeine's effects on cognitive, physical and occupational performance. *Neuroscience & Biobehavioral Reviews*, 71, 294-312.
- Mekhail, G. M., Kamel, A. O., Awad, G. A. S., & Mortada, N. D. (2012). Anticancer effect of atorvastatin nanostructured polymeric micelles based on stearyl-grafted chitosan. *International Journal of Biological Macromolecules*, 51(4), 351-363.

- Meler, J., Szczesniak, M., Grimling, B., & Pluta, J. (2013). Application of chitosan in the formulation of hydrogels applied on skin. *Progress on Chemistry and Application of Chitin and Its Derivatives*, 18, 181-186.
- Meng, S., Liu, Z., Zhong, W., Wang, Q., & Du, Q. (2007). Phosphorylcholine modified chitosan: Appetent and safe material for cells. *Carbohydrate Polymers*, 70(1), 82-88.
- Mi, F. L., Peng, C. K., Huang, M. F., Lo, S. H., & Yang, C. C. (2005). Preparation and characterization of *N*-acetylchitosan, *N*-propionylchitosan and *N*-butyrylchitosan microspheres for controlled release of 6-mercaptopurine. *Carbohydrate Polymers*, 60(2), 219-227.
- Min, K. H. Park, K., Kim, Y. S., Bae, S. M., Lee, S., Jo, H. G., Park, R. W., Kim, I. S., Jeong, S. Y., Kim, K., & Kwon, I. C. (2008). Hydrophobically modified glycol chitosan nanoparticles-encapsulated camptothecin enhance the drug stability and tumor targeting in cancer therapy. *Journal of Controlled Release*, 127(3), 208-218.
- Miwa, A., Ishibe, A., Nakano, M., Yamahira, T., Itai, S., Jinno, S., & Kawahara, H. (1998). Development of novel chitosan derivatives as micellar carriers of taxol. *Pharmaceutical Research*, 15(12), 1844-1850.
- Mo, R., Jin, X., Li, N., Ju, C., Sun, M., Zhang, C., & Ping, Q. (2011). The mechanism of enhancement on oral absorption of paclitaxel by *N*-octyl-*O*-sulfate chitosan micelles. *Biomaterials*, 32(20), 4609-4620.
- Moazeni, E., Gilani, K., Najafabadi, A. R., Reza Rouini, M., Mohajel, N., Amini, M., & Barghi, M. A. (2012). Preparation and evaluation of inhalable itraconazole chitosan based polymeric micelles. *DARU Journal of Pharmaceutical Sciences*, 20(1), 85.
- Monnier, C. A., Thevenaz, D. C., Balog, S., Fiore, G. L., Vanhecke, D., Rothen-Rutishauser, B., & Petri-Fink, A. (2015). A guide to investigating colloidal nanoparticles by cryogenic transmission electron microscopy: Pitfalls and benefits. *AIMS Biophysics*, 2(3), 245-258.
- Moore, A., Collins, S., Carroll, D., & McQuay, H. (1997). Paracetamol with and without codeine in acute pain: a quantitative systematic review. *Pain*, 70(2-3), 193-201.
- Mora-Huertas, C. E., Fessi, H., Elaissari, A. (2010). Polymer-based nanocapsules for drug delivery. *International Journal of Pharmaceutics*, 385(1-2), 113-142.
- Morgado, P. I., Miguel, S. P., Correia, I. J., & Aguiar-Ricardo, A. (2017). Ibuprofen loaded PVA/chitosan membranes: A highly efficient strategy towards an improved skin wound healing. *Carbohydrate Polymers*, 159, 136-145.

- Morimoto, M., Saimoto, H., Usui, H., Okamoto, Y., Minami, S., & Shigemasa, Y. (2001). Biological activities of carbohydrate-branched chitosan derivatives. *Biomacromolecules*, 2(4), 1133-1136.
- Mothilal, M., Nagalakshmi, M., Swati, P. S., Damodharan, N., Manimaran, V., & Lakshmi, K. S. (2012). Optimisation and characterisation of chitosan microspheres of aceclofenac. *International Journal of Pharma Sciences and Research*, 3(2), 305-315.
- Mourya, V. K., & Inamdar, N. N. (2008). Chitosan-modifications and applications: Opportunities galore. *Reactive and Functional Polymers*, 68(6), 1013-1051.
- Munmaya, M. (2015). *Handbook of encapsulation and controlled release* (pp. 278). Boca Raton, Florida, USA: CRC Press.
- Muzzarelli, R. A. A., & Muzzarelli, C. (2005). Chitosan Chemistry: Relevance to the Biomedical Sciences. In T. Heinze (Eds.), *Polysaccharides I: Structure, characterization and use* (pp. 151-209). Berlin, Heidelberg, Germany: Springer.
- Nagavarma, B. V. N., Yadav, H. K. S., Ayaz, A., Vasudha, L. S., Shivakumar, H. G. (2012). Different techniques for preparation of polymeric nanoparticles-Review. *Asian Journal of Pharmaceutical and Clinical Research*, 5(3), 16-23.
- Nair, R., Ashok Kumar, C. K., & Vishnu Priya, K. (2011). Formulation and *in vitro-in vivo* evaluation of sustained release chitosan microspheres containing mefenamic acid. *Journal of Pharmaceutical Science & Technology*, 3(3), 563-569.
- Nam, J. P., Park, S. C., Kim, T. H., Jang, J. Y., Choi, C., Jang, M. K., & Nah, J. W. (2013). Encapsulation of paclitaxel into lauric acid-*O*-carboxymethyl chitosan-transferrin micelles for hydrophobic drug delivery and site-specific targeted delivery. *International Journal of Pharmaceutics*, 457(1), 124-135.
- Nam, K. S., Choi, Y. R., & Shon, Y. H. (2001). Evaluation of the antimutagenic potential of chitosan oligosaccharide: Rec, Ames and Umu tests. *Biotechnology Letters*, 23(12), 971-975.
- Namazi, H., Fathi, F., & Heydari, A. (2012). Nanoparticles based on modified polysaccharides. In Hashim, A. A. (Eds.), *The Delivery of Nanoparticles*. Retrieved on February 10, 2016, from <https://www.intechopen.com/books/the-delivery-of-nanoparticles/nanoparticles-based-on-modified-polysaccharides>.
- Namburi, B. V. N., Yadav, H. K. S., S, H., Ahmed, A., Sureddy, V. L., & Shivakumar, H. G. (2014). Formulation and evaluation of polymeric nanoparticulate gel for topical delivery. *International Journal of Polymeric Materials and Polymeric Biomaterials*, 63(9), 476-485.

- Narayanan, D., Ninan, N., Jayakumar, R., Nair, S. V., & Menon, D. (2014). *O*-carboxymethyl chitosan nanoparticles for controlled release of non-steroidal anti-inflammatory drugs. *Advanced Science, Engineering and Medicine*, 6(5), 522-530.
- Nehlig, A. (2010). Is caffeine a cognitive enhancer? *Journal of Alzheimer's Disease*, 20, S85-94.
- Nicholson, B. (2000). Gabapentin use in neuropathic pain syndromes. *Acta Neurologica Scandinavica*, 101(6), 359-371.
- Nitta, S. K., & Numata, K. (2013). Biopolymer-based nanoparticles for drug/gene delivery and tissue engineering. *International Journal of Molecular Sciences*, 14, 1629-1654.
- Novak, K., Cupp, M. J., & Tracy, T. S. (2003). Chitosan. In M. J. Cupp & T. S. Tracy (Eds.), *Dietary supplements: Toxicology and clinical pharmacology* (pp. 33-39). Totowa, New Jersey: Humana Press.
- Ortona, O., D'Errico, G., Mangiapia, G., & Ciccarelli, D. (2008). The aggregative behavior of hydrophobically modified chitosans with high substitution degree in aqueous solution. *Carbohydrate Polymers*, 74(1), 16-22.
- Ozbas-Turan, S., & Akbuga, J. (2011). Plasmid DNA-loaded chitosan/TPP nanoparticles for topical gene delivery. *Drug Delivery*, 18(3), 215-222.
- Ozbas-Turan, S., Akbuga, J., & Sezer, A. D. (2010). Topical application of antisense oligonucleotide-loaded chitosan nanoparticles to rats. *Oligonucleotides*, 20(3), 147-153.
- Panyam, J., & Labhasetwar, V. (2003). Biodegradable nanoparticles for drug and gene delivery to cells and tissue. *Advanced Drug Delivery Reviews*, 55(3), 329-347.
- Paradkar, M. M., & Irudayaraj, J. (2002). A rapid FTIR spectroscopic method for estimation of caffeine in soft drinks and total methylxanthines in tea and coffee. *Journal of Food Science*, 67(7), 2507-2511.
- Park, I. K., Yang, J., Jeong, H. J., Bom, H. S., Harada, I., Akaike, T., Kim, S. I., & Cho, C.S. (2003). Galactosylated chitosan as a synthetic extracellular matrix for hepatocytes attachment. *Biomaterials*, 24(13), 2331-2337.
- Park, K. (2014). Controlled drug delivery systems: Past forward and future back. *Journal of Controlled Release*, 190, 3-8.
- Park, P. J., Je, J. Y., Jung, W. K., Ahn, C. B., & Kim, S. K. (2004). Anticoagulant activity of heterochitosans and their oligosaccharide sulfates. *European Food Research and Technology*, 219(5), 529-533.

- Patnaik, A. (2012). Non-covalent approaches to facile synthesis of dimension-specific H and J-aggregates. In Kobayashi, T., *J-Aggregates*, Vol. 2 (pp. 343-401). Singapore: World Scientific.
- Patel, M. P., Patel, R. R., & Patel, J. K. (2010). Chitosan mediated targeted drug delivery system: A review. *Journal of Pharmacy and Pharmaceutical Sciences*, 13(4), 536-557.
- Paulose-Ram, R., Hirsch, R., Dillon, C., Losonczy, K., Cooper, M., & Ostchega, Y. (2003). Prescription and non-prescription analgesic use among the US adult population: results from the third National Health and Nutrition Examination Survey (NHANES III). *Pharmacoepidemiology and Drug Safety*, 12(4), 315-326.
- Peer, D., Karp, J. M., Hong, S., Farokhzad, O. C., Margalit, R., Langer, R. (2007). Nanocarriers as an emerging platform for cancer therapy. *Nature Nanotechnology*, 2, 751-760.
- Peng, H. T., & Shek, P. N. (2009). Development of in situ-forming hydrogels for hemorrhage control. *Journal of Materials Science: Materials in Medicine*, 20(8), 1753-1762.
- Peng, Y., Han, B., Liu, W., & Xu, X. (2005). Preparation and antimicrobial activity of hydroxypropyl chitosan. *Carbohydrate Research*, 340(11), 1846-1851.
- Peniche, C., Elvira, C., & San Roman, J. (1998). Interpolymer complexes of chitosan and polymethacrylic derivatives of salicylic acid: preparation, characterization and modification by thermal treatment. *Polymer*, 39(25), 6549-6554.
- Petkova, V., Valchanova, V., Ibrahim, A., Nikolova, I., Benbasat, N., & Dimitrov, M. (2014). Marketing approaches for OTC analgesics in Bulgaria. *Biotechnology & Biotechnological Equipment*, 28(2), 360-365.
- Philippova, O. E., & Korchagina, E. V. (2012). Chitosan and its hydrophobic derivatives: Preparation and aggregation in dilute aqueous solutions. *Polymer Science Series A*, 54(7), 552-572.
- Philippova, O. E., Volkov, E. V., Sitnikova, N. L., Khokhlov, A. R., Desbrieres, J., & Rinaudo, M. (2001). Two types of hydrophobic aggregates in aqueous solutions of chitosan and its hydrophobic derivative. *Biomacromolecules*, 2(2), 483-490.
- Pogorielov, M. V., & Sikora, V. Z. (2015). Chitosan as a hemostatic agent: Current state. *European Journal of Medicine: Series B*, 2(1), 24-33.
- Poornima, B., & Korrapati, P. S. (2017). Fabrication of chitosan-polycaprolactone composite nanofibrous scaffold for simultaneous delivery of ferulic acid and resveratrol. *Carbohydrate Polymers*, 157, 1741-1749.

- Popiel, W. J. (1978). *Introduction to colloid science* (pp. 151). New York, USA: Exposition Press, Inc.
- Prabaharan, M. (2015). Chitosan-based nanoparticles for tumor-targeted drug delivery. *International Journal of Biological Macromolecules*, 72, 1313-1322.
- Prabaharan, M., & Mano, J. F. (2004). Chitosan-based particles as controlled drug delivery systems. *Drug Delivery*, 12(1), 41-57.
- Prabu, S., Swaminathan, M., Sivakumar, K., & Rajamohan, R. (2015). Preparation, characterization and molecular modeling studies of the inclusion complex of caffeine with beta-cyclodextrin. *Journal of Molecular Structure*, 1099, 616-624.
- Qiu, Y., Zhu, J., Wang, J., Gong, R., Zheng, M., & Huang, F. (2013). Self-assembled phytosterol-fructose-chitosan nanoparticles as a carrier of anticancer drug. *Journal of Nanoscience and Nanotechnology*, 13(8), 5935-5941.
- Qu, G., Yao, Z., Zhang, C., Wu, X., & Ping, Q. (2009). PEG conjugated *N*-octyl-*O*-sulfate chitosan micelles for delivery of paclitaxel: *In vitro* characterization and *in vivo* evaluation. *European Journal of Pharmaceutical Sciences*, 37(2), 98-105.
- Quinones, J. P., Gothelf, K. V., Kjems, J., Caballero, A. M. H., Schmidt, C., & Covas, C. P. (2013). *N,O*6-partially acetylated chitosan nanoparticles hydrophobically-modified for controlled release of steroids and vitamin E. *Carbohydrate Polymers*, 91(1), 143-151.
- Quintarelli, G., Cifonelli, J. A., & Zito, R. (1971). On phosphotungstic acid staining. II. *Journal of Histochemistry & Cytochemistry*, 19(11), 648-653.
- Raja, M. A., Arif, M., Feng, C., Zeenat, S., & Liu, C. G. (2017). Synthesis and evaluation of pH-sensitive, self-assembled chitosan-based nanoparticles as efficient doxorubicin carriers. *Journal of Biomaterials Applications*, 31(8), 1182-1195.
- Ramesh, H. P., & Tharanathan, R. N. (2003). Carbohydrates-the renewable raw materials of high biotechnological value. *Critical Reviews in Biotechnology*, 23(2), 149-173.
- Rao, P., & Knaus, E. E. (2008). Evolution of nonsteroidal anti-inflammatory drugs (NSAIDs): cyclooxygenase (COX) inhibition and beyond. *Journal of Pharmacy and Pharmaceutical Sciences*, 11(2), 81s-110s.
- Reddy, A., Manjula, B., Jayaramudu, T., Sadiku, E., Anand Babu, P., & Periyar Selvam, S. (2016). 5-Fluorouracil loaded chitosan-PVA/NaMMT nanocomposite films for drug release and antimicrobial activity. *Nano-Micro Letters*, 8(3), 260-269.

- Reger, D. L., Goode, S. R., & Ball, D. W. R. (2009). *Chemistry: Principles and practice* (pp. 125). Boston, United States: Cengage Learning.
- Rekha, M. R., & Sharma, C. P. (2008). Phthalyl chitosan–poly(ethylene oxide) semi-interpenetrating polymer network microparticles for oral protein delivery: An *in vitro* characterization. *Journal of Applied Polymer Science*, 110(5), 2787-2795.
- Rekha, M. R., & Sharma, C. P. (2009). Synthesis and evaluation of lauryl succinyl chitosan particles towards oral insulin delivery and absorption. *Journal of Controlled Release*, 135(2), 144-151.
- Ribeiro, H., Marto, J., Raposo, S., Chiari, B. G., Silva, A. N., Duarte, A., Correa, M. A., Isaac, V. (2013). Rheological characterisation and effect of abiotic factors on the antimicrobial efficacy of chitosan-based hydrogels containing alpha-hydroxy acids. *World Journal of Pharmacy and Pharmaceutical Sciences*, 2(5), 3567-3580.
- Rinaudo, M., Auzely, R., Vallin, C., & Mullagaliev, I. (2005). Specific interactions in modified chitosan systems. *Biomacromolecules*, 6(5), 2396-2407.
- Rouget, M. C. (1859). Des substances amylacees dans les tissus des animaux, specialement des Articules (chitine). *Comptes Rendus Chimie*, 48, 792-795.
- Rumengan, I. F. M., Suryanto, E., Modaso, R., Wullur, S., Tallei, T. E., & Limbong, D. (2014). Structural characteristics of chitin and chitosan isolated from the biomass of cultivated rotifer, *Brachionus rotundiformis*. *International Journal of Fisheries and Aquatic Sciences*, 3(1), 12-18.
- Sadeghi, A. M. M., Amini, M., Avadi, M. R., Siedi, F., Rafiee-Tehrani, M., & Junginger, H. E. (2008). Synthesis, characterization, and antibacterial effects of trimethylated and triethylated 6-NH₂-6-Deoxy Chitosan. *Journal of Bioactive and Compatible Polymers*, 23(3), 262-275.
- Sahoo, D., Sahoo, S., Mohanty, P., Sasmal, S., & Nayak, P. L. (2009). Chitosan: a new versatile bio-polymer for various applications. *Designed Monomers and Polymers*, 12(5), 377-404.
- Samuels, R. J. (1981). Solid state characterization of the structure of chitosan films. *Journal of Polymer Science Part B: Polymer Physics*, 19(7), 1081-1105.
- Savjani, K. T., Gajjar, A. K., & Savjani, J. K. (2012). Drug solubility: Importance and enhancement techniques. *ISRN Pharmaceutics*, 2012, 195727, 10 pages.
- Schmidt, B. (2005). Methylxanthine therapy for apnea of prematurity: evaluation of treatment benefits and risks at age 5 years in the international Caffeine for Apnea of Prematurity (CAP) trial. *Biology of the Neonate*, 88(3), 208-213.

- Senel, S., & McClure, S. J. (2004). Potential applications of chitosan in veterinary medicine. *Advanced Drug Delivery Reviews*, 56(10), 1467-1480.
- Senyigit, T., Sonvico, F., Barbieri, S., Ozer, O., Santi, P., & Colombo, P. (2010). Lecithin/chitosan nanoparticles of clobetasol-17-propionate capable of accumulation in pig skin. *Journal of Controlled Release*, 142(3), 368-373.
- Seo, W. G., Pae, H. O., Kim, N. Y., Oh, G. S., Park, I. S., Kim, Y. H., Kim, Y. M., Lee, Y. H., Jun, C. D., & Chung, H. T. (2000). Synergistic cooperation between water-soluble chitosan oligomers and interferon- γ for induction of nitric oxide synthesis and tumoricidal activity in murine peritoneal macrophages. *Cancer Letters*, 159(2), 189-195.
- Shao, W., Wu, J., Wang, S., Huang, M., Liu, X., & Zhang, R. (2017). Construction of silver sulfadiazine loaded chitosan composite sponges as potential wound dressings. *Carbohydrate Polymers*, 157, 1963-1970.
- Shelma, R., Paul, W., & Sharma, C. P. (2010). Development and characterization of self-aggregated nanoparticles from anacardoylated chitosan as a carrier for insulin. *Carbohydrate Polymers*, 80(1), 285-290.
- Shelma, R., & Sharma, C. P. (2010a). Hydrophobically Modified Acylated Chitosan Particles for Drug Delivery Applications. In Kim, S. K., *Chitin, chitosan, oligosaccharides and their derivatives* (pp. 507-517). Boca Raton, Florida, USA: CRC Press.
- Shelma, R., & Sharma, C. P. (2010b). Acyl modified chitosan derivatives for oral delivery of insulin and curcumin. *Journal of Materials Science: Materials in Medicine*, 21(7), 2133-2140.
- Shelma, R., & Sharma, C. P. (2011a). Development of lauroyl sulfated chitosan for enhancing hemocompatibility of chitosan. *Colloids and Surfaces B: Biointerfaces*, 84(2), 561-570.
- Shelma, R., & Sharma, C. P. (2011b). Submicroparticles composed of amphiphilic chitosan derivative for oral insulin and curcumin release applications. *Colloids and Surfaces B: Biointerfaces*, 88(2), 722-728.
- Shi, L., & Caldwell, K. D. (2000). Mucin adsorption to hydrophobic surfaces. *Journal of Colloid and Interface Science*, 224(2), 372-381.
- Shigemasa, Y., Usui, H., Morimoto, M., Saimoto, H., Okamoto, Y., Minami, S., & Sashiwa, H. (1999). Chemical modification of chitin and chitosan 1: preparation of partially deacetylated chitin derivatives via a ring-opening reaction with cyclic acid anhydrides in lithium chloride/N,N-dimethylacetamide. *Carbohydrate Polymers*, 39(3), 237-243.

- Shon, Y. H., Park, I. K., Moon, I. S., Chang, H. W., Park, I. K., & Nam, K. S. (2002). Effect of chitosan oligosaccharide on 2,3,7,8-tetrachlorodibenzo-p-dioxin-induced oxidative stress in mice. *Biological and Pharmaceutical Bulletin*, 25(9), 1161-1164.
- Siafaka, P. I., Zisi, A. P., Exindari, M. K., Karantas, I. D., & Bikiaris, D. N. (2016). Porous dressings of modified chitosan with poly(2-hydroxyethyl acrylate) for topical wound delivery of levofloxacin. *Carbohydrate Polymers*, 143, 90-99.
- Siddique, M. I., Katas, H., Iqbal Mohd. Amin, M. C., Ng, S. F., Zulfakar, M. H., Buang, F., & Jamil, A. (2015). Minimization of local and systemic adverse effects of topical glucocorticoids by nanoencapsulation: *In vivo* safety of hydrocortisone-hydroxytyrosol loaded chitosan nanoparticles. *Journal of Pharmaceutical Sciences*, 104(12), 4276-4286.
- Siew, A., Le, H., Thiovolet, M., Gellert, P., Schatzlein, A., & Uchegbu, I. (2012). Enhanced oral absorption of hydrophobic and hydrophilic drugs using quaternary ammonium palmitoyl glycol chitosan nanoparticles. *Molecular Pharmaceutics*, 9(1), 14-28.
- Sihorkar, V., & Vyas, S. P. (2001). Potential of polysaccharide anchored liposomes in drug delivery, targeting and immunization. *Journal of Pharmacy and Pharmaceutical Sciences*, 4(2), 138-158.
- Silverstein, R. M., Webster, F. X., Kiemle, D. J., & Bryce, D. L. (2014). *Spectrometric Identification of Organic Compounds* (8th Ed.) (pp. 80-108). New Jersey, USA: John Wiley & Sons, Inc.
- Simunek, J., Koppova, I., Filip, L., Tishchenko, G., & Belzecki, G. (2010). The antimicrobial action of low-molar-mass chitosan, chitosan derivatives and chitoooligosaccharides on bifidobacteria. *Folia Microbiologica*, 55(4), 379-382.
- Singh, R., & Lillard Jr., J. W. (2009). Nanoparticle-based targeted drug delivery. *Experimental and Molecular Pathology*, 86(3), 215-223.
- Singla, A. K., & Chawla, M. (2001). Chitosan: some pharmaceutical and biological aspects-an update. *Journal of Pharmacy and Pharmacology*, 53(8), 1047-1067.
- Sinha, V. R., Singla, A. K., Wadhawan, S., Kaushik, R., Kumria, R., Bansal, K., & Dhawan, S. (2004). Chitosan microspheres as a potential carrier for drugs. *International Journal of Pharmaceutics*, 274(1-2), 1-33.
- Snel, J., & Lorist, M. M. (2011). Effects of caffeine on sleep and cognition. *Progress in Brain Research*, 190, 105-117.

- Sogias, I. A., Khutoryanskiy, V. V., & Williams, A. C. (2010). Exploring the Factors Affecting the Solubility of Chitosan in Water. *Macromolecular Chemistry and Physics*, 211(4), 426-433.
- Sole, I., Vilchez, S., Miras, J., Montanya, N., Garcia-Celma, M. J., & Esquena, J. (2017). DHA and L-carnitine loaded chitosan hydrogels as delivery systems for topical applications. *Colloids and Surfaces A: Physicochemical and Engineering Aspects*, 525, 85-92.
- Soltani, H. A., & Aghadavoudi, O. (2002). The effect of different lidocaine application methods on postoperative cough and sore throat. *Journal of Clinical Anesthesia*, 14(1), 15-18.
- Son, S., Chae, S. Y., Choi, C., Kim, M. Y., Ngugen, V. G., Jang, M. K., Nah, J. W., & Kweon, J. K. (2004). Preparation of a hydrophobized chitosan oligosaccharide for application as an efficient gene carrier. *Macromolecular Research*, 12(6), 573-580.
- Sonam, Chaudhary, H., Arora, V., Kholi, K., & Kumar, V. (2013). Effect of physicochemical properties of biodegradable polymers on nano drug delivery. *Polymer Reviews*, 53(4), 546-567.
- Soni, S., Verma, N., Verma, A., & K. Pandit, J. (2017). Gelucire based floating emulsion gel beads: A potential carrier for sustained stomach specific drug delivery. *Farmacia*, 65(1), 142-152.
- Sonia, T. A., Rekha, M. R., & Sharma, C. P. (2011). Bioadhesive hydrophobic chitosan microparticles for oral delivery of insulin: *In vitro* characterization and *in vivo* uptake studies. *Journal of Applied Polymer Science*, 119(5), 2902-2910.
- Sonia, T. A., & Sharma, C. P. (2011). Chitosan and its derivatives for drug delivery perspective. In Jayakumar, R., Prabakaran, M., & Muzzarelli, R. A. A., *Chitosan for Biomaterials I* (Vol. 243, pp. 23-53). Berlin, Heidelberg: Springer-Verlag GmbH.
- Soppimath, K. S., Aminabhavi, T. M., Kulkarni, A. R., & Rudzinski, W. E. (2001). Biodegradable polymeric nanoparticles as drug delivery devices. *Journal of Controlled Release*, 70(1-2), 1-20.
- Stein, C. (1995). The control of pain in peripheral tissue by opioids. *The New England Journal of Medicine*, 332(25), 1685-1690.
- Strand, S. P., Issa, M. M., Christensen, B. E., Varum, K. M., & Artursson, P. (2008). Tailoring of chitosans for gene delivery: Novel self-branched glycosylated chitosan oligomers with improved functional properties. *Biomacromolecules*, 9(11), 3268-3276.

- Suksaeree, J., Monton, C., Madaka, F., Sakunpak, A., Pichayakorn, W., & Boonme, P. (2014). Physicochemical properties study of Plai patches for topical applications. *International Journal of Pharmacy and Pharmaceutical Sciences*, 6(5), 253-256.
- Sun, T., Yao, Q., Zhou, D., & Mao, F. (2008). Antioxidant activity of *N*-carboxymethyl chitosan oligosaccharides. *Bioorganic & Medicinal Chemistry Letters*, 18(21), 5774-5776.
- Sun, T., Zhu, Y., Xie, J., & Yin, X. (2011). Antioxidant activity of *N*-acyl chitosan oligosaccharide with same substituting degree. *Bioorganic & Medicinal Chemistry Letters*, 21(2), 798-800.
- Swerdlow, M., & Cundill, J. G. (1981). Anticonvulsant drugs used in the treatment of lancinating pain. A comparison. *Anaesthesia*, 36(12), 1129-1132.
- Tamura, H., & Furuike, T. (2014). Chitin and chitosan. In Kobayashi, S. & Mullen, K., *Encyclopedia of Polymeric Nanomaterials* (pp. 1-4). Berlin, Heidelberg: Springer-Verlag GmbH.
- Tan, H. W., & Misran, M. (2013). Polysaccharide-anchored fatty acid liposome. *International Journal of Pharmaceutics*, 441(1-2), 414-423.
- Tan, Q., Liu, W., Guo, C., & Zhai, G. (2011). Preparation and evaluation of quercetin-loaded lecithin-chitosan nanoparticles for topical delivery. *International Journal of Nanomedicine*, 6, 1621-1630.
- Tan, Y. L., & Liu, C. G. (2009). Self-aggregated nanoparticles from linoleic acid modified carboxymethyl chitosan: Synthesis, characterization and application *in vitro*. *Colloids and Surfaces B: Biointerfaces*, 69(2), 178-182.
- Tang, D. L., Song, F., Chen, C., Wang, X. L., & Wang, Y. Z. (2013). A pH-responsive chitosan-b-poly(p-dioxanone) nanocarrier: formation and efficient antitumor drug delivery. *Nanotechnology*, 24(14), 145101.
- Tang, J., & Ge, Y. (2015). Preparation and characterization of chitosan film loaded citronella oil. *Huagong Xinxing Cailiao*, 43(10), 85-87.
- Teixeira, G. Q., Leite Pereira, C., Castro, F., Ferreira, J. R., Gomez-Lazaro, M., Aguiar, P., Barbosa, M. A., Neidlinger-Wilke, C., & Goncalves, R. M. (2016). Anti-inflammatory chitosan/poly- γ -glutamic acid nanoparticles control inflammation while remodeling extracellular matrix in degenerated intervertebral disc. *Acta Biomaterialia*, 42, 168-179.
- Terzi, M., Altun, G., Sen, S., Kocaman, A., Kaplan, A. A., Yurt, K. K., & Kaplan, S. (2017). The use of non-steroidal anti-inflammatory drugs in neurological diseases. *Journal of Chemical Neuroanatomy*, *In press*.

- Thakur, A., Lariya, N. K., Agarwal, A., Tiwari, B. K., Kharya, A. K., Agrawal, H., & Agrawal, G. P. (2013). Nanoparticles-in-microspheres based dual drug delivery system for topical delivery of anti-acne drugs. *International Journal of Advanced Research*, 1(5), 176-188.
- Thanou, M., Florea, B. I., Geldof, M., Junginger, H. E., & Borchard, G. (2002). Quaternized chitosan oligomers as novel gene delivery vectors in epithelial cell lines. *Biomaterials*, 23(1), 153-159.
- The National Pharmaceutical Council & Joint Commission Accreditation of Healthcare Organization. (2001). *Pain: Current Understanding of Assessment, Management, and Treatments (Vol. Section III: Types of treatments)*. Washington, USA: The National Pharmaceutical Council & Joint Commission Accreditation of Healthcare Organization.
- Tian, F., Liu, Y., Hu, K., & Zhao, B. (2003). The depolymerization mechanism of chitosan by hydrogen peroxide. *Journal of Materials Science*, 38(23), 4709-4712.
- Tian, M., Tan, H., Li, H., & You, C. (2015). Molecular weight dependence of structure and properties of chitosan oligomers. *RSC Advances*, 5(85), 69445-69452.
- Tikhonov, V. E., Stepnova, E. A., Babak, V. G., Yamskov, I. A., Palma-Guerrero, J., Jansson, H.B., Lopez-Llorca, L. V., Salinas, J., Gerasimenko, D. V., Avdienko, I. D., & Varlamov, V. P. (2006). Bactericidal and antifungal activities of a low molecular weight chitosan and its *N*-2(3)-(dodec-2-enyl)succinoyl/-derivatives. *Carbohydrate Polymers*, 64(1), 66-72.
- Tiwari, B. K., Valdramidis, V. P., O' Donnell, C. P., Muthukumarappan, K., Bourke, P., & Cullen, P. J. (2009). Application of natural antimicrobials for food preservation. *Journal of Agricultural and Food Chemistry*, 57(14), 5987-6000.
- Tiwari, G., Tiwari, R., Sriwastawa, B., Bhati, L., Pandey, S., Pandey, P., & Bannerjee, S. K. (2012). Drug delivery systems: An updated review. *International Journal of Pharmaceutical Investigation*, 2(1), 2-11.
- Toffey, A., & Glasser, W. G. (2001). Chitin derivatives III formation of amidized homologs of chitosan. *Cellulose*, 8(1), 35-47.
- Tommeraas, K., Varum, K. M., Christensen, B. E., & Smidsrod, O. (2001). Preparation and characterisation of oligosaccharides produced by nitrous acid depolymerisation of chitosans. *Carbohydrate Research*, 333(2), 137-144.
- Tsai, C. Y., Woung, L. C., Yen, J. C., Tseng, P. C., Chiou, S. H., Sung, Y. J., Liu, K. T., & Cheng, Y. H. (2016). Thermosensitive chitosan-based hydrogels for sustained release of ferulic acid on corneal wound healing. *Carbohydrate Polymers*, 135, 308-315.

- Tsai, G. J., Su, W. H., Chen, H. C., & Pan, C. L. (2002). Antimicrobial activity of shrimp chitin and chitosan from different treatments and applications of fish preservation. *Fisheries Science*, 68(1), 170-177.
- Ubaidulla, U., Sultana, Y., Ahmed, F. J., Khar, R. K., & Panda, A. K. (2007). Chitosan phthalate microspheres for oral delivery of insulin: Preparation, characterization, and *in vitro* evaluation. *Drug Delivery*, 14(1), 19-23.
- Ueno, H., Mori, T., & Fujinaga, T. (2001). Topical formulations and wound healing applications of chitosan. *Advanced Drug Delivery Reviews*, 52(2), 105-115.
- Umadevi, S. K., Thiruganesh, R., Suresh, S., & Reddy, K. B. (2010). Formulation and evaluation of chitosan microspheres of aceclofenac for colon-targeted drug delivery. *Biopharmaceutics & Drug Disposition*, 31(7), 407-427.
- United States Pharmacopeia and National Formulary. (2000). *The United States Pharmacopeia XXIV and the National Formulary XIX*. Rockville, Maryland: United States Pharmacopeial Convention Inc.
- Varum, F. J. O., McConnell, E. L., Sousa, J. J., Veiga, F., & Basit, A. W. (2008). Mucoadhesion and the gastrointestinal tract. *Critical Reviews in Therapeutic Drug Carrier Systems*, 25(3), 207-258.
- Vasnev, V. A., Tarasov, A. I., Markova, G. D., Vinogradova, S. V., & Garkusha, O. G. (2006). Synthesis and properties of acylated chitin and chitosan derivatives. *Carbohydrate Polymers*, 64(2), 184-189.
- Velasco, M. V., Tano, C. T., Machado-Santelli, G. M., Consiglieri, V. O., Kaneko, T. M., & Baby, A. R. (2008). Effects of caffeine and siloxanetriol alginate caffeine, as anticellulite agents, on fatty tissue: histological evaluation. *Journal of Cosmetic Dermatology*, 7(1), 23-29.
- Venter, J. P., Kotze, A. F., Auzely-Velty, R., & Rinaudo, M. (2006). Synthesis and evaluation of the mucoadhesivity of a CD-chitosan derivative. *International Journal of Pharmaceutics*, 313(1-2), 36-42.
- Verheul, R. J., Amidi, M., van der Wal, S., van Riet, E., Jiskoot, W., & Hennink, W. E. (2008). Synthesis, characterization and *in vitro* biological properties of *O*-methyl free N,N,N-trimethylated chitosan. *Biomaterials*, 29(27), 3642-3649.
- Vieira, A. P., Badshah, S., & Airoidi, C. (2013). Ibuprofen-loaded chitosan and chemically modified chitosan—Release features from tablet and film forms. *International Journal of Biological Macromolecules*, 52, 107-115.

- Wang, C. C., Lin, L. H., Lee, H. T., & Ye, Y. W. (2011). Surface activity and micellization properties of chitosan-succinyl derivatives. *Colloids and Surfaces A: Physicochemical and Engineering Aspects*, 389(1–3), 246-253.
- Wang, S. L., Lin, S. Y., & Wei, Y. S. (2002). Transformation of metastable forms of acetaminophen studied by thermal Fourier transform infrared (FT-IR) microspectroscopy. *Chemical and Pharmaceutical Bulletin*, 50(2), 153-156.
- Wang, X. H., Tian, Q., Wang, W., Zhang, C. N., Wang, P., & Yuan, Z. (2012). *In vitro* evaluation of polymeric micelles based on hydrophobically-modified sulfated chitosan as a carrier of doxorubicin. *Journal of Materials Science: Materials in Medicine*, 23(7), 1663-1674.
- Wang, Y. S., Liu, L. R., Jiang, Q., & Zhang, Q. Q. (2007). Self-aggregated nanoparticles of cholesterol-modified chitosan conjugate as a novel carrier of epirubicin. *European Polymer Journal*, 43(1), 43-51.
- Wang, Y., Wang, J., Han, H., Liu, J., Zhao, H., Shen, M., Xu, Y., Xu, J., Li, L., & Guo, X. (2016). Self-assembled micelles of *N*-phthaloylchitosan-g-poly (*N*-vinylcaprolactam) for temperature-triggered non-steroidal anti-inflammatory drug delivery. *Journal of Materials Science*, 51(3), 1591-1599.
- Wassmer, S., Rafat, M., Fong, W. G., Baker, A. N., & Tsilfidis, C. (2013). Chitosan microparticles for delivery of proteins to the retina. *Acta Biomaterialia*, 9(8), 7855-7864.
- Wei, X. H., Niu, Y. P., Xu, Y. Y., Du, Y. Z., Hu, F. Q., & Yuan, H. (2010). Salicylic acid-grafted chitosan oligosaccharide nanoparticle for paclitaxel delivery. *Journal of Bioactive and Compatible Polymers*, 25(3), 319-335.
- Whang, H. S., Kirsch, W., Zhu, Y. H., Yang, C. Z., & Hudson, S. M. (2005). Hemostatic agents derived from chitin and chitosan. *Journal of Macromolecular Science: Part C: Polymer Reviews*, C45(4), 309-323.
- Win, P. P., Shin-ya, Y., Hong, K. J., & Kajiuchi, T. (2003). Formulation and characterization of pH sensitive drug carrier based on phosphorylated chitosan (PCS). *Carbohydrate Polymers*, 53(3), 305-310.
- Wishart, D. S., Knox, C., Guo, A. C., Shrivastava, S., Hassanali, M., Stothard, P., Chang, Z., & Woolsey, J. (2006). DrugBank: A comprehensive resource for in silico drug discovery and exploration. *Nucleic Acids Research*, 34(Database issue), D668-672.
- Xiangyang, X., Ling, L., Jianping, Z., Shiyue, L., Jie, Y., Xiaojin, Y., & Jinsheng, R. (2007). Preparation and characterization of *N*-succinyl-*N'*-octyl chitosan micelles

as doxorubicin carriers for effective anti-tumor activity. *Colloids and Surfaces B: Biointerfaces*, 55(2), 222-228.

- Xie, Y., Liu, X., & Chen, Q. (2007). Synthesis and characterization of water-soluble chitosan derivate and its antibacterial activity. *Carbohydrate Polymers*, 69(1), 142-147.
- Xing, R., Liu, S., Guo, Z., Yu, H., Zhong, Z., Ji, X., & Li, P. (2008). Relevance of molecular weight of chitosan-*N*-2-hydroxypropyl trimethyl ammonium chloride and their antioxidant activities. *European Journal of Medicinal Chemistry*, 43(2), 336-340.
- Xu, Y., Du, Y., Huang, R., & Gao, L. (2003). Preparation and modification of *N*-(2-hydroxyl) propyl-3-trimethyl ammonium chitosan chloride nanoparticle as a protein carrier. *Biomaterials*, 24(27), 5015-5022.
- Yaneva, Z. L., Staleva, M. S., & Georgieva, N. V. (2015). Study on the host-guest interactions during caffeine encapsulation into zeolite. *European Journal of Chemistry*, 6(2), 169-173.
- Yang, L., Guo, C., Jia, L., Liang, X., Liu, C., & Liu, H. (2010). Dual responsive copolymer micelles for drug controlled release. *Journal of Colloid and Interface Science*, 350(1), 22-29.
- Yang, Z., Fang, Y., & Ji, H. (2016). Controlled release and enhanced antibacterial activity of salicylic acid by hydrogen bonding with chitosan. *Chinese Journal of Chemical Engineering*, 24(3), 421-426.
- Yen, M. T., Yang, J. H., & Mau, J. L. (2008). Antioxidant properties of chitosan from crab shells. *Carbohydrate Polymers*, 74(4), 840-844.
- Yin, H., Du, Y., & Zhang, J. (2009). Low molecular weight and oligomeric chitosans and their bioactivities. *Current Topics in Medicinal Chemistry*, 9(16), 1546-1559.
- Yoo, H. S., Lee, J. E., Chung, H., Kwon, I. C., & Jeong, S. Y. (2005). Self-assembled nanoparticles containing hydrophobically modified glycol chitosan for gene delivery. *Journal of Controlled Release*, 103(1), 235-243.
- Yoshioka, H., Nonaka, K., Fukuda, K., & Kazama, S. (1995). Chitosan-derived polymer-surfactants and their micellar properties. *Bioscience, Biotechnology, and Biochemistry*, 59(10), 1901-1904.
- You, J., Hu, F. Q., Du, Y. Z., & Yuan, H. (2007). Polymeric micelles with glycolipid-like structure and multiple hydrophobic domains for mediating molecular target delivery of paclitaxel. *Biomacromolecules*, 8(8), 2450-2456.

- Yuan, X. B., Li, H., & Yuan, Y. B. (2006). Preparation of cholesterol-modified chitosan self-aggregated nanoparticles for delivery of drugs to ocular surface. *Carbohydrate Polymers*, 65(3), 337-345.
- Yuan, Z., Ye, Y., Gao, F., Yuan, H., Lan, M., Lou, K., & Wang, W. (2013). Chitosan-graft-beta-cyclodextrin nanoparticles as a carrier for controlled drug release. *International Journal of Pharmaceutics*, 446(1-2), 191-198.
- Yuen, C. W. M., Yip, J., Liu, L., Cheuk, K., Kan, C. W., Cheung, H. C., & Cheng, S. Y. (2012). Chitosan microcapsules loaded with either miconazole nitrate or clotrimazole, prepared via emulsion technique. *Carbohydrate Polymers*, 89(3), 795-801.
- Zhang, C., Ding, Y., Yu, L., & Ping, Q. (2007a). Polymeric micelle systems of hydroxycamptothecin based on amphiphilic *N*-alkyl-*N*-trimethyl chitosan derivatives. *Colloids and Surfaces B: Biointerfaces*, 55(2), 192-199.
- Zhang, C., Ping, Q., Zhang, H., & Shen, J. (2003a). Preparation of *N*-alkyl-*O*-sulfate chitosan derivatives and micellar solubilization of taxol. *Carbohydrate Polymers*, 54(2), 137-141.
- Zhang, C., Ping, Q., Zhang, H., & Shen, J. (2003b). Synthesis and characterization of water-soluble *O*-succinyl-chitosan. *European Polymer Journal*, 39(8), 1629-1634.
- Zhang, C., Qineng, P., & Zhang, H. (2004). Self-assembly and characterization of paclitaxel-loaded *N*-octyl-*O*-sulfate chitosan micellar system. *Colloids and Surfaces B: Biointerfaces*, 39(1-2), 69-75.
- Zhang, C., Qu, G., Sun, Y., Yang, T., Yao, Z., Shen, W., Shen, Z., Ding, Q., Zhou, H., & Ping, Q. (2008). Biological evaluation of *N*-octyl-*O*-sulfate chitosan as a new nano-carrier of intravenous drugs. *European Journal of Pharmaceutical Sciences*, 33(4-5), 415-423.
- Zhang, J., Chen, X. G., Huang, L., Han, J. T., & Zhang, X. F. (2012). Self-assembled polymeric nanoparticles based on oleic acid-grafted chitosan oligosaccharide: biocompatibility, protein adsorption and cellular uptake. *Journal of Materials Science: Materials in Medicine*, 23(7), 1775-1783.
- Zhang, J., Han, J., Zhang, X., Jiang, J., Xu, M., Zhang, D., & Han, J. (2015). Polymeric nanoparticles based on chitoooligosaccharide as drug carriers for co-delivery of all-trans-retinoic acid and paclitaxel. *Carbohydrate Polymers*, 129, 25-34.
- Zhang, L., Radovic-Moreno, A. F., Alexis, F., Gu, F. X., Basto, P. A., Bagalkot, V., Jon, S., Langer, R. S., Farokhzad, O. C. (2007b). Co-delivery of hydrophobic and hydrophilic drugs from nanoparticle-aptamer bioconjugates. *ChemMedChem*, 2(9), 1268-1271.

- Zhang, N., Wardwell, P. R., & Bader, R. A. (2013a). Polysaccharide-based micelles for drug delivery. *Pharmaceutics*, 5(2), 329-352.
- Zhang, P., Liu, X., Hu, W., Bai, Y., & Zhang, L. (2016). Preparation and evaluation of naringenin-loaded sulfobutylether- β -cyclodextrin/chitosan nanoparticles for ocular drug delivery. *Carbohydrate Polymers*, 149, 224-230.
- Zhang, X., Ercelen, S., Duportail, G., Schaub, E., Tikhonov, V., Slita, A., Zarubaev, V., Babak, V., & Mely, Y. (2008). Hydrophobically modified low molecular weight chitosans as efficient and nontoxic gene delivery vectors. *Journal of Gene Medicine*, 10(5), 527-539.
- Zhang, Y., Huo, M., Zhou, J., Yu, D., & Wu, Y. (2009). Potential of amphiphilically modified low molecular weight chitosan as a novel carrier for hydrophobic anticancer drug: Synthesis, characterization, micellization and cytotoxicity evaluation. *Carbohydrate Polymers*, 77(2), 231-238.
- Zhang, Y., Huo, M., Zhou, J., Zou, A., Li, W., Yao, C., & Xie, S. (2010). DDSolver: An add-in program for modeling and comparison of drug dissolution profiles. *AAPS Journal*, 12(3), 263-271.
- Zhang, Y., Wu, S., Xu, J., Chen, W., & Lv, Y. (2013b). Preparation and performance characterization of electrospun drug loaded poly (vinyl alcohol)/chitosan nanofibrous membrane. *Zhejiang Da Xue Xue Bao, Yi Xue Ban*, 42(6), 644-648.
- Zhang, Z., Wang, X., Zhao, M., & Qi, H. (2014). *O*-acetylation of low-molecular-weight polysaccharide from *Enteromorpha linza* with antioxidant activity. *International Journal of Biological Macromolecules*, 69, 39-45.
- Zhao, Z., He, M., Yin, L., Bao, J., Shi, L., Wang, B., Tang, C., & Yin, C. (2009). Biodegradable nanoparticles based on linoleic acid and poly(beta-malic acid) double grafted chitosan derivatives as carriers of anticancer drugs. *Biomacromolecules*, 10(3), 565-572.
- Zheng, F., Shi, X. W., Yang, G. F., Gong, L. L., Yuan, H. Y., Cui, Y. J., Wang, Y., Du, Y. M., & Li, Y. (2007). Chitosan nanoparticle as gene therapy vector via gastrointestinal mucosa administration: Results of an *in vitro* and *in vivo* study. *Life Sciences*, 80(4), 388-396.
- Zheng, L. Y., & Zhu, J. F. (2003). Study on antimicrobial activity of chitosan with different molecular weights. *Carbohydrate Polymers*, 54(4), 527-530.
- Zhong, Z., Ji, X., Xing, R., Liu, S., Guo, Z., Chen, X., & Li, P. (2007). The preparation and antioxidant activity of the sulfanilamide derivatives of chitosan and chitosan sulfates. *Bioorganic & Medicinal Chemistry*, 15(11), 3775-3782.

Zhong, Z., Xing, R., Liu, S., Wang, L., Cai, S., & Li, P. (2008). Synthesis of acyl thiourea derivatives of chitosan and their antimicrobial activities *in vitro*. *Carbohydrate Research*, 343(3), 566-570.

Zhou, H., Yu, W., Guo, X., Liu, X., Li, N., Zhang, Y., & Ma, X. (2010a). Synthesis and characterization of amphiphilic glycidol–chitosan–deoxycholic acid nanoparticles as a drug carrier for doxorubicin. *Biomacromolecules*, 11(12), 3480-3486.

Zhou, Y. Y., Du, Y. Z., Wang, L., Yuan, H., Zhou, J. P., & Hu, F. Q. (2010b). Preparation and pharmacodynamics of stearic acid and poly (lactic-co-glycolic acid) grafted chitosan oligosaccharide micelles for 10-hydroxycamptothecin. *International Journal of Pharmaceutics*, 393(1-2), 144-152.

University of Malaya

LIST OF PUBLICATIONS AND PAPERS PRESENTED

a) Publications

1. **Tiew, S. X.**, & Misran, M. (2018). Thermal properties of acylated low molecular weight chitosans. *Journal of the Chemical Society of Pakistan*. (Accepted).
2. **Tiew, S. X.**, & Misran, M. (2017). Physicochemical properties of acylated low molecular weight chitosans. *International Journal of Polymeric Materials and Polymeric Biomaterials*. In press. DOI: 10.1080/00914037.2017.1362637
3. **Tiew, S. X.**, & Misran, M. (2017). Encapsulation of salicylic acid in acylated low molecular weight chitosan for sustained release topical application. *Journal of Applied Polymer Science*, 45273, 11 pages.
4. Voon, S. H., **Tiew, S. X.**, Kue, C. S., Lee, H. B., Kiew, L. V., Misran, M., Kamkaew, A., Burgess K., & Chung., L. Y. (2016). Chitosan-coated poly(lactic-co-glycolic acid)-diiodinated boron-dipyrromethene nanoparticles improve tumor selectivity and stealth properties in photodynamic cancer therapy. *Journal of Biomedical Nanotechnology*, 12, 1431-1452.

b) Oral presentations

1. **Tiew, S. X.**, & Misran, M. Acylated low molecular weight chitosan for sustained release of salicylic acid. The International Polymer Conference of Thailand (PCT-7), 1st-2nd June 2017, Amari Watergate Hotel, Bangkok, Thailand.
2. **Tiew, S. X.**, & Misran, M. Water-soluble chitosan nanoparticles from acylation of short chain hydrophobic alkyl group. 2nd AMDI International Biohealth Sciences Conferences 2016, 27-28th January 2016, Universiti Sains Malaysia Penang, Malaysia.

c) Poster presentation

1. **Tiew, S. X.**, & Misran, M. Low Molecular Weight Chitosan Nanoparticles as Halal Compliant Nanocarriers. Program Halal Research in UM (HARUM) 2016, 29th September 2017, Akademi Pengajian Islam, Universiti Malaya, Kuala Lumpur, Malaysia.